

AD-A150 802

RESEARCH ON COMPOSITE MATERIALS FOR STRUCTURAL DESIGN

1/4

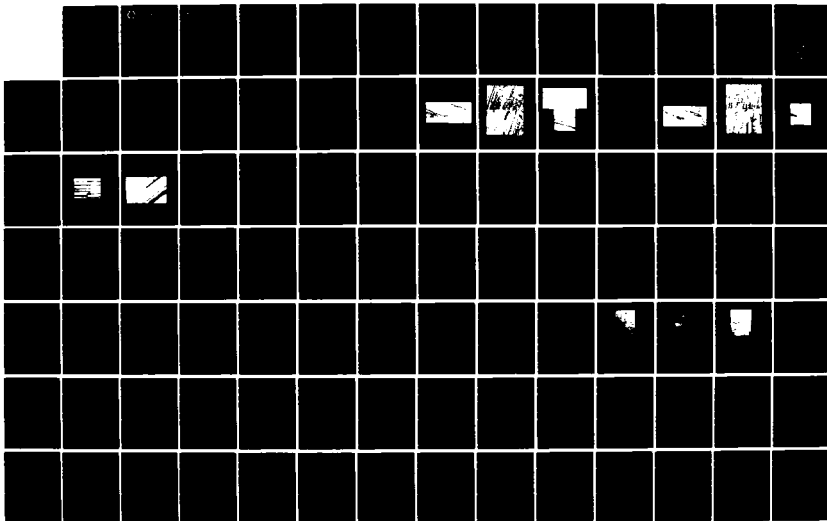
(U) TEXAS A AND M UNIV COLLEGE STATION MECHANICS AND  
MATERIALS RE. . D ALLEN ET AL. APR 84 MM-4665-84-5

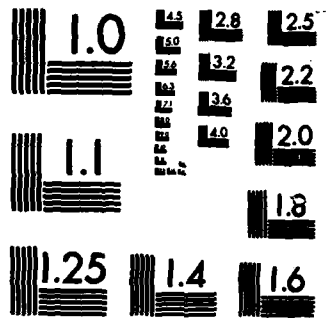
UNCLASSIFIED

AFOSR-TR-85-0226 F49620-82-C-0057

F/G 11/9

NL





MICROCOPY RESOLUTION TEST CHART  
NATIONAL BUREAU OF STANDARDS-1963-A

2



**Mechanics and Materials Center  
TEXAS A&M UNIVERSITY  
College Station, Texas**

---

RESEARCH ON COMPOSITE MATERIALS FOR  
STRUCTURAL DESIGN  
FINAL TECHNICAL REPORT

AD-A150 802

DTIC FILE COPY

SEARCHED  
SERIALIZED  
INDEXED  
FILED

AIR FORCE OFFICE OF SCIENTIFIC RESEARCH  
OFFICE OF AEROSPACE RESEARCH  
UNITED STATES AIR FORCE  
CONTRACT No. F49620-82-C-0057

MM 4665-84-5

APRIL 1984

This document has been approved  
for public release and sale; its  
distribution is unlimited.

UNCLASSIFIED

SECURITY CLASSIFICATION OF THIS PAGE (When Data Entered)

REPORT DOCUMENTATION PAGE		READ INSTRUCTIONS BEFORE COMPLETING FORM
1. REPORT NUMBER <b>AFOSR-STR- 85-0226</b>	2. GOVT ACCESSION NO.	3. RECIPIENT'S CATALOG NUMBER
4. TITLE (and Subtitle) RESEARCH ON COMPOSITE MATERIALS FOR STRUCTURAL DESIGN		5. TYPE OF REPORT & PERIOD COVERED FINAL 1 Jan 82 - 15 Feb 84
		6. PERFORMING ORG. REPORT NUMBER MM 4665-84-5
7. AUTHOR(s) D. Allen, W. Bradley, S. Groves, J. Ham, B. Harbert, C. Hoeve, R. Schapery, R. Tonda, R. Weatherby, Y. Weitsman		8. CONTRACT OR GRANT NUMBER(s) F46920-82-C-0057
9. PERFORMING ORGANIZATION NAME AND ADDRESS TEXAS A&M UNIVERSITY MECHANICS & MATERIALS CENTER COLLEGE STATION, TX 77843		10. PROGRAM ELEMENT, PROJECT, TASK AREA & WORK UNIT NUMBERS 6/102F 2307/B2
11. CONTROLLING OFFICE NAME AND ADDRESS AIR FORCE OFFICE OF SCIENTIFIC RESEARCH BLDG. 410 BOLLING AIR FORCE BASE, D.C. 20332		12. REPORT DATE April 1984
14. MONITORING AGENCY NAME & ADDRESS (if different from Controlling Office)		13. NUMBER OF PAGES 97 + Appendix
		15. SECURITY CLASS. (of this report) UNCLASSIFIED
		15a. DECLASSIFICATION/DOWNGRADING SCHEDULE
16. DISTRIBUTION STATEMENT (of this Report)  Approved for public release; distribution unlimited		
17. DISTRIBUTION STATEMENT (of the abstract entered in Block 20, if different from Report)		
18. SUPPLEMENTARY NOTES		
19. KEY WORDS (Continue on reverse side if necessary and identify by block number) Composite Materials      Delamination      Fracture Resins      Residual Stresses      Damage Adhesives      Viscoelasticity		
20. ABSTRACT (Continue on reverse side if necessary and identify by block number) Summarized are research activities related to advanced fiber reinforced plastics in the areas of fracture, delamination, distributed damage, residual stresses, moisture effects, and toughening mechanisms in elastic and viscoelastic materials. Also included are abstracts of the six M.S. theses and one Ph.D. dissertation completed during the project period. The Appendix contains full papers and additional abstracts of work done on the project. <i>(Additional keywords: resins, adhesives, fracture (mechanics), structural mechanics, polymers)</i>		

DD FORM 1 JAN 73 1473

UNCLASSIFIED

SECURITY CLASSIFICATION OF THIS PAGE (When Data Entered)



RESEARCH ON COMPOSITE MATERIALS

FOR STRUCTURAL DESIGN

Final Technical Report

Submitted

by the

TEXAS A&M UNIVERSITY

MECHANICS AND MATERIALS CENTER

Accession For	
NTIS GRA&I	<input checked="" type="checkbox"/>
DTIC TAB	<input type="checkbox"/>
Unannounced	<input type="checkbox"/>
Justification	
By	
Distribution/	
Availability Codes	
Dist	Avail and/or Special
A-1	



to the

Air Force Office of Scientific Research

Office of Aerospace Research

United States Air Force

AIR FORCE OFFICE OF SCIENTIFIC RESEARCH (AFSC)  
NOTICE OF TRANSMITTAL TO DTIC  
This technical report has been reviewed and is  
approved for public release in accordance with AFR 190-12.  
Distribution is unlimited.  
MATTHEW J. KERPER  
Chief, Technical Information Division

MM 4665-84-5

Contract No. F49620-82-C-0057

April 1984

## TABLE OF CONTENTS

	Page
1. INTRODUCTION.....	1
1.1 Summary.....	1
1.2 Statement of Work.....	2
2. MICROMECHANISMS OF MATRIX CONTROLLED FRACTURE OF GRAPHITE/EPOXY COMPOSITES.....	3
2.1 Introduction.....	3
2.2 Qualitative Models for Mode I Delamination.....	3
2.3 Qualitative Model for Mixed Mode Delamination.....	8
2.4 Experimental Work to Study Qualitative Delamination Fracture Models.....	8
2.5 Experimental Results and Discussion.....	9
2.6 Summary.....	22
2.7 References.....	25
3. MATRIX CONTROLLED DEFORMATION AND FRACTURE ANALYSIS OF FIBROUS COMPOSITES.....	26
3.1 Introduction.....	26
3.2 Deformation and Fracture Theory for Composites with Distributed Damage.....	26
3.3 Evaluation of Energy Release Rates in Unidirectional Split Laminate Specimens.....	27
3.4 Slow, Stable Delamination in Graphite/Epoxy Composites.....	29
3.5 Analysis of Crack Growth in Damaged Media Using a Generalized J-Integral.....	30
3.6 Characterization of Damage Using a Pseudo Potential.....	33
3.7 References.....	42
4. A DAMAGE MODEL FOR CONTINUOUS FIBER COMPOSITES.....	43
4.1 Introduction.....	43
4.2 Development of the Damage Model.....	44

5. RESIDUAL STRESSES AND ENVIRONMENTAL EFFECTS IN COMPOSITES.....	50
5.1 Introduction.....	50
5.2 Time-Temperature Behavior of Hercules 3502 Resin.....	50
5.3 Chemical Cure-Shrinkage Effects on Residual Stresses in Epoxy Resins.....	52
5.4 Hygrothermal Stresses in Unsymmetric Cross-Ply Graphite/Epoxy Laminates.....	52
5.5 Hygrothermal Effects on Damage in AS4/3502 Composites.....	55
5.6 Investigations of Moisture Diffusion in Composites.....	59
6. RESIN STUDIES.....	67
6.1 Improving the Ductility of Epoxy Resins.....	67
6.2 Structure and Behavior of Water in Resins.....	73
6.3 Molecular Models of Resins.....	73
7. DEVELOPMENT OF ELASTIC STRAIN RATIO TRANSLATOR (ESRT) GAGE.....	76
7.1 Introduction.....	76
7.2 Description.....	76
7.3 Results and Discussion.....	78
8. GRADUATE RESEARCH ASSISTANT ACTIVITIES.....	81
8.1 Summary.....	81
8.2 Abstracts of M.S. Theses and Ph.D. Dissertation.....	82
9. PROFESSIONAL PERSONNEL INFORMATION.....	91
9.1 Faculty Research Assignments.....	91
9.2 Additional Professional Staff.....	92
9.3 Spoken Papers and Presentations, Publications, and Other Professional Activities of the Faculty.....	92
APPENDIX.....	98

## 1. INTRODUCTION

### 1.1 Summary

Primary activities consisted of (i) conducting research in accordance with the Statement of Work given in Section 1.2; (ii) preparing sixteen technical papers and reports, six M.S. Theses, one Ph.D. dissertation, and one invention disclosure; and (iii) various interactions of the faculty with the technical community.

Sections 2-8 summarize the research activities. The professional personnel associated with the project and the outside composites-related activities of the faculty are given in Section 9. Six faculty members had responsibility for the research activities, as shown in Section 9.1. Sections 2-6 were prepared by them or under their direction: Walter Bradley (2); Richard Schapery (3); David Allen (4); Jack Weitsman (5); Cor Hoeve and Joe Ham (6). In some cases graduate students assisted in writing the sections: Randy Weatherby (3); Richard Tonda (3); Scott Groves (4). A device for measuring large uniaxial deformations in adverse environments was developed by Bob Harbert, a research engineer in the Mechanics and Materials Center, and this work is discussed in Section 7.

Details of completed studies appear in the seven theses and dissertation, whose abstracts are given in Sections 8.2, and in the sixteen publications. Seven of the papers or reports were completed during the second year of the contract, and they are reproduced in their entirety in the Appendix. The other nine publications identified in the Appendix were included with the 1983 Annual Technical Report (Texas A&M University Report No. MM 4665-83-4, April 1983).

## 1.2 Statement of Work

Specific areas to be investigated are:

1. micro- and macro-mechanisms of fracture of resins and composites, with emphasis on processes involved in delamination growth
2. effects of transient temperatures and moisture content on deformation and fracture properties, including consideration of residual stresses and their effect on intraply and interply cracking (delamination)
3. behavior and structure of water in resins and model resin systems, and its effect on basic deformation and fracture properties
4. toughening mechanisms in high temperature resins, including study of the separate effects of energy absorption in crack-tip failure processes and far-field deformation and micro-damage processes
5. improved theoretical models for characterizing and predicting deformation and failure behavior of resins and composites

## 2. MICROMECHANISMS OF MATRIX CONTROLLED FRACTURE OF GRAPHITE/EPOXY COMPOSITES\*

### 2.1 Introduction

The objective of this work has been to relate the macroscopic delamination fracture behavior as quantified using fracture mechanics to the micromechanisms of fracture observed directly by fracturing specimens in the scanning electron microscope. Such an approach should guide in the development of qualitative models of delamination as an intermediate step in the development of quantitative micromechanics models for delamination fracture. The principal results from this effort will be summarized next.

### 2.2 Qualitative Models for Mode I Delamination

The energy dissipation during delamination fracture can result from resin deformation and/or microcracking and from fiber pullout and/or breakage. The relative contribution of these two processes to the total fracture energy depends on the toughness of the resin and the interfacial bonding strength. Furthermore, whether the delamination toughness of the composite material is greater or less than the toughness of the neat material also depends on the toughness of the resin and the interfacial bond strength.

Addition of Brittle Fibers to Brittle Resin: The addition of stronger brittle fibers to a weaker brittle resin should increase the resistance to fracture, even for the delamination mode of fracture. The reason is that while the crack moves nominally through the resin rich region between plies, it will occasionally impinge on misaligned fibers. Since the fibers

---

\*Prepared by W.L. Bradley

are much stronger than the resin, interaction of the crack tip with the graphite fibers increases resistance to crack growth. Furthermore, a thin resin rich region between plies can give rise to a corrugated topography for the fractured surface. The crack will prefer to move through the weaker resin rather than breaking the stronger fiber, but there is no plane containing only resin if the resin rich region between plies has an average thickness of less than one fiber diameter. The thinner the resin rich region, the more corrugated will be the fracture surface and the more frequent will be the crack tip interaction with the fibers. Each of these effects should increase the energy absorbed per unit area of crack extension in a brittle fiber/brittle resin system. Thus, the addition of strong brittle fibers to a brittle resin should give a delamination fracture toughness greater than the neat resin fracture toughness, with the increase in fracture toughness being greatest for the minimum possible thickness of the resin rich region. Going the other direction, as the resin rich region approaches 5-10 fiber diameters (if processing would allow this), one might expect the delamination toughness to approach a lower limit value which would be equal to the neat resin toughness.

The preceding discussion assumes that the cracking propagates principally through the resin rather than at the resin/fiber interface. If the interfacial toughness is less than the resin toughness, then considerable cracking may occur at the interface giving debonding and involving more fibers in the delamination fracture process. Depending on how much less energy is dissipated by cracking at the interface than in the resin and how much more energy is dissipated in fiber debond and breakage, the delamination fracture energy may either increase or decrease with increased fiber debonding.

In summary the delamination fracture energy of a graphite

fiber/brittle epoxy should be greater than the neat material with the increase being greatest for a very thin resin rich region between plies.

Addition of Brittle Fibers to Ductile Resin: Crack extension in a ductile resin will generally be preceded by a significant process zone where extensive deformation and/or microcracking occurs. The energy dissipation in this process zone prior to fracture is normally much larger than the energy associated with creation of new surface and constitutes the bulk of the energy absorbed per unit area of crack extension.

The addition of graphite fibers to such a system may significantly reduce the extent of the process zone and will reduce the volume of material available to deform/microcrack and absorb energy in the process zone (since the fibers act like rigid filler). While crack tip interaction with the fibers might give an incremental increase in the energy absorbed in crack extension, the loss of material absorbing energy in the process zone gives a much greater decrease in fracture energy, resulting in a net decrease in the delamination fracture toughness.

A second reason for loss in toughness in a resin with the introduction of brittle fibers is the additional constraint imposed on the resin. If energy dissipation in a given resin is by shear deformation, the reduced shear stresses that result from fiber constraint could be particularly deleterious to the resin toughness so essential to delamination toughness in such a system. The loss in toughness due to loss in height of a suitably defined crack-tip process zone and local strain to fracture could be quantified in a micromechanical model using an equation of the form

$$G_{IC} \approx \int_0^h \int_0^{c_f} \sigma d\epsilon dy \quad (1)$$

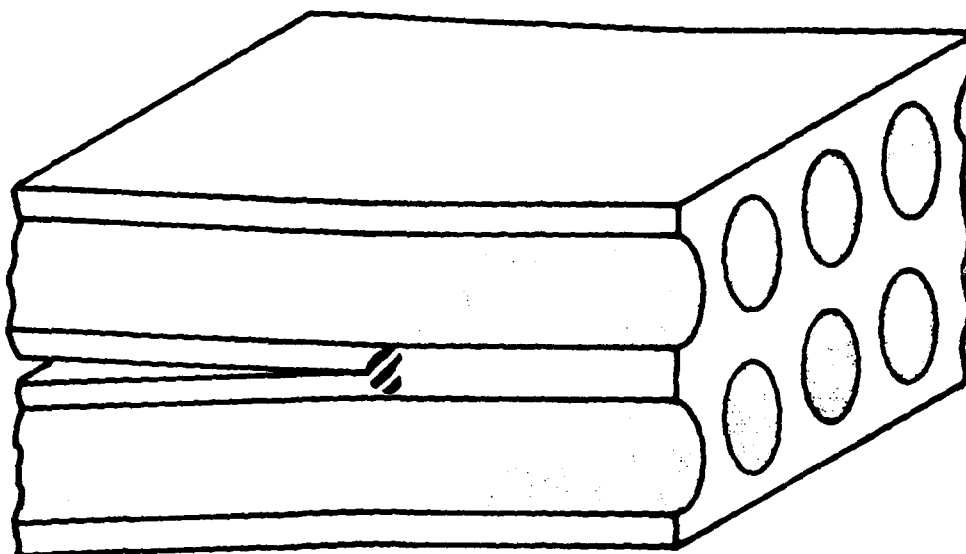


where  $\epsilon_f = f(x,y,z)$  and represents the local strain at various points in the process zone during crack extension and  $h$  represents the height of this zone of inelastic deformation above and below the crack tip which acts as an energy dissipating sink. (See [1, p. 29-33] for details.)

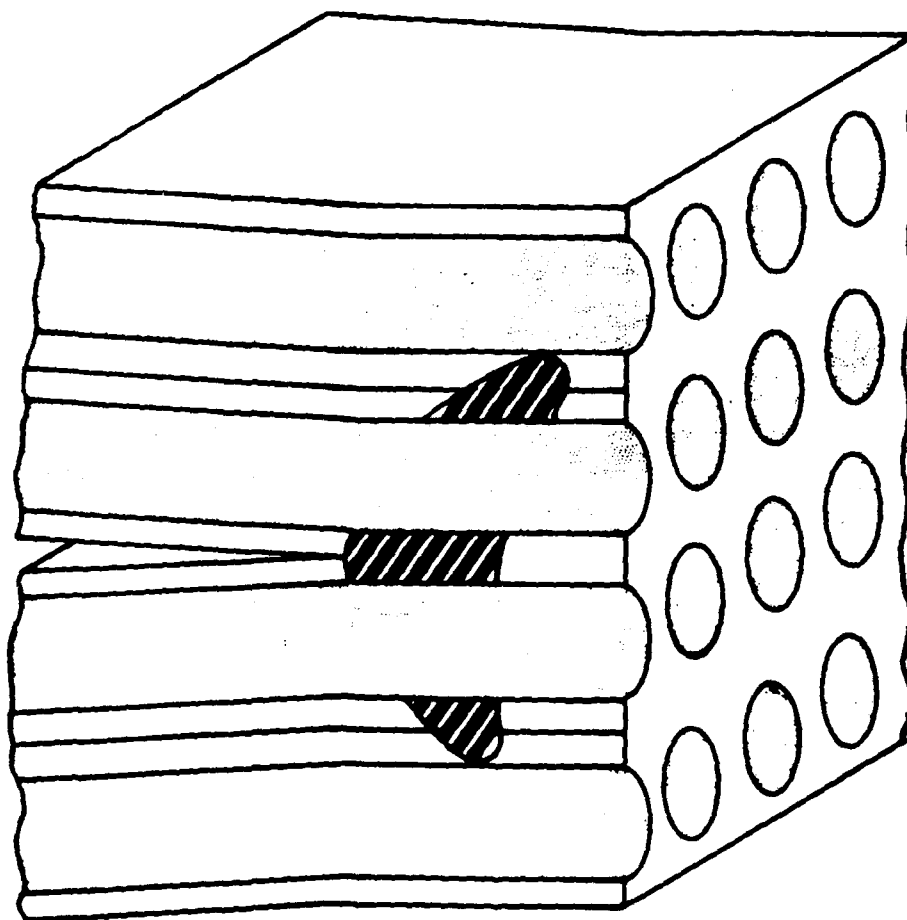
In summary, we are predicting that the delamination toughness of a graphite fiber/ductile resin composite will generally be less than the neat material toughness. This prediction is in sharp contrast to the results predicted for a brittle resin composite material. For brittle resins, the process zone is so small that the addition of fibers has no effect on it. This difference is illustrated in Figure 1.

For a graphite/fiber ductile epoxy composite, a thicker resin rich region should increase the delamination toughness by increasing the process zone size. In the limit as the resin rich region between plies is made sufficiently thick to contain the entire process zone (if it were possible to make such a composite), the delamination fracture toughness should approach that of the neat material. The lower limit of delamination fracture toughness should be observed as the resin rich region between plies approaches zero thickness. In this case not only is the process zone reduced in size but also the effect of constraint of the fibers on resin ductility is maximized.

In summary, a ductile resin reinforced with brittle fibers will have a delamination fracture toughness that is less than the neat material toughness, with the minimum toughness observed for the minimum thickness of the resin rich region between plies. It should be emphasized that this prediction is just opposite to that predicted for a brittle resin/brittle fiber composite.



**A. Brittle Resin**



**B. Ductile Resin**

Figure 1. Schematic of crack damage zone size in a delaminating composite with a brittle matrix and in a delaminating composite with a ductile matrix.

### 2.3 Qualitative Model for Mixed Mode Delamination

The superposition of mode II loading on mode I loading should have some predictable influence on the delamination fracture behavior. If the resin is brittle, the fracture on a microscopic scale may still occur on the principal normal stress plane with the principal effect of the mode II loading being to change the orientation of this plane from parallel to the plies to some acute angle. This would give a much more frequent interaction of the crack tip with the fiber which, as previously noted for a brittle fiber/brittle resin system, should increase the resistance to delamination.

In a ductile resin/brittle fiber composite, by contrast, the effects of the mode II loading on process zone size will dominate. The effect of the mode II loading should be to increase the size of the process zone if deformation occurs principally by shear. Thus, one might expect increasing the mode II loading component would increase the delamination fracture energy.

### 2.4 Experimental Work to Study Qualitative Delamination Fracture Models

The experimental program was designed to test the qualitative predictions of the models in two ways. First, macromechanics tests were run to measure the delamination fracture toughness. Variables studied included thickness of resin rich region, resin ductility, interfacial strength and state of stress (pure mode I versus mixed mode I/mode II). Second, real time observations of delamination fracture were made in the scanning electron microscope (SEM) for the same composite systems studied macroscopically. Post mortem fractographic observations were also made in the SEM on the delaminated specimens. This portion of the study allowed the micromechanisms of the fracture process to be correlated with

macromechanics measurements of delamination fracture toughness.

## 2.5 Experimental Results and Discussion

### Macroscopic Measurements of Delamination and Transverse Fracture

Toughness: The fracture toughness measurements made using split laminates and compact tension specimens are summarized in Table I.

(a) Ductile Resins - For the two systems with ductile resin (F155 and F185), the predicted decrease in fracture toughness (for crack propagation parallel to the fibers) for decreasing thickness of resin rich region is observed. Note the neat material represents the limiting case of a material with an "infinitely" thick resin rich region whereas the transverse cracking corresponds to the opposite limit of an essential zero thickness resin rich region. Delamination represents an intermediate case between these extremes.

If one assumes (1) that the process zone for the neat material is the same size as that in the composite and (2) that the toughness comes principally through energy dissipation in the resin, then one might expect the decrease in toughness comparing neat material to delamination or transverse cracking to correlate with the volume fraction of fibers; i.e.,

$$G_{IC} \text{ (delamination or transverse cracking)} = G_{IC} \text{ (neat material)} \times (1 - V_f) \quad (2)$$

where  $V_{f1}$  represents the average volume fraction of fiber over the volume of the process zone. For these systems the average volume fraction of fiber over the whole composite is between 55 and 60%, which should also be the  $V_f$  used for transverse cracking. For delamination cracking, the process zone averages the resin rich region between plies with the higher volume fraction of fibers within a given ply. The larger the process zone, the

Table I. Summary of mode I energy release rates for four materials and two types of tests.

Material	Type of Fracture	Avg. $\dot{a}$ (m/S)	$G_C$ J/m <sup>2</sup>
Neat 3502 Resin		$5.0 \times 10^{-5}$	69[10]
AS1/3502	Delamination	$6.1 \times 10^{-5}$	155[4]
AS1/3502	Transverse	$5.7 \times 10^{-5}$	225[10]
AS4/3502	Delamination	$2.8 \times 10^{-5}$	225
AS4/3502	Transverse	$1.7 \times 10^{-5}$	120
Neat F155 Resin		*	730[11]
T6C190/F155	Delamination	$3.5 \times 10^{-5}$	600
T6C190/F155	Transverse	$3.8 \times 10^{-5}$	410
Neat F185 Resin		*	6000[12]
T6T145/F185	Delamination	$3.0 \times 10^{-5}$	2700
T6T145/F185	Transverse	$3.8 \times 10^{-5}$	1525

\*Test performed by others; crack growth rate not indicated.

higher would be the average  $V_f$  value since a larger fraction of the total process zone would be ply rather than resin rich region between plies. A reasonable estimate for  $V_f$  might be 40% for delamination in the F185 and 30% for the F155, which has a smaller process zone. These estimates are based on the in-situ fracture results to be presented later.

The use in equation 2 of these values of  $V_f$  for transverse and delamination cracking of T6T145/F185 overestimates the observed  $G_{IC}$  results. This implies that the presence of the fibers further degrades the resin toughness in some other way(s). These might include the effect of fiber constraint in resin strain to fracture, fiber debonding prior to extraction of all of the intrinsic toughness from the resin, or reduction of the process zone size with the addition of fibers.

A similar analysis for T6C190/F155, again using equation 2 and the estimated values for  $V_f$ , underestimates the transverse and delamination toughness values as compared to those observed in the fracture mechanics testing. This implies that the additional increments of toughness must be due to fiber debond, tie zone formation and fiber breakage in addition to resin deformation. Note the net effect of fiber constraint on resin strain to fracture and fiber debonding leading ideally to tie zone formation and fiber fracture varies from system to system giving an increase in the F155  $G_{IC}$  but a decrease in the F185  $G_{IC}$ .

In summary, the trend in toughness from neat material to delamination to transverse cracking predicted by Equation 2 for ductile resins (based on effect of volume fraction of fibers on resin deforming in process zone) is well supported by the results of the two ductile resins, F155 and F185. The lack of exact numerical agreement implies that other factors not accounted for by this equation are also important, as previously discussed.

(b) Brittle Resins - For the two systems with brittle resins studied, the predicted increase in  $G_{IC}$  with fiber additions (for crack propagation parallel to the fibers) was observed. If one assumes (1) that the fracture energy is proportional to surface area on the fracture surface and (2) that the cracking occurs through the resin rather than at the interface, then the ratio of the  $G_{IC}$  for composite material compared to neat material would have a maximum value of  $\pi/2$  for a fully "corrugated" fracture surface compared to a flat one. The 3502 neat resin does give a glassy smooth fracture surface [3]; and the delamination of the composite gives a very corrugated fracture surface, as will be shown later in this paper.

The increases in  $G_{IC}$  with fiber additions reported in Table I for the 3502 resin system are much greater than the  $\pi/2$  prediction, which implies in general that crack tip interaction with the fibers, fiber debond and fiber breakage make a significant contribution to the total energy dissipation in the fracture process in a composite with a brittle resin. For AS1/3502 the predicted increase in  $G_{IC}$  with decreasing thickness of the resin rich zone (neat to delamination to transverse cracking) is observed. For AS4/3502 the transverse cracking actually gave a lower  $G_{IC}$ , possibly due to a significant amount of cracking at the fiber matrix interface rather than through the matrix itself. The AS4 fibers debonded much more readily than did the AS1 fibers, which almost never debonded in our study. The AS4 fibers are smoother fibers which give a higher strain to fracture and strength. However, the interfacial bonding in the graphite fiber/3502 system must have a significant mechanical contribution in the rougher fiber AS1/3502 which is substantially lost in the smooth fiber AS4/3502 system.

(c) Mixed-Mode Delamination - The mixed mode delamination results are summarized in Figure 2. The expected increase in  $G_{Total} = G_I + G_{II}$  with increasing mode II shear is observed in the two systems with a brittle

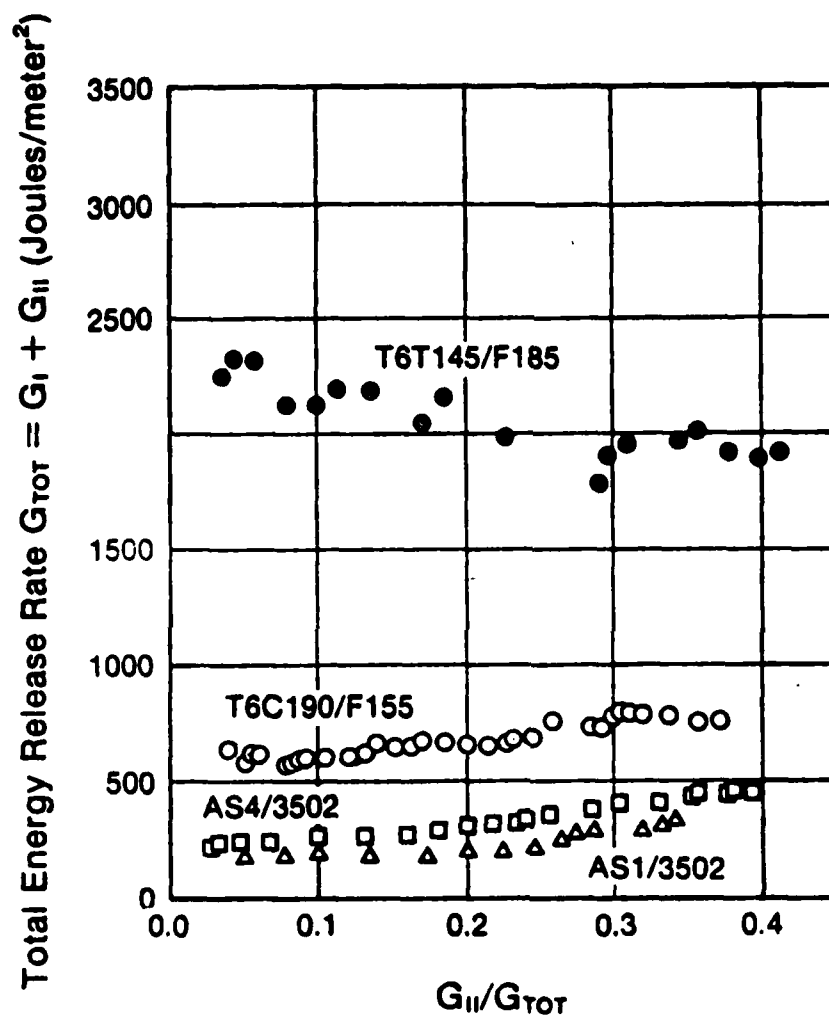


Figure 2. Total critical energy release rate for mixed mode delamination for four composite material systems.



resin; namely, AS1 and AS4/3502. A slight increase in the T6C/F155  $G_{Total}$  with increasing mode II is noted whereas the  $G_{Total}$  for the T6T/F185 decreases. The reason for this last observation is not known and in fact seems to be at odds with results by O'Brien, Johnston, Morris and Simonds obtained with a different test coupon and analysis [2]. It is possibly significant that they were using a multidirectional lay up where we were using unidirectional.

Microscopic Observation of Fracture Process: (a) T6T145/F185 - In-situ fracture of T6T145/F185 is shown in Figure 3 with post-mortem fractography shown in Figures 4 and 5. Figure 3 shows the crack tip region during delamination for a thin and thick resin rich region between plies. It has previously been suggested that the process zone (or damage zone) for this composite should be much larger than the resin rich region between plies. This is clearly seen to be the case. Typically microcracking can be seen over a region of  $\pm 3-5$  fiber diameters from the plane of the primary crack.

The extensive microcracking around the crack tip will result in the scalloped fracture surface often seen in delamination fracture if the resin rich region is not too thick. Where it is thicker and the resin is ductile the primary fracture will show more gross deformation and the fracture surface may resemble to some extent the dimpled fracture surface seen in ductile fracture of metals. Figure 4 shows this duplex appearance of the fracture surface due to variation in thickness of the resin rich region. At higher magnification, some scalloping that results from coalescence of microcracks is seen.

Fiber breakage (or bundle breakage) is generally initiated by fiber debond which allows the fiber (or bundle) to span the crack opening. As the crack opening increases, the fiber is eventually bent until it breaks,

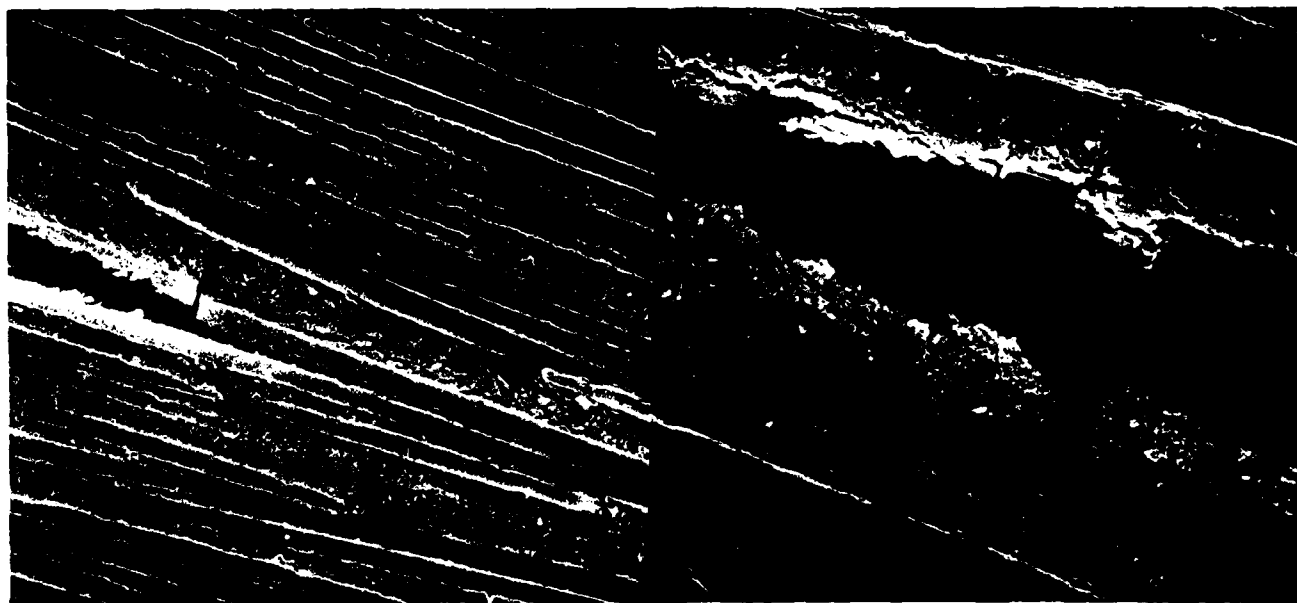


Figure 3. In-situ delamination fracture of T6T145/F185 composite at 500X (left) and 1000X (right). Note the extent of the damage zone as indicated by the secondary cracking.



Figure 4. Post-mortem fractography of delaminated T6T115/F185 composite material. Note great variety of artifacts on fracture surface due to variation in thickness of resin rich region. (Upper-left and right, 700X; lower-left, 1000X; lower-right, 2000X).

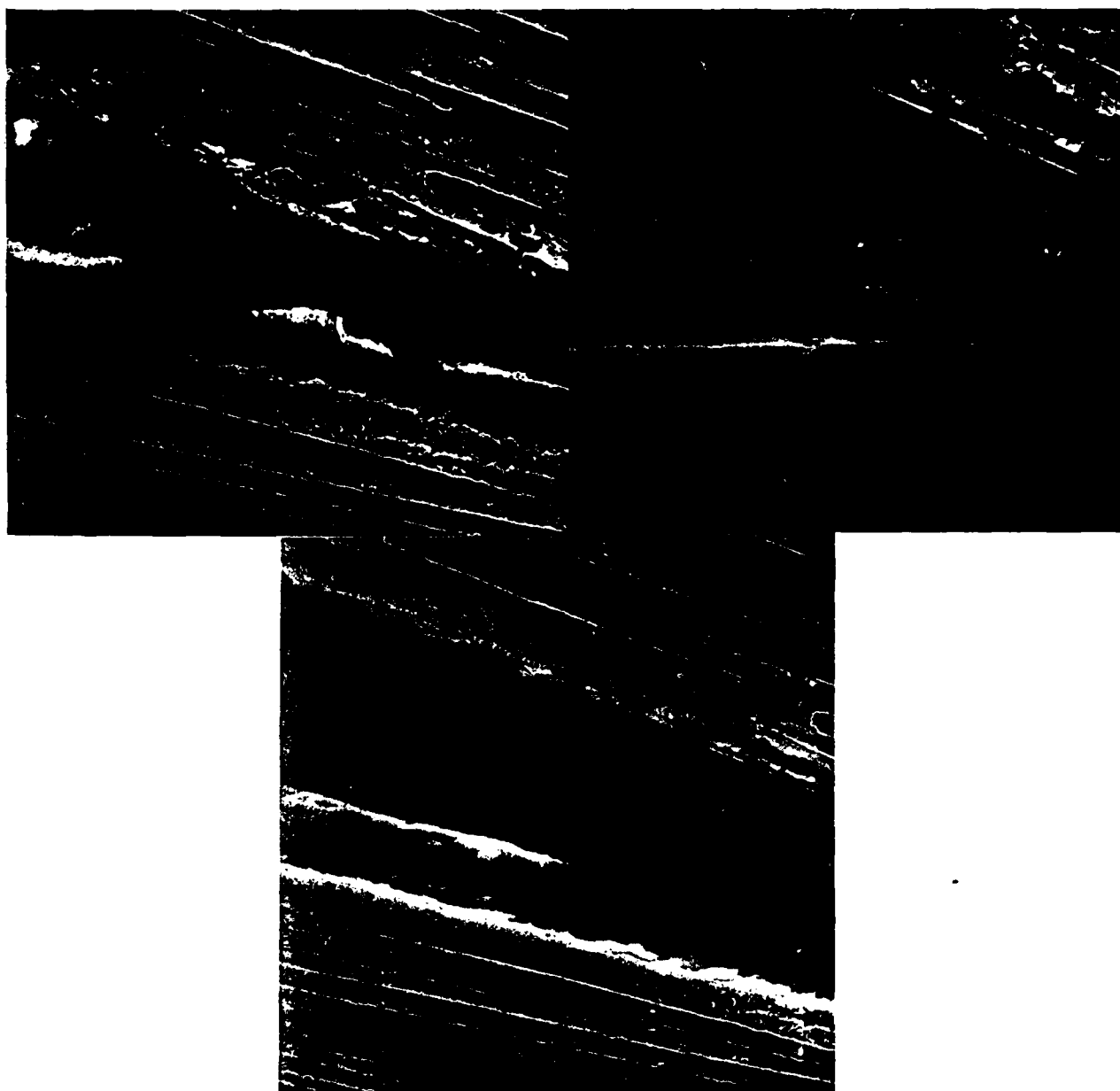


Figure 5. In-situ delamination showing bundle breakage in T6T145/F185 composite. Fiber or bundle breakage almost always begins with debond and follows the pattern shown in these pictures. (Upper-left, 500X; right, 1300X; center-500X).

as seen in Figure 5. Where the resin is fairly ductile and compliant, the bending of the fiber (or bundle) to the point of breaking is more difficult, allowing a significant tie zone to form behind the crack tip. Such a tie zone has the effect of increasing the energy dissipated in fracture, and thus, the delamination  $G_{IC}$ .

(b) T6C190/F155 - In-situ fracture of the T6C190/F155 is seen in Figure 6. Note fracture in this region is occurring in a relatively thick resin rich zone between plies. It should also be noted that the damage zone is more localized than it was in the F185, giving a much lower delamination  $G_{IC}$ .

The toughening of the F155 and F185 is accomplished through the introduction of rubber particles with a bimodal size distribution. The fracture behavior in Figure 6 suggests that the rubber particle spatial distribution is heterogeneous, leaving the matrix hard and brittle in some regions and soft and ductile in others. Some fiber debond is also noted.

The heterogeneity in the fracture behavior that results from a nonuniform distribution of rubber particles, variation in thickness of resin rich region and variation in fracture mechanism (fiber debond versus resin rupture) is clearly seen in Figure 7 which shows post-mortem fractography.

(c) AS4/3502 - In-situ fracture in the brittle AS4/3502 is seen in Figure 8. The volume fraction of fibers in this system is seen to be much greater than in the two ductile systems with no significant resin rich region. This is due to the fact that the 3502 resin during processing has a very low viscosity, allowing almost all excess resin to bleed off. The process zone, or damage zone is seen to be very localized to the crack tip with no indication of microcracking elsewhere.

Post-mortem fractography seen in Figure 9 shows the expected

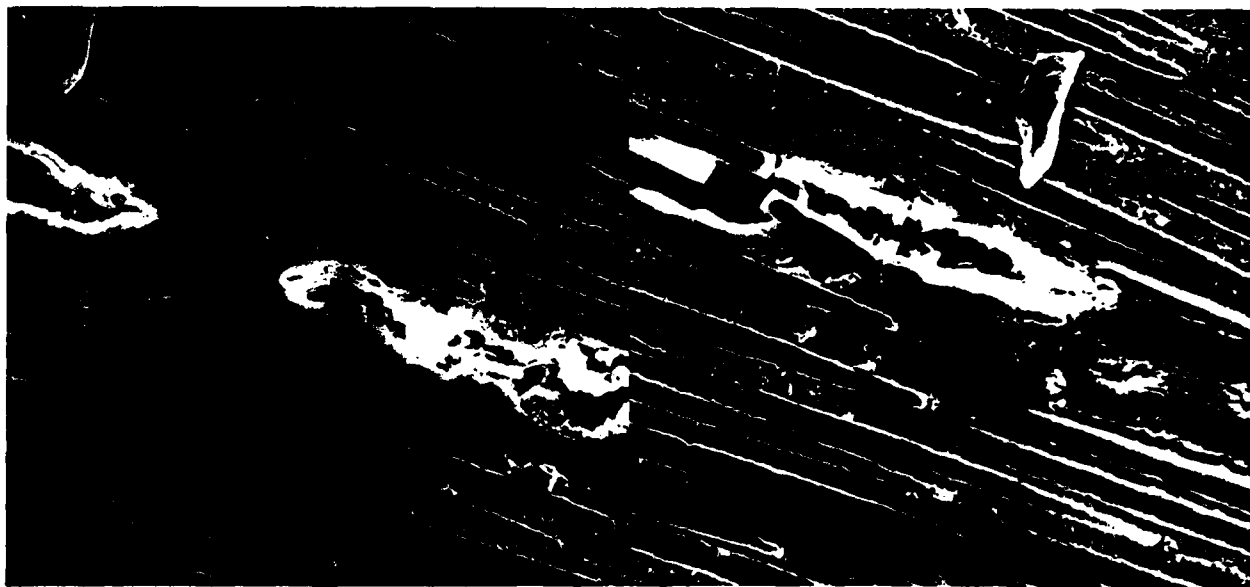


Figure 6. In-situ delamination fracture in T6C190/F155. Heterogeneity of resin is apparent with hard brittle region just ahead of crack tip and soft, more ductile region further ahead of crack tip (left). (Left, 600X; right, 650X).



Figure 7. Post-mortem fractography of a delaminated T6C190/F155 composite. Note the variety of artifacts due to variations in thickness of resin rich region and variations in fracture mechanism: namely, debond versus resin fracture. Dimples are thought to be due to rubber particles rather than voids introduced during manufacturing. Scallop is a result coalescence of microcracks.

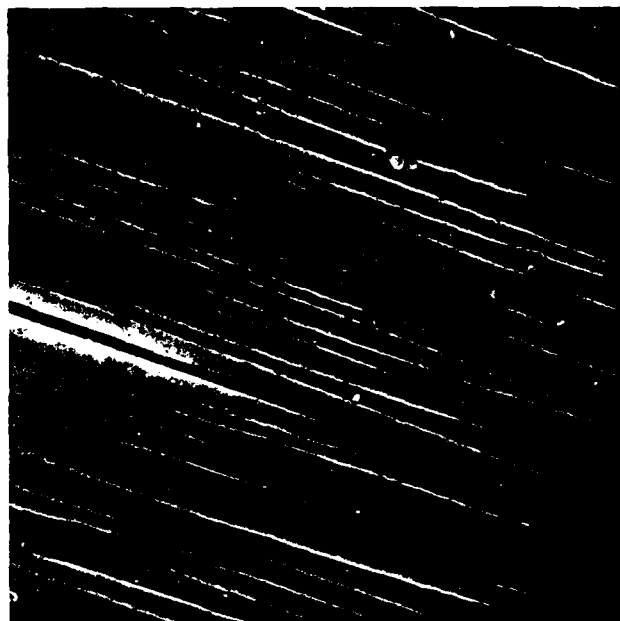


Figure 8. In-situ delamination fracture in AS4/3501. Because of brittle character of resin, crack opening displacement is very small and exact location of crack tip is uncertain. No damage zone around crack tip is indicated. 500X.



corrugated fracture surface with some scalloping for matrix fracture between fibers. While it is not clear whether the fracture surface seen in Figure 9 is through the matrix or along the fiber/matrix interface, Figure 10 suggests debonding and fracture along the interface dominates. It should be noted that previously published fractography on AS1/3502 indicates fracture through the matrix, with very little debonding [4], in contrast to the results presented here for AS4/3502.

## 2.6 Summary

The fracture process and resultant fracture toughness for delamination of graphite/epoxy composites is seen to be sensitive to the following factors: (1) resin toughness, (2) interfacial strength, and (3) thickness of resin rich region (or volume fraction of fibers). Ideally, the interfacial strength should be just strong enough to allow deformation of the resin to the point of fracture before debonding occurs. This would allow energy dissipation by both the matrix and the fibers. Too weak an interface will allow mainly fiber breakage without extraction of the resin's intrinsic toughness. Too strong an interface will allow energy dissipation from the matrix alone.

The optimal thickness of the resin rich region (thick versus thin) depends on whether the resin is ductile or brittle. For a ductile resin, a thicker resin rich region (or lower average volume fraction of fibers) will increase the resistance to delamination, though at the expense of stiffness and in-plane strength. Recently completed work at TAMU ("Effect of Resin Content on the Delamination Fracture Behavior of Graphite Epoxy Laminates" - see Appendix) [5] has indicated that the T6C190/F155 will have a 2x variation in delamination  $G_{IC}$  comparing a bled to an unbled panel. For a brittle resin the optimal thickness of the resin rich region between plies



Figure 9. Post-mortem fractography of delaminated AS4/3502 composite. Note the smooth corrugations due to debond at the matrix/fiber interface with coalesced microcracks giving scalloped regions between the fiber debonds. 2000X

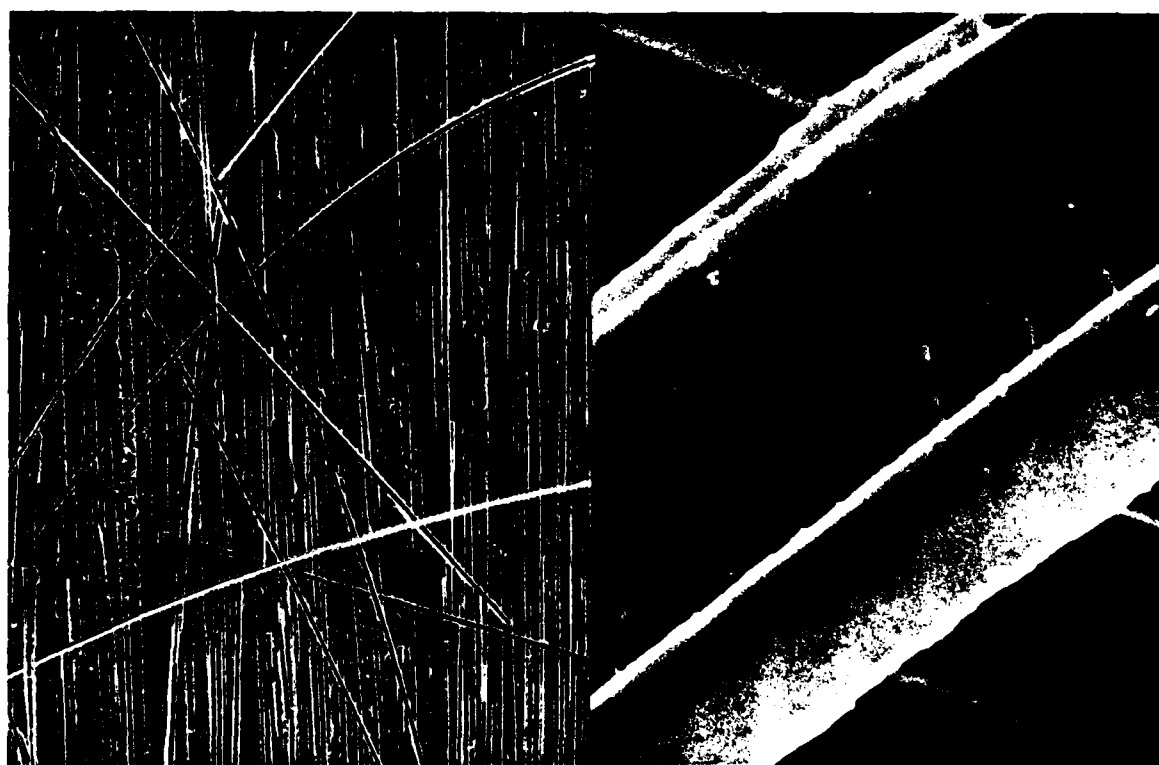


Figure 10. Post-mortem fractography of delaminated AS4/3502 composite emphasizing the weak interface in this system. Only in this system were loose fibers found strewn on the delaminated fracture surface. The enlargement shows the bare fiber resulting from debonding and the cracked resin between adjacent fibers. No such observations were ever made on the AS1/3502 composites, which apparently had much stronger interfacial bonding: (left, 100X; right, 4500X.)

would be zero, or as small as processing can produce.

Finally, the lower delamination fracture toughness as compared to neat material toughness for a ductile resin can be rationalized principally in terms of a decrease in the amount of resin being deformed in the process zone due to the presence of fibers, with fiber constraint and debond also important in modifying the toughness.

## 2.7 References

1. Schapery, R.A., "Correspondence Principles and a Generalized J Integral for Large Deformation and Fracture Analysis of Viscoelastic Media", Int. J. Fracture Mechanics. (In press.) Texas A&M University Report MM 4665-83-7, April 1983.
2. O'Brien, T.K., Johnston, N.J., Morris, D.H. and Simonds, R.A., "Determination of Interlaminar Fracture Toughness and Fracture Mode Dependence of Composites Using Edge Delamination Test", Proceedings of Conference on Testing, Evaluation and Quality Control of Composites, TEQC 83, Sept. 1983, U. of Surrey, Guildford, United Kingdom (Butterworth Scientific Ltd.) pp. 223-232.
3. Williams, D.R., "Mode I Cracking in an Epoxy and a Graphite/Epoxy Composite", Master's Thesis, Texas A&M University, College Station, TX, December 1981. Texas A&M University Report MM 3724-81-16, December 1981.
4. Vanderkley, P.S., "Mode I - Mode II Delamination Fracture Toughness of a Unidirectional Graphite/Epoxy Composite", Master's Thesis, Texas A&M University, College Station, TX, December 1981. Texas A&M University Report MM 3724-81-15, December 1981.
5. Jordan, W.M. and Bradley, W.L., "Effect of Resin Content on the Delamination Fracture Behavior of Graphite Epoxy Laminates", to be presented at Annual SAMPE Meeting, Reno, April 1984. Texas A&M University Report MM 4665-84-1, January 1984.

### 3. MATRIX CONTROLLED DEFORMATION AND FRACTURE ANALYSIS OF FIBROUS COMPOSITES

#### 3.1 Introduction\*

Summarized in this section is theoretical and experimental work on matrix-dominated processes of deformation and fracture. The constitutive and fracture theory which forms the basis for some of our current activities is discussed in Section 3.2. Sections 3.3 and 3.4 give the principal results from two M.S. theses on the double-cantilevered beam specimen, which is used in many of the fracture investigations on this project. Current activities on modeling of crack growth, such as delamination, in materials with distributed micro-damage and the development of specific constitutive equations which account for this micro-damage are described in Sections 3.5 and 3.6, respectively. This constitutive theory has a form which is especially convenient for use in analysis of macro-crack growth. Other constitutive equations which are in some respects more general are discussed in Section 4.

#### 3.2 Deformation and Fracture Theory for Composites with Distributed Damage

Methods of quasi-static deformation and fracture analysis have been developed for nonlinear elastic, viscous, and viscoelastic materials; see Abstracts No. 5 and 6 in the Appendix. The correspondence principles which provide the basis for the viscoelastic analysis are not limited to crack growth; they apply to crack closing and healing as well as to other types of problems involving ablation and interfacial contact and separation. However, only crack growth examples are given. The crack-growth theory,

---

\*Sections 3.1-3.4 prepared by R.A. Schapery

which uses a generalized  $J$  integral and allows for distributed, microscale damage, is not much more involved than that of nonlinear elasticity or special cases of linear viscoelasticity. This simplicity, compared to what one might expect, is a direct result of the particular constitutive equations and mechanical variables selected to characterize rheological behavior. We believe the deformation and fracture theory provides a practical approach to the development of realistic damage and global fracture models for nonlinear elastic, viscous, and viscoelastic media. It is potentially applicable to the mathematical modeling of crack tip regions, such as the delamination tip in fibrous composites (cf. Section 2, Fig. 3).

### 3.3 Evaluation of Energy Release Rates in Unidirectional Split Laminate Specimens

An improved theory for the double-cantilevered beam (Fig. 1) which accounts for deformation around the crack tip is described in the M.S. thesis by J.R. Weatherby; see Section 8 for the Abstract. The primary findings are:

- (i) Deformation occurring ahead of the crack front in DCB specimens under symmetric loading, such as illustrated in Fig. 1, affects both the stiffness and the energy release rate. This effect becomes less important as the crack length increases.
- (ii) For symmetric loading a model consisting of a beam supported at the crack tip by a torsion spring can be used to predict stiffness and energy release rate accounting for deformation ahead of the crack front. When the crack is sufficiently long, the spring constant is independent of crack length.
- (iii) An approximate analytical prediction of the mode I spring constant agrees well with finite element solutions.
- (iv) For crack lengths of interest in split laminate specimens, shear deformation in the separated beams has a much smaller effect on energy release rate calculations than does the deformation ahead of the crack front.

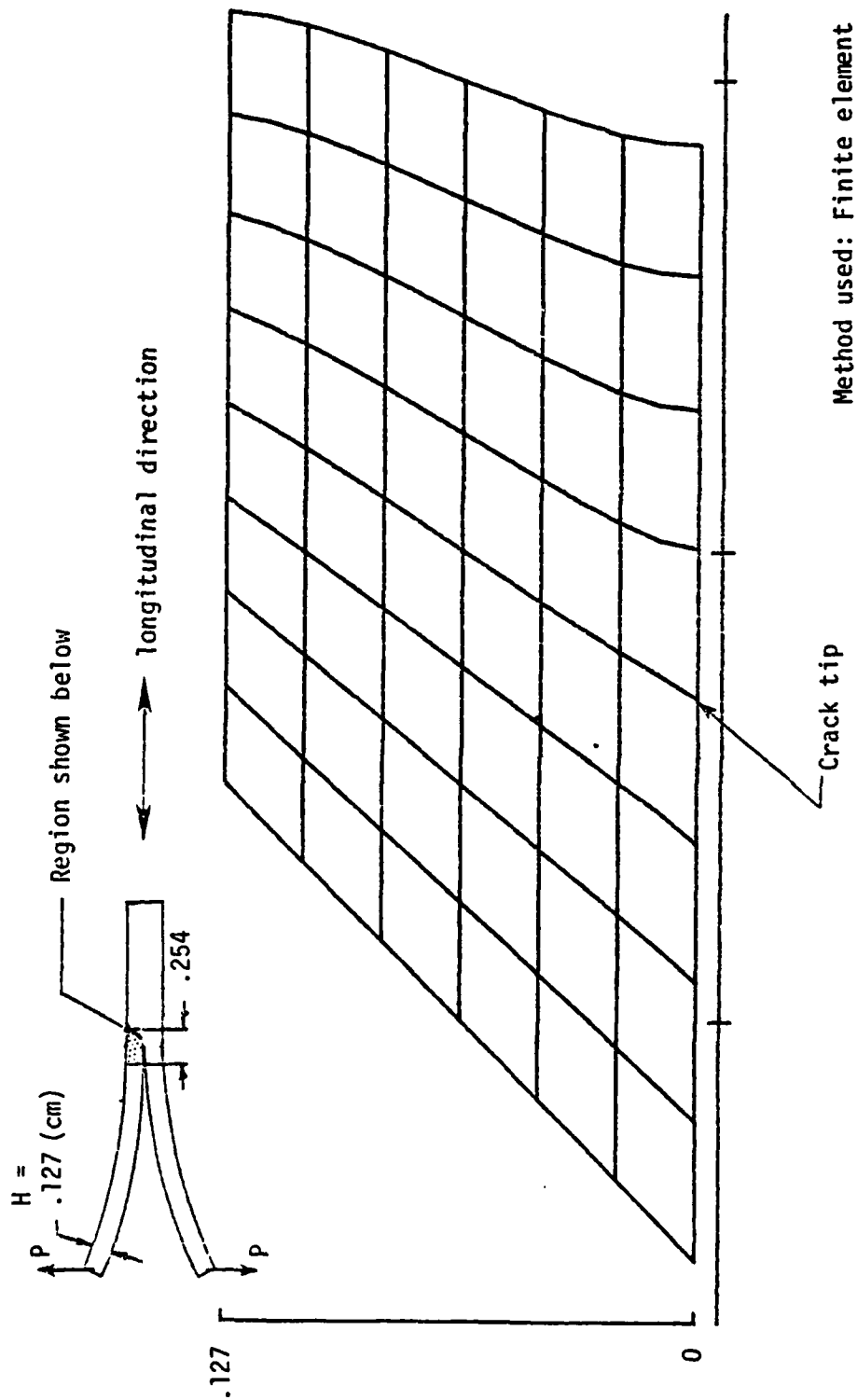


Figure 1. Horizontal displacements near the crack tip for mode I loading of a graphite/epoxy split-laminate specimen. ( $0^\circ$  Fiber Angle)

- (v) For split laminate specimens where the delamination length is much greater than the height of the specimen, energy release rates can be evaluated accurately by using an "effective" crack length in the unmodified beam theory energy release rate equations. The difference  $a_0$  between the actual length of the crack and the effective crack length is given by a simple approximate equation involving the orthotropic elastic constants. For isotropic materials with a Poisson's ratio of .3, this relation gives  $a_0 \approx .58H$  (where  $H$  = half-height of the uncracked beam) which is in close agreement with the experimental results of .6H obtained by Mostovoy et al. [1]. For AS/3501-6 graphite/epoxy unidirectional material,  $a_0 \approx 1.5H$  is predicted from the theory.
- (vi) Pure mode II loading distorts the cross section of the specimen much less than does mode I loading. As a result, in a limited study, it was found that the unmodified beam theory gives a better approximation of energy release rate for mode II loading than for mode I loading.

#### 3.4 Slow, Stable Delamination in Graphite/Epoxy Composites

Using symmetrically loaded unidirectional, split laminates under fixed-grip conditions, the relation between crack speed,  $\dot{a}$ , and energy release rate,  $G$ , was found for one tough composite (Hexcel F185) and one brittle composite (Hercules AS4/3502). This study is reported in the M.S. thesis by H. Razi; its Abstract is in Section 8. The principal conclusions are:

- (i) The energy release rate during slow growth is approximately 15% less than the initiation value  $G_c$  for the brittle system (3502) and 30% less than  $G_c$  for the tough system (F185).
- (ii) For the brittle system,  $G \approx 203\dot{a}^{.0045}$  (45% RH, RT) and  $G \approx 195\dot{a}^{.0046}$  (95% RH, RT) where  $G$  is  $J/m^2$  and  $\dot{a}$  is cm/s.
- (iii) For the tough system,  $G \approx 1665\dot{a}^{.022}$  (dry, RT).



### 3.5 Analysis of Crack Growth in Damaged Media Using a Generalized J-Integral\*

It has been shown that the J-integral is a useful fracture parameter for correlating data on initial crack extension in metals even when yielding occurs on a scale which is comparable to specimen dimensions [2]. The purpose of this research effort is to study and verify the applicability of a generalized J-integral theory [3] to both crack initiation and propagation in metals undergoing plastic deformation and fiber reinforced composite materials with damage. An idealized failure zone (which is a thin layer of damaged and failing material) is included in the crack tip model to eliminate singularities in stress and strain. A ligament of material in the failure zone is assumed to break when a certain amount of work has been done on it by the surrounding continuum [4] or, alternatively, when the displacement between the ends of the ligament reaches a specified value.

The approach being followed is to first study crack growth in isotropic materials which deform according to a  $J_2$  deformation theory of plasticity on the first loading, with linear elastic unloading. In this situation the necessary restriction for the J-integral to be path independent is that the maximum value of the octahedral shear strain in the unloading region enclosed by the path of integration be independent of the coordinate which runs parallel to the crack plane. The question of whether this condition is met will be studied numerically for both the small scale yielding problem and crack problems associated with large scale plasticity. In extending the study to initially orthotropic materials, the approach currently being considered is to characterize the matrix phase of

---

\*Prepared by J.R. Weatherby

the composite using the same type of deformation theory mentioned previously while the fiber phase is assumed to remain linearly elastic.

At this time, all of the necessary numerical tools have been developed for studying crack growth in the isotropic material. This has required both the incorporation of a plasticity model into a finite element code as well as the development of a new element to model the failure zone at the crack tip. It was found necessary to modify the usual deformation plasticity theory in order to get physically acceptable stress-strain relationships when reyielding occurs. Relyielding is of concern since some authors report the existence of a small zone of reyielding material behind the tip of an advancing crack. The modified plasticity model agrees exactly with deformation theory for the first loading of the material. In general, if the material is unloaded and subsequently reyielded, use of the usual deformation theory coupled with elastic unloading gives rise to discontinuous stresses or strains (depending on which is taken as the input) while our modified plasticity model does not. Several test cases with known solutions have been considered in order to verify that the computer code is working properly. Test cases with a single element under homogeneous states of stress and strain were used to verify the ability of the code to handle stress histories involving loading, unloading, and reyielding of the material. The problem of an elastic-perfectly plastic thick wall cylinder subjected to internal pressure was modeled; the resulting stress distribution was found to agree with that found in [5]. Also, a crack problem with small scale yielding near the crack tip was studied. Numerical results clearly show the transition from a square root stress singularity far away from the plastic zone to a HRR singularity [6,7] within the plastic zone.

The failure zone which is present in the crack tip model is

represented by a special element. This element is used to impose limits on the magnitudes of shear and normal stress in the crack plane ahead of the apparent crack tip. Each failure zone element is one dimensional and consists of six nodes with three nodes on both the upper and lower surfaces. A constitutive equation relating tractions on the surface of the element to relative displacements of initially coincident points on the upper and lower surfaces must be specified by the user. This traction-displacement relationship can be nonlinear and for such cases is represented by a piecewise linear curve. Typically, the traction acting at a point on the surface of a failure zone element vanishes after the crack opening displacement reaches a critical value. Thus, as the applied loads (or specified boundary displacements) are increased, the crack tip region advances continuously (not node by node) without any need for node splitting or modification of the boundary conditions in the crack tip region. The method of crack advance is consistent with the fundamental fracture criterion that a ligament in the failure zone ceases to carry load when the work input to the ligament exceeds a critical value.

In order to verify that the failure zone elements had been properly implemented in the finite element code, two test cases with known solutions were considered. The first of these was the problem of an elastic beam loaded by a point load and supported by an elastic-perfectly plastic foundation. Here the failure zone elements were used to represent the foundation. Displacements obtained from the finite element model agreed very well with displacements from the beam theory solution. The second problem considered bears strong resemblance to a split laminate specimen where fibers at the crack tip bridge across the crack faces and form something very similar to the idealized failure zone. This problem was

modeled (using 2-D continuum elements) as a cantilevered beam connected to a beam on an elastic-perfectly plastic foundation. Again, the special failure zone elements were used to represent the foundation. In this case the traction in the failure zone was assumed to vanish when the opening displacement exceeded a critical value, which for our model is equivalent to a critical energy criterion. Figure 2 shows the resulting deflections as predicted by beam theory and as predicted by the finite element model for two different values of deflection at the tip of the cantilever. When the beam tip deflection was increased from .285 (in.) to .375 (in.) the traction free surface of the beam increased by a length of approximately five inches. This increase in traction free surface was a result of the specified traction-displacement relation in the failure zone elements (no boundary conditions were altered other than the beam tip deflection) and demonstrates the usefulness of the element in studying problems with advancing cracks.

### 3.6 Characterization of Damage Using a Pseudo Potential\*

This portion of the research effort is intended to first develop laboratory and analytical techniques which will enable one to determine if graphite/epoxy composite material can be characterized by a potential which is analogous to strain energy density, but with allowance for behavior which is different for loading and unloading. If such is possible, the form of these functions will be determined. Our preliminary investigations have focused on investigation of the literature which relates to this concept, development of a generalized methodology to evaluate the approach, and analysis of those specimen geometries which appear fruitful.

---

\*Prepared by R.D. Tonda and R.A. Schapery

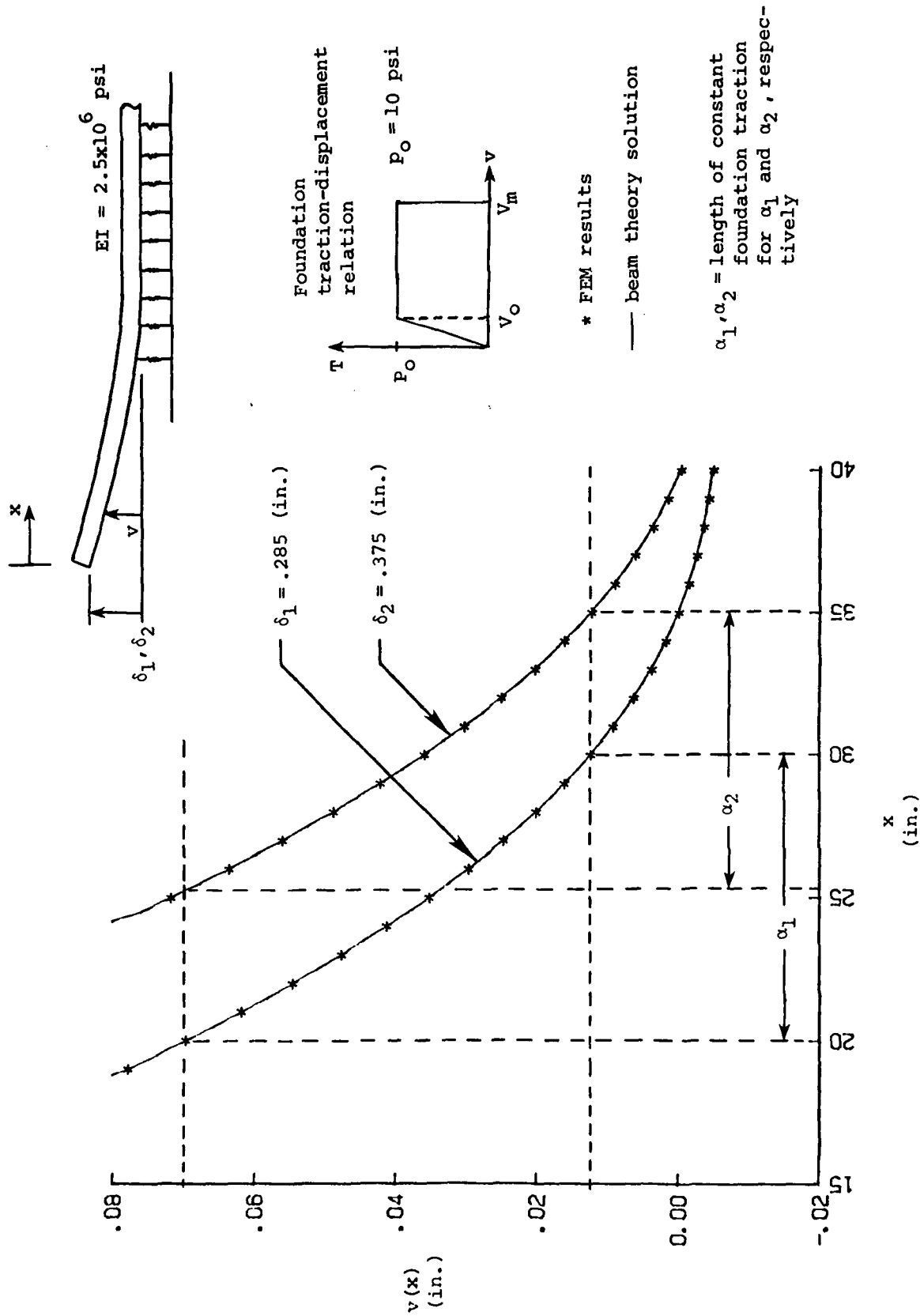


Figure 2. Deflections in a cantilever supported by an elastic plastic foundation in which the tractions vanish above a critical displacement.

The literature is replete with analytical treatments of nonlinear elastic materials where forms of strain energy potentials are evaluated using essentially the experimental techniques described in Green and Adkins [8]. Rivlin [9], Treloar [10], and Tshoegl [11] have used strain energy in predicting the response of elastomers and these techniques have correlated well with experimental data and modified network theories. The approach described by Tshoegl [12] is especially promising when investigating composites. He and Rivlin [9] demonstrate that "(from) a phenomenological ... point of view it is perfectly admissible to formulate an elastic potential as a non-integral exponent of the deformation tensor". The success of this application with nonlinear viscoelastic networks of elastomeric material indicate considerable promise for the application of a similar treatment to composites. For example, a potential of the form

$$\Phi = C_N J_b(N)$$

where  $C_N$  is a shear compliance which may be a function of time, position, etc.,  $J_b(N)$  is an invariant function of the stresses, and  $N$  is the dimensionless material parameter which appears as a non-integral exponent, might be a good candidate for evaluation. Our experience with the power law behavior of some composites reinforces this formulation.

Development of the methodology to evaluate this approach, whether or not power law behavior exists, is straight-forward. It is our intention to first test several uni-directional tensile specimens in various off-axis configurations. The data developed in these tests can then be examined to determine if the "cross-derivatives" are equal. This concept perhaps deserves some additional explanation. For a time-independent material, it is supposed that the three in-plane stresses  $\sigma_1$ ,  $\sigma_2$  and  $\tau_{12}$  can be

represented as functions of the corresponding strains  $\epsilon_1$ ,  $\epsilon_2$  and  $\gamma_{12}$  when referred to the material directions 1 and 2. The material direction 1 is chosen to correspond to the fiber direction while the 2-direction is orthogonal to and in the same plane as the sample and the 1-direction. Hence we can write that (upon loading);

$$\sigma_1 = \sigma_1(\epsilon_1, \epsilon_2, \gamma_{12}) ,$$

$$\sigma_2 = \sigma_2(\epsilon_1, \epsilon_2, \gamma_{12}) , \text{ and}$$

$$\tau_{12} = \tau_{12}(\epsilon_1, \epsilon_2, \gamma_{12}) .$$

Upon unloading, it is reasonable to assume that the functional dependence will also include the maximum values of the strains, or alternatively the maximum value of some function of the strains like the maximum octahedral shear strain in the matrix. In any event, if a potential  $\phi$  is to exist, where

$$\sigma_1 = \partial\phi/\partial\epsilon_1, \quad \sigma_2 = \partial\phi/\partial\epsilon_2, \quad \tau_{12} = \partial\phi/\partial\gamma_{12}$$

then it is necessary that (for example),

$$\left. \frac{\partial\sigma_2}{\partial\gamma_{12}} \right|_{\epsilon_1, \epsilon_2 = \text{CONST.}} = \left. \frac{\partial\tau_{12}}{\partial\epsilon_2} \right|_{\gamma_{12}, \epsilon_1 = \text{CONST.}} .$$

If the data are analyzed and it appears that the identity is satisfied, it will then be worthwhile to pursue more detailed analysis of the data, including numerical differentiation and nonlinear curve-fitting techniques to postulate and develop reasonable forms for the potential functions (i.e. one for loading and another for unloading).

In parallel with the above efforts, we are examining specimen configurations which hold promise of offering stress states which will be useful in analyzing composites. In particular, we have looked at uniaxial, rail-shear, and A-H-V (Arcan) tests [13, 14]. Each one indicates some promise for a particular stress state, but the A-H-V specimen, if it can be properly optimized, appears to offer the widest range of available stress states and conditions. The difficulties with the A-H-V specimen are in fabrication and bonding of thin samples. The effects of the bonding layer and the dramatic change in properties across the boundary are questionable, and although not yet determined, may influence the test results. The A-H-V specimen should not be discounted because of these potential weaknesses, however. The rail-shear method, for example, has the potential for all the same weaknesses, while the A-H-V specimen has uniform shear distributed over at least 90 percent of the significant section.

Our future plans include verification of the methodology, data acquisition and reduction techniques, and curve-fitting methods to be employed, by uniaxial testing of the unidirectional specimens mentioned earlier. We will also continue evaluation of similar techniques for the A-H-V and other specimens to be used later in the study after the above verifications are completed, assuming that the alternative geometries are deemed particularly useful or instructive.

Testing of the off-axis uniaxial tensile specimens has begun. Both Hercules AS4/3502 and Hexcel F-155 specimens are included in the test plan. The first phase of the testing involves ramp loading tests to failure to determine the ultimate strength of the specimen configuration. This series is followed by ramp-hold-unload sequences at 25%, 50% and 75% of the nominal ultimate strength. Each of the ramp-hold-unload specimens is then



again ramped to 75% of ultimate, this load held for a short time, and the ramp is then continued to failure, or reduced in level, or the sample is unloaded. Strain gage data taken by a 45-45-90 rosette in the 1-direction and at  $\pm 45^\circ$  is monitored throughout the testing. These measured strains are transformed into strains in the 1, 2 and axial directions and stored in separate data files for later manipulation, plotting and analysis. Figure 3 depicts a load vs. time plot for a specimen of AS4/3502 composite showing one history developed to characterize the material behavior and to investigate any time dependence which might be present. Figures 4 and 5 show, respectively, axial stress and shear stress on a plane oriented in the fiber-direction. Figure 5 also shows a "virgin" response curve and its relationship to the cyclic response. The cyclic response curve clearly shows the difference between loading and unloading behavior with an increased hysteresis level as the load is increased. The material also exhibits significant levels of nonlinearity and time-dependence which one cannot neglect in a study of damage.

Observe that there is considerable creep during the constant load periods (segments 8 and 10) and that the specimen strain gradually vanishes when the load is removed (segment 12). Microcrack growth during constant load segment 8 may be significant, but it is probably negligible for segments 10 and 12. A method for accounting for this viscoelastic behavior in damage modeling is developed in [3], and will be evaluated in subsequent work. Specifically, one uses "pseudo strains" (which are related to actual strains through a hereditary integral) in place of the actual strains in developing the potential  $\phi$ . In this case  $\phi$  is called a "pseudo potential" [3].

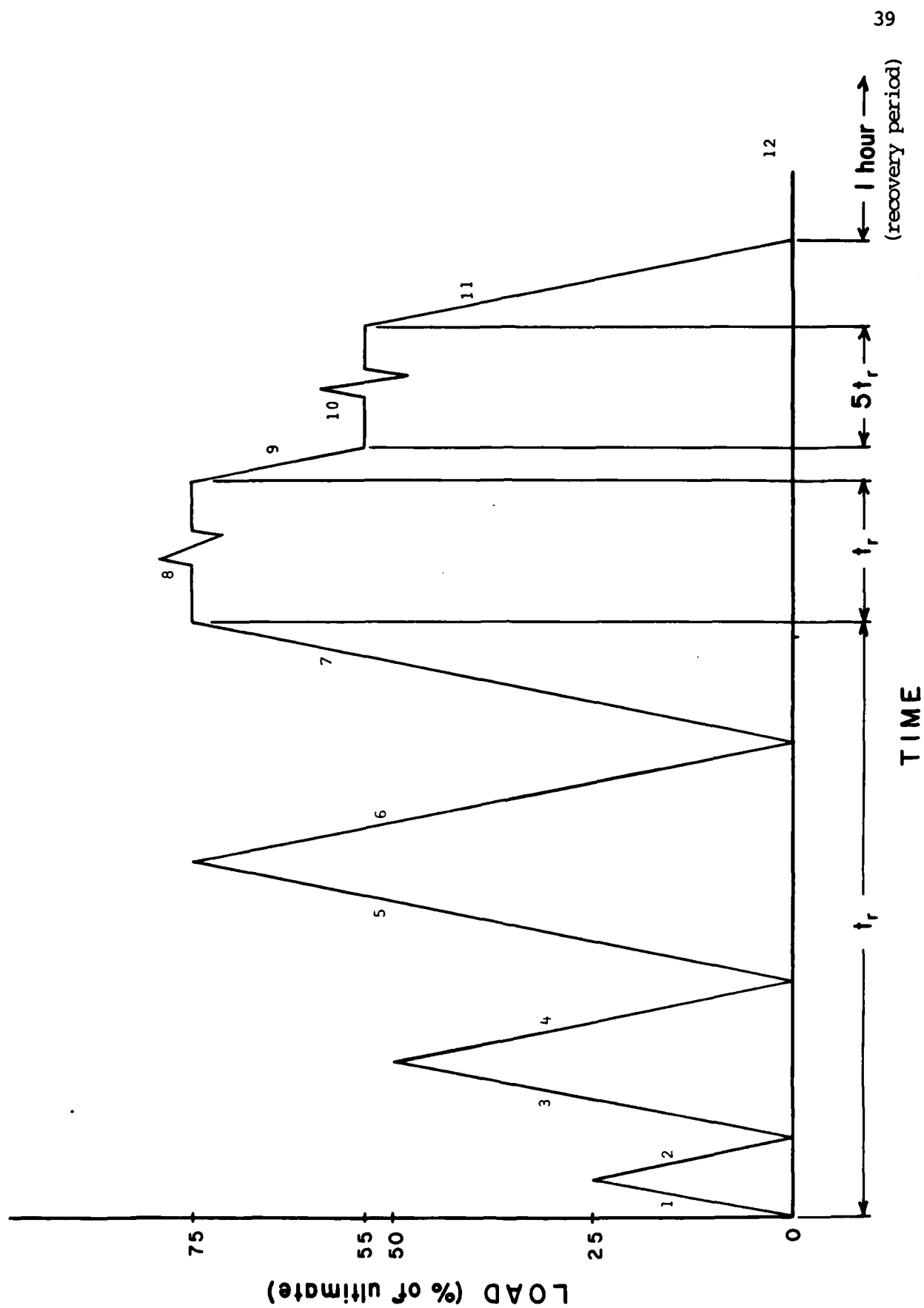


Figure 3. Load-time history used in 30° off-axis tests. ( $t_r = 210$  sec.)

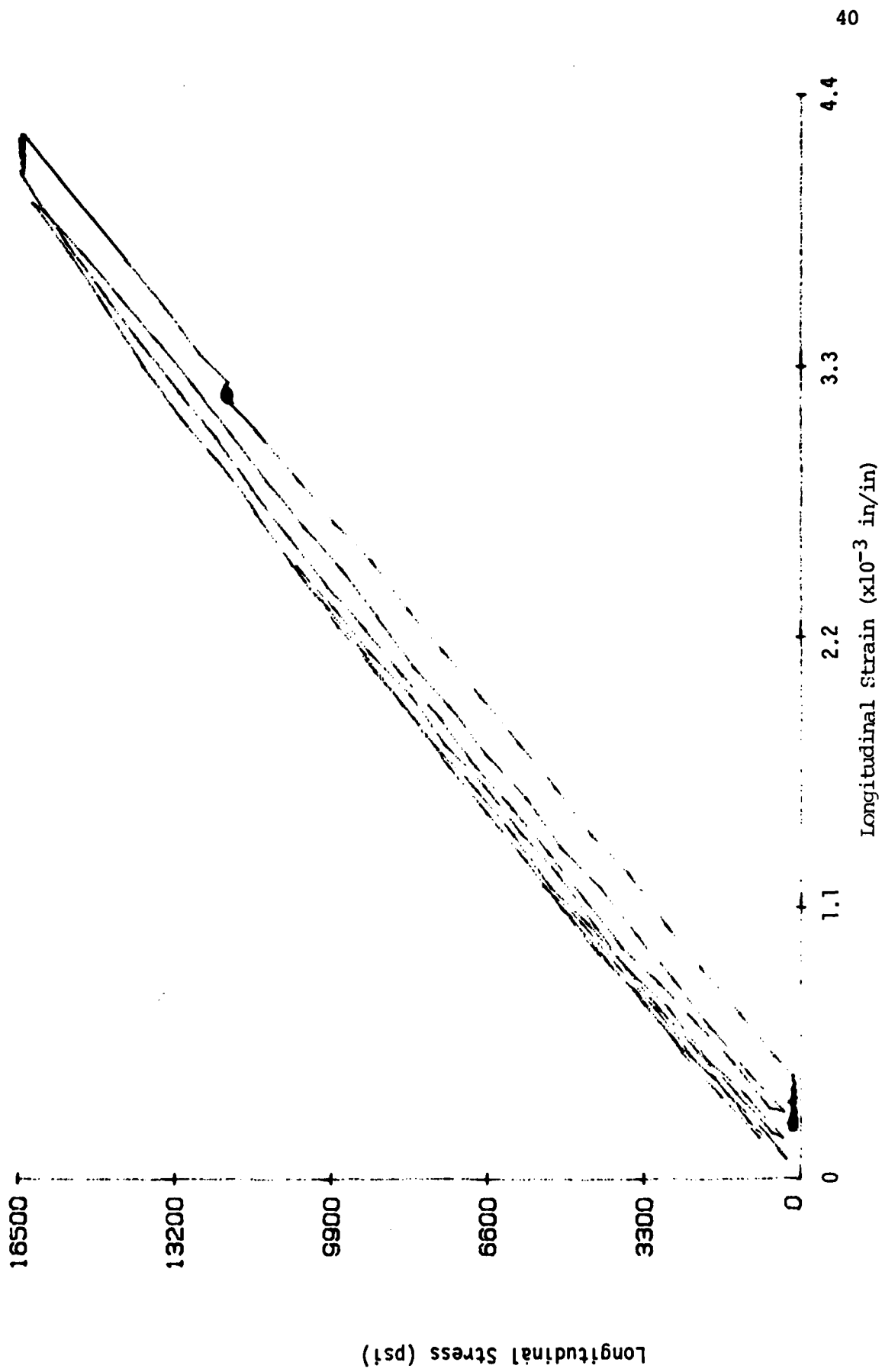
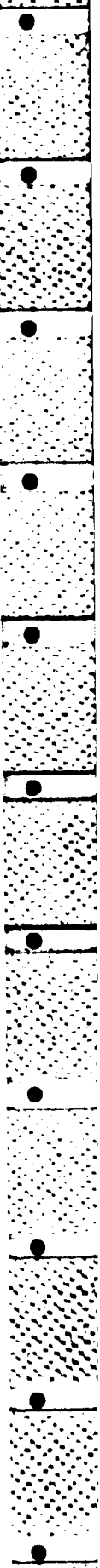


Figure 4. Axial stress vs. axial strain for loading in Fig. 3.



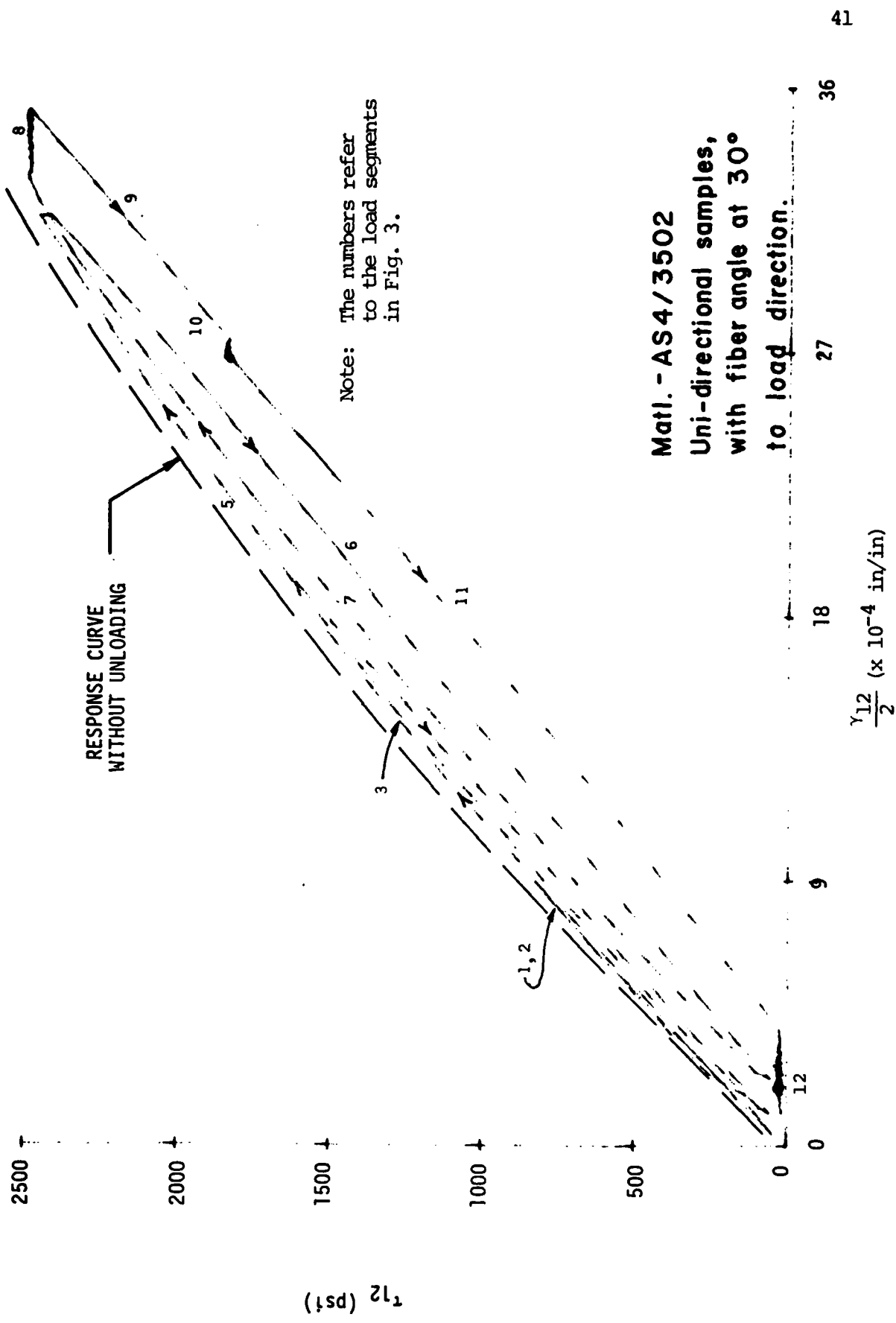


Figure 5. Shear stress (in fiber direction) vs. shear strain for loading in Fig. 3.

### 3.7 References

1. Mostovoy, S., P.B. Crosley and E.J. Ripling, "Use of Crack-Line-Loaded Specimens for measuring Plane Strain Fracture Toughness", Journal of Materials, Vol. 2, No. 3, September 1967, pp. 661-681.
2. Begley, J.A. and J.D. Landes, "The J Integral as a Fracture Criterion", ASTM STP 514, American Society for Testing and Materials, Philadelphia, 1972, pp. 1-20.
3. Schapery, R.A., "Correspondence Principles and a Generalized J-Integral for Large Deformation and Fracture Analysis of Viscoelastic Media", Texas A&M University Report No. MM 4665-83-7, April 1983.
4. Schapery, R.A., "A Theory of Crack Initiation and Growth in Viscoelastic Media, Part I", International Journal of Fracture, Vol II, 1975, pp. 141-159.
5. Hodge, P.G. and G.N. White, "A Quantitative Comparison of Flow and Deformation Theories of Plasticity", Journal of Applied Mechanics, June 1950, pp. 180-184.
6. Hutchinson, J.W., "Singular Behavior at the End of a Tensile Crack in a Hardening Material", J. Mech. Phys. Solids, Vol. 16, 1968, pp. 13-31.
7. Rice, J.R. and G.F. Rosengren, "Plane Strain Deformation Near a Crack Tip in a Power-Law Hardening Material", J. Mech. Phys. Solids, Vol. 16, 1968, pp. 1-12.
8. Green and Adkins, Large Elastic Deformations, 2nd Edition, Clarendon Press, Oxford, 1970.
9. Rivlin, R.S. and K.S. Sawyers, "Large Elastic Deformations", Transactions of the Society of Rheology, Vol. 20, 1976.
10. Treloar, L.R.G., The Physics of Rubber Elasticity, 2nd Edition, Clarendon Press, Oxford, 1958.
11. Tshoegl, N.W., "Constitutive Equations for Elastomers", Rubber Chem. Tech., Vol. 45, No. 1, March 1972.
12. Tshoegl, N.W., "Phenomenological Aspects of the Deformation of Elastomeric Networks", Polymer, Vol. 20, pp. 1365-1370, 1979.
13. Whitney, James M., Isaac M. Daniel and R. Byron Pipes, Experimental Mechanics of Fiber Reinforced Composite Materials, SESA Monograph No. 4, Society for Experimental Stress Analysis, Brookfield Center, CT, 1982.
14. Arcan, M., Z. Hashin and A. Voloshin, "Method to Produce Uniform Plane-Stress States With Applications to Fiber-reinforced Materials", Experimental Mechanics, 1978.

#### 4. A DAMAGE MODEL FOR CONTINUOUS FIBER COMPOSITES\*

##### 4.1 Introduction

It is now well known that ultimate failure of continuous fiber composites is preceded by a sequence of microstructural events such as microvoid growth, transverse cracking, fiber-matrix debonding, interlaminar cracking, edge delamination, and fiber fracture which are all loosely termed damage. The significance of a specific damage state lies in the fact that global material properties such as strength and stiffness may be substantially altered during the life of the component.

The model being developed proceeds from a continuum mechanics approach for predicting the thermomechanical constitution of continuous fiber composites subjected to both monotonic and cyclic fatigue loadings. In this method the damage is characterized by a set of vector valued internal state variables representing locally average measures of specific damage states such as transverse cracks, matrix microvoids, or any other damage state as previously mentioned. History dependent constitutive equations are posed utilizing constraints imposed from thermodynamics with internal state variables as well as current microphenomenological observations and fracture mechanics.

In surveying the literature on composite damage one finds a variety of available material. Past research has been primarily experimental and has concentrated on detailing the various types of damage and their possible causes. There has also been a considerable amount of work in analytically modeling a specific damage mode. Only recently has significant attention

---

\*Prepared by D.H. Allen and S.E. Groves

been given to actually predicting the resulting damage state from a specified load history. An extensive survey is contained in the report "A Survey on Damage in Continuous Fiber Composites" by S.E. Groves and D.H. Allen, which is in the Appendix.

#### 4.2 Development of the Damage Model

The Helmholtz free energy, which is used to obtain the stress and thus the constitutive equations, is modified to account for the local surface energy formed due to damage. All damage is assumed to be reflected through these constitutive equations as long as the damage in the constitutive specimens is statistically homogeneous. This implies that the total newly created surface area (which includes internal surfaces) may be of the same order of magnitude as the virginal external surface area. Large scale changes in the external surface such as edge delaminations, however, are not applicable since they lead to statistical inhomogeneity. Under the condition of statistical homogeneity all continuous based conservation laws are assumed to be valid on a global scale. Since the material is assumed to be elastic outside the damaged areas, the rate of surface energy created during the damage process can be related to the critical energy release rate via

$$\dot{u}_L^C = \frac{G_{CL}}{\rho_L V_L} \dot{S}_2 \quad (1)$$

where  $u_L^C$  is the surface energy,  $\rho_L$  and  $V_L$  are the local density and volume, respectively,  $S_2$  is the total surface area of cracks, and  $G_{CL}$  is the local volume averaged critical energy release rate required for crack propagation. Since equation (1) is history dependent and not observable due to the changing nature of  $G_{CL}$  and  $S_2$ , it is proposed that  $u_L^C$  be modeled

by a set of vector valued internal state variables, each describing a locally averaged specific damage mode such as transverse cracking and fiber fracture. In function form this energy for a unit of new surface is

$$u_L^C = u_L^C(\epsilon_{k\ell}, T, \alpha_i^j), \quad (2)$$

where  $\epsilon_{k\ell}$  is the second order infinitesimal strain tensor,  $T$  is the temperature, and  $\alpha_i^j$  are the components of internal state variables with  $j$  ranging from one to number of damage modes. For an undamaged material the local Helmholtz free energy is given by

$$h_L \equiv u_L - Ts = h_{E_L} = h_{E_L}(\epsilon_{ij}, T), \quad (3)$$

where  $u_L$  and  $s_L$  are the local internal energy and entropy per unit mass and  $h_{E_L}$  is the locally average Helmholtz free energy. In order to incorporate the damage terms the local Helmholtz free energy is modified as follows

$$h_L \equiv u_L - u_L^C - Ts = h_{E_L} - u_L^C. \quad (4)$$

To determine the stress-strain equations, the Helmholtz free energy function is expanded in a Taylor series expansion which is second order in  $\epsilon_{k\ell}$ , and  $\alpha_i^j$  as well as first order in  $T$  and then differentiated with respect to strain  $\epsilon_{k\ell}$ . The free energy function can be simplified by noting that the damage reflected in  $u_L^C$  is symmetric about a plane\*, that is  $u_L^C(\alpha) = u_L^C(-\alpha)$ . Therefore, all linear terms in damage can be neglected. This results in the following constitutive equations,

---

\*Talreja, Ramesh, "A Continuum Mechanics Characterization of Damage in Composite Materials," DCAMM Report No. 268, Proc. Royal Society London, 1984 (in press).



$$\begin{aligned}
\sigma_{Lij} = & \rho_L (B_{Lij} + C_{Lijkl} \epsilon_{Lkl} + E_{Lij} \Delta T_L - L_{ijkl}^{pq} \alpha_k^p \alpha_\ell^q \\
& - P_{mnijkl}^{pq} \alpha_m^p \alpha_n^q \epsilon_{Lkl} - Q_{ijkl}^{pq} \alpha_k^p \alpha_\ell^q \Delta T_L \\
& - T_{mnijkl} \alpha_m^p \alpha_n^q \epsilon_{Lkl} \Delta T_L) , \quad (5)
\end{aligned}$$

where the subscript L denotes the locally averaged quantities,  $\Delta T_L \equiv T_r - T$  where  $T_r$  is the locally averaged reference temperature, and the superscripts p and q denote specific damage modes. Equation (5) may be written in the following convenient form

$$\sigma_{Lij} = \sigma_{Lij}^R + C'_{Lijkl} (\epsilon_{Lkl} - \epsilon_{kl}^T) \quad (6)$$

where

$$\sigma_{Lij}^R \equiv \rho_L (B_{Lij} - L_{ijkl} \alpha_k^p \alpha_\ell^q) , \quad (7)$$

are the residual stress terms and

$$C'_{Lijkl} \equiv \rho_L (C_{Lijkl} - P_{mnijkl}^{pq} \alpha_m^p \alpha_n^q - T_{mnijkl} \alpha_m^p \alpha_n^q \Delta T_L) , \quad (8)$$

is called the effective modulus tensor, and

$$\epsilon_{kl}^T = C_{Lijkl}^{-1} \rho_L (E_{Lij} - Q_{mnij}^{pq} \alpha_m^p \alpha_n^q \Delta T_L) , \quad (9)$$

is called the thermal strain. Equations (6) are the completed description of the constitutive relationships.

For transversely isotropic media equations (5) through (9) may be simplified by utilizing material symmetry to the following form in material

coordinates

$$\sigma_{L\alpha} = \sigma_{L\alpha}^R + C_{L\alpha\beta}' (\epsilon_{L\beta} - \epsilon_{\beta}^T) , \quad (10)$$

where

$$\sigma_{L\alpha}^R \equiv \rho_L (B_{\alpha} - L_{kl\alpha\beta}^{pq} \alpha_k^p \alpha_l^q) , \quad (11)$$

$$C_{L\alpha\beta}' \equiv \rho_L (C_{\alpha\beta} - P_{mn\alpha\beta}^{pq} \alpha_m^p \alpha_n^q - T_{mn\alpha\beta}^{pq} \alpha_m^p \alpha_n^q \Delta T_L) , \quad (12)$$

and

$$\epsilon_{\beta}^T \equiv C_{\alpha\beta}^{-1} \rho_L (E_{\alpha} - Q_{mn\alpha}^{pq} \alpha_m^p \alpha_n^q \Delta T_L) , \quad (13)$$

where  $\alpha, \beta$  range from 1 to 6.

In order to completely characterize the constitutive equations shown in equations (10) through (13) one must be able to describe the damage terms  $\alpha_i^j$  as well as determine the material constants in each of the tensors shown. The damage growth laws are constructed in the following manner

$$\dot{\alpha}_i^j = \Omega_i^j (\epsilon_{Lkl}, T_L, \alpha_m^p) , \quad (14)$$

where the dot denotes time differentiation.

The precise nature of equations (14) can be determined only through an experimental testing program coupled with an understanding of the micromechanics of the medium. Indeed, these so called internal state variable growth laws are without doubt the most difficult link in the model development.

As an example, a first generation growth law is constructed assuming the damage to be only transverse cracks. The growth law is postulated to be given by

$$\begin{aligned}
 |\dot{\alpha}_1| &= K_1 \left[ \left( \frac{\epsilon_o - \epsilon_{o_{\min}}}{\epsilon_{o_{\max}} - \epsilon_{o_{\min}}} \right) \right]^{n_1} \frac{d\epsilon_o}{dt} \quad \text{if } \epsilon_o - \epsilon_{o_{\min}} > 0, \\
 &= 0 \quad \text{if } \epsilon_o - \epsilon_{o_{\min}} \leq 0 \quad \text{or} \quad \epsilon_o - \epsilon_{o_{\min}} \geq \epsilon_{o_{\max}} - \epsilon_{o_{\min}} \quad (15)
 \end{aligned}$$

where  $\epsilon_o$  is the octahedral shear strain,  $\epsilon_{o_{\min}}$  is the value of  $\epsilon_o$  at which the onset of transverse cracking is observed,  $\epsilon_{o_{\max}}$  is the value of  $\epsilon_o$  at which transverse cracking saturates, and  $K_1$  and  $n_1$  are material constants. Equation (15) will result in general saturation at the CDS, as shown in Fig. 1.

The above model has also been cast in a laminate analysis scheme suitable for comparison to experimental results. Efforts are currently underway to compare the predictive ability of the model to analytical results obtained by the finite element method for laminates with transverse cracks. Efforts in the near future will shift toward comparison of the model to experimental results. Although the first generation model is essentially complete at this time, public dissemination is being withheld until comparative results are obtained.

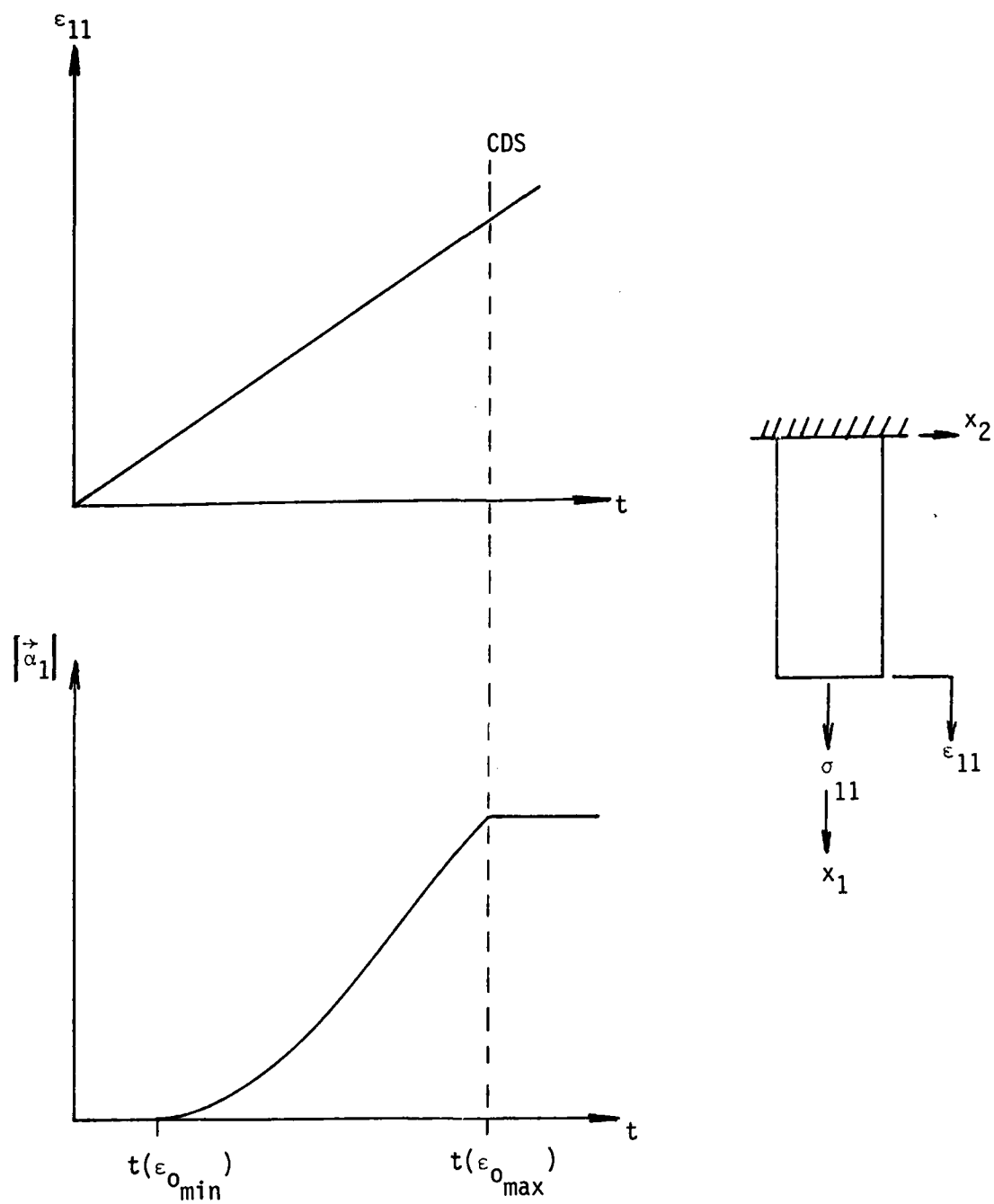


Fig. 1. Typical Growth Mechanisms in a Specimen With Transverse Cracks

## 5. RESIDUAL STRESSES AND ENVIRONMENTAL EFFECTS IN COMPOSITES\*

### 5.1 Introduction

The work reported in sections 5.2-5.6 constituted the Ph.D. thesis of B.D. Harper, titled "On the Effects of Post-Cure Cool-Down and Environmental Conditioning on Residual Stresses in Composite Laminates", (August 1983); the M.Sc. thesis of E.J. Porth, titled "Effect of an External Stress on Moisture Diffusion in Composite Laminates", (Dec. 1983); the M.Sc. thesis of D.L. Clark, titled "Moisture Absorption in Hybrid Composites", (Dec. 1983); and the M.Sc. thesis of S.P. Jackson, titled "Hygrothermal Effects in an Anti-Symmetric Cross-Ply Graphite/Epoxy Material", (completed Feb. 1984).

### 5.2 Time-Temperature Behavior of Hercules 3502 Resin

Like all polymeric materials, the 3502 resin creeps under load and the creep response is strongly affected by temperature. A detailed characterization of this time-dependent behavior is required for the following reasons: (a) it enables the determination of residual thermal stresses when the deformation of the resin is confined by the presence of stiff fibers, (b) it enables us to make predictions about long-time behavior from short-time data, and (c) it enables the computation of thermal stresses due to fluctuating temperatures.

An improved thermoviscoelastic characterization is obtained when creep is measured under sudden temperature-drop circumstances, in addition to isothermal conditions. A theoretical scheme that was developed earlier under this contract ("On the Thermoviscoelastic Characterization of

---

\*Prepared by Y. Weitsman

Adhesives and Composites", Proc. ICCM IV, pp. 771-779, 1982) was applied to the specific case of 3502 resin. It was found that under varying temperatures and stresses the creep of this material can be successfully related by

$$\epsilon - \alpha \Delta T = D_0 g_0(T) \sigma + g_1(T) D_1 \int_0^t [\xi(t) - \xi(\tau)]^n \frac{d[g_2(T) \sigma]}{d\tau} d\tau$$

where  $\epsilon$  is strain,  $\sigma$  stress,  $\alpha$  coefficient of thermal expansion,  $T$  temperature,  $t$  time,  $D_0$ ,  $D_1$ ,  $n$  are material constants and  $g_0(T)$ ,  $g_1(T)$ ,  $g_2(T)$  are (material) functions of temperature. Also, the "reduced time"  $\xi = t/a_T(T)$ , where  $a_T$  is the shift-factor. It was found that

$$\alpha = 30 \times 10^{-6} \text{ m/m/}^\circ\text{C}, \quad D_0 = 233 \times 10^{-6} \text{ (Mpa)}^{-1},$$

$$n = 0.31, \quad D_1 = 2.24 \times 10^{-6} \text{ (Mpa} \cdot \text{(Sec)}^n)^{-1}.$$

Furthermore

$$a_T = \exp\left[-\gamma_0 \left(\frac{T-T_R}{T_R}\right)^{\gamma_1}\right]$$

$$g_0 = \exp\left[-\beta_0 \left(\frac{T-T_R}{T_R}\right)^{\beta_1}\right]$$

$$g_1 = \exp\left[-g_0 \left(\frac{T-T_R}{T_R}\right)^{g_1}\right]$$

$$g_2 = \exp\left[r_0 \left(\frac{T-T_R}{T_R}\right)^{r_1}\right]$$

where  $T$  is in  $^\circ\text{K}$ ,  $T_R = 303^\circ\text{K}$  and  $\gamma_0 = 12.9$ ,  $\gamma_1 = 0.95$ ,  $\beta_0 = 0.68$ ,  $\beta_1 = 0.77$ ,  $g_0 = 9.83$ ,  $g_1 = 1.13$ ,  $r_0 = 11.2$ ,  $r_1 = 2$ .

Verification tests, where both stress  $\sigma$  and temperature  $T$  fluctuated in several manners resulted in strains that were matched by the analytical

expression to within 1%-2%.

A manuscript based on this work was accepted for publication in the Journal of Rheology. The work was presented at a meeting of the Rheology Society in Nov. 1983.

### 5.3 Chemical Cure-Shrinkage Effects on Residual Stresses in Epoxy Resins

The details of this work were reported in the Annual Technical Report for 1982. Therefore, only the main conclusions will be restated here.

In resins that are cured below their glass transition temperature  $T_g$ , the chemical-shrinkage strains develop against a material modulus of substantial magnitude - thus resulting in significant stresses. For instance, in the Hercules 3502 resin the cure-shrinkage stresses are about 30% of the total residual stress at the termination of cool-down. On the other hand, when resins are cured above their  $T_g$ , the modulus during the curing process is very low indeed, and the resulting stresses are negligible. Such a circumstance exists, for instance, for the FM-73 adhesive.

The above conclusions were derived from experimental investigations.

A paper titled "Assessment of Chemical Cure-Shrinkage Stresses in Two Technical Resins" by B. Harper, D. Peretz and Y. Weitsman was presented at the 24th SDM meeting in Lake Tahoe and appeared in the Proceedings of that conference (pp. 29-35).

### 5.4 Hygrothermal Stresses in Unsymmetric Cross-Ply Graphite/Epoxy Laminates

The effects of moisture and temperature on residual stresses in AS4/3502 composites were investigated by periodic measurement of curvatures in non-symmetric  $[0/90/0_4/90_4/0/90]_T$  square plates. The lay-up, as well as the size of the plates (4" x 4"), was selected to prevent premature

cracking, while at the same time yielding measureable curvatures which still remain within the range of linear plate theory. The plates were cured at 350°F according to manufacturer's specifications and then cooled to 75°F, where they deformed into a "saddle shape" due to residual thermal stresses. Subsequently, the plates were exposed to various levels of relative-humidity and temperature as shown in Table 1 below.

$\begin{matrix} \text{RH}\% \\ \text{T} (^{\circ}\text{K}) \end{matrix}$	0	13	75	95
298		X	[X]	[X]
327	X	X	[X]	[X]
339	X	X	[X]	[X]
346				[X]

Table 1: Conditioning Scheme\*

Preliminary studies were performed to characterize the process of moisture diffusion and relate the diffusivity  $D$  to temperature  $T$ . The moisture swelling coefficients  $\beta_T$  and  $\beta_L$ , in directions along and transverse to the fibers, were also measured. In addition, data regarding the creep behavior at various levels of temperature  $T$  and moisture content  $m$  was employed and expressed by means of a moisture-temperature shift factor function  $a_{Tm}$ .

Expressions for the time-dependent curvature  $k$  of the plate were derived for the transient moisture states, employing both linear elasticity and viscoelasticity. In the elastic case the curvature  $k$  is given by

---

\*A symbol  $[X]$ , indicates that absorption and saturation were followed by a desorption test.  $[X]$  indicates that desorption is not yet complete.



$$k = \frac{3h_3(Q_L + Q_T + 2Q_{LT}) \{g_1(P - Q)\Delta T + (R - S)G\}}{h_3^4 \{(Q_L + Q_T)^2 - 4Q_{LT}^2\} - 3g_1^2(Q_L - Q_T)^2} \quad (1)$$

$$\frac{-3g_1(Q_L - Q_T) \{h_3(P + Q)\Delta T + (R + S)F\}}{h_3^4 \{(Q_L + Q_T)^2 - 4Q_{LT}^2\} - 3g_1^2(Q_L - Q_T)^2}$$

where

$h_3$  = half laminate thickness

$$P = Q_L \alpha_L + Q_T \alpha_T$$

$$Q = Q_{LT} \alpha_L + Q_T \alpha_T$$

$$R = Q_L \beta_L + Q_{LT} \beta_T$$

$$S = Q_{LT} \beta_T + Q_T \beta_T$$

$$g_1 = \frac{1}{2} h_3^2 + h_1^2 - h_2^2$$

$$F(t) = \int_0^{h_3} m_e(z, t) dz$$

$$G(t) = \int_0^{h_3} m_e(z, t) z dz - 2 \int_{h_1}^{h_2} m_e(z, t) z dz$$

while in the viscoelastic case  $k$  must be determined from the simultaneous solution of four integral equations of the form

$$\sigma_x(t) = \int_0^t Q_L(\xi - \xi') \left\{ \frac{\partial \epsilon_x^0(\tau)}{\partial \tau} + z \frac{\partial k_x(\tau)}{\partial \tau} - \frac{\partial (\alpha_L \Delta T(\tau))}{\partial \tau} - \beta_L \frac{\partial m_e(z, \tau)}{\partial \tau} \right\} d\tau$$

$$+ \int_0^t Q_{LT}(\xi - \xi') \left\{ \frac{\partial \epsilon_x^0(\tau)}{\partial \tau} - z \frac{\partial k_x(\tau)}{\partial \tau} - \frac{\partial (\alpha_T \Delta T(\tau))}{\partial \tau} - \beta_T \frac{\partial m_e(z, \tau)}{\partial \tau} \right\} d\tau \quad (2)$$

where

$$\xi = \xi(z, t) = \int_0^t \frac{ds}{a_{TM}(m(z, s), T(s))}$$

$$\xi' = \xi'(z, \tau) = \int_0^\tau \frac{ds}{a_{TM}(m(z, s), T(s))}$$

The solution of the viscoelastic case required a numerical scheme, with discretization in both the time domain and along the thickness of the plate.

In many cases, curvature measurements during the first absorption stage agreed better with viscoelastic predictions, as shown for instance in Fig. 1. However, upon desorption the data departed from any theoretical prediction. The reason for this departure was subsequently attributed to irreversible damage.

In addition, several saturated laminates were exposed to subsequent cycles of dry/humid ambient environments, some fluctuating every 9 days, others every 16 days (Figs. 2 and 3). Curvatures and moisture weight-gains were measured, resulting in departures from predictions of both Fick's law for moisture diffusion and plate theory analysis (elastic or viscoelastic) for curvatures. These departures were also related subsequently to irreversible damage within the laminate.

A manuscript based upon this investigation was submitted for publication in the International Journal of Solids and Structures.

### 5.5 Hygrothermal Effects on Damage in AS4/3502 Composites

As noted in section 5.4 above, departures between theory and experiments were observed with the onset of desorption. To understand the causes for these discrepancies, the plate specimens were sectioned and

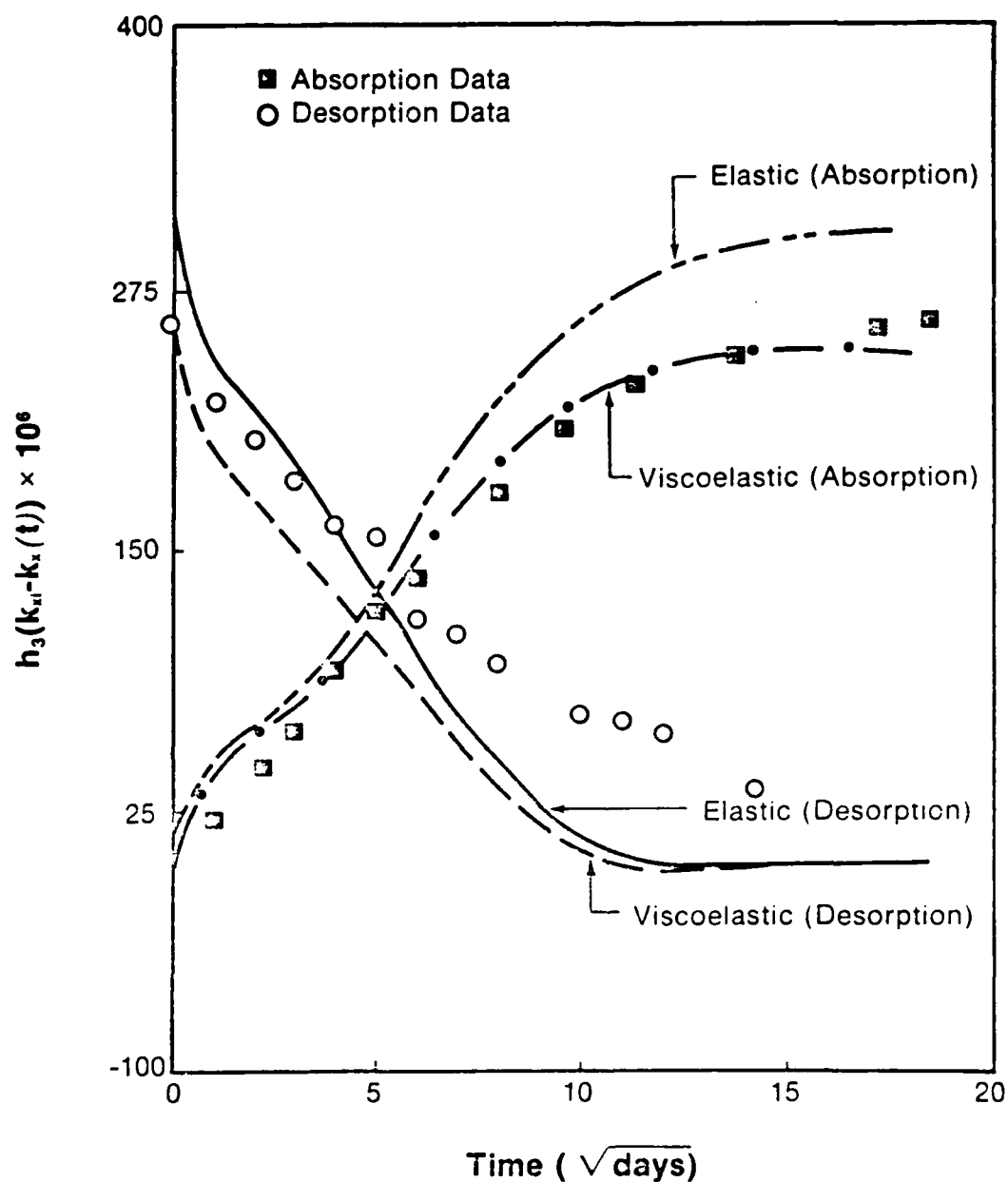


Figure 1. Time-dependent curvature change of (0/90/04/904/0/90)<sub>T</sub> AS4/3502 graphite/epoxy laminates at 130°F. Absorption data was obtained at 75% relative humidity.

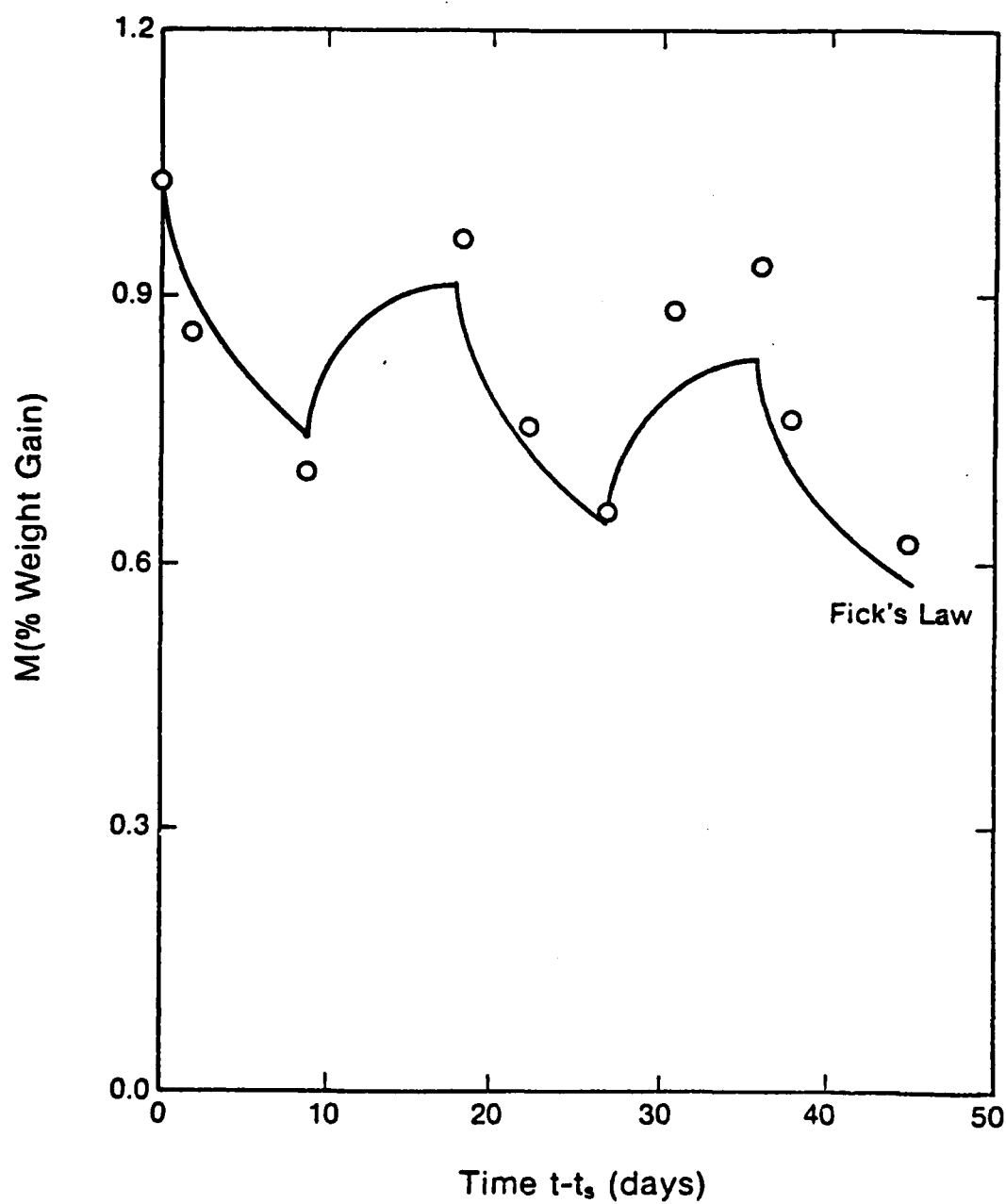


Figure 2. Moisture content (in % weight gain) during cyclic exposure to 0 and 95% relative humidities at 327°K (130°F), with cycle interval of 9 days.

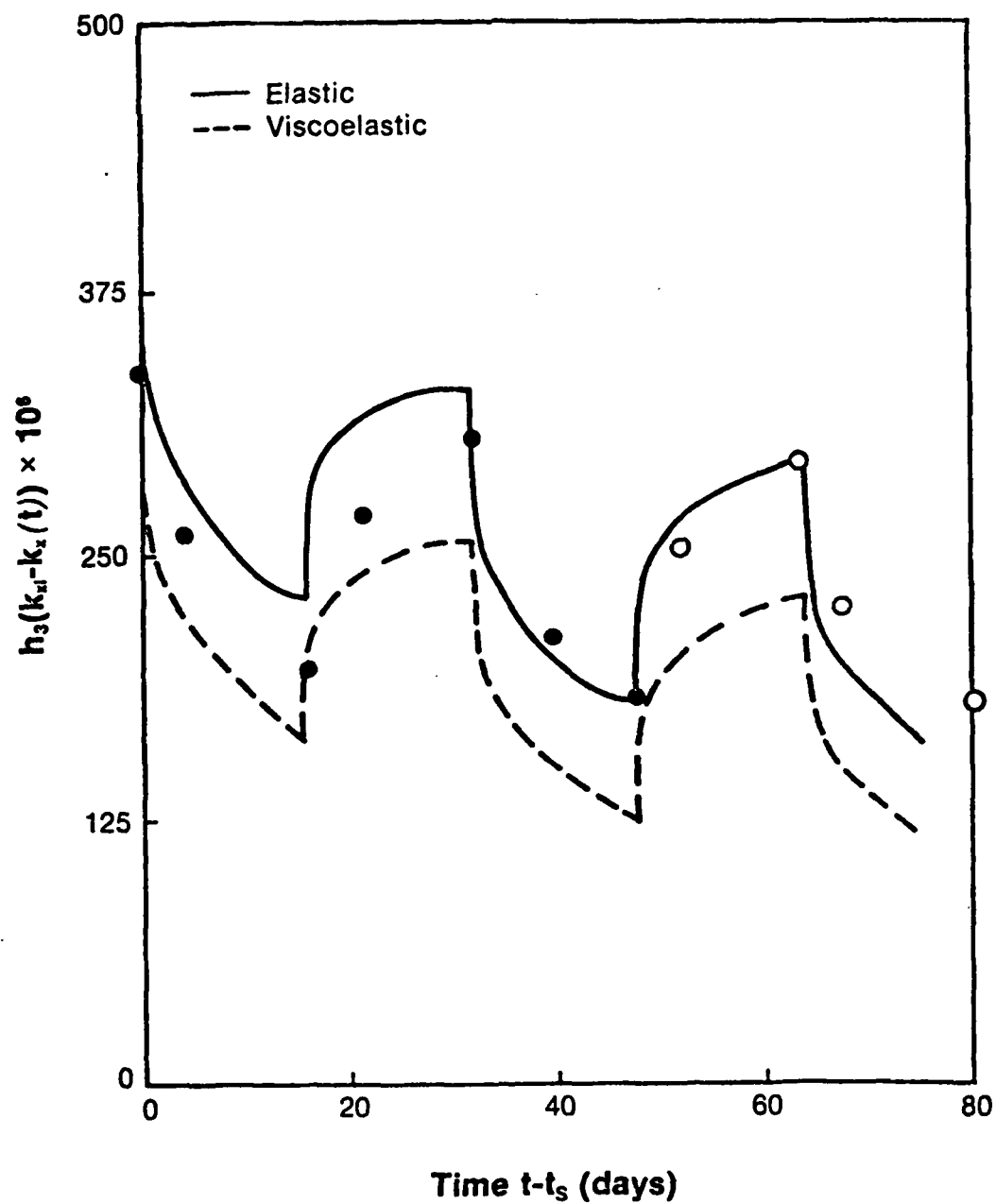


Figure 3. Time-dependent curvature change of  $(0/90/0_4/90_4/0/90)_T$  AS4/3502 graphite/epoxy laminates during cyclic exposure to 0% and 95% relative humidities at 130°F, with cycle interval of 16 days.

cores from the center portion were examined by SEM. No damage was detected in virgin and in fully saturated specimens. With the onset of desorption some damage was observed in places that corresponded to the locations of highest residual stress, as predicted by linear viscoelasticity. With the progress of desorption, or with further cycles in the ambient humidity, the damage became more and more wide spread. In all cases, the damage had the typical form of debond at the fiber/matrix interfaces (Figs. 4-6).

The results of this investigation indicate that the severity of damage due to moisture cycling increases with the amplitude and number of environmental cycles. As stated above, damage was in the form of individual cracks that initiated at the matrix/fiber interfaces and then coalesced into continuous cracks that meandered along those interfaces. Such damage may be very detrimental for laminates subjected to shear and compressive loads, because in those circumstances the matrix no longer provides the necessary support for the load bearing fibers.

It is worth noting that the earliest cracks developed in locations of highest transverse tensile stresses, as predicted by viscoelasticity theory. Subsequent cracking could not be correlated with theoretical predictions since no fracture was incorporated into the analyses. In many circumstances, particularly under moisture cycling at 9 or 16 days intervals, many cracks formed in directions parallel to the free surfaces of the laminate. This geometric feature indicates that stresses on the micro-level, rather than at the laminate level, play an important role in failure due to moisture.

#### 5.6 Investigations of Moisture Diffusion in Composites

Two investigations were performed regarding some basic mechanisms of moisture transport in composites.

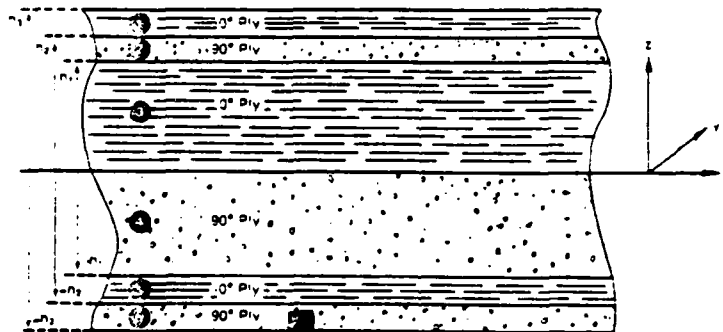
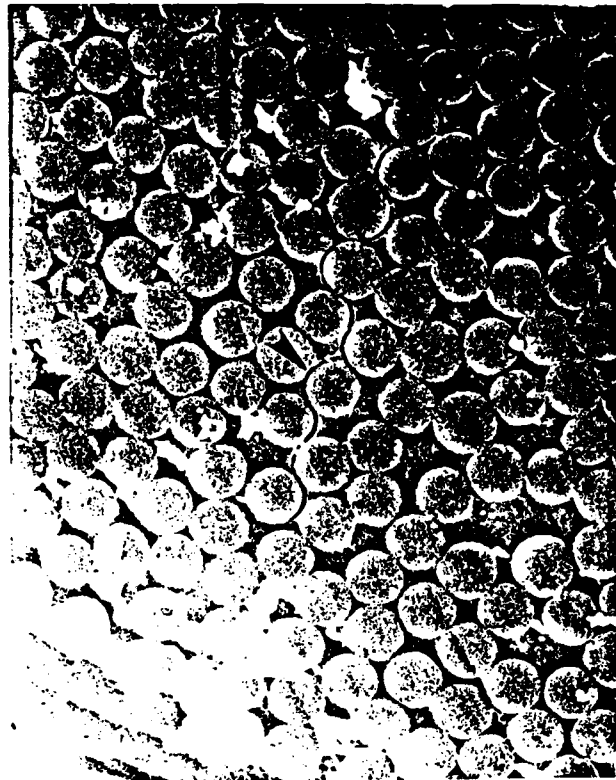


Figure 4. Vertical microcrack starting just underneath the surface of a laminate that was initially saturated, (95% R.H. and 130°F), and then cycled at 9 day intervals between 95% and 0% R.H. at 130°F, 1000X.

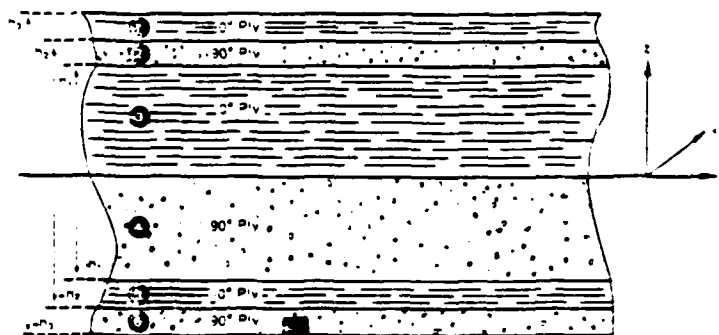
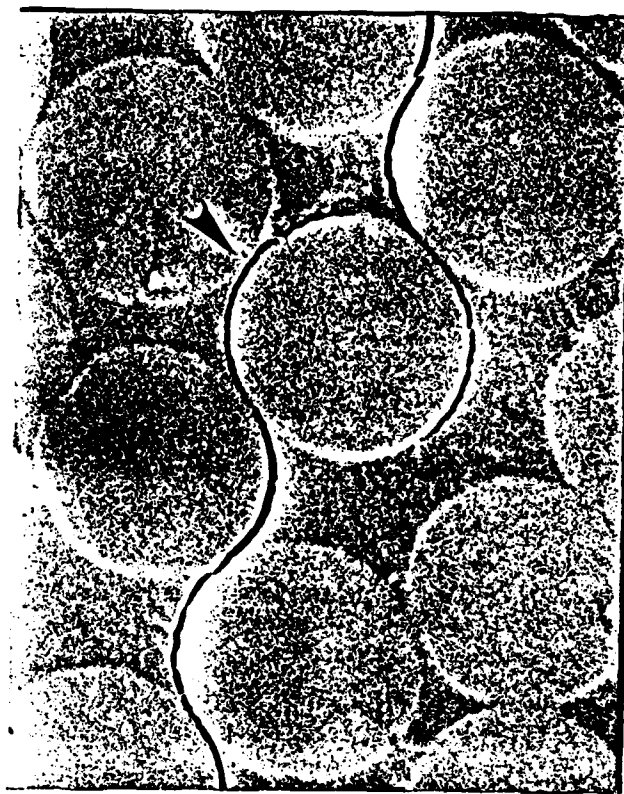


Figure 5. Same as figure 4 but at higher magnification, 4500X.



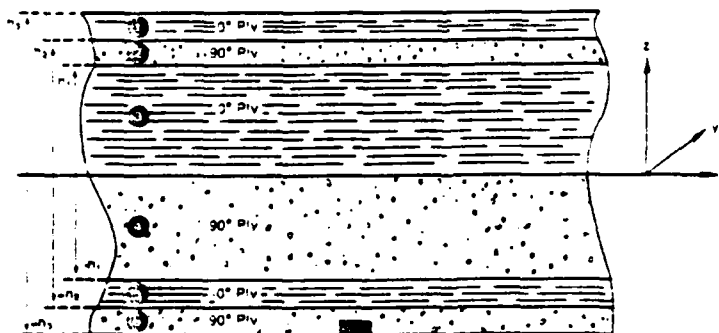
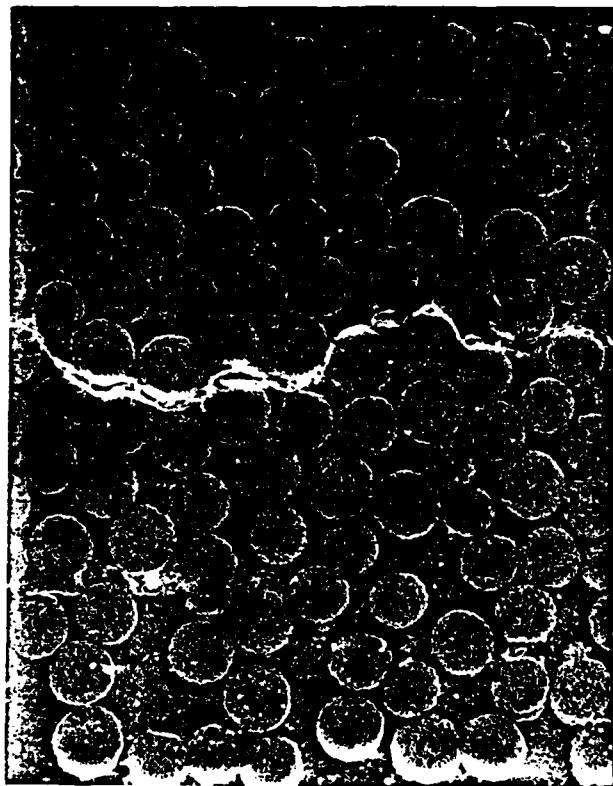


Figure 6. A horizontal microcrack caused by ply-level stresses. Laminate was initially dry then cycled at 9 day intervals between 95% and 0% R.H. at 150°F, 100X.

The first study involved the absorption of moisture in hybrids of rubber-toughened graphite/epoxy composites. Uni-directional coupons were formed of Hexcel F155 and F185 composites and moisture up-take was recorded in F185<sub>2</sub>/F155<sub>4</sub>/F185<sub>2</sub>, F155<sub>2</sub>/F185<sub>4</sub>F155<sub>2</sub> samples. The major advantage in this particular choice of materials was that they could be manufactured under the same cure cycle. Measurements were performed at two temperatures (24°C and 49°C), each at three levels of ambient relative humidity (55%, 75%, and 95% RH). Saturation levels and moisture diffusivities for each component material were determined from absorption data of F185<sub>4</sub> and F155<sub>4</sub> coupons, at the above mentioned levels of RH and temperature.

A mathematical solution for diffusion in hybrids was developed under the assumption that at the interface between the materials there is continuity of mass flux

$$D_1 \frac{\partial m_1}{\partial x} = D_2 \frac{\partial m_2}{\partial x}$$

and a jump discontinuity in the moisture content which is proportional to the discontinuity in the saturation levels; namely, at the interface

$$m_1 = \alpha m_2$$

where

$$\alpha = \frac{m_{1\infty}}{m_{2\infty}}$$

The solution to the one dimensional diffusion equation with the above interface conditions was obtained by means of a Fourier series, employing the concept of the "extended inner product".

Moisture profiles were obtained by numerical summation of a sufficient number of terms in the series to within a pre-determined degree of

accuracy. For short times (several hours) this procedure required taking about forty terms in the series, but fewer terms sufficed for longer times.

A typical comparison between experimental and theoretical predictions of weight-gain data is shown in Fig. 7.

The second study concerned the effect of an external stress on moisture diffusion in composite materials.

Uni-directional 90° four ply coupons of Hexcel F155 were manufactured and loaded on creep frames at 0%, 14%, 20% and 27% of ultimate stress (dry) ( $\sigma_{ult. dry} \approx 9000$  MPa). The frames were located in humidity chambers which were maintained at 93% RH and 41°C and at 97% RH and 13°C, respectively. The load frames were constructed with a quick load release mechanism which enabled a periodic weighing of the coupons. Poor environmental control and unexpected power failures caused severe disturbances in the 97% RH, 13°C chamber and rendered the data unreliable. The remaining results are shown in Fig. 8.

It should be noted that the curves in Fig. 8 give the average of data from two coupons, and the actual data at the various stress levels overlap on several occasions.

This investigation is now being repeated with "neat" resin coupons, under another contract.

The investigations described in the present section indicate that basic understanding is still lacking regarding moisture up-take in composites. The mechanism is still not fully recognized and no suitable theory seems to exist at the present time regarding the coupling between stress and diffusion. The latter effect may be especially significant near crack-tips.

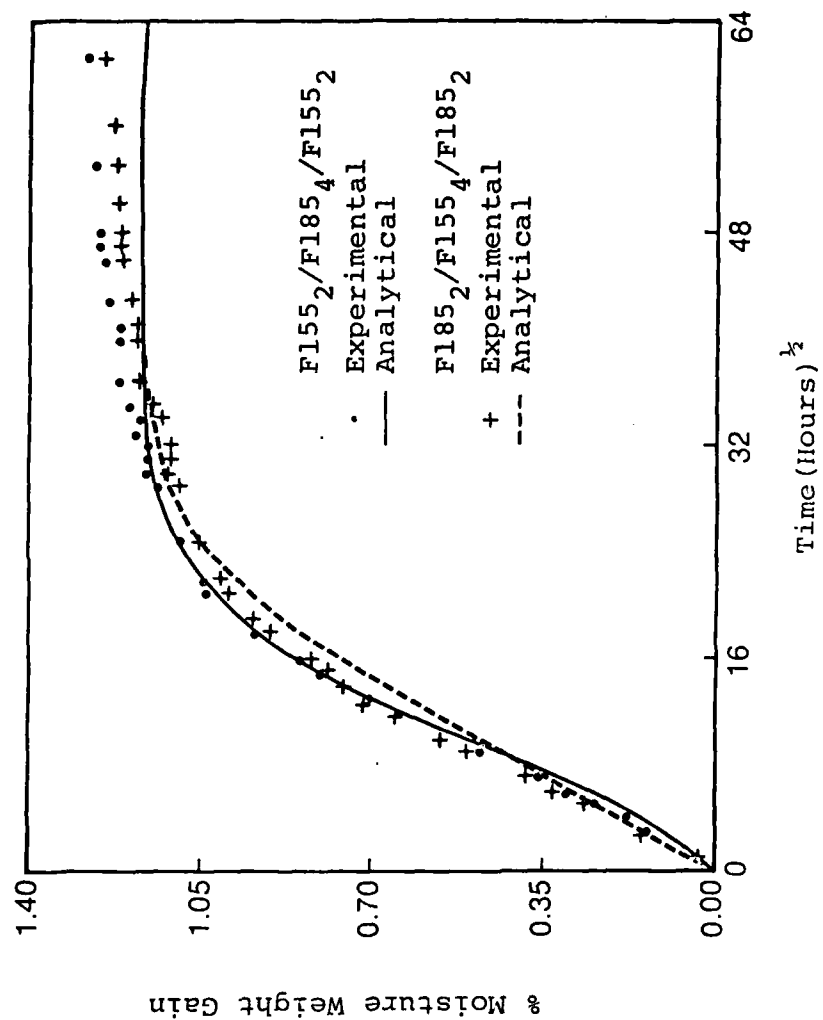


Figure 7 . Moisture Weight Gain in Hybrid Composite  
Specimens: 49°C, 95% RH.

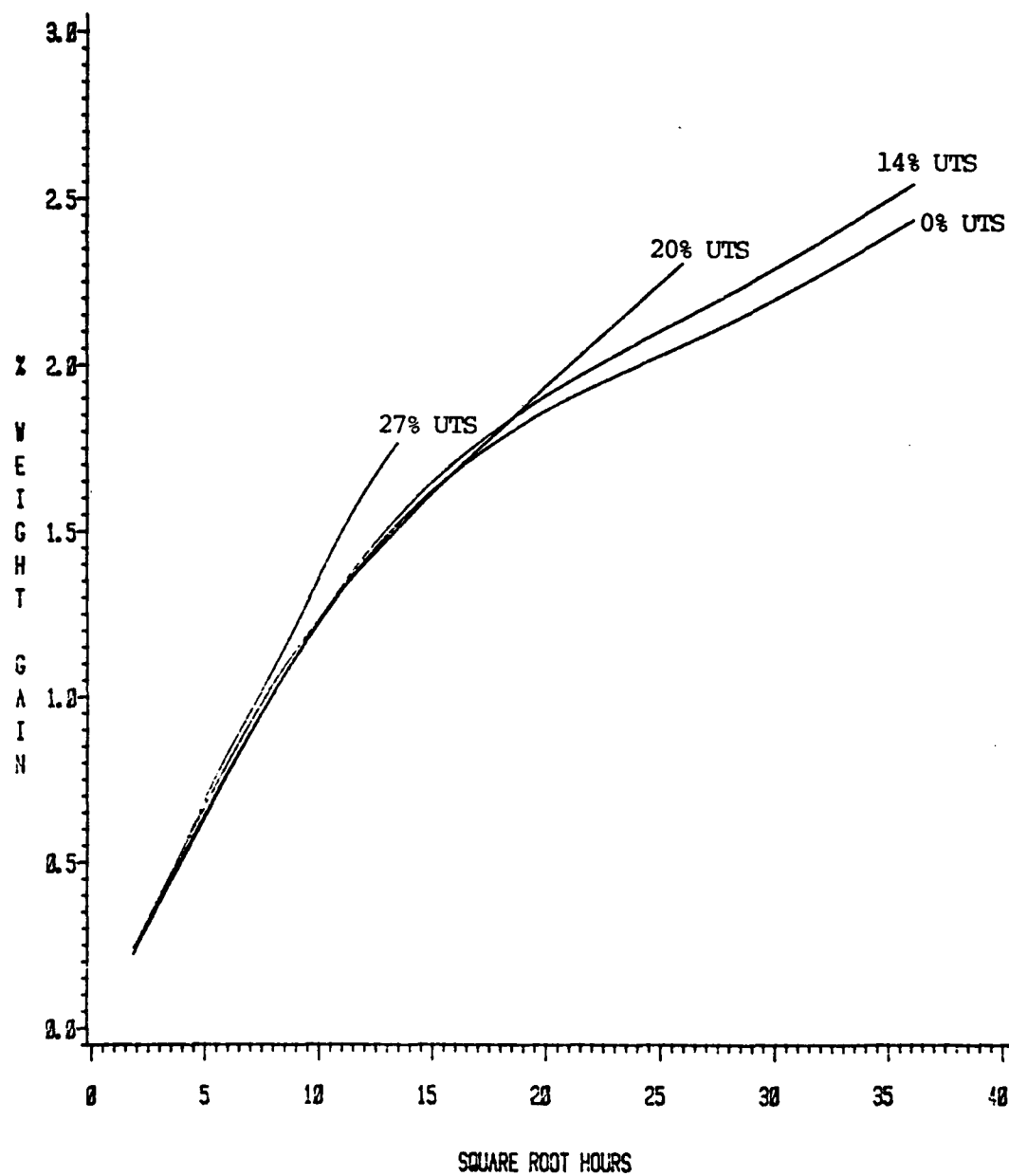
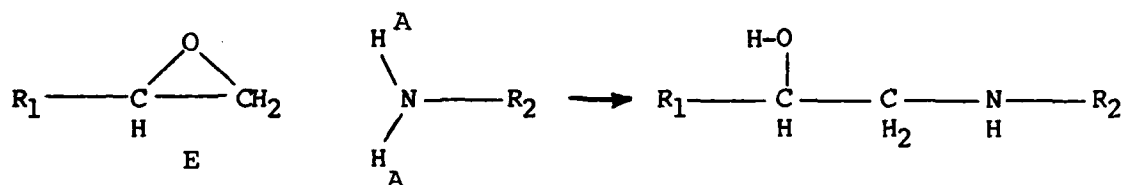


Figure 8 . Percent Weight Gain in Tensile Coupons Subjected to Different Stress Levels During Exposure to 41°C and 93% R.H.

## 6. RESIN STUDIES

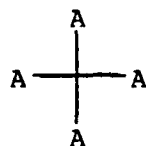
6.1 Improving the Ductility of Epoxy Resins\*

Introduction: At present it is possible to synthesize ranges of different epoxies based on a variety of monomers. The basic reaction between the functional groups is



where the epoxy group (E) reacts with one of the N-H groups (A). Depending on the number of these groups in the monomers (functionality) a different architecture is obtained.

The mechanical properties of the matrix, including its fracture behavior, are governed by this architecture. In general, the modulus increases if the functionality increases. Until recently, most research was directed towards this goal. In this case highly crosslinked networks are produced with great strength. The glass transition temperature,  $T_g$ , can be elevated to above 200°C. The larger is the number of amine groups, the tighter is the resulting network. As an example a diamine has four N-H groups and can be represented as follows:



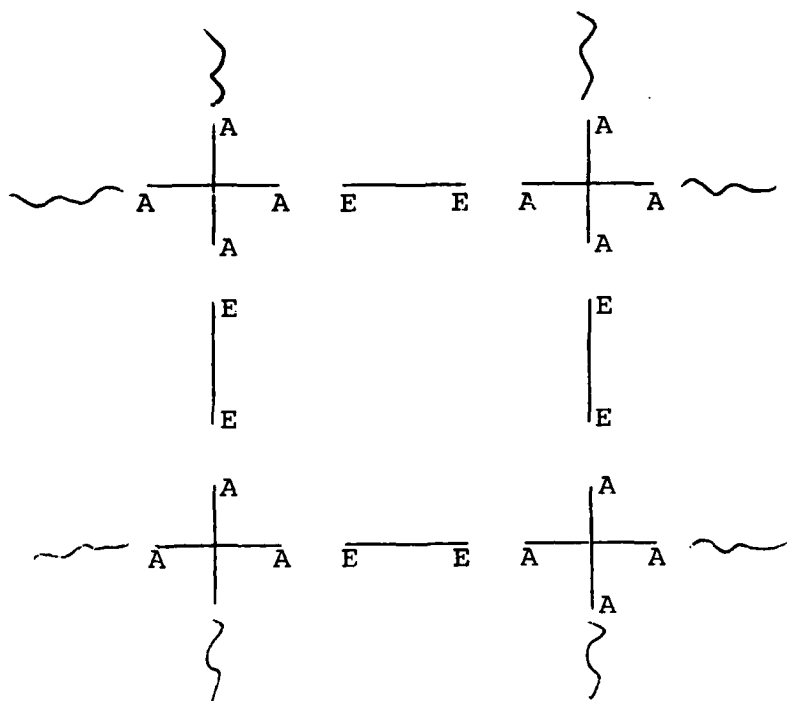

---

\*Sections 6.1 and 6.2 prepared by C.A.J. Hoeve

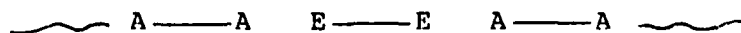
For a difunctional epoxy we have the schematic representation



In this case the crosslinked network produced can be represented as follows:



The drawback of these highly crosslinked polymers is, however, that the samples are brittle. Better ductility can be obtained by lowering the functionality and, thereby,  $T_g$ . This can be achieved by starting with a monoamine  $\text{A} \text{ --- } \text{A}$  and a diepoxy  $\text{E} \text{ --- } \text{E}$ . In this case linear polymers are obtained, as is represented by



These polymers have low glass points, since no network structure is present. Some of these have glass points below room temperature and are then rubbery in ambient environments. It is true that they have then a low

modulus; they are, however, extremely ductile.

By combining the properties of highly crosslinked, high-modulus polymers with those of linear, rubbery polymers, superior results can be obtained. An outstanding example is that of Kraton, manufactured by the Shell Company.

Our objective is to produce similar epoxy copolymers. If the two components are sufficiently different, phase separation occurs spontaneously. The matrix can then be represented schematically as shown in Fig. 1.

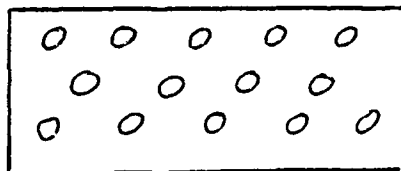


Figure 1

The spherical inclusions constitute the rubber particles, whereas the continuous phase is the glass, high-modulus phase. It is known that this type of two-phase system is quite ductile and yet has a high modulus. On impact the hard continuous phase offers resistance, and the soft domains retard or prevent development of large cracks. Furthermore, the soft inclusions serve as nucleation sites for the initiation of microcracks. It is now well established that the larger the number of cracks is, the larger is the energy required to rupture the sample, and thus the larger is the ductility.

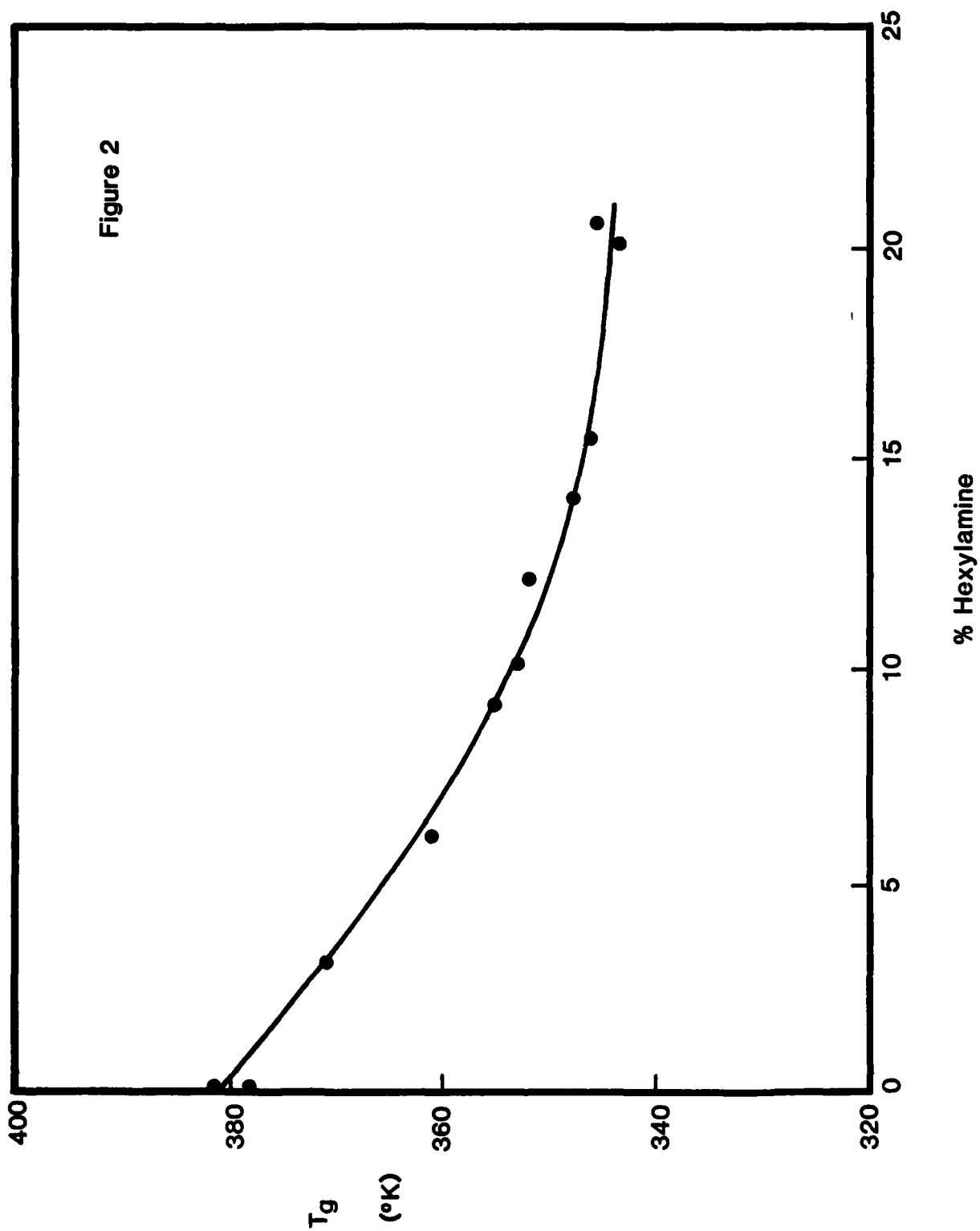
Experimental: Glass transition temperatures were measured with the Perkin Elmer DSC-2 instrument, a differential scanning calorimeter. Usually a scanning rate of  $10^{\circ}\text{C}$  per minute was used. The inflection point

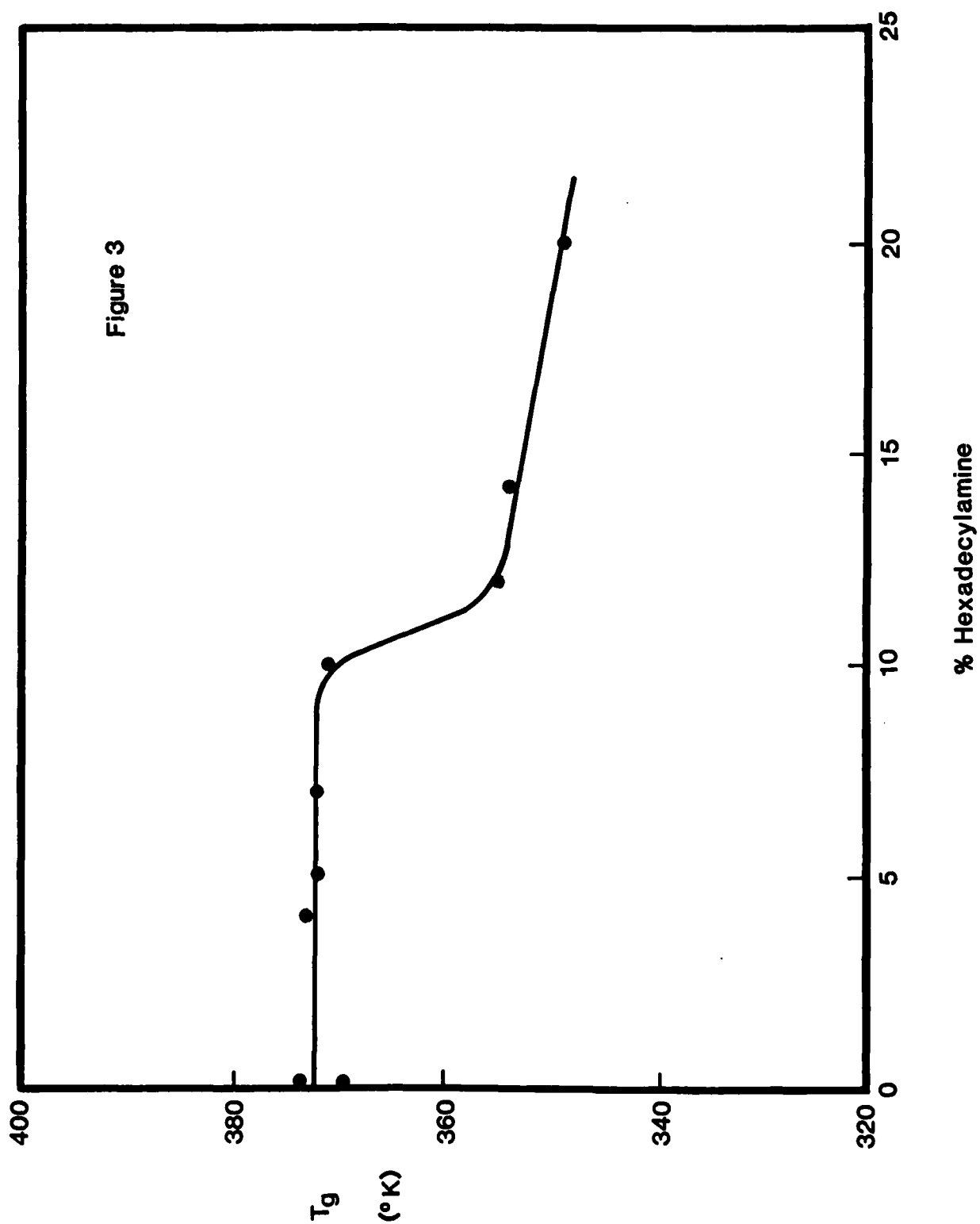


in the curve was taken to be the glass point. Samples of Epon were obtained from the Shell Company. The monomers are essentially bifunctional epoxies and can be represented by  $E\text{---}E$ . Samples of 1,4 diamino butane, hexadecylamine and hexylamine were 99% pure, or better. All polymerizations were carried out with stoichiometric amounts of amine hydrogen (A) and epoxy groups (E). Polymerizations were carried out at 100°C for 8 hours. This time was sufficient for completion of the reaction.

Results and Discussion: With 1,4 diamino butane and Epon a glassy polymer is produced with a  $T_g$  of 100°C. Copolymerization with various amounts of hexylamine produces polymers with lowered glass points, as shown in Fig. 2. This behavior is to be expected, since hexylamine has a lower functionality (2) than 1,4 diaminobutane (4). As a result the network is not as tightly crosslinked, resulting in a lower  $T_g$ . The continuous decrease in  $T_g$  indicates a homogeneous mixture of the different units.

In contrast, as shown in Fig. 3, when hexadecylamine is used as the monomer,  $T_g$  remains constant, until a concentration of 10% is reached. Subsequently, at still higher concentrations  $T_g$  decreases. This behavior is abnormal. It was to be expected that hexadecylamine would depress  $T_g$  more than hexylamine, since the long side chains of hexadecylamine (16 C-atoms) are bulkier than those of hexylamine (6 C-atoms). The bulkier the groups are, the more the network is diluted. These abnormal results can only be interpreted if we assume that a two-phase system exists. Apparently, the long non-polar tails are sufficiently different from the more polar matrix to spontaneously separate out as small inclusions, shown in Fig. 1. In that case we expect to find two glass points, the lower  $T_g$  being that for the inclusions. Indeed, we have confirmed that the lower  $T_g$  value at 12°C is that for the rubber inclusions. We have thus produced a





two-phase epoxy system, where both components are epoxies. On increasing the concentration of hexadecylamine beyond 10%, we see (Fig. 3) that  $T_g$  is lower, indicating that now the linear chains become also incorporated into the network. Below 10%, however, we have an excellent phase-separated system.

Usually, as in Hexcel's F155 and F185 resin, the rubber phase is physically mixed with the epoxy matrix. In this case the rubber particles are necessarily heterogeneous in size. When the two components are chemically linked, however, the size distribution of the inclusions can be made narrow, as in Kraton. Our new two-phase epoxy systems may have superior mechanical properties, but these have not yet been studied.

The results of this work are being prepared for publication.

## 6.2 Structure and Behavior of Water in Resins

Water absorption in epoxy resins often has undesirable effects on the mechanical properties. Although the maximum amount of water absorbed is only several percent, irreversible damage can result. The basic mechanism of the water-resin interaction is, however, not understood. We are engaged in a long-term program to study the water-resin interaction. One model study was carried out with methylcellulose on this project. The article entitled "Heat Capacity of Water Absorbed in Methylcellulose" by D.A. Kinard and C.A.J. Hoeve has been accepted for publication in the Journal of Polymer Science; its abstract is in the Appendix.

## 6.3 Molecular Models of Resins\*

Work has progressed along two lines. The first has to do with the

---

\*Prepared by J.S. Ham

molecular basis for toughness in resins, particularly in the polysulfones. The second is an attempt to understand the observed creep behavior in terms of basic material parameters.

Included in the Appendix is a short paper on some intermolecular interactions in the polysulfones. Its thesis is that the high  $T_g$  of the polysulfones is only in part due to the polarity of the sulfone group, but mainly is due to a relatively sluggish motion of the backbone chains. Discussions at the meeting where the paper was presented made clear that tighter arguments are needed to convince the holders of the conventional wisdom that the high  $T_g$  is primarily a consequence of polarity. The presentation of the evidence in a convincing format has yet to be done.

This concept is of importance in that high temperature resin candidates must have a high  $T_g$ . This can come either from polarity or from the stiffness interactions described in the paper. Presently, the dominant weakness in these candidates is the lack of toughness. The use of polarity to attain high  $T_g$  is thought to result in a brittle resin while increased chain stiffness promotes toughness. Therefore, this concept, when accepted, can help in the search for tougher resin candidates.

Also in the Appendix is a draft of a paper not quite ready for submission to a journal. This paper attempts to relate molecular parameters to creep characteristics. The molecular models of Rouse and Bueche from some years ago attempt to describe the polymer solutions and polymer melts in terms of chain dynamics. More recently, quasidimensional arguments (De Gennes) have been made as to the behavior where chain interaction predominates. The present paper is an extension of the latter to take into account the statistical distribution of time constants likely to be found in the solid polymer. By taking these into account, approximate power law behavior in creep time is predicted, although it is

difficult to obtain a log-log slope quite as small as that found empirically in some of the resins used in composites.

This type of study is related to a major unresolved question of the presence and importance of microstructural heterogeneities in the cured resin. The observation of such regions by electron microscopy has been questioned by many as an artifact but this does not prove that these regions do not exist. A comparison of actual creep behavior with that predicted from molecular models with and without heterogeneities should be helpful in identifying the nature of the microstructure and its effect on mechanical characteristics such as toughness.

## 7. DEVELOPMENT OF ELASTIC STRAIN RATIO TRANSLATOR (ESRT) GAGE\*

### 7.1 Introduction

A device for measuring uniaxial strains was developed which is believed will greatly enhance experimental capabilities in the mechanical characterization of fibrous composites and other materials. Efforts culminated in the filing of a "Disclosure of Invention" through the Texas A&M University System, dated Oct. 22, 1982. We have complied with Air Force requirements regarding disclosure submittal and the completion of the Air Force Systems Command Abstracts of New Technology (ANT).

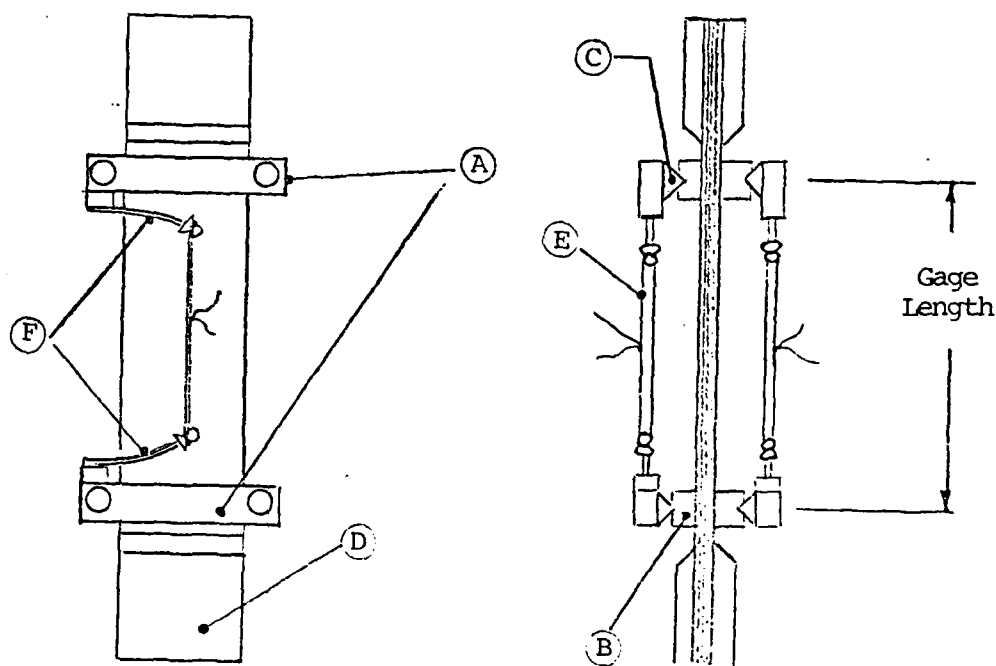
### 7.2 Description

Figure 1 is a schematic showing the basic elements of operation of the "ESRT" gage. Two stainless steel clamps, A, are secured to a uniaxial test specimen by pressure applied from the clamps through a pressure foot, B. Fixation of the position of the clamp to the pressure foot is accomplished by indentation indexing through an arrangement of steel balls or a knife edge.

Two such clamps are located on the test specimen, D, with the gage length being determined by the on-center spacing between the two clamps. The longitudinal strain sensing elements of the device are composed of two electrical resistant strain loops, E, which are made of very small diameter alloy wires coated with enamel. These loops are in turn placed in a condition of pre-tension through the cantilever springs, F. Subsequent axial straining of the test specimen produces

---

\*Prepared by B.C. Harbert



- A. Stainless steel gage clamps secured to test specimen at two locations. Gage length determined by on-center distance between clamps.
- B. Pressure foot or raised surface.
- C. Recessed hardened steel ball or knife edge.
- D. Typical 'tabbed end' uniaxial test specimen.
- E. Electrical resistant strain loop.
- F. Cantilever loading spring.

Figure 1. ESRT Gage Mounted on a Uniaxial Specimen



changes in the wire tension and the electrical resistance of the strain loops. The electrical changes can be treated in the usual manner as with standard bonded resistance strain gages, regarding electrical circuitry, signal conditioning, and analysis.

### 7.3 Results and Discussion

Operation of the ESRT gage on uniaxial test specimens has been performed to check out various gage characteristics such as accuracy, repeatability, sensitivity, calibration, linearity, fatigue limit and, to a lesser degree, gage sensitivity to temperature and humidity. Accuracy of the gage was established in part by comparing strains measured with the gage and two independent strain measuring techniques; a uniaxial graphite/epoxy composite test specimen subjected to a sinusoidal loading history was used. Figure 2 shows the comparison of mean cyclic strain measured by a conventional bonded resistance strain gage, an Instron type extensometer and the ESRT gage. Cyclic loading was performed on an Instron test machine at room temperature and humidity. Loading was essentially linear at 0.5 Hertz, with a typical cycle initially being a 300 lb. peak decreasing to 100 lb. The different steps on this curve reflect upward changes in the peak loading and corresponding changes in the low level during the cycle. The final cyclic load variation at the time of specimen failure was 750/200 lbs. The correlation between the ESRT gage and the clip gage extensometer is very good over the entire test range including the point of failure. Initially the agreement between the conventional bonded strain gage was good; however, disagreement between the strain gage and the other two devices increased with each increase in cyclic load level, until at a mean strain of 0.85% the

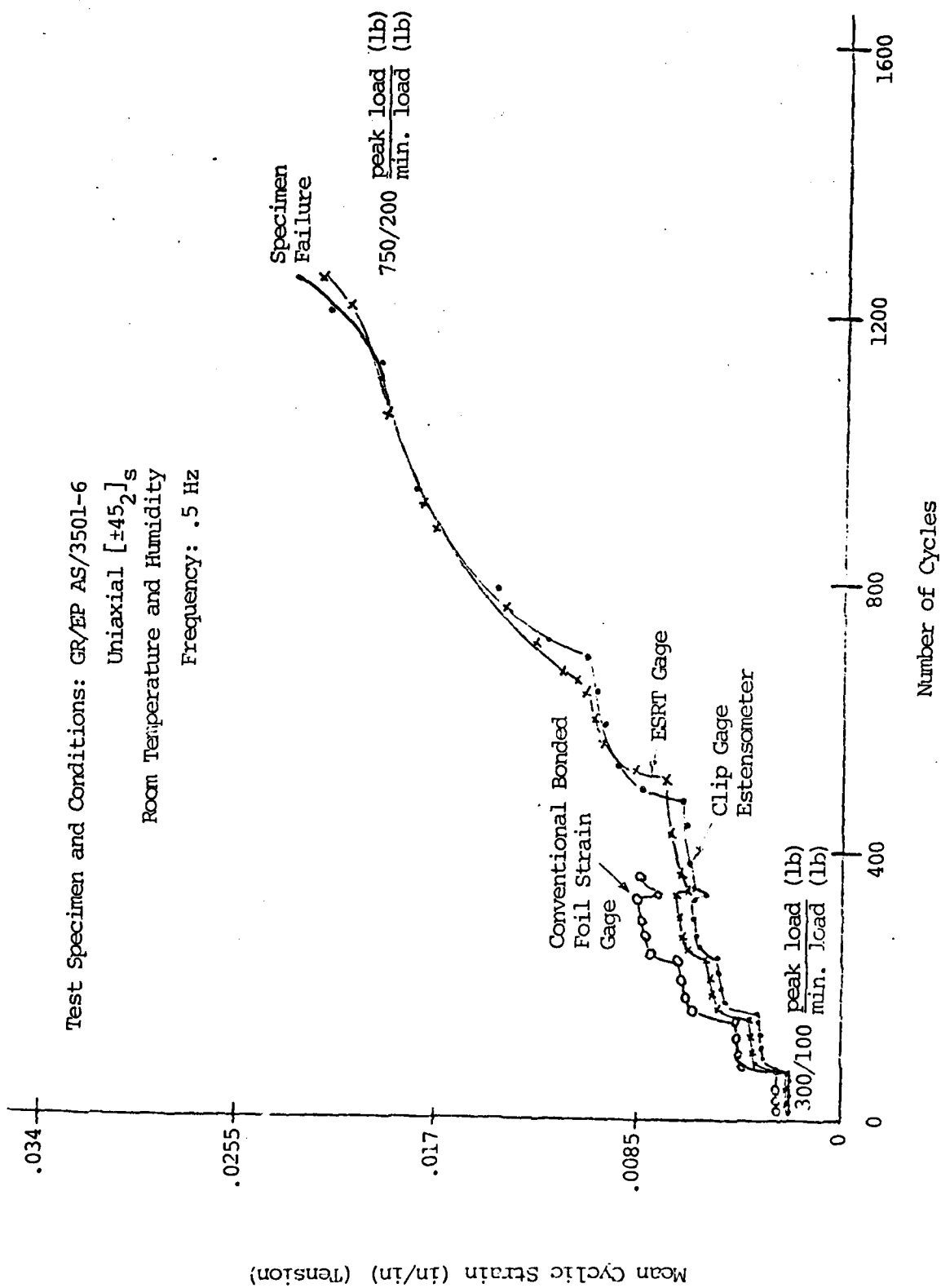


Figure 2. Performance of ESRT Gage Compared to Conventional Bonded Strain Gage and Instron Extensometer on  $[\pm 45_2]_s$  Graphite/Epoxy Composite Material.

conventional strain gage failed. Typical of these bonded gages, a considerable zero shift occurs under cyclic loading above 0.2% strain, increasing exponentially as the strain level increases. Therefore, even though the conventional strain gage continued to provide data, it was greatly in error by virtue of the zero shift which increased with each increase of load at strains above 0.2%. In contrast, we have obtained excellent agreement between the ESRT gage and a conventional bonded strain gage on an aluminum specimen tested at a constant strain rate of  $.01 \text{ min}^{-1}$ .

With additional experience and refinements it is believed the ESRT gage will become a very valuable experimental tool because it offers certain advantages over conventional strain measuring techniques:

Large strains can be measured (in excess of 5% if desired) because of the translation ratio imparted by the springiness of the cantilevered beams (as opposed to a 1:1 relationship for a bonded strain gage).

Since the strain loops are coupled through elastic metallic elements, no adhesive bonding is required; thus performance of the gage is not degraded at the high temperatures and high humidities at which polymeric adhesives creep.

The "ESRT" has been demonstrated to function very reliably under conditions of fatigue loading, both at high and low strain levels, as illustrated in Figure 2, and observed during many other tests. The levels of strain measured under fatigue loadings greatly exceed the capabilities of conventional strain gages.

## 8. GRADUATE RESEARCH ASSISTANT ACTIVITIES

### 8.1 Summary

The fourth and fifth groups of graduate engineering students to participate on the M.S. level in the AFOSR research project entered the program in September 1981 and 1982. They have now completed all of their requirements for a Master of Science degree, and the results of the research are reported in the following theses:

1. Cohen, R.N., "Effect of Resin Toughness on Fracture Behavior of Graphite/Epoxy Composites", December 1982.
2. Razi, H., "Slow, Stable Delamination in Graphite/Epoxy Composites", December 1982.
3. Weatherby, J.R., "Evaluation of Energy Release Rates in Unidirectional Double Cantilevered Beam Fracture Toughness Specimens", December 1982.
4. Porth, E.J., "Effect of an External Stress on Moisture Diffusion in Composite Laminates", December 1983.
5. Clark, D.L., "Moisture Absorption in Hybrid Composites", December 1983.
6. Jackson, S.P., "Hygrothermal Effects in an Anti-Symmetric Cross-Ply Graphite/Epoxy Material", February 1984.

The first Ph.D. student on the project graduated in August 1983, and his dissertation is:

Harper, B.D., "On the Effects of Post-Cure Cool-Down and Environmental Conditioning on Residual Stresses in Composite Laminates", August 1983.

The abstracts are in Section 8.2. Copies of the theses and dissertation will be provided upon written request to the Principal Investigator (R.A. Schapery).

To date, twenty five M.S. students and one Ph.D. student have participated in the project and graduated. Emphasis of the graduate program shifted from the M.S. level to the Ph.D. level in 1981. The

current group consists of one M.S. and eight Ph.D. students.

8.2 Abstracts of M.S. Theses and Ph.D. Dissertation

See pages 83-90

## ABSTRACT

Effect of Resin Toughness on Fracture Behavior  
of Graphite/Epoxy Composites (December 1982)

Ronald Nelson Cohen, B.S., Purdue University

Chairman of Advisory Committee: Dr. Walter L. Bradley

Energy release rates for delamination and transverse fracture have been experimentally determined for three different graphite/epoxy systems. Various combinations of mode I (opening)/mode II (in-plane shear) load ratios for delamination fracture have been investigated to determine the effect of resin toughness on delamination fracture. The micromechanisms of fracture were determined using in-situ fracture in a scanning electron microscope along with subsequent fractography on fractured surfaces. The energy release rate for delamination fracture and transverse fracture is less than the energy release rate for the neat material for a tough resin system. For a brittle resin system, the delamination and transverse toughness is greater than for the neat material. The results have been interpreted in terms of the relative contributions of resin deformation and fiber pullout and breakage to the total energy dissipated during fracture.

## ABSTRACT

Slow, Stable Delamination in  
Graphite/Epoxy Composites (December 1982)

Hamid Razi, B.S. Mechanical Engineering

University of Washington

Chairman of Advisory Committee: Dr. R.A. Schapery

Split laminated beam specimens tested under a fixed-grip condition are used to obtain relationships between the opening-mode energy release rate and crack speed in one brittle and one tough unidirectional, graphite/epoxy composite with moisture contents corresponding to ambient humidity, 45% RH, and 95% RH. The analysis employs a linear elastic fracture mechanics approach coupled with nonlinear beam theory to account for large deflections and rotations produced during the delamination tests.

## ABSTRACT

Evaluation of Energy Release Rates in  
Unidirectional Double Cantilevered Beam  
Fracture Toughness Specimens (December 1982)

Joe Randall Weatherby, B.S. Mechanical Engineering  
Texas A&M University

Co-Chairmen of Advisory Committee: Dr. R.A. Schapery  
Dr. M. Henriksen

An improved beam theory model is proposed for calculating energy release rates in symmetrically loaded unidirectional double cantilevered beam fracture toughness specimens having longitudinally oriented fibers. The proposed model consists of a beam supported at the crack front by a torsion spring. Here the spring is used to account for the strain energy in the region ahead of the crack front. Values for the spring constant are obtained from a two dimensional approximate analytical solution and from finite element models. Energy release rate calculations based on the beam and spring model are compared to those obtained by numerical evaluation of Irwin's crack closure integral. Comparisons are also made with results from techniques previously used in the analysis of isotropic double cantilevered beam specimens.



## ABSTRACT

Effect of an External Stress on Moisture  
Diffusion in Composite Materials (December 1983)  
Edward John Porth, B.S., University of Colorado  
Chairman of Advisory Committee: Dr. Y. Weitsman

This work concerns the coupling effects between mechanical stress and strain fields and moisture diffusion in fiber reinforced polymeric composites. It is noted that stresses give rise to two types of coupling. The first type causes an increase in the moisture saturation level, thus increasing the moisture boundary value. The second kind of coupling modifies the moisture diffusion process, thus altering the form of the field equation through a stress-diffusion coupling term.

Diffusion experiments conducted on composite tensile coupons stressed uniaxially detected the first type of coupling, but due to the uniformity of the stress field, determination of the second kind of coupling was not possible. An analytical study demonstrated that detection of both the stress-diffusion coupling effects would require a complex experimental setup.

## ABSTRACT

## Moisture Absorption in Hybrid Composites (December 1983)

Dan Laro Clark, B.S. Aerospace Engineering

Texas A&amp;M University

Co-Chairmen of Advisory Committee: Dr. Y. Weitsman  
Dr. W.J. Horn

This thesis presents an analytical and experimental investigation of moisture absorption in single component and hybrid graphite/epoxy composites. The main purpose of this effort was to evaluate the applicability of the classical diffusion equation, modified to account for interfacial conditions, in predicting moisture weight gain in a hybrid graphite/epoxy composite. The hybrid was made of Hexcel F155 and Hexcel F185 graphite fiber reinforced/epoxy resin systems. Moisture uptake was measured under three fixed relative humidities at each of two temperature levels. Reasonably good agreement was obtained between experimental data and analytical predictions based on Fick's Law, the classical diffusion equation. The circumstances of poorer agreement can be attributed to the non-Fickian diffusion behavior of the F155 material at the higher temperature. Improved agreement was attained for the cases of higher relative humidities. Several analytical solutions were evaluated for additional hypothetical lay-ups to provide further insight to the diffusion process in hybrids and to assess the effect of coatings in minimizing moisture uptake in hybrids. These cases indicated that the optimum coating material, to retard moisture absorption by the laminate, would be one with both low diffusivity and low moisture saturation level.

## ABSTRACT

Hygrothermal Effects in an Anti-Symmetric  
Cross-Ply Graphite/Epoxy Material (May 1984)  
Steven Paul Jackson, B.S., Aerospace Engineering  
Texas A&M University

Chairman of Advisory Committee: Dr. Y. Weitsman

This thesis concerns the effects of moisture and temperature (i.e. hygrothermal) conditioning on anti-symmetric AS4/3502 graphite/epoxy cross-ply laminates. Experimental measurements of the curvatures of hygrothermally conditioned cross-ply laminates were compared with linear elastic and linear viscoelastic theoretical predictions. Measurements of experimental moisture weight gain of the laminates are also compared against theoretical predictions derived from the classical, one-dimensional diffusion equation.

The differences between the experimental results and the theoretical predictions were most likely caused by irreversible damage due to the moisture and temperature conditioning. The presence of such damage was detected by scanning electron microscopy (SEM) and an attempt was made to relate the location and extent of damage to the history of the hygrothermal conditioning.

## ABSTRACT

On the Effects of Post Cure Cool Down  
and Environmental Conditioning on  
Residual Stresses in Composite  
Laminates. (August 1983)

Brian Douglas Harper, B.S., Texas A&M University  
M.S., Texas A&M University

Co-Chairmen of Advisory Committee: Dr. Yechiel Weitsman  
Dr. Thomas Kozik

This dissertation consists of four investigations, all of which concern the effects of post cure cool down path and environmental conditioning upon the residual thermal stresses that develop in composite laminates.

The main theme involves an analysis which considers the effects of temperature and moisture upon the time-dependent behavior of the material and all calculations employ recent data on the hygrothermo-viscoelastic response of the AS/3502 graphite/epoxy system. The analysis was accompanied by an experimental investigation, where curvatures of anti-symmetric, cross-ply AS/3502 graphite/epoxy laminates were measured as a function of time and compared against theoretical viscoelastic predictions.

Additional topics involved a thermoviscoelastic characterization of the Hercules 3502 epoxy resin system, and an assessment of the effects of chemical cure shrinkage strains upon residual stresses.

These two subjects involved experimental work, supplemented by appropriate mathematical models.

The fourth subject concerns optimal cool down paths which minimize the residual thermal stresses occurring in balanced, symmetric cross-ply laminates. Solutions were obtained analytically, based upon variational principles.

## 9. PROFESSIONAL PERSONNEL INFORMATION

### 9.1 Faculty Research Assignments

Each participating faculty member has been responsible for the research conducted in at least one specific area of investigation, as shown below. In addition, most have served as chairmen of one or more of the graduate advisory committees for M.S. and Ph.D. students and, as such, directed their students' research projects. The faculty also contributed to other research activities on the project by serving on student advisory committees, through technical meetings, informal discussions, and, in some cases, through specific research. It should also be observed that there is considerable overlap between the areas in the Statement of Work, and therefore most of the faculty have been involved in more than one area of activity.

Besides the listed faculty, Dr. Walter Haisler (Aerospace Engineering) has contributed significantly to the project. He provided valuable advice on numerical solution methods and served on several graduate advisory committees.

The Principal Investigator (R.A. Schapery) had responsibility for overall technical direction and coordination and for project management. In addition he had direct responsibility for certain research work, as noted below.

<u>Faculty Member/Departmental Affiliation</u>	<u>Primary Research Responsibility</u>
Dr. David Allen/Aerospace Engineering	(5)* theoretical models/formulation and numerical solution methods

---

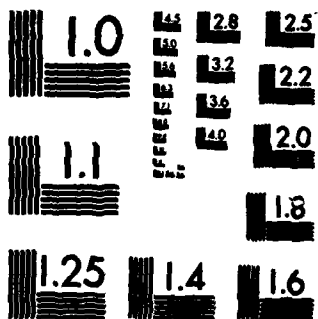
\*Number in parentheses indicates area in State of Work (Section 1).

AD-A150 802 RESEARCH ON COMPOSITE MATERIALS FOR STRUCTURAL DESIGN  
(U) TEXAS A AND M UNIV COLLEGE STATION MECHANICS AND  
MATERIALS RE. D ALLEN ET AL. APR 84 MM-4665-84-5

UNCLASSIFIED AFOSR-TR-85-0226 F49620-82-C-0057

214

NL



MICROCOPY RESOLUTION TEST CHART  
NATIONAL BUREAU OF STANDARDS-1963-A



Dr. Walter Bradley/Mechanical Engineering	(1) delamination fracture properties and SEM studies
Dr. Joe Ham/Physics	(4) toughening mechanisms (molecular aspects)
Dr. Cornelius Hoeve/Chemistry	(3) toughening mechanisms and water in polymers
Dr. Richard Schapery/Aerospace and Civil Engineering	(5) theoretical models/formulation and analysis
Dr. Jack Weitsman/Civil Engineering	(2) temperature and moisture effects/residual stresses

## 9.2 Additional Professional Staff

### Mechanics and Materials Center

Ms. Jennifer Wells - Systems Analyst

Mr. Carl Fredericksen - Electronics Technician

Mr. Bob Harbert - Assistant Research Engineer

Mr. Richard Tonda - Laboratory Manager

## 9.3 Spoken Papers and Presentations, Publications, and Other Professional Activities of the Faculty

The activities shown in this section are only those that are directly related to research on composite materials. Most of the faculty had many other outside involvements including consulting with industry as well as research, publishing, and lecturing on other topics.

D.H. Allen

### Publications:

"A Survey on Damage in Continuous Fiber Composites", (with S.E. Groves), Texas A&M Report No. MM 5023-84-6, 1984.

"A Damage Model for Continuous Fiber Composites", (with S.E. Groves and R.A. Schapery). To be presented at SES Annual Meeting, Oct. 1984 (In preparation).

W.L. Bradley

Conference Presentations:

"Delamination and Transverse Fracture in Graphite/Epoxy Composite Materials", Gordon Research Conference on Composite Materials, Ventura, CA, January 1982.

"Mixed Mode Delamination Fracture in Graphite/Epoxy Composite Materials", Society of Engineering Science 19th Annual Meeting, Rolla, Missouri, October 1982.

"In-Situ Fractographic Study of Graphite/Epoxy Composite Materials", Sixth Conference on Fibrous Composites in Structural Design, New Orleans, January 1983.

"Delamination Fracture in Ductile and Brittle Epoxies Reinforced with Graphite", NASA Workshop, RPI, July 1983.

"Delamination and Transverse Fracture in Graphite/Epoxy Composite Materials", Fourth International Conference on Mechanical Behavior of Materials, Sweden, August 1983.

"Matrix Deformation and Fracture in Graphite Reinforced Epoxies", ASTM Symposium on Delamination and Debonding of Materials, Pittsburgh, November 1983.

Publications:

"In-Situ Fractographic Study of Graphite/Epoxy Composite Materials", (with R.N. Cohen) Proc. 6th Conference on Fibrous Composites in Structural Design, New Orleans, January 1983.

"Delamination and Transverse Fracture in Graphite/Epoxy Composite Materials", (with R.N. Cohen) Proc. Fourth Int. Conf. on Mechanical Behavior of Materials, Sweden, August 1983.

"The Effect of Resin Content on the Delamination Fracture Behavior of Graphite Epoxy Laminates", (with W.M. Jordan) accepted for presentation and publication, SAMPE Annual Meeting, Reno, Nevada, April 1984.

"In-situ Delamination Study of Graphite/Epoxy Composite Material in the Scanning Electron Microscope", (with E.A. Chakachery) accepted for presentation and publication at 6th International Conference on Fracture to be held in Delhi, India, November 1984.

"Matrix Deformation and Fracture in Graphite Reinforced Epoxies", (with R.N. Cohen) presented at ASTM Symposium on Delamination and Debonding of Materials, under review for publication in STP for same conference, Pittsburgh, November 1983.

J.S. Ham

Conference Presentation:

"Effects of Chain Stiffness in a Polysulfone", American Chemical Society Annual Meeting, Kansas City, September 1982; also poster session at American Physical Society Annual Meeting, Dallas, March 1982.

Publications:

"Effects of Chain Stiffness in a Polysulfone", Polymer Preprints, No. 23, 1982.

"A Molecular Model for Creep in a Viscoelastic Polymer", Texas A&M University Report No. MM 4665-84-8, April 1984.

C.A.J. Hoeve

Lectures:

"The Molecular Weight Distribution of Poly-condensation Reactions", Dow Chemical Co., Freeport, TX, April 1982.

"The Glass Transition of Polymers and Its Connection With the Mechanical Properties", Shell Co., Houston, TX, September 1982.

"How Can We Change the Structure of Epoxies to Improve Their Properties", Dow Chemical Co., Freeport, TX, May 1983.

Publications:

"Heat Capacity of Water Absorbed in Methylcellulose", with D.A. Kinard, J. Polymer Science. (In press.)

"Two-phase Epoxy Resins", with J. Latham, J. Polymer Science, (in preparation).

R.A. Schapery

Lectures and Conference Presentations:

"Time-Dependent Deformation and Failure Behavior of Composite Materials", 1982 Midwest Mechanics Lecture Series at Eight Universities: Michigan, Michigan State, Wisconsin, Minnesota, Notre Dame, Illinois Institute of Tech., Illinois, Purdue.

"Models for Damage Growth and Fracture in Nonlinear Viscoelastic Particulate Composites", Ninth U.S. National Congress of Applied Mechanics, Cornell University, June 1982.

"Characterization of Damage Growth and Fracture in Filled Elastomers", IUPAC International Symposium on Macromolecules, University of Mass., July 1982.

"Research on Composite Materials for Structural Design", Eighth Annual Mechanics of Composites Review, Dayton, Ohio, October 1982.

"Micro-Damage Analysis for Composite Materials", University of Texas, Austin, December 1982.

"Analysis of Damage Growth and Fracture of Viscoelastic Composites", Gordon Conference on Composites, Santa Barbara, January 1983.

"Crack Growth in Tires", Plenary session lecture at the annual meeting of the Tire Society, March 1983.

"Composite Materials Research at TAMU", Dow Chemical and Shell Development Companies, March 1983.

"Effect of Polymer Properties on Fracture Toughness of Composites", American Chemical Society Meeting, Freeport, March 1983.

"On the J Integral for Analysis of Crack Growth in Viscoelastic Adhesives", VPI & SU Workshop on Adhesion Science, Blacksburg, May 1983.

"Correspondence Principles and a J Integral for Analysis of Viscoelastic Materials", Seminar at Caltech, Pasadena, May 1983.

"Time-Dependent and Fracture Behavior of Short Fiber Composites", Caltech Conference on Polymers and Composites, Pasadena, May 1983.

"Viscoelastic Effects in Crack Propagation", National Bureau of Standards Conference on Fracture, Washington, June 1983.

"Time-Dependent Fracture of Composite Materials", ASME Applied Mechanics Conference, Univ. of Houston, June 1983.

"Constitutive Equations for Solid Propellant with Distributed Damage", ONR Workshop on Dynamic Deformation, Fracture, and Transient Combustion, Chestertown MD, July 1983.

"A Generalized J Integral for Fracture Analysis of Viscoelastic Materials", Seminar at Cornell University, Ithaca, October 1983.

#### Publications:

"Models for Damage Growth and Fracture in Nonlinear Viscoelastic Particulate Composites", Proc. Ninth U.S. National Congress of Applied Mechanics, 1982.

"Continuum Aspects of Crack Growth in Time Dependent Materials", Encyclopedia of Materials Science and Engineering, Pergamon Press. (In press.)

"Correspondence Principles and a Generalized J Integral for Large Deformation and Fracture Analysis of Viscoelastic Media", Int. J. Fracture Mechanics. (In press.)

Deformation and Fracture Analysis of Viscoelastic Media", Int. J. Fracture Mechanics. (In press.)

#### Additional Activities:

Air Force Materials Lab. consultant to W.B. Jones on fracture of resins, 1982. Also member of editorial board, Composites Technology Review (1982-present) and member of the Structural Composites Working Group, OSD/IDA Reliability and Maintainability Study (1983).

Y. Weitsman

#### Lectures and Conference Presentations:

"On the Thermoviscoelastic Characterization of Adhesives and Composites", 4th International Conference on Composite Materials, Tokyo, October 1982.

"Optimal Cooling of Cross-Ply Composite Laminates and Adhesive Joints", Winter Annual Meeting of ASME, Phoenix, November 1982.

"The Modeling of Craze in Polymers", Technion, Haifa, Israel, December 1982.

"Models of Craze", Seminar at the University of Texas, Austin, TX, April 14, 1983.

"Residual Stresses in Composite Materials", lecture at Hercules Corp., Magna, UT, April 1983.

"The Characterization of the Thermorheologically Complex Behavior of Two Technical Resins", 1983 Annual Meeting of the Society of Rheology, Knoxville, TN, Oct. 1983.

"Modeling of Craze in Polymers", Seminar at Virginia Polytechnic Institute and State University, Blacksburg, VA, Oct. 1983.

"Environmental Effects in Composites", presentation at the Composite Materials Review Meeting, Dayton, OH, Oct. 1983.

#### Publications:

"The Non-Linear Viscoelastic Characterization of FM-73 Adhesive", with D. Peretz, J. of Rheology, Vol. 26, No. 3, pp. 245-261, 1982.

"On the Thermoviscoelastic Characterization of Adhesives and Composites", In Progress in Science and Engineering of Composites, Proceedings of the 4th International Conference of Composite Materials Tokyo Japan, T. Hayashi, Editor, Vol. 1, pp. 771-779, 1982.

"Optimal Cooling of Cross-Ply Composite Laminates and Adhesive Joints", with B.D. Harper, J. of Applied Mechanics, ASME, Vol. 49, No. 4, pp. 735-739, 1982.

"The Non-Linear Thermoviscoelastic Characterization of a Structural Adhesive", with D. Peretz, J. of Rheology, Vol. 27, No. 2, pp. 97-114, April 1983.

"Assessment of Chemical Cure-Shrinkage Stresses in Two Technical Adhesives", with B.D. Harper, Proc. Joint AIAA/ASME/ASCE/AHS 24th Structures, Structural Dynamics and Materials Conference, Part 1, pp. 29-35, 1983.

"Deformation and Stress Intensities Due to a Craze in an Extended Elastic Material", with J.R. Walton, J. of Applied Mechanics, Vol. 51, No. 1, pp. 84-92, March 1984.

"Viscoelastic Effects on Stresses and Stress Intensities in Crazes", In Recent Developments in Applied Mathematics, F.F. Ling and I.G. Tadjbakhsh, Editors, Rensselaer Press, pp. 220-234, 1983.

"A Characterization Method for a Class of Thermorheologically Complex Materials", with B.D. Harper, Journal of Rheology. (In press.)

"On the Effects of Environmental Conditioning on Residual Stresses in Composite Laminates", with B.D. Harper, submitted for publication in the International Journal of Solids and Structures.

**Additional Activities:**

Member of the ASME Committee and AIAA Sub-Committee on Composite Materials.

## APPENDIX

Publications of Research  
AFOSR Contract

## LIST OF CONTENTS:

Abstracts/Research Summary (1982-83)

(The complete publications were in the 1983 Annual Report)

1. "Delamination and Transverse Fracture in Graphite/Epoxy Materials", by W.L. Bradley and R.N. Cohen.
2. "In-Situ Fractographic Study of Graphite/Epoxy Composite Materials", by W.L. Bradley and R.N. Cohen.
3. "Effects of Chain Stiffness in a Polysulfone", (Research Summary) by J.S. Ham.
4. "Heat Capacity of Water Absorbed in Methylcellulose", by D.A. Kinard and C.A.J. Hoeve.
5. "Continuum Aspects of Crack Growth in Time Dependent Materials", by R.A. Schapery.
6. "Correspondence Principles and a Generalized J Integral for Large Deformation and Fracture Analysis of Viscoelastic Media", by R.A. Schapery.
7. "Assessment of Chemical Cure-Shrinkage Stresses in Two Technical Resins", by B.D. Harper, D. Peretz and Y. Weitsman.
8. "On the Thermoviscoelastic Characterization of Adhesives and Composites", by Y. Weitsman.
9. "Optimal Cooling of Cross-Ply Composite Laminates and Adhesive Joints", by Y. Weitsman and B.D. Harper.

New Publications (1983-84)

1. "A Survey of Damage in Continuous Fiber Composites", by S.E. Groves and D.H. Allen.
2. "In-Situ Delamination Study of Graphite/Epoxy Composite Materials in the Scanning Electron Microscope", by E.A. Chakachery and W.L. Bradley.
3. "Matrix Deformation and Fracture in Graphite/Epoxy Reinforced Epoxies", by W.L. Bradley and R.N. Cohen.

4. "Effect of Resin Content on the Delamination Fracture Behavior of Graphite Epoxy Laminates", by W.M. Jordan and W.L. Bradley.
5. "A Molecular Model for Creep in a Viscoelastic Polymer", by J.S. Ham.
6. "A Characterization Method for a Class of Thermorheologically Complex Materials", by B.D. Harper and Y. Weitsman.
7. "On the Effects of Environmental Conditioning on Residual Stresses in Composite Laminates", by B.D. Harper and Y. Weitsman.



Texas A&M University Report No. MM 4665-83-5  
August 1983

DELAMINATION AND TRANSVERSE FRACTURE  
IN GRAPHITE/EPOXY MATERIALS\*

W.L. Bradley  
and  
R.N. Cohen\*\*

ABSTRACT

Four graphite/epoxy composite materials systems have been studied to determine the transverse and delamination fracture behavior. Measured critical energy release rates have been correlated with micromechanisms of fracture determined using in-situ fracture in a SEM and post-mortem fractographic examinations.

---

\*Published in Proc. Fourth Int. Conf. on Mechanical Behavior of Materials, Sweden, August 1983.

\*\*Now at General Dynamics, San Diego.

Texas A&M University Report No.MM 4665-83-20  
January 1983

IN-SITU FRACTOGRAPHIC STUDY  
OF GRAPHITE/EPOXY COMPOSITE MATERIALS\*

W.L. Bradley  
and  
R.N. Cohen\*\*

ABSTRACT

Fractography may be used to better understand the micromechanisms of fracture in composite materials as a guide to improving the fracture strength and toughness. However, the fracture behavior of composite materials is quite complicated and post-mortem interpretation of the artifacts on the fracture surface is not straightforward. In-situ fracture of composite materials specimens in the SEM has been used to observe directly the fracture processes and the formation of the various artifacts usually observed in post-mortem fractography. These results have clarified the significance of many of the features commonly observed on the fracture surface of composite materials.

---

\*Published in Proc. 6th Conference on Fibrous Composites in Structural Design, New Orleans, January 1983.

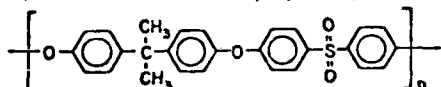
\*\*Now at General Dynamics, San Diego.

# EFFECTS OF CHAIN STIFFNESS IN A POLYSULFONE\*

by  
Joe S. Ham  
Department of Physics  
Texas A&M University, College Station, TX 77841

It is credible that short molecular chains between crosslinks in a tightly crosslinked thermosetting material will produce only a short elongation at break. However, whether longer chains between the crosslinks will permit greater elongation at break is not clear. In thermosets, as in elastomers, a greater length between crosslinks will possibly increase the elongation at break until entanglements replace the crosslinks as load bearing. Therefore, a study of entanglements in a polysulfone was part of an Air Force program to develop a family of acetylene-terminated sulfones. The polysulfone was selected to correspond to the molecular chain in the thermoset.

A sample of the commercial polyether, P-1800 (Union



Carbide), was crudely fractionated into five fractions. Dilute and concentrated solution viscosities were measured in a series of capillary viscometers using standard methods. High temperature measurements in a Rheometric Mechanical Spectrometer, using parallel plate geometry and small strains, determined the melt viscosity.

The expression  $[\eta] = 1.03 \times 10^{-3} M^{0.55}$  found by Allen and coworkers<sup>1</sup> for this polysulfone in dimethylformamide solvent determined the molecular weights from the intrinsic viscosity. They used light scattering to standardize this expression. Jenner used osmotic measurements to standardize the expression  $[\eta] = 1.22 \times 10^{-3} M^{0.59}$  in the same solvent.<sup>2</sup> If the difference between the number and weight average molecular weights is considered, these expressions are consistent. Allen and coworkers found  $M_w/M_n = 1.6$  for samples fractionated in a fashion similar to that used here. The molecular weights of the five fractions studied are shown in Table I. In addition, an unfractionated sample of low molecular weight is listed. The molecular weight listed for this sample should be considered only as indicative since it is beyond the calibration range of the equation.

Measurements of the real and imaginary parts of the complex modulus were made for each molecular weight sample over a temperature range from 280 to 380 °C. A master curve was obtained by standard shifting techniques. Measurements of fractions 3, 4 and 5 were in a spectral region where the imaginary part of the complex modulus was proportional to the frequency and the real part was proportional to the square of the frequency. This implies that the frequencies are low compared to the inverse relaxation times. Measurements at lower temperatures and thus at higher reduced frequencies involved stresses that were too large to be measured with our geometry and load cell.

Fraction 1 shows a clear deviation from the above frequency behavior in both the real and imaginary parts of the complex modulus, indicating that our range of measurements included some relaxation times in this fraction. Fraction 2 shows only a slight deviation from the frequency dependence of fractions 3, 4 and 5.

The melt viscosity involved no corrections to low frequencies in fractions 3, 4 and 5 and only a small correction in fraction 2. The melt viscosity is consistent with the often observed law  $\eta \propto M^{1.5}$ . Only fraction 1 deviated from this law with a larger viscosity due either to imprecise extrapolation to low frequencies or to the presence of a high molecular weight tail.

None of the fractions showed evidence of a viscosity

characteristic of the molecular weight range where entanglements are not important. Nor were measurements obtained that indicate a plateau region in the relaxation spectrum. Within a plateau region the steady state shear compliance determines a molecular weight between entanglements.

Ferry established that the entanglement length can be determined from the viscosity of concentrated solutions in samples that have a molecular weight larger than that between entanglements.<sup>3</sup> Grässley has criticized this approach<sup>4</sup> and he and others<sup>5</sup> have proposed theoretical models.

According to Ferry, the critical concentration multiplied by the molecular weight should be a constant. In other words, each part of a chain can give rise to an entanglement so that the onset of entanglements occurs when the product of the contour length of the chain and the polymer concentration is a critical value. This implies  $cM = \text{constant}$ .

The viscosity of each fraction was measured at various concentrations. A change in the form of the concentration dependence occurred in the solutions between the concentration of 2 and 7 g/dl. To determine the concentration at which this change occurred, the logarithm of the viscosity was plotted against the logarithm of the concentration and shifted along the concentration axis until the curves for each molecular weight would fall upon the same master curve. The concentration at which the change in dependence occurred is listed in Table I.

Table I shows that  $cM$  is not a constant but  $cM^{1/2}$  is much closer to a constant. If the volume occupied by the chains in a random walk conformation determine the critical concentration, then the total volume in the chains is proportional to  $cM^{1/2}$ . The low critical concentrations show that the chains entangle at a low polymer concentration.

Mills<sup>6</sup> described the strong forces between the sulfone groups as a possible contribution to entanglements. This is separate from the entanglements of chains wrapped around their neighbors. However, little thermodynamic interaction seems to occur between the sulfone groups in solution. Allen found the exponents in the Mark-Houwink equation almost 0.50 for three solvents. Only in chloroform does the exponent (0.72) deviate appreciably from the theoretical 0.5. The values of the second virial coefficient estimated from the concentration dependence of the dilute solution viscosity indicate little nonideality in all of the solvents. In chloroform the Flory interaction parameter is 0.37 compared to the value of 0.5 under  $\theta$  conditions. Although these thermodynamic quantities are the result of an average over all the forces between the molecules and are the differences between the solvent-polymer and the polymer-polymer forces, they show nothing unusual in the forces between the chains in several different solvents. One would not expect strong forces to cancel out in such varied solvents. Therefore, the entanglements do not appear to be due to strong forces between the sulfone groups within the polymer.

Allen has shown conclusively that the polysulfone has a random walk conformation in dilute solution. He found from the measurements of the intrinsic viscosity and from calculations assuming reasonable bond lengths and angles that  $[\eta] = (802 + 20) \times 10^{-11}$  cm. The rigid aromatic groups spread out the chain so it is unlikely to curl back upon itself, creating steric effects which limit bond angles. This produces a very low value of 2 for  $C_\infty = \langle r^2 \rangle_0 / nl^2$ .

Mills<sup>6</sup> estimated from the steady state compliance the entanglement molecular weight in the melt to lie between 2500 and 5000. Other mechanical properties supported this short entanglement length. The compressive yield stress

\*Published in Polymer Preprints, 1982.

reached a plateau value at relatively small molecular weights and the fracture toughness showed little molecular weight dependence with only the sample of molecular weight about 5300 showing an absence of plastic deformation. Bersted lists  $M_c = 6300$  and Aharoni lists  $N_c = 320$  which corresponds to  $M_c = 8600$ . These values are all high compared to the concentrated solution entanglements in this paper.

The ability of this polysulfone to entangle so readily is attributed to its stiffness. A chain may have a random walk conformation but if the rotation about the bonds is slow, it will then sluggishly change its shape. Two such chains will entangle more readily if each chain is so stiff that it cannot readily change its conformation. If a chain is completely stiff, it will entangle severely at a concentration where the chains first begin to overlap. In an undiluted polymer very little flow could occur.

Changes in conformation must occur in this polysulfone during viscous flow because the volume of the hydrodynamic spheres at the critical concentrations found in Table I show the molecules must overlap. In addition, the viscous flows in the undiluted state require changes in conformation. Yet, if these chains have some stiffness, they can entangle at low concentrations without equilibrium measurements showing strong interaction between the chains.

In contrast to this hypothesis of stiffness, Aharoni classifies polymers as flexible or rigid, using two parameters: the number of backbone chain atoms between entanglements ( $N_c$ ) and  $C_m$ . The values of  $N_c = 320$  and  $C_m = 2$  definitely classifies polysulfone with the flexible polymers. Even though a much smaller value of  $N_c$  is predicted from entanglements in concentration solution, he would continue to classify polysulfone as a flexible polymer since  $N_c = 320$  is already high compared to his best correlation for flexible polymers of  $N_c$  versus  $C_m$ . A definite value for  $N_c$  is not deduced from the data in Table I since the solutions do not follow the dependence of  $cM = \text{constant}$ .

The presence of sulfone groups in a polymer promotes a high glassy transition temperature. This high value can result from either strong forces between chains or from stiffness within a single chain so that any motion will require simultaneous movement of many atoms. If the strong intermolecular forces are excluded because of the small second virial coefficients in solution, then a stiffness of the chain could be the source of the high glassy transition temperature.

Inelastic scattering of light or neutrons should be capable of detecting stiffness within the chains. The dependence of viscosity upon shear rate should also depend upon this assumed stiffness, but the interpretation of such data is not as direct as for inelastic scattering.

Acknowledgements: Thanks are due Tim Heinrichs for taking much of the data and to T. Helminiak, C. L. Fenner, and W. F. Jones for their advice and encouragement. The experimental data were collected during two summers at the Air Force Materials Laboratory-Wright-Patterson Air Force Base and the analysis was supported in part by grant F49620-72-C-0057 from the Air Force Office of Scientific Research to Texas A&M University.

#### REFERENCES

1. G. Allen, J. McInash, and C. Strazielle, *Europ. Polymer J.* **5**, 319 (1969).
2. C. L. Fenner, unpublished results.
3. G. E. Berry and T. G. Fox, *Adv. Polymer Sci.* **5**, 261 (1967).
4. W. K. Graessley, *Adv. Polymer Sci.* **19**, 1 (1974); *Polymer* **21**, 278 (1980); W. K. Graessley and S. F. Edwards, *Polymer* **22**, 1329 (1981).

5. P. G. deGennes, *J. Chem. Phys.* **55**, 572 (1971).
6. N. J. Mills, *Rheol. Acta* **13**, 185 (1974).
7. B. H. Bersted, *J. Appl. Polymer Sci.* **24**, 37 (1979).
8. S. H. Aharoni, *Polymer Preprints* **23**, 275 (1982).

Table I

Fractions	$[\eta]$ in dl/gm.	$M_w$	$c$ in gm/dl.	$cM^{1/2}$ x $10^2$	$cM$ x $10^5$	$\log r$
1	0.628	116,000	2.63	8.96	3.05	11.9
2	0.512	80,000	3.31	9.36	2.65	10.3
3	0.480	71,000	3.63	9.67	2.58	9.7
4	0.396	50,000	4.07	9.10	2.04	8.7
5	0.24	20,000	6.91	9.77	1.38	
Low	0.15	8,600	10.7	9.92	0.92	

The viscosity is reduced to 138 °C. Sample 4 shifted differently from the higher molecular weight samples.

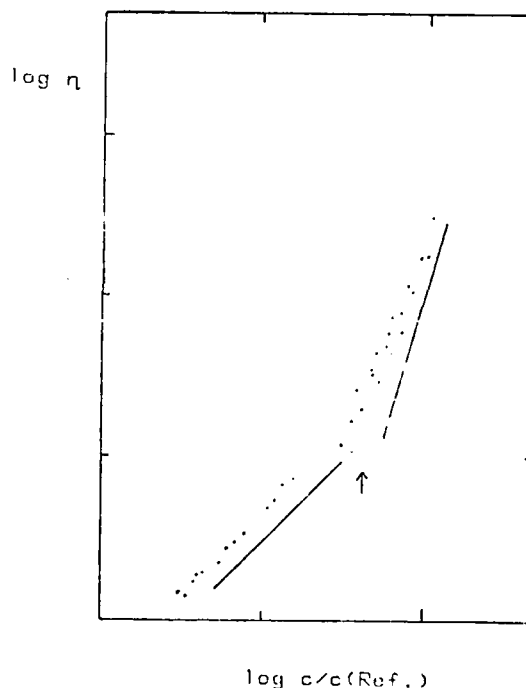


FIGURE 1. REDUCED VISCOSITY CURVES FOR CONCENTRATED SOLUTIONS OF P-1500 IN DMAC. THE CURVES HAVE BEEN SHIFTED ONLY ALONG THE LOGARITHMIC CONCENTRATION AXIS. THE LINES INDICATE SLOPES OF 1 AND 0.5.

Texas A&M University Report No. MM 4665-83-21  
1983

HEAT CAPACITY OF WATER  
ABSORBED IN METHYLCELLULOSE\*

D.A. Kinard\*\*  
and  
C.A.J. Hoeve

ABSTRACT

The heat capacity of methylcellulose is determined at various water contents over a wide range of temperatures, down to 125K. From the data the partial specific heat capacity of water has been obtained. The results show that water should be considered as a single, mobile phase. No evidence exists for bound water. Near 130K water becomes immobilized in a glassy state.

---

\*To be published in J. Polymer Science (in press).

\*\*Now at Cosden Oil and Chemical Company, Big Spring, TX

Texas A&M University Report No. MM 4665-83-2  
February 1983

CONTINUUM ASPECTS OF CRACK GROWTH IN  
TIME DEPENDENT MATERIALS\*

R.A. Schapery

ABSTRACT

The effect of time dependent rheological properties on crack growth in a class of nonlinear continua is studied. Starting with a single-integral, nonlinear viscoelastic constitutive equation for a monolithic or composite material, an elastic-viscoelastic correspondence principle is introduced, which leads to crack growth criteria expressed in terms of a generalized J integral. Rheological properties of the continuum are reflected in the value of the J integral and a creep compliance, both of which appear explicitly in the equations for time of initiation of growth and speed of continuous growth. Concluding discussions include comparison of the present results with some existing fracture models for materials which exhibit linear viscoelasticity or nonlinear transient and steady-state creep. A generalization of the theory to materials whose rheological properties account for certain types of distributed damage is given in the Appendix.

---

\*To be published in Encyclopedia of Materials Science and Engineering, Pergamon Press (in press).

CORRESPONDENCE PRINCIPLES AND A GENERALIZED J INTEGRAL FOR LARGE  
DEFORMATION AND FRACTURE ANALYSIS OF VISCOELASTIC MEDIA\*

R.A. Schapery

## ABSTRACT

Methods of quasi-static deformation and fracture analysis are developed for a class of nonlinear viscoelastic media and sample applications are given. Selection of the class of media is guided by actual rheological behavior of monolithic and composite materials as well as the need for simplicity to be able to understand the effect of primary material and continuum parameters on crack growth behavior. First, pertinent aspects of J integral and energy release rate theory for nonlinear elastic media are discussed. Nonlinear viscoelastic constitutive equations are then given, and correspondence principles which establish a simple relationship between mechanical states of elastic and viscoelastic media are developed. These principles provide the basis for the subsequent extension of J integral theory to crack growth in viscoelastic materials. Emphasis is on predicting mechanical work available at the crack tip for initiation and continuation of growth; some examples show how viscoelastic properties and the J integral affect growth behavior. Included is the problem of a crack in a thin layer having different viscoelastic properties than the surrounding continuum. The Appendix gives an apparently new constitutive theory for elastic and viscoelastic materials with changing microstructure (e.g. distributed damage) and indicates the conditions under which the fracture theory in the body of the report is applicable.

---

\*To be published in Int. J. Fracture Mechanics (in press).

Texas A&M University Report No. MM 4665-83-1  
January 1983

# ASSESSMENT OF CHEMICAL CURE-SHRINKAGE

## STRESSES IN TWO TECHNICAL RESINS\*

B.D. Harper\*  
D. Peretz\*\*  
and  
Y. Weitsman

### ABSTRACT

This paper concerns the effects of chemical cure-shrinkage on the residual stresses which arise in geometrically constrained resins. Results are presented for the FM-73U adhesive, and for the Hercules 3502 resin used in graphite/epoxy composites. It is shown that when cure occurs above the glass transition temperature  $T_g$ , like in FM-73U, the stresses are negligible. On the other hand, when cure takes place below  $T_g$ , the chemical cure-shrinkage stresses are significant.

---

\*Published in Proc. AIAA/ASME/ASCE/AHS 24th Structures, Structural Dynamics and Materials Conference, Part 1, pp. 29-35, 1983.

\*\*Now at Ohio State University.

\*\*\*Now at Armament Development Authority, Israel.



Texas A&M University Report No. MM 4665-82-12  
December 1982

ON THE THERMOVISCOELASTIC CHARACTERIZATION  
OF ADHESIVES AND COMPOSITES\*

Y. Weitsman

ABSTRACT

This paper presents a method to characterize the time and temperature behavior of adhesives and polymeric resins within the linear range of stress-strain response.

The method involves an experimental scheme to determine in a non-ambiguous way if the time-dependent behavior is thermorheologically simple or complex and provides suitable analytical expressions to predict the behavior in either case. Some experimental results are discussed and the differences between the predictions of the thermorheologically simple and complex models are assessed for the particular data at hand.

The subject is related to the design of geometrically stable structures.

---

\*Published in Progress in Science and Engineering of Composites, Proceedings of the 4th International Conference of Composite Materials, Tokyo Japan, Vol. 1, pp. 771-779, 1982.

Texas A&M University Report No. MM 4665-82-13  
December 1982

OPTIMAL COOLING OF CROSS-PLY COMPOSITE  
LAMINATES AND ADHESIVE JOINTS\*

Y. Weitsman  
and  
B.D. Harper\*\*

ABSTRACT

This paper concerns the optimal cooling of symmetric, balanced, cross-ply composite laminates and adhesive joints so as to minimize the residual thermal stresses upon termination of the cool-down process. The computations are based on a recently developed analytical scheme and employ up-to-date data on graphite/epoxy laminas. The calculations consider the thermoviscoelastic response of the polymeric resins and incorporate the temperature dependence of the coefficients of thermal expansion. It is shown that the viscoelastic behavior may contribute to a significant reduction of the residual stresses.

---

\*Published in Journal of Applied Mechanics, pp. 735-739, Dec. 1982.

\*\*Now at Ohio State University.

A SURVEY OF DAMAGE  
IN CONTINUOUS FIBER COMPOSITES

by

S.E. Groves and D.H. Allen

Aerospace Engineering Department  
Texas A&M University, College Station, TX 77843

ABSTRACT

In this paper a brief detail of some of the past and present work related to the characterization of damage is discussed. The objective of this survey was to obtain a solid foundation on the difficulties and current techniques in damage modeling. The goal of the current on-going research is to develop a precise damage model for continuous fiber graphite/epoxy laminates subjected to complex load histories.

# A SURVEY OF DAMAGE IN CONTINUOUS FIBER COMPOSITES

## Introduction

Composite materials have for some time been known for their extreme efficiency of strength to weight in application to aerospace structures. Nevertheless, up to this time their application to aerospace structures has been limited to so-called non-critical areas because of a lack of understanding of the behavior of composite materials subjected to fatigue type load histories. The amount of material degradation, damage, or loss in strength and stiffness over any complex load history is extremely vital if the structural designer is to maximize the use of composite materials. The goal of the current research is to develop a precise damage model for some specific composite materials, mainly continuous fiber graphite epoxy laminates. It is therefore the objective of this section to briefly detail some of the past and present work related to the characterization of this damage state.

In surveying the literature on composite damage one finds a variety of available material. Past research has been primarily experimental and has concentrated on detailing the various types of damage and their possible causes. There has also been a considerable amount of work in analytically modeling a specific damaged mode. This consists of determining the stress and deformation fields of the damaged area. Only recently has significant attention been given to actually predicting the resulting damage state from a specified load history.

In detailing these various stages of damage modeling, four main categories will be covered and in doing so no real attempt will be made to follow a chronological order. These four categories are: 1) experimental observation of damage, 2) analysis of stress and deformation in damage laminates, 3) general analytic theory, and 4) prediction of damage.

### Experimental Observation of Damage

This section will be concerned with describing the various types of damage generally found in continuous fiber composites as well as some of the experimental techniques used to observe them. Also mentioned will be some of the various sources of damage data available in the literature.

There are five main types of cumulative damage which have been observed and which are of interest in the damage model. These are as follows: matrix dominant transverse cracking, spherical cavitation, interlaminar delamination, fiber-matrix debonding, and fiber breaking. These five types of damage can further be divided into fatigue damage or quasi-static. Fatigue damage will be defined as that damage which causes a reduction of residual strength of a laminate below the quasi-static loading value [3]. Combined tension-compression loadings seem to degrade strength properties more readily [5], assuming the loads are well below buckling loads. This area will be treated only lightly in developing the model. Transverse cracks are small macro cracks and are generally situated normal to the fiber direction [1,2,4]. It has been observed that as this type of damage accumulates in a laminate, i.e., an increase in the density of cracks, during fatigue loading, a saturation density of cracks is reached. This saturation density of cracks is defined as the characteristic damage state (CDS), (see Fig. 1), and implies a stable or equilibrium state for the laminate [1,3]. The CDS is hypothesized to be a laminate property controlled by the properties of the individual laminate and its corresponding stacking sequence. The CDS occurs in both fatigue damage and monotonic loading, however, it is usually undeveloped in the quasi-static case. Transverse cracking may imply two different mechanisms. It can be a relief for locally high stress concentrations, or it may be a source

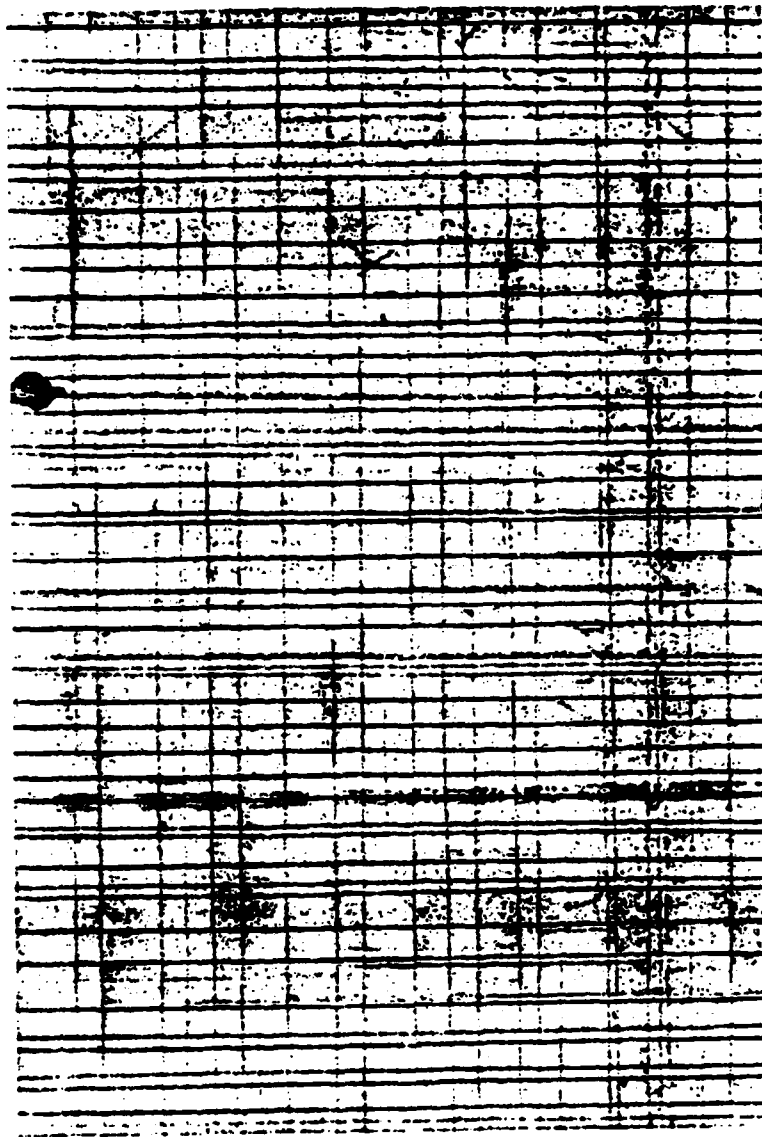


Fig. 1: Radiograph of a  $[0,90_2]_s$  graphite epoxy laminate shows a high saturation of transverse cracks as well as some internal delaminations which appear as darkened areas in the lower third of the picture [ref. 93].

generator of the stress concentrator if present due to localized failure or fabrication flaw. Thus two levels of crack parameters might be necessary. Initial fabrication flaws or cracks caused by residual stresses from post cure, or micro cracks formed during peak stresses.

Spherical cavitation is the formation of very small spherical voids in the matrix (0.1 - 0.2  $\mu\text{m}$  in diameter). One cause of these voids results from deformation of second phase elastomer particles followed by their rupture and cavitation [6]. It is also possible these spherical voids are present due to post cure residual effects. These small voids directly decrease the overall strength and stiffness of the laminate by only a small amount. However, due to a small loss in cross-sectional area several voids may coalesce and form a transverse crack which is in general a more serious type of damage. It is unknown at this point whether a saturation density of spherical voids occurs.

Interlaminar delamination occurs when two plies of a laminate begin to debond or separate, see Figure 1. This separation is generally caused by the interlaminar normal stresses which develop between the plies [7] and usually initiates at the free edge [8,9,10]. Delamination generally results in loss of strength, stiffness, and life in the composite laminate. Currently there is substantial research being conducted to develop matrix resins with improved resistance to delamination. One current method is to include liquid and solid elastomers in the resin compounds.

A laminate property associated with delamination is the interlaminar fracture toughness,  $G_c$ . The fracture toughness is defined to be the critical value of the strain energy release rate,  $G$ , necessary for the delamination to propagate. The strain energy release rate,  $G$ , represents the energy lost

per unit area when a delamination creates new surface area [6]. Considerable research has been performed to characterize  $G_c$  as well as to calculate  $G$  for various laminates and crack geometries [6,11,12,13,14,15,16,17].

Fiber matrix debond or breakage is simply the failure or pulling out of the individual fibers of the composite laminate. Fiber breakage is caused by high tensile stresses in local regions of the laminate or by local shearing in the matrix. In separate form high strength composite fibers are extremely brittle and easy to break in shear. Ultimate failure of a laminate occurs when all fibers have broken.

Most of the damage that occurs in a laminate during static or fatigue loading usually occurs in subcritical elements, i.e., off axis plies. However, this resulting damage must redistribute the stresses in order to maintain equilibrium, and thus affects the overall structural integrity of the laminate, i.e., the stiffness, etc., and thus ultimate failure behavior. If critical enough, this resulting state of damage can lead to more damage and might be stable or unstable. Stable damage would lead to the characteristic damage state whereas unstable damage causes rapid failure of the laminate, see Figure 2 for a flaw diagram of damages. And so as with all composite laminates, highly dependent on the orientation of the plies, stacking sequence, and material properties. Even in quasi-isotropic laminates different stacking sequences affect the damage, unlike the self similar manner in which damage occurs in metallic structures [1]. Thus, damage is more complex in composites than in metals, but not necessarily as critical.

There are a wide variety of experimental techniques used to observe the five types of damage previously mentioned. Some of these methods are ultrasonics, acoustic emission, x-ray radiography, stereo radiography, thermography,



## FLOW CHART OF DAMAGE

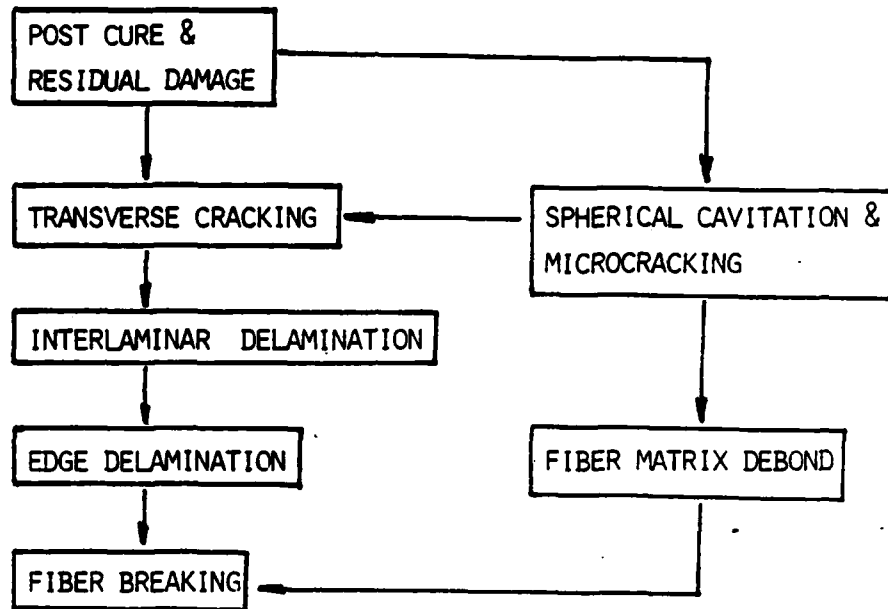


Fig. 2: Flow Chart of Damage

die penetrants, holography, stiffness measurements, edge replication, Moire Interferometry, SEM, TEM, and deplying techniques [1,3,4,18,19,20,21,22,23]. These methods can be classified in either of two types, nondestructive testing (NDT) and destructive testing. The advantages of NDT are obvious, however, initially one must verify the NDT techniques through destructive testing.

The field of ultrasonics concerns the use of acoustic waves of low intensity and high-frequency sound energy [92] to detect internal flaws as well as actually determine various material properties. Basically the technique uses transducers to propagate as well as receive the acoustic waves. The received acoustic wave through interaction of damage loses some of its energy. A common ultrasonic technique is called C-scan. This method uses a continuous pulsing transducer which can scan a specified surface. Energy losses in the acoustic wave are translated to voltage changes supplied to an electronic pen. The major set back of this method is that the depth of the actual flaw is not easily distinguished. Another application of ultrasonics is to carefully examine the received acoustic wave. An internal flaw will show up as a deviation from the standard wave of an undamaged material. This method would require an extreme amount of destructive correlation.

Acoustic emission is the study of the stress waves emitted during creation of internal flaws or damage [2]. However, one must always monitor the material to determine the extent of damage and thus vast amounts of data must be analyzed and correlated which presently has been unattainable.

X-ray radiography is the use of soft x-rays to determine a detailed map of the internal damage across a given width. X-ray stereo radiography provides even more information, yielding some detail of damage through the thickness [2] provided the damage is in a relatively uncomplicated state, i.e.,

a transverse crack, delamination, etc. A stereo radiography is developed by viewing two slightly different orientated images of an object at the same time. This produces a perception of depth which allows one to distinguish the various types of damage.

Thermography is the technique of visualizing the surface temperatures on an object. As internal damage is formed heat is created which can be recorded using a video thermographic camera [2,19]. Again, as with an NDT technique, rigorous correlation with destructive testing is required to distinguish the damage modes. Similar problems occur less with acoustic emission. Continuous testing is required for mapping the damage.

Dye penetrants are used to enhance the damage state present within a composite laminate so as to make it easier to ascertain the given damage. These penetrants are generally used along with x-ray stereo radiography. They are also used with deplying techniques to identify a given damaged area.

Deplying is a destructive testing method by which the composite laminate is heated to very high temperatures (about 700°F for graphite epoxy) to loosen or destroy the bonding between the individual plies of the laminate. Examination of these individual plies after deplying, if successful, can yield valuable information about the actual damage which developed on the composite laminate. An alternate form of deplying is to place the laminate in liquid nitrogen which freezes and marks various modes of damage. This method requires a highly delaminated laminate which can be pulled apart with sudden application of force.

Direct stiffness measurement has also been used to measure the damage in a composite laminate. This technique does not reveal the type or location of the actual damage but instead attempts to measure overall amount of

damage present. This technique is highly questionable because damage can exist without actually affecting the stiffness, while affecting other material properties.

Edge replication is a technique used to record or imprint the surface topography at the edge of a laminate [2,93]. To develop the replication one requires cellulose acetate tape and a softening agent such as acetone. Once the edge surface has been prepared or polished the softened tape is pressed against the surface to record the topography. The acetone is then allowed to evaporate and a permanent record of damage is obtained. A microfiche reader can be used to examine the detail of the tape. In order to gain more information about the meaning of the replication, correlation with destructive sectioning would be required. It has been shown in some cases that the edge replication is a good indication of the internal damage.

Moire Interferometry can be used to study the crack-tip deformation and in particular actual deformations on a laminate surface [94,95]. The ability to measure surface deformations should prove invaluable in reasoning the damage process. The Moire fringe pattern is obtained by using two gratings which must be overlaid. One of the gratings is used for the reference. The fringes are then produced by transmitting light through the overlay. The accuracy of the fringe pattern is related to the definition or spacing in the grid pattern.

Scanning electron microscopy, SEM, and transmission electron microscopy, TEM, can be used to achieve extremely detailed micrographics of a specified damage area. This method is usually a destructive technique requiring the laminate to be sectioned and polished for use in the microscope. The SEM and TEM are generally used more for correlation of the various nondestructive test methods rather than actual damage measurement.

No NDT technique discussed thus far has been shown to be sufficiently adequate for measuring the actual forms of damage in a laminate. More correlation would be required with destructive test in order to develop a useful NDT. One of the major problems with any NDT measure of internal damage can be the local anisotropy or non-uniform distribution size of fibers in a given laminate as shown by the micrographs in Figure 3. This local non-uniformity alone may be enough, under a given load, to create local high stresses or failure of the resin material or fiber which may be sufficient to create or drive local cracks.

Sources of experimental data on damage to composite laminates are somewhat limited because the extreme variability of damage requires many experimental tests to be repeated. In order to have a useful damage model one would prefer to use the least amount of experimental input possible. This is a formidable task due to the vast amount of different material properties available. Sources of data encountered in this research are contained in the following references [1,4,5,6,11,12,13,24,25,26,27,28,93].

#### Analysis of Stress and Deformation in Damaged Laminates

This section will be concerned with describing the various numerical and analytic methods used to model the stress and deformation fields for specific damage states in composite laminates. Current methods used to analyze the damaged area are finite elements, finite difference, analytical, shear lag, and modified classical lamination theory.

The use of finite element methods (F.E.M.) as well as finite differences to solve for the stress and deformation fields in solid composite bodies have been utilized often in the literature. Although finite difference techniques give accurate solutions and yield full field solutions, i.e., all 6 stress

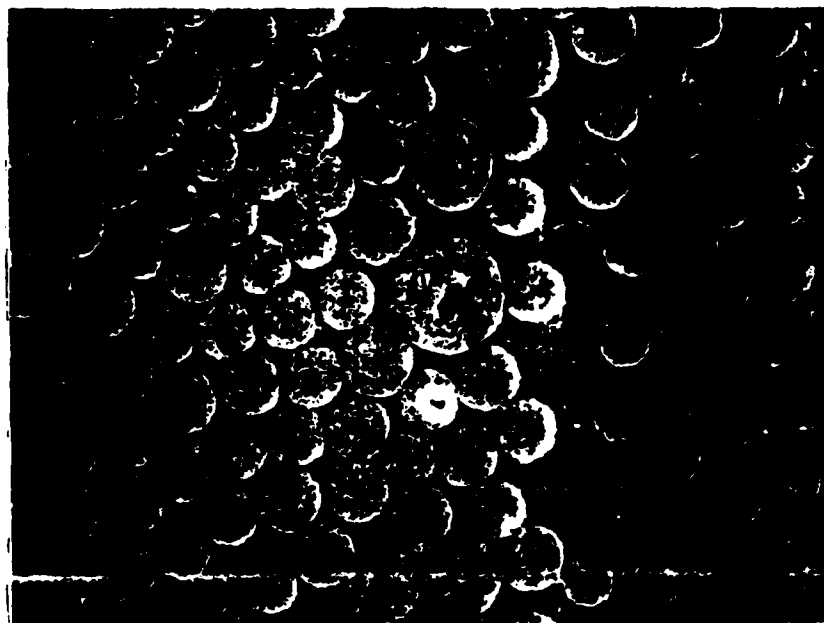
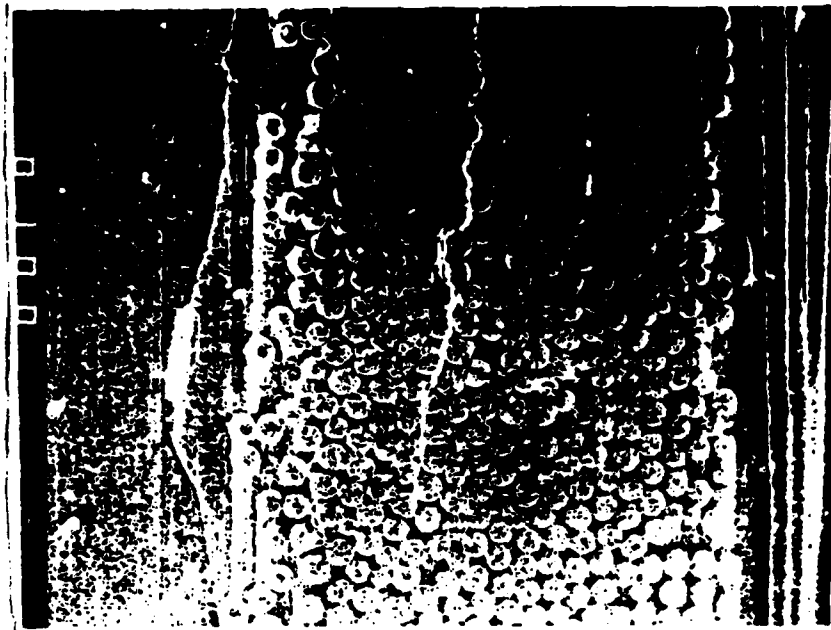


Fig. 3: Typical micrographs of graphite/epoxy laminate [ref. 96].

components, they are limited in user ability and require larger core computer memory than finite element techniques [4,29]. There has been much F.E.M. research in both undamaged and damaged composite laminates. This research ranges from 2-D analysis to quasi-3D analysis to full 3-D analysis incorporating several methods ranging from simple constant strain triangular elements (CST's) to advanced hybrid stress finite elements with complex crack geometries [1,6,11,12,13,14,16,30,31,32,33,34,35,36].

The results from these models range from solutions for the strain energy release rates [6,11,12,13,14,15,16,17] for given cracks or delaminations, to the CDS [1,4,36] to stress intensity factors [30,31,34,35]. One analytical technique consists of simple fracture mechanics principals applied to simple beam geometries, etc., to solve for strain energy release rates and stress intensity factors [37]. Another analytic technique is shear lag modeling [38]. Shear lag is based on the stress singularity which arises near a transverse crack and which exponentially dies out some distance away from the crack. As the stress singularity dies out, it is possible for a new crack to form and this in turn leads to the CDS.

Modified classical lamination theory consists of modifying the properties of a specified ply or region in a laminate to reflect damage or degradation in stiffness and strength and thus modify the overall global response [6,12,13,14,17]. This usually results in globally averaged laminate properties for the damaged laminate. A rule of mixtures approach is sometimes incorporated to modify the laminate. This technique does not lend itself very well to general B.V.P., i.e., irregular geometries or detailed analysis of specified regions.

Comparing all of the solution techniques, the F.E.M. seems to be the most appropriate technique for solving damage problems. This is due to the ability of the F.E.M. to handle diverse boundary conditions. However, over the course of the research to come, it may become necessary to use more than one method.

#### General Analytic Theory

This section will briefly discuss some of the analytical techniques which have some connection to the modeling or prediction of damage. Most of the pure analytic damage models have their roots in classical fracture mechanics associated with isotropic metals with special closed form solutions to simple single crack geometries [39,40,41,42,43,44,45,46,47,48,49]. Other analytical models are based on linear and nonlinear viscoelastic theories such as those of Schapery [50]. This work was followed by application of fracture mechanics to composites [51]. Again, these studies are very specialized. Erdogan and Gupta [40] have examined an interface flaw and Sih, et al., [49] have studied interaction of works with fibers and the effect of fiber volume fraction on crack behavior. More recently Wang and Choi [52,53] have studied the interface crack between dissimilar anisotropic composite materials. All of the theories discussed generally result in singular integral equations which make application of them to modeling cumulative damage very difficult, especially the characteristic damage state. The difficulties associated with the crack problem in composites involves not only the singular crack-tip stress but also the significant coupling between inplane and interlaminar deformations, that is the simultaneous existence of mode I, mode II, and mode III fracture due to material anisotropy [52].



### Prediction of Damage

The development of cumulative damage models has followed three paths; 1) fracture mechanics, 2) empirical, and 3) internal state variable theories based on thermodynamics.

Fracture mechanics has been incorporated by Chou, Wang, and Miller [25, 26,36], Backlund [54], and Schapery [55,56,57], as well as many others. Chou, et al., first investigated the initiation and growth processes of transverse cracking and edge delamination. Their experimental observations suggest that monotonic and fatigue damage are similar and imply the concept of a constant damage state. Their damage model incorporates growth rate equations based on fracture mechanics and are somewhat similar to Miner's rule. A computer program using a "Monte Carlo" simulation has been incorporated to simulate an actual damage development. This model is also largely empirical because it requires the determination of many material parameters and thus considerable experimental data.

Backlund [54] investigated a method called the fictitious crack model which essentially examines notches or cracks which develop near stress concentrations. This fictitious crack more accurately represents a damaged zone rather than a typical sharp crack and its basic principle is to gather all microcracks and local fractures into a fictitious crack. Some of the earlier work applying fracture mechanics to composites was done by Waddoups, et al. [59], Hahn [60], Morris and Hahn [61], and Brinson, et al. [62,63,64].

Schapery [55,56,57,58] has applied both fracture mechanics and nonlinear viscoelasticity to nonhomogeneous media. Developed therein are single integral nonlinear equations for predicting the behavior of the media. These equations are generally difficult to solve. Particulate composites such as

solid rockets propellants are emphasized, although it is believed these equations are general enough to be applicable to continuous fiber composites. The damage modeled is microcracking and growth is predicted using the J integral theory developed for viscoelasticity. This theory, as with Chou, et al. and others, is still lacking extensive experimental verification.

Empirical or heuristic attempts at modeling damage have been numerous. The major drawback emanates from no sound physical bases as well as in general requiring voluminous experimental data. Usually, these theories tend to be very specific in form.

Chou and Croman [65] developed a model based on the equal rank assumption which was first introduced by Hahn and Kim [66]. The equal rank assumption implies that the rank in the fatigue life distribution is the same as that rank in the static case. Hahn and Kim developed their model without regards to any specific crack but instead developed empirical relations for the global decrease in residual strength. This contains some merit because individually examining or predicting each crack in a damaged laminate would be fruitless. Chou and Croman found this model to be overly restrictive. They inserted an open empirical fit parameter to accomodate different residual strength distributions. Yuan-Sheng [67] developed a model based on an effective cross-sectional area reduction which was applied to concrete. This area reduction was tied to the variation in the stress. The damage parameter is evaluated using Kachanov's hypothesis [68]. Even though this damage parameter was not developed for composites and thus has no experimental correlation, it too contains some merit because if one recalls, the formation of the characteristic damage state or even one transverse crack in the laminate it is obvious there is a slight reduction in cross section with each crack.

Hashin and co-workers [69-79] have studied and developed various techniques for modeling damage. One of their first attempts [69-70] consisted of a series of damage curves or surfaces and equivalent loading conditions (similar to equal rank assumption). These curves are based on the familiar S-N curves for metal fracture, where S is the stress amplitude and N is the number of cycles to failure at a given stress, S. A Miner's rule type derivative is used to predict resulting global damage. Again, considerable experimental data are necessary to characterize the damage surfaces. Later work has concentrated on obtaining effective material properties due to accumulation of cracks [71-74]. Upper and lower bounds on these effective properties have been determined using variational theorems of elasticity and globally averaged properties. Next, failure criteria have been developed in terms of quadratic stress polynomials [75-79]. These polynomials have been expressed in terms of the transversely isotropic stress invariants and globally averaged stresses. These polynomials along with much experimental data are used to construct the damage surfaces. No experimental correlation is given for this model.

Researchers at General Dynamics [27] have also looked at damage modeling. However, most of this work is in early stages and more or less a damage program outline. Initial work has established a methodology of cumulative damage mechanisms. A crude model has been developed which uses a damage rate modifier equation similar in form to Miner's equation.

Internal state variable theories based on thermodynamics and continuum mechanics have recently begun to appear in the area of cumulative damage modeling. These theories proceed from the assumption that one or more internal state variables characterized by continuum mechanic or thermodynamic constraints can be incorporated to describe the state of damage within the

composite laminate. These internal state variables may be scalar, vector, or possibly tensor valued damage parameters. It is believed that the damage functions must be at least vector valued because a scalar field assumes that the orientations of the cracks or damage has no effect on the global response.

Talreja [83,84] proposed that damage in a composite material can be modelled by a set of independent vector fields based on continuum mechanics. He follows the approach laid out by Coleman and Noll [85], Coleman and Gurtin [86] and Truesdell and Toupin [87]. An actual microphysical definition of the damage vectors is not given, however their respective magnitudes are proportional to the number of cracks per unit volume, the average area of the crack surface, and a crack shape parameter. No experimental correlation is given for this model. Krajcinovic and Fonseka [88,89,90] have developed a damage law based on general thermodynamics and derived from a dissipation potential related to the stress intensity factors. However, this theory is applied only to perfectly brittle materials and not composites. One of the damage variables is very similar to the evolution of the plastic strain in metals. Again, no experimental correlation is given. Allen [91] proposes a model based on a continuum/thermodynamics approach. As with the two previous models the damage is characterized by a set of internal state variables which in turn are reflected through the local constitutive equations. A set of energy dissipative local functions reflect the energy of cracking is proposed for characterizing the internal state variables. A unique feature of this model is that the local damage variables as well as the constitutive equations are globally averaged over the volume of the laminate in question. The resulting globally averaged internal state variables of damage are vector valued history dependent functions. This approach appears to be very promising, even though no current experimental correlation is given for the proposed model.

### Conclusion

Many models and techniques have been discussed in brief detail, however one should by now realize that no one damage model or experimental observation technique has been shown to be adequate in predicting the accumulation of damage in a composite material. One can only hope that through careful rigorous model development and extensive experimental support can a useful model be developed. This effort must obviously be supported by the almost endless supply of knowledge from the research community.

## REFERENCES

1. Stinchcomb, W.W., Reifsnider, K.L., Yeung, P., and Masters, J., "Effect of Ply Constraint on Fatigue Damage Development in Composite Material Laminates," Fatigue of Fibrous Composite Materials, ASTM STP 723, pp. 65-84.
2. Reifsnider, K.L., Henneke, E.G., Stinchcomb, W.W., and Duke, J.C., "Damage Mechanics and NDE of Composite Laminates," Mechanics of Composite Materials, 1982, pp. 399-420.
3. Reifsnider, K.L. and Jamison, K., "Fracture of Fatigue-loaded Composite Laminates," Int. J. Fatigue, October 1982, pp. 187-197.
4. Highsmith, A.L., Stinchcomb, W.W., and Reifsnider, K.L., "Stiffness Reduction Resulting From Transverse Cracking in Fiber-Reinforced Composite Laminates," VPI-E-81.33, Virginia Polytechnic Institute, November 1981.
5. Starnes, J.H. and Williams, J.G., "Failure Characteristics of Graphite-Epoxy Structural Components Loaded in Compression," NASA TM 84552, September 1982.
6. O'Brien, T.K., Johnston, N.J., Morris, D.H., and Simonds, R.H., "A Simple Test For the Interlaminar Fracture Toughness of Composites," SAMPE Journal, July/August 1982, pp. 8-15.
7. Pipes, R.B. and Pagano, N.J., "Interlaminar Stresses in Composite Laminates Under Uniform Axial Tension," J. Composite Materials, Vol. 4, October 1970, pp. 538-548.
8. Wang, A.S.D. and Crossman, F.W., "Some New Results on Edge Effects in Symmetric Composite Laminates," J. Composite Materials, Vol. 11, January 1977, pp. 92-106.
9. Spilker, R.L. and Chou, S.C., "Edge Effects in Symmetric Composite Laminates: Importance of Satisfying the Traction-Free-Edge Condition," J. Composite Materials, Vol. 14, January 1980, pp. 2-19.
10. Altus, E., Rotem, A., and Shmveli, M., "Free Edge Effect in Angle Ply Laminates - A New Three Dimensional Finite Difference Solution," Journal Composite Materials, Vol. 14, January 1980, pp. 21-30.
11. Wang, S.S. and Wang, H.T., "Interlaminar Crack Growth in Fiber Reinforced Composites During Fatigue," Journal of Engineering Materials and Technology, Vol. 101, January 1979, pp. 34-41.
12. O'Brien, T.K., "The Effect of Delamination on the Tensile Strength of Unnotched Quasi-Isotropic, Graphite/Epoxy Laminates," Proc. 1982 Joint Conference on Experimental Mechanics, SESA and JSME, May 23-28, pp. 236-243.

13. O'Brien, T.K., "Characterization of Delamination Onset and Growth in a Composite Laminate," Damage in Composite Materials, ASTM STP 775, 1982, pp. 140-167.
14. O'Brien, T.K., "Mixed Mode Strain-Energy Release Rate Effects on Edge Delamination of Composites," NASA TM 84592, January 1983.
15. Han, K.S. and Koutsky, J., "The Interlaminar Fracture Energy of Glass Fiber Reinforced Polyester Composites," J. Composite Materials, Vol. 15, July 1981, pp. 371-388.
16. Rybicki, E.F., Schmueser, D.W., and Fox, J., "An Energy Release Rate Approach For Stable Crack Growth in the Free-Edge Delamination Problem," J. Composite Materials, Vol. 11, October 1977, pp. 470-487.
17. Arenburg, R.T., "Analysis of the Effect of Matrix Degradation on Fatigue Behavior of a Graphite/Epoxy Laminate," Thesis, Texas A&M University, May 1982.
18. Chatterjee, S.N., Hashin, Z., and Pipes, R.B., "Definition and Modeling of Critical Flows in Graphite Fiber Reinforced Resin Matrix Composite Materials," MSC TFR 1105/1008, NADC-77278-30, Naval Air Development Center, August 1979.
19. Wilson, D.W. and Charles, J.A., "Thermographic Detection of Adhesive-bond and Interlaminar Flaws in Composites," Experimental Mechanics, July 1981, pp. 276-280.
20. DeCharentenay, F.X., Bethmont, M., Benzeggagh, M., and Chretien, J.F., "Delamination of Glass Fiber Reinforced Polyester, An Acoustic Emission Study," Mechanical Behavior of Materials, Vol. 13, ICM 3, August 1979, pp. 241-251.
21. DeCharentenay, F.X., Harry, J.M., Prel, Y., and Benzeggagh, M., "Characterizing the Effect of Delamination Defect By Mode I Delamination Test," Effect of Defect in Composite Materials, ASTM STP XXX, 1983.
22. DeCharentenay, F.X., Kamimura, K., and Lemascon, A., "Fatigue Delamination in Unidirectional Carbon-Epoxy Composites," Proc. of Fatigue '81, Materials, Experimentation, and Design in Fatigue, pp. 199-209.
23. Oplinger, D.W., Gandhi, K.R., and Parker, B.S., "Studies of Tension Test Specimens for Composite Materials Testing," AMMRC TR 82-27, Army Materials and Mechanics Research Center, April 1982.
24. Wu, E.M., Moore, R.L., and Nguyen, N.Q., "Matrix-Dominated Time-Dependent Deformation and Damage of Graphite Epoxy Composite Experimental Data Under Ramp Loading," AFWAL-TR-82-3076, Air Force Wright Aeronautical Laboratories, November 1982.
25. Chou, P.C. and Wang, A.S.D., "Cumulative Damage Model for Advanced Composite Materials," Interim Tech Report 4, Contract No. F33615-80-C-5039, Air Force Wright Aeronautical Laboratories, February 1983.

26. Chou, P.C. and Wang, A.S.D., "Cumulative Damage Model for Advanced Composite Materials," Interim Tech. Report 3, Contract No. F33615-80-C-5039, Air Force Wright Aeroanautical Laboratories, August 1982.
27. General Dynamics, "Cumulative Damage Model for Advanced Composite Materials," Progress Report No. 3, Contract No. F33615-81-C-5049, Air Force Materials Laboratory, September 1982.
28. Whitcomb, J.D., "Experimental and Analytical Study of Fatigue Damage in Notched Graphite/Epoxy Laminates," Fatigue of Fibrous Composite Materials, ASTM STP 723, 1981, pp. 48-63.
29. Talug, A., "Analysis of Stress Fields in Composite Laminates With Interior Cracks," Thesis, Doctor of Philosophy, College of Engineering, Virginia Polytechnic Institute, September 1978.
30. Rybicki, E.F. and Kanninen, M.F., "A Finite Element Calculation of Stress Intensity Factors by a Modified Crack Closure Integral," Engineering Fracture Mechanics, Vol. 9, 1977, pp. 931-938.
31. Kobayashi, A.S., "Numerical Analysis in Fracture Mechanics," UWA/DME/TR-83/45, ONR, January 1983.
32. Melosh, H.J. and Raetsky, A., "A Simple and Efficient Method for Introducing Faults into Finite Element Computations," Bulletin of the Seismological Society of America, Vol. 71, October 1981.
33. Kobayashi, A.S., "Hybrid Experimental-Numerical Stress Analysis," UWA/DME/TR-83/47, ONR, April 1983.
34. Sandhu, R.S., Sendeckyj, G.P., and Gallo, R.L., "Modelling of the Failure Process in Notched Laminates," Mechanics of Composite Materials, 1982, pp. 179-189.
35. Kanninen, M.F., Rybicki, E.F., Griffity, W.I., and Broek, D., "Fundamental Analysis of the Failure of Polymer-Based Fiber Reinforced Composites," NASA-CR-2689.
36. Chou, P.C., Wang, A.S.D., and Miller, H., "Cumulative Damage Model for Advanced Composite Materials," AFWAL-TR-82-4083, Air Force Wright Aeroanautical Laboratories, April 1982.
37. Devitt, D.F., Schapery, R.A., and Bradley, W.L., "A Method for Determining the Mode I Delamination Fracture Toughness of Elastic and Viscoelastic Composite Materials," J. Composite Materials, Vol. 14, October 1980, pp. 270-285.
38. Reifsnider, K.L., "Some Fundamental Aspects of the Fatigue and Fracture Response of Composite Materials," Proc. 14th Annual Society of Engineering Science Meeting, Lehigh University, November 14-16, 1979.
39. Liebowitz, H., Subramonian, N., and Lee, J.D., "Mechanics of Fracture - Fundamentals and Some Recent Developments," Israel Journal of Technology, Vol. 17, 1979, pp. 273-294.



40. Erdogan, F. and Gupta, G.D., "Layered Composites With an Interface Flaw," Int. J. Solids Structures, Vol. 7, 1971, pp. 1089-1107.
41. Rice, J.R. and Rivlin, A.L., "Stability of Steady Frictional Slipping," Journal of Applied Mechanics, 83-APM-16, June 1983.
42. Rice, J.R., "A Path Independent Integral and the Approximate Analysis of Strain Concentration by Notches and Cracks," Journal of Applied Mechanics, June 1968, pp. 379-389.
43. Kinra, V.K. and Vu, B.Q., "Brittle Fracture of Plates in Tension - Virgin Waves and Boundary Reflections," Journal of Applied Mechanics, Vol. 47, March 1980, pp. 45-50.
44. Badaliance, R. and Sih, G.C., "An Approximate Three-Dimensional Theory of Layered Plates Containing Through Thickness Cracks," Engineering Fracture Mechanics, 1975, Vol. 7, pp. 1-22.
45. Tada, H., Paris, P.C., and Irwin, G.R., The Stress Analysis of Cracks Handbook, Del Research Corporation, Hellertown, Pennsylvania, 1973.
46. Altus, E. and Rotem, A., "A 3-D Fracture Mechanics Approach to the Strength of Composite Materials," Engineering Fracture Mechanics, Vol. 14, pp. 637-644.
47. Chen, E.P. and Sih, G.C., "Stress Intensity Factor For a Three-Layered Plate With a Crack in the Center Layer," Engineering Fracture Mechanics, Vol. 14, pp. 195-214.
48. Sih, G.C. and Chen, E.P., "Sudden Stretching of a Four-Layered Composite Plate," Engineering Fracture Mechanics, Vol. 15, 1981, pp. 243-252.
49. Sih, G.C., Hilton, P.D., Badaliance, R., Shenberger, P.S., and Villarreal, G., "Fracture Mechanics for Fibrous Composites," Analysis of the Test Methods for High Modulus Fibers and Composites, ASTM STP 521, 1973, pp. 98-132.
50. Schapery, R.A., "Correspondence Principles and a Generalized J-Integral For Deformation and Fracture Analysis of Nonlinear Viscoelastic Media," MM 3724-80-16, Air Force Office of Scientific Research, November 1980.
51. Alexander, R.M., Schapery, R.A., Jerina, K.L., and Sanders, B.A., "Fracture Characterization of a Random Fiber Composite Material," MM 1979-80-20, Texas A&M University, April 1980.
52. Wang, S.S. and Choi, I., "The Interface Crack Between Dissimilar Anisotropic Composite Materials," Journal of Applied Mechanics, 83-APM-6, Transactions of the ASME, June 1983.
53. Wang, S.S. and Choi, I., "The Interface Crack Behavior in Dissimilar Anisotropic Composites Under Mixed-Mode Loading," Journal of Applied Mechanics, 83-APM-7, Transactions of the ASME, June 1983.

54. Backlund, J., "Fracture Analysis of Notched Composites," Computers and Structures, Vol. 13, pp. 145-154, 1981.
55. Schapery, R.A., "A Method for Predicting Crack Growth in Nonhomogeneous Viscoelastic Media," Int. Journal of Fracture, Vol. 14, 1978, pp. 293-309.
56. Schapery, R.A., "On Viscoelastic Deformation and Failure Behavior of Composite Materials With Distributed Flaws," Advances in Aerospace Structures and Materials, AD-01, 1981, pp. 5-20.
57. Schapery, R.A., "Models for Damage Growth and Fracture in Nonlinear Viscoelastic Particulate Composites," MM 3168-82-5, Mechanics and Materials Center, Texas A&M University, August 1982.
58. Schapery, R.A., "Continuum Aspects of Crack Growth in Time Dependent Materials," MM 4665-83-2, Texas A&M University, February 1983.
59. Waddoups, M.E., Eisenmann, J.R., and Kaminski, B.E., "Macroscopic Fracture Mechanics of Advanced Composite Materials," J. Composite Materials, Vol. 5, pp. 446-454, 1971.
60. Hahn, H.T., "Fracture Behavior of Composite Laminates," Proc. Int. Conference on Fracture Mechanics and Technology, Sigthoff, Noordhoff, Hong Kong, 1977.
61. Morris, D.H. and Hahn, N.T., "Fracture Resistance Characterization of Graphite/Epoxy Composites," In Composite Materials: Testing and Design, ASTM STP 617, pp. 5-17, 1977.
62. Brinson, H.F. and Yeow, Y.T., "An Experimental Study of the Fracture Behavior of Laminated Graphite/Epoxy Composites," Composite Materials: Testing and Design, ASTM STP 617, pp. 18-38, 1977.
63. Yeow, Y.T., Morris, D.H., and Brinson, H.F., "The Fracture Behavior of Graphite Epoxy Laminates," Experimental Mechanics, Vol. 19, pp. 1-8, 1979.
64. Yeow, Y.T., Morris, D.H., and Brinson, H.F., "A Correlative Study Between Analysis and Experiment on the Fracture Behavior of Graphite/Epoxy Composites," Journal Testing Evaluation, Vol. 7, pp. 117-125, 1979.
65. Chou, P.C. and Croman, R., "Residual Strength in Fatigue Based on the Strength-Life Equal Rank Assumption," Journal Composite Materials, Vol. 12, April 1978, pp. 177-194.
66. Hahn, H.T. and Kim, R.Y., "Proof Testing of Composite Materials," Journal Composite Materials, Vol. 9, July 1975, pp. 297-311.
67. Yuan-Sheng, C., "A Review on the Law of Continuous Damage for Non-Aging Materials," Engineering Fracture Mechanics, Vol. 17, 1983, pp. 211-217.

68. Odqvist, F.K.G., On Theories of Creep Rupture, Second-Order Effects in Elasticity, Plasticity, and Fluid Dynamics, Edited by M. Reiner and D. Abir, MacMillan, New York, 1964.
69. Hashin, Z. and Rotem, A., "A Cumulative Damage Theory of Fatigue Failure," AFOSR 76-3015, TAU-SOE/395-77, February 1977.
70. Hashin, Z. and Laird, C., "Cumulative Damage Under Two Level Cycling: Some Theoretical Predictions and Test Data," N00014-78-C-0544, TR-3, August 1979.
71. Hashin, Z., "Analysis of Properties of Fiber Composites With Anisotropic Constituents," Journal of Applied Mechanics, Vol. 46, September 1979.
72. Gottesman, T., Hashin, Z., Brull, M.A., "Reduction of Elastic Moduli of Fiber Composites by Fatigue Crack Accumulation," N00014-78-C-0544, TR-4, April 1980.
73. Gottesman, T., Hashin, Z., Brull, M.A., "Effective Elastic Moduli of Cracked Fiber Composites," N00014-70-C-0544, Office of Naval Research, Tel-Aviv University.
74. Gottesman, T., Hashin, Z., Brull, M.A., "Effective Elastic Properties of Cracked Materials," N00014-78-C-0544, TR-6, ONR, May 1981.
75. Hashin, Z., "Failure Criteria for Unidirectional Fiber Composites," Journal of Applied Mechanics, Vol. 47, June 1980, pp. 329-334.
76. Hashin, Z., "A Reinterpretation of the Palmgren-Miner Rule for Fatigue Life Prediction," Journal of Applied Mechanics, Vol. 47, June 1980, pp. 324-329.
77. Hashin, Z., "Fatigue Failure Criteria for Combined Cyclic Stress," Int. J. of Fracture, Vol. 17, No. 2, April 1981, pp. 101-104.
78. Hashin, Z., "Fatigue Failure Criteria For Unidirectional Fiber Composites," Journal of Applied Mech., Vol. 48, December 1981, pp. 846-852.
79. Hashin, Z., "Static and Fatigue Failure Criteria For Unidirectional Fiber Composites," N00014-78-0544, ONR, Tel Aviv University, 1982.
80. Phoenix, S.L., "Statistical Modeling of the Time and Temperature Failure of Fibrous Composites," D.O.E., DEAC02-76-ER04027., Cornell University.
81. Chou, P.C., Wang, A.S.D., Croman, R., Miller, H., and Alper, J., "Statistical Analysis of Strength and Life of Composite Materials," AFWAL-TR-80-4049, Air Force Wright Aeronautical Laboratories, April 1980.
82. Chou, P.C. and Wang, A.S.D., "Statistical Analysis of Fatigue of Composite Materials," AFML-TR-18-96, Air Force Wright Aeronautical Laboratories, July 1978.

83. Talreja, R., "Fatigue of Composite Materials: Damage Mechanisms and Fatigue-Life Diagrams," Proc. R. Soc. Lond., A 378, pp. 461-475, 1981, Printed in Great Britain.
84. Talreja, R., "A Continuum Mechanics Characterization of Damage in Composite Materials," Visiting Scientist, ESM, Virginia Polytechnic Institute, 1982.
85. Coleman, B.D. and Noll, W., "The Thermodynamics of Elastic Materials With Heat Conduction and Viscosity," Archives of Rational Mech. and Anal., Vol. 13, 1963, pp. 167-178.
86. Coleman, B.D. and Gurtin, M.E., "Thermodynamics With Internal State Variables," J. of Chem. Phys., Vol. 47, No. 2, 1967, pp. 597-613.
87. Truesdell, C. and Toupin, R.A., "The Classical Field Theories," Encyclopedia of Physics, ed. S. Flugge, Vol. 3/1, Springer-Verlag, Berlin, 1960, pp. 226-793.
88. Krajcinovic, D. and Fonseka, G.U., "The Continuous Damage Theory of Brittle Materials, Part 1: General Theory," Journal of Applied Mechanics, Vol. 48, 1981, pp. 809-815.
89. Fonseka, G.U. and Krajcinovic, D., "The Continuous Damage Theory of Brittle Materials, Part 2: Uniaxial and Plane Response Modes," Journal of Applied Mechanics, Vol. 48, 1981, pp. 816-824.
90. Krajcinovic, D., "Constitutive Equations for Damaging Materials," Journal of Applied Mechanics, Transactions of the ASME, 83-APM-12, Houston, June 1983.
91. Allen, D.H., "A Damage Model for Continuous Fiber Composites," Mechanics and Materials Center, Texas A&M University, in preparation.
92. Ho, C.L., "Ultrasonic Surface-Wave Detection Technique," SESA, Experimental Techniques in Fracture Mechanics, 2, edited by A.S. Kobayashi, 1975.
93. Jamison, R.D. and Reifsnider, K.L., "Advanced Fatigue Damage Development in Graphite Epoxy Laminates," AFWAL TR-82-3103, December 1982.
94. Liu, H.W. and Ke, J.S., "Moire Method," SESA, Experimental Techniques in Fracture Mechanics, 2, edited by A.S. Kobayashi, 1975.
95. Dally, J.W. and Riley, W.F., "Experimental Stress Analysis," McGraw-Hill, 1978.
96. Jackson, S.P., "Hygrothermal Effects in an Anti-Symmetric Cross-Ply Graphite/Epoxy Material," Thesis, Texas A&M University, Mechanics and Materials Center, May 1984.

**IN-SITU DELAMINATION STUDY OF GRAPHITE/EPOXY  
COMPOSITE MATERIALS IN THE SCANNING ELECTRON MICROSCOPE**

**Elizabeth A. Chakachery\* and Walter L. Bradley\*\***

**\*Graduate Assistant and \*\*Professor of Mechanical Engineering  
Texas A&M University, College Station, Texas 77843**

**ABSTRACT**

In situ delamination of two graphite/epoxy composites have been conducted in the scanning electron microscope to study the effect of rubber particle toughening of the matrix on the micromechanisms leading to fracture. Extensive tearing and microcracking along with dimple formation in the resin correlate well with critical energy release rates previously reported for these materials. A study of coated versus uncoated regions in the specimens have proved conclusively that coating enhances picture quality without introducing any artifacts into the micrographs. The entire delamination sequence has been videotaped off the SEM to provide a dynamic record of the actual fracture process.

**INTRODUCTION**

Weight critical structures such as aircraft and spacecraft are best designed with materials possessing low thermal expansion coefficients and high specific strengths and stiffness. Fibre reinforced resin laminates are ideally suited since they can be tailored to meet these exacting requirements. The relative ease with which complex shapes can be fabricated from these materials is an added advantage. Much effort is therefore being directed towards utilizing these materials commercially, the major hurdle being the vulnerability of these materials to transverse and delamination cracking.

The fibres are strong and stiff and are the major load-bearing components. The composite laminate is thus highly anisotropic and inherently weak to loading conditions that do not allow the fibres to participate. Tensile stresses transverse to the fibres and shear stresses in the plane of the laminate subject the matrix to severe loading and result in easy fracture. Thus the choice of a reasonably strong and tough matrix is clearly indicated. However, the improvement in these properties must be achieved without adversely affecting either bonding properties or the glass transition temperature. A relatively inexpensive way is to disperse small particles of an elastomeric material as a second phase within the resin matrix (Moulton and Ting, 1981). Recent studies (Bradley and Cohen, 1983) on graphite/epoxy composite laminates, in which the epoxy resin matrix was modified by an acrylonitrile butadiene elastomer, have shown that a considerable improvement in the critical energy release rate,  $G_c$ , can be achieved. Our focus in this study is to correlate the macrolevel observables with micromechanisms operative in these systems. To this end the same materials studies by Bradley and Cohen

(1983) were subjected to in-situ mode I delamination in the SEM and micrographs of both the fracture process and of the fracture surfaces were obtained. The entire delamination sequence was also videotaped off the scanning electron microscope to obtain a dynamic picture of the actual fracture process.

#### EXPERIMENTAL DETAILS

The composite laminates observed in this study were prepared from Hexcel T6T145/F185 and T6C190/F155 cloth supplied by the manufacturer. The resin matrix in these systems are toughened through a bimodal distribution of pre-reacted solid elastomeric particles with average particle size of 2  $\mu$ m and 8  $\mu$ m and through the addition of liquid CTBN which copolymerizes with the epoxy during cure to precipitate out as particles with sizes varying from 0.1  $\mu$ m to 10  $\mu$ m (Bascom et al, 1980). The rubber particles constitute 6.0% and 14% by volume of the F155 and F185 resins respectively. Unidirectional laminate panels, (30 cm x 30 cm) six ply thick were prepared from each of these systems as per the curing schedule suggested by the manufacturer. Two cm. wide teflon strips were placed between the third and fourth plies to provide an initial debonded region to be used as a crack starter. The specimens were cut to size (3 cm x 0.5 cm) with a Micromatic Precision Slicing Machine employing a diamond wheel blade ensuring that one end had an initial debond region approximately 5 mm long. They were then ground on the long edge using graded emery paper followed by a finishing polish with diamond paste (0.6  $\mu$ m) to achieve high surface gloss. Degreasing was achieved by cleaning with Freon following which the specimens were cleaned in a Branson B221 ultrasonic vibrator using petroleum ether as solvent. Specimens were then coated by vapour deposition of a gold-palladium alloy in a Technics Hummer to give a coating thickness of 200 Å. In order to obtain direct comparison between coated and uncoated specimens the following procedure was adopted. Prior to coating, strips of 2 mm wide tape were laid down 3 mm apart on the long edge of the specimens and removed subsequently. This resulted in a surface with alternate coated and uncoated regions running perpendicular to the direction of crack propagation.

All specimens were delaminated in-situ in a JEOL JSM-35 SEM using a special JEOL 35-TS2 tensile stage. Delamination was achieved by driving a blunt-nosed wedge between the central plies via the initial pre-crack from which the teflon had been removed. The crack growth was viewed along the edge of the specimen and a dynamic record of the actual fracture processes made by videotaping the entire delamination sequence on a RCA VHS Selectavision Videocassette recorder employing Scotch T120 3M videocassette tapes. A TV Scanning videotape interface JEOL 35-TVS was used to obtain the dynamic picture on the TV monitor.

#### RESULTS AND DISCUSSION

Experimentally determined values of critical energy release rate,  $G_c$ , for mode I delamination have been reported by Bradley and Cohen (1982) to be 60 and 2600 J/m for T6C 190/F155 and T6T 145/F185

systems respectively. The critical energy release rates reported for the toughened F155 and F185 neat resins are 730 and 6500 J/m respectively (Moulton, 1982). Thus the presence of the fibres in the matrix results in a decrease in toughness. The features of the delamination sequence and the fractographs carry enough evidence to explain this behaviour. Detailed observations on the individual systems follow.

#### T6C145/F185

Micrographs of typically observed events in the delamination process are shown Figures 1(a)-1(d). In each of these pictures the direction of the crack propagation is from bottom left to top right. Fibre participation via debond, followed by breakage or fragmentation, are depicted in Figures 1(a) and 1(b). This is a rather frequent event and is often accompanied by crack wander over a few fibres to an adjacent resin rich region. The onset of such an event is noticeable in Figure 1(c). Significant microcracking is visible in the vicinity of the primary crack and is noticeably present several fibre diameters away. The crack often jumps to adjacent resin rich regions severing the intermediate fibres. Since the crack surges ahead during every fibre break event, attempts to photograph the actual crack drift result in blurred images. However, since the TV interface uses the rapid scan mode, similar events have been dynamically recorded on videotape. The micrographs reveal that the damage zone in the resin is really large and this is clearly the source of the high toughness exhibited by the resin. The presence of the fibres limits the damage zone both by imposing physical constraints on the amount of deformation and by reducing the effective volume of deformed region. The composite, therefore, has a much poorer toughness than the neat resin.

The microcracking evident in Figure 1(c) suggests that the resin cracks in a rather brittle manner whereas Figure 1(d) shows very soft tearing in ductile plastic material. The resin alternately exhibits ductile and brittle behaviour suggesting microlevel inhomogeneity in the matrix. This could either be due to varying amounts of crosslinking in different regions of the matrix or due to an overall non-uniformity of rubber particle distribution. Crosslink density within a lamina would be high and lead to brittle cracking whereas between plies lower crosslink density could give rise to ductile tearing. A cross-sectional view [Figure 2(a)] shows that the lamina are rather wavy. During crack propagation the crack could possibly be traversing in and out of plies, thus exhibiting both types of cracking patterns.

Alternatively rubber particles clusters could lead to regions where soft tearing predominates. That such clusters actually exist in the matrix is evident from Figure 2(c). Here the dimpled surface features typically associated with ruptured particles are clearly visible as localized groupings. Bascom et al (1980) suggest that the dimples are created by dilation followed by tearing and collapse of the precipitated elastomeric particles leading to a thin coating of rubbery material within the dimple. Figure 2(c) shows that a ductile tearing is far more prominent in the vicinity of the dimples than in

the surrounding area. This is borne out further by the low magnification picture of Figure 2 (b). Thus clustering of the elastomeric particles may indeed be the explanation for the heterogenous nature of crack propagation in the resin.

T6C 145/F155

Essentially the behaviour of this system is very similar to that of the T6T 190/F185. This is borne out by the micrographs [Figure 3] which show fibre participation in the delamination process and microcracking in the resin. The micrographs of Figure 3(a) shows both ductile tearing and brittle cracking occurring side by side. The brittle region of Figure 3(a) is shown at a higher magnification in Figure 3(b). An interesting feature of the fractographs in Figures 4(a) and 4(b) is that ductile tearing is restricted to narrow bands along the fibre direction separated by larger regions of low resin content. This is an indication of waviness of the laminae perpendicular to the fibre direction. No such waviness has been observed along the fibre direction. The primary effect of ply waviness is probably to give variability in the thickness of the resin rich region, which in turn influences the degree of resin flow preceding fracture.

It may be noted that fibre participation as an event in the delamination process may occur either due to fibre misalignment within the matrix or due to lamina waviness in the composite. A view of the fracture surface would show broken fibres resulting from both these sources. However the point being made here is that along any longitudinal section lamina waviness cannot contribute much to fibre participation.

#### EFFECT OF COATING

The results of this study are presented in the micrographs of Figures 5(a)-5(d). Both at low and high magnification it is evident that resolution and picture quality are distinctly improved on the coated specimens. The micrograph, Figure 5(b), shows microcracking in the resin on the uncoated specimen proving conclusively that the microcracking is not an artifact introduced by the coating itself. All features observed in the coated regions were present in the uncoated regions and direct comparison was possible using the alternately strip coated specimens. We have satisfied ourselves that the coating does not introduce any artifacts of its own but contributes towards improving picture quality.

#### SUMMARY

The main objective of this study was to observe microscopically the mechanisms leading to delamination fracture and to attempt to correlate these with the reported critical energy release rates. The in-situ delamination in the SEM showed that both fibre and resin participate in the fracture process. The resin exhibits both brittle and ductile behaviour suggesting that the incorporation of rubber particles in the matrix gave extra ductility through an inhomogeneous



distribution of the particles in the matrix. The presence of fibres resulted in a decrease in the volume of the resin deforming in the crack tip region and explains why a large increase in neat resin toughness gets translated into a more modest increase in composite toughness. A careful study shows that the Au/Pd coating does not introduce any artifacts into the micrographs and definitely improves picture quality.

#### ACKNOWLEDGEMENTS

The authors wish to acknowledge the generous financial support of the Air Force Office of Scientific Research (Major David Glasgow: project monitor) Marjorie Andler and Laurie Veeder were instrumental in the scanning electron microscopy work. Their excellent work is gratefully acknowledged.

#### REFERENCES

Bascom, W.D., Bitner, J.L., Moulton, R.J., and Siebert, A.R., "The Interlaminar Fracture of Organic-matrix, Woven Reinforcement Composites," *Composites*, January 1980, p. 9.

Bradley, W.L., and Cohen, R.N., "Delamination and Transverse Fracture in Graphite/Epoxy Materials," *Proceedings of the 4th International Conference on Mechanical Behaviour of Materials*, Stockholm, Sweden, August 1983.

Moulton, R.J., and Ting, R.Y., "Thermostat Matrix Modification- A Model Study for Enhanced Toughness in HMG Composites," *Internal Report- Naval Research Laboratory and Hexcel Corporation*, September 1981.

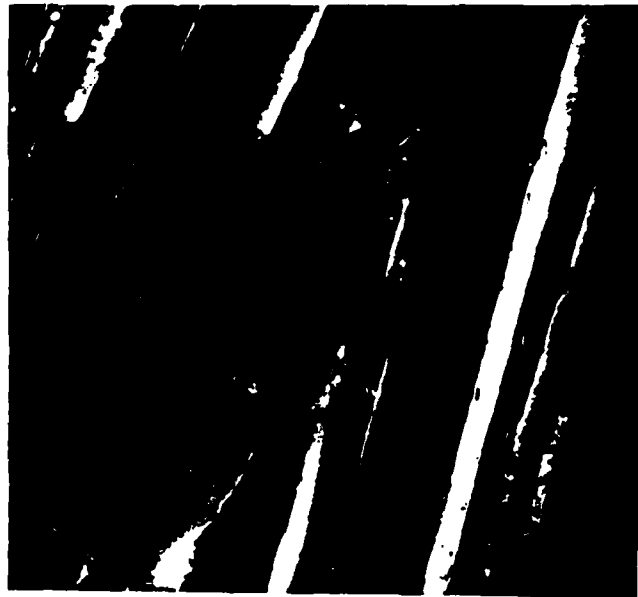
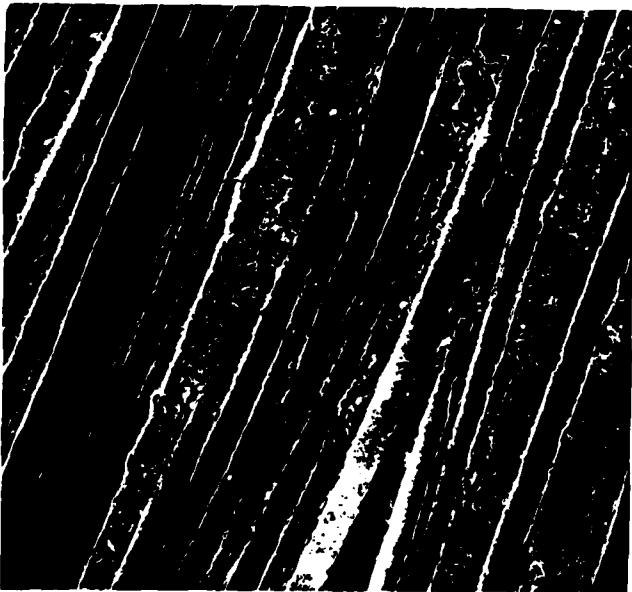


Figure 1. T6T 145/F185 photographed during in-situ fracture in the SEM showing top left (a) fibre participation in the delamination process at 650x; top right (b) fibre breakage and fragmentation at 1500x; bottom left (c) extensive microcracking in the resin at 650x; and bottom right (d) soft plastic tearing of the resin at 650x.

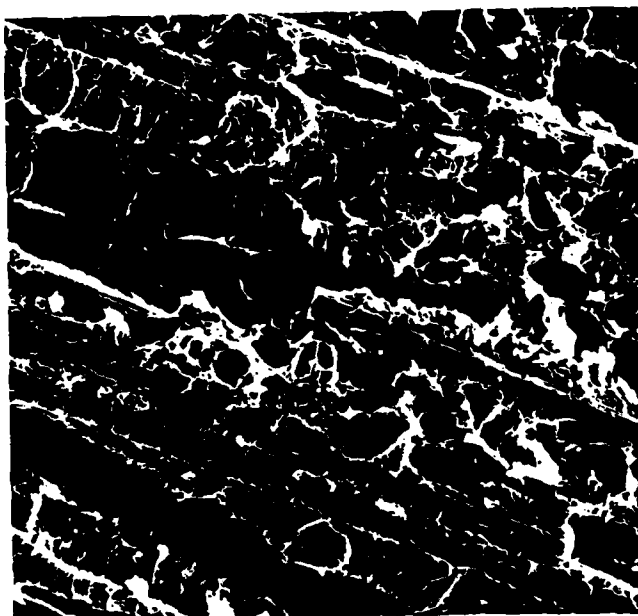
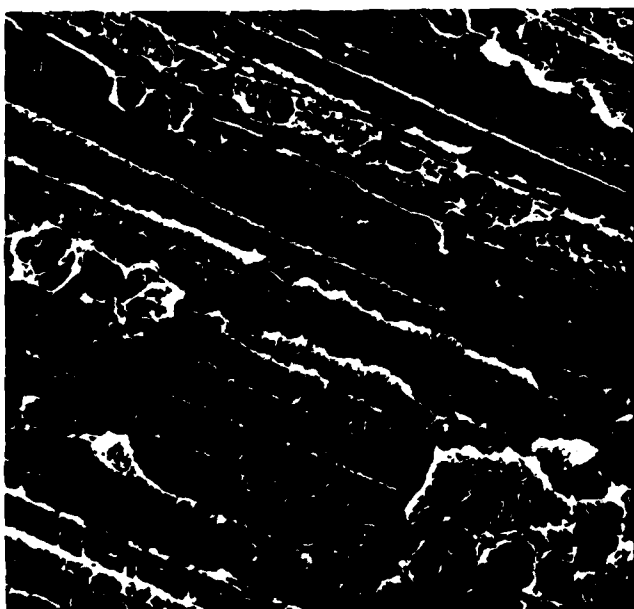
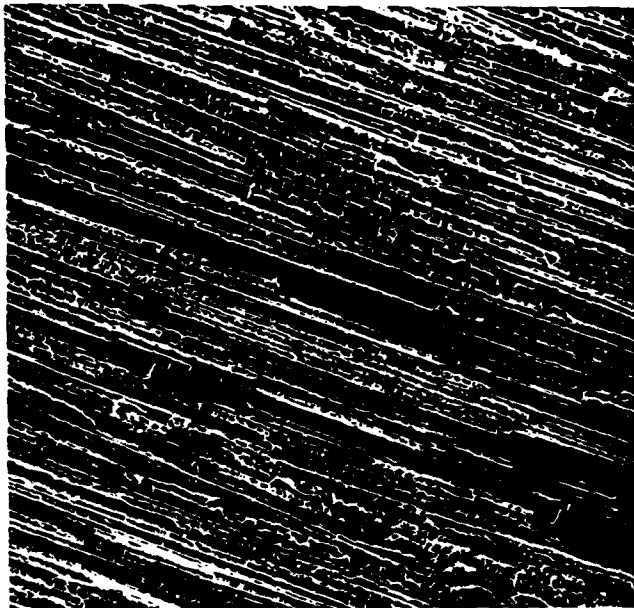
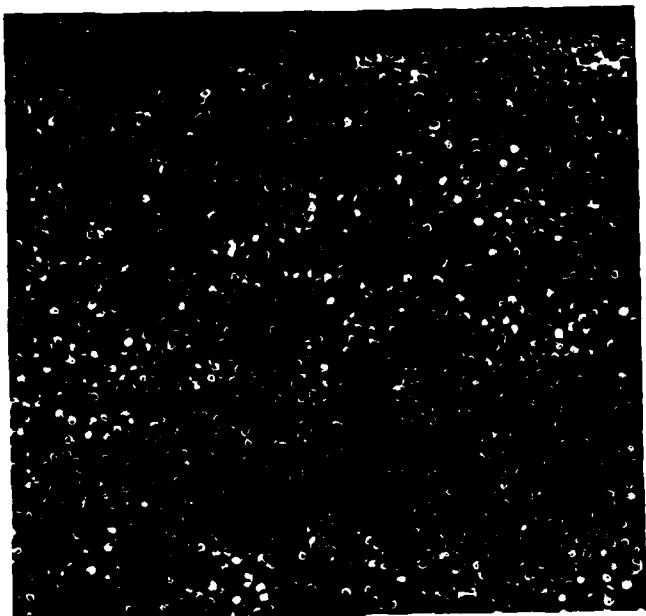


Figure 2. T6T 145/F185 top left (a) cross-sectional view at 200x showing interlaminar resin rich regions and waviness of plies; top right (b) fractograph at 100x showing extensive fibre breakage and localized plasticity in the resin; note clusters of dimpled regions in the bottom left and bottom right regions; bottom (c) and (d) magnified view at 800x showing extensive deformation in the vicinity of the dimples and localized clustering of dimples.



Figure 3. T6C 190/F155 photographed during in-situ delamination in the SEM. (a) Micrograph at 600x showing ductile plastic tearing and brittle cracking in the resin occurring side by side; and (b) magnified view at 3300x of the brittle region.

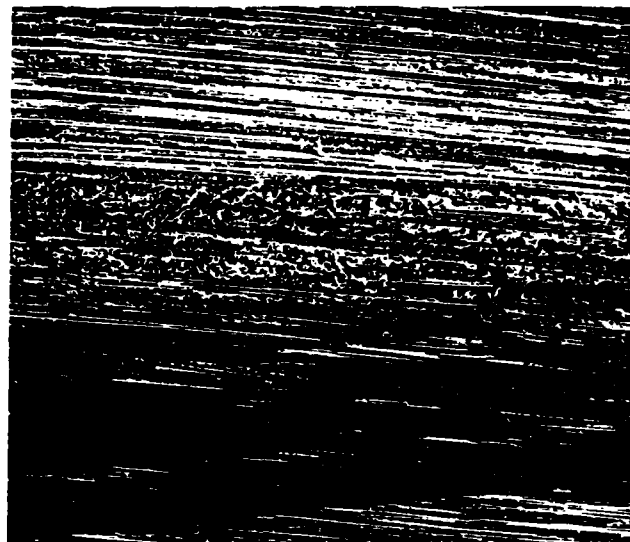


Figure 4. T6C 190/F155 fractographs at progressively increasing magnification: top left (a) at 15x and top right (b) at 40x showing alternate fibre rich and resin rich regions running parallel to the fibres indicating lamina waviness perpendicular to fibre direction; bottom left (c) at 200x and bottom right (d) at 1000x in a resin rich region showing extensive resin deformation.

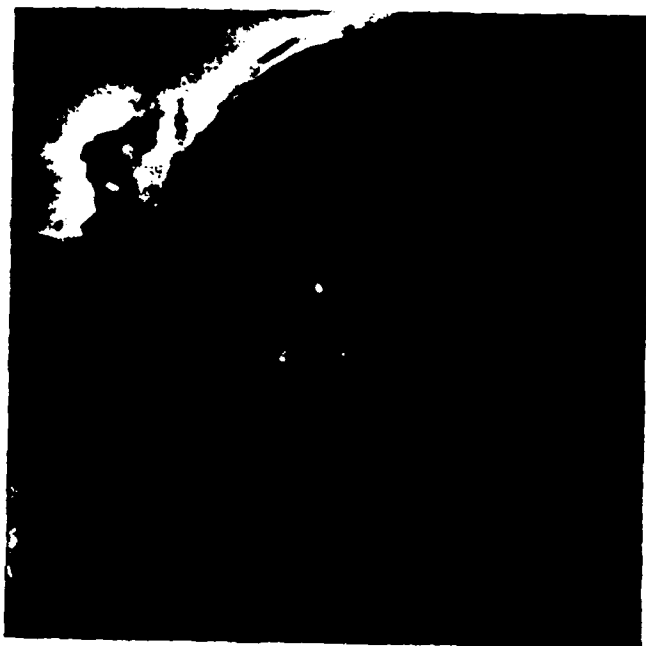


Figure 5. Top T6T 145/F185 at 3000x left (a) with 200 Å thick Au/Pd coating and right (b) uncoated. Bottom T6C 190/F155 at 1200x left (a) coated as above and right (b) uncoated. The difference in detail and picture quality are evident.

Texas A&M University Report No. MM 4665-84-2  
November 1983

**MATRIX DEFORMATION AND FRACTURE  
IN GRAPHITE REINFORCED EPOXIES\***

W.L. Bradley  
Mechanical Engineering  
Texas A&M University  
College Station, TX 77843

R.N. Cohen  
General Dynamics  
San Diego, CA 92124

presented at  
ASTM Symposium  
on  
DELAMINATION AND DEBONDING OF MATERIALS  
Pittsburg, PA  
November 8-10, 1983

---

\*This work performed at Texas A&M University was supported by United States Air Force Office of Scientific Research with Major David Glasgow as project monitor.

## ABSTRACT

The resin dominated fracture behavior of several graphite/epoxy composites has been studied using delamination of split laminates and transverse cracking of compact tension specimens. Pure mode I and mixed mode I/mode II fracture behavior have been studied using specimens cut from unidirectional laminates with the critical energy release rates  $G_{IC}$  or  $G_{I,IIc}$  being measured. The effect on  $G_{IC}$  of variations in resin ductility, thickness of resin rich region through which cracking occurs and fiber debonding have been investigated. In-situ delamination fracture in a scanning electron microscope and post-mortem fractography have been used to determine the micromechanisms of fracture which control  $G_{IC}$ . A qualitative micromechanics model of delamination has been proposed and used to interpret the observed variations in  $G_{IC}$ .

KEY WORDS: composite material, delamination, transverse cracking, mixed mode, mode I, graphite/epoxy.



## LIST OF SYMBOLS

$a$	crack length in compact tension specimen
$B$	specimen thickness
$C$	compliance of test coupon
$E$	elastic modulus in the fiber direction
$G_I$	energy release rate for mode I loading (opening mode)
$G_{II}$	energy release rate for mode II loading (in plane shear)
$G_{IC}$	critical energy release rate for stable crack growth
$I_1$	moment of inertia for uncracked portion of split laminate
$L_C$	crack length in split laminate
$P_a$	asymmetric load component (see Fig. 2)
$P_s$	symmetric load component (see Fig. 2)
$P_u$	load applied to upper half of split laminate (see Fig. 2)
$P_L$	load applied to lower half of split laminate (see Fig. 2)

## LIST OF FIGURES

1. Schematic of crack damage zone size in a delaminating composite with a brittle matrix and in a delaminating composite with a ductile matrix.
2. Schematic showing how asymmetric loading of split laminate can introduce a mixed mode I/mode II state of stress at the crack tip.
3. Total critical energy release rate for mixed mode delamination for four composite material systems.
4. In-situ delamination fracture of T6T145/F185 composite at 500X (left) and 1000X (right). Note the extent of the damage zone as indicated by the secondary cracking.
5. Post-mortem fractography of delaminated T6T145/F185 composite material. Note great variety of artifacts on fracture surface due to variation in thickness of resin rich region. (Upper-left and right, 700X; lower-left, 2000X).
6. In-situ delamination showing bundle breakage in T6T145/F185 composite. Fiber or bundle breakage almost always begins with debond and follows the pattern shown in these pictures. (Upper-left, 500X; right, 1300X; center, 500X).
7. In-situ delamination fracture in T6C190/F155. Heterogeneity of resin is apparent with hard, brittle region just ahead of crack tip and soft, more ductile region further ahead of crack tip (left). (Left, 600X; right, 650X).
8. Post-mortem fractography of a delaminated T6C190/F155 composite. Note the variety of artifacts due to variations in thickness of resin rich region and variations in fracture mechanism; namely, debond versus resin fracture. Dimples are thought to be due to rubber particles rather than voids introduced during manufacturing. Scalloping is a result of coalescence of microcracks.
9. In-situ delamination fracture in AS4/3504. Because of brittle character of resin, crack opening displacement is very small and exact location of crack tip is uncertain. No damage zone around crack tip is indicated. 500X.
10. Post-mortem fractography of delaminated AS4/3502 composite. Note the smooth corrugations due to debond at the matrix/fiber interface with coalesced microcracks giving scalloped regions between the fiber debonds. 2000X.
11. Post-mortem fractography of delaminated AS4/3502 composite emphasizing the weak fiber/matrix interface in this system. Only in this system were loose fibers found strewn on the delaminated fracture surface. The enlargement shows the bare fiber resulting from debonding and the cracked resin between adjacent fibers. No such observations were ever made on AS1/3502 composites, which apparently had much stronger interfacial bonding: (left, 100X; right 4500X.)

## INTRODUCTION

Graphite/epoxy composite materials are very attractive for a variety of aerospace applications due to their high strength and stiffness to weight ratios and their low coefficient of thermal expansion. The limiting design strains for aircraft applications at present is approximately 0.0035-0.004, with compressive buckling being the failure mechanism which drives the design. The relatively low resistance to delamination in composite materials is primarily responsible for these low design strains. It is anticipated that an increased resistance to delamination could potentially increase the design strains to 0.006 where fatigue or other failure mechanisms would then drive the design.

The first generation resin systems developed for high performance composite materials (e.g., Hercules 3502 and Narmco 5208) were designed to maximize the glass transition temperature and resin stiffness. It was only subsequently that the delamination problem surfaced. Strength and fracture resistance for in plane loading are dominated by the mechanical properties of the graphite fibers. However, the response of the composite to out of plane loading will be dominated by the mechanical properties of the resin. Thus, it is not surprising that the first generation high performance graphite/epoxy composites are vulnerable to delamination induced fracture. The very high cross link density required to achieve high  $T_g$  and stiffness would predictably give a very low toughness.

Currently, efforts are under way to develop new resins, for use in high performance composites, that will give an increased resistance to delamination with a minimal penalty in stiffness and  $T_g$ . The initial efforts to effect an increased resistance to composite delamination through the use of much tougher resins have been disappointing, though not

necessarily surprising. The use of much tougher resins has in general produced only modest increases in delamination toughness [1, 2].

In this paper we will present several physically based qualitative models for delamination fracture that indicate the significance of resin strength and ductility, interfacial strength, thickness of resin rich region between plies, and mode of loading. Experiments designed to test these results will then be described. Results and comparison with model predictions will follow.

#### QUALITATIVE MODELS FOR MODE I DELAMINATION

The energy dissipation during delamination fracture can result from resin deformation and/or microcracking and from fiber pullout and/or breakage. The relative contribution of these two processes to the total fracture energy depends on the toughness of the resin and the interfacial bonding strength. Furthermore, whether the delamination toughness of the composite material is greater or less than the toughness of the neat material also depends on the toughness of the resin and the interfacial bond strength.

#### Addition of Brittle Fibers to Brittle Resin

The addition of stronger brittle fibers to a weaker brittle resin should increase the resistance to fracture, even for the delamination mode of fracture. The reason is that while the crack moves nominally through the resin rich region between plies, it will occasionally impinge on misaligned fibers. Since the fibers are much stronger than the resin, interaction of the crack tip with the graphite fibers increases resistance to crack growth. Furthermore, a thin resin rich region between plies can give rise to a corrugated topography for the fractured surface. The crack

will prefer to move through the weaker resin rather than breaking the stronger fiber, but there is no plane containing only resin if the resin rich region between plies has an average thickness of less than one fiber diameter. The thinner the resin rich region, the more corrugated will be the fracture surface and the more frequent will be the crack tip interaction with the fibers. Each of these effects should increase the energy absorbed per unit area of crack extension in a brittle fiber/brittle resin system. Thus, the addition of strong brittle fibers to a brittle resin should give a delamination fracture toughness greater than the neat resin fracture toughness, with the increase in fracture toughness being greatest for the minimum possible thickness of the resin rich region. Going the other direction, as the resin rich region approaches 5-10 fiber diameters (if processing would allow this), one might expect the delamination toughness to approach a lower limit value which would be equal to the neat resin toughness.

The preceding discussion assumes that the cracking propagates principally through the resin rather than at the resin/fiber interface. If the interfacial toughness is less than the resin toughness, then considerable cracking may occur at the interface giving debonding and involving more fibers in the delamination fracture process. Depending on how much less energy is dissipated by cracking at the interface than in the resin and how much more energy is dissipated in fiber debond and breakage, the delamination fracture energy may either increase or decrease with increased fiber debonding.

In summary the delamination fracture energy of a graphite fiber/brittle epoxy should be greater than the neat material with the increase being greatest for a very thin resin rich region between plies.

### Addition of Brittle Fibers to Ductile Resin

Crack extension in a ductile resin will generally be preceded by a significant process zone where extensive deformation and/or microcracking occurs. The energy dissipation in this process zone prior to fracture is normally much larger than the energy associated with creation of new surface and constitutes the bulk of the energy absorbed per unit area of crack extension.

The addition of graphite fibers to such a system may significantly reduce the extent of the process zone and will reduce the volume of material available to deform/microcrack and absorb energy in the process zone (since the fibers act like rigid filler). While crack tip interaction with the fibers might give an incremental increase in the energy absorbed in crack extension, the loss of material absorbing energy in the process zone gives a much greater decrease in fracture energy, resulting in a net decrease in the delamination fracture toughness.

A second reason for loss in toughness in a resin with the introduction of brittle fibers is the additional constraint imposed on the resin. If energy dissipation in a given resin is by shear deformation, the reduced shear stresses that result from fiber constraint could be particularly deleterious to the resin toughness so essential to delamination toughness in such a system. The loss in toughness due to loss in process zone volume and local strain to fracture could be quantified in a micromechanical model using an equation of the form

$$G_{Ic} \approx \int_0^{V_p} \int_0^{\epsilon_f} \sigma d\epsilon dv \quad (1)$$

where  $\epsilon_f = f(x,y,z)$  and represents the local strain at various points in

the process zone at the moment of crack extension and  $V_p$  represents the zone of nonlinear deformation ahead of the crack tip which acts as an energy dissipating sink.

In summary, we are predicting that the delamination toughness of a graphite fiber/ductile resin composite will generally be less than the neat material toughness. This prediction is in sharp contrast to the results predicted for a brittle resin composite material. For brittle resins, the process zone is so small that the addition of fibers has no effect on it. This difference is illustrated in Figure 1.

For a graphite/fiber ductile epoxy composite, a thicker resin rich region should increase the delamination toughness by increasing the process zone size. In the limit as the resin rich region between plies is made sufficiently thick to contain the entire process zone (if it were possible to make such a composite), the delamination fracture toughness should approach that of the neat material. The lower limit of delamination fracture toughness should be observed as the resin rich region between plies approaches zero thickness. In this case not only is the process zone reduced in size but also the effect of constraint of the fibers on resin ductility is maximized.

In summary, a ductile resin reinforced with brittle fibers will have a delamination fracture toughness that is less than the neat material toughness, with the minimum toughness observed for the minimum thickness of the resin rich region between plies. It should be emphasized that this prediction is just opposite to that predicted for a brittle resin/brittle fiber composite.

## QUALITATIVE MODEL FOR MIXED MODE DELAMINATION

The superposition of mode II loading on mode I loading should have some predictable influence on the delamination fracture behavior. If the resin is brittle, the fracture on a microscopic scale may still occur on the principal normal stress plane with the principal effect of the mode II loading being to change the orientation of this plane from parallel to the plies to some acute angle. This would give a much more frequent interaction of the crack tip with the fiber which, as previously noted for a brittle fiber/brittle resin system, should increase the resistance to delamination.

In a ductile resin/brittle fiber composite, by contrast, the effects of the mode II loading on process zone size will dominate. The effect of the mode II loading should be to increase the size of the process zone if deformation occurs principally by shear. Thus, one might expect increasing the mode II loading component would increase the delamination fracture energy.

## EXPERIMENTAL PROCEDURES AND ANALYSIS

The experimental program was designed to test the qualitative predictions of the models in two ways. First, macromechanics tests were run to measure the delamination fracture toughness. Variables studied included thickness of resin rich region, resin ductility, interfacial strength and state of stress (pure mode I versus mixed mode I/mode II). Second, real time observations of delamination fracture were made in the scanning electron microscope (SEM) for the same composite systems studied macroscopically. Post mortem fractographic observations were also made in the SEM on the delaminated specimens. This portion of the study allowed



the micromechanisms of the fracture process to be correlated with macromechanics measurements of delamination fracture toughness.

### Fracture Mechanics Testing and Analysis

Materials and Fabrication - The composite materials selected for this study were Hexcel T6C190/F155, Hexcel T6T145/F185, Hercules AS1/3502, and Hercules AS4/3502. Prepreg tape was used to lay up unidirectional panels 30.5 x 30.5 cm. square, generally 20 to 28 plies thick. The panels were subsequently processed in a thermomechanical press according to vendor's specification. A 2.5 cm. wide piece of teflon was placed between the center plies along one edge of the panels to serve as a crack starter.

The panels were subsequently cut into 2.5 cm. by 30.5 cm. split laminate specimens with the fibers running along the length of the laminate, parallel to the direction of subsequent crack growth. A few compact tension specimens 6.5 cm. by 6.1 cm. were also cut out of these panels. The slot and notch were cut parallel to the fiber direction. Thus, the subsequent cracking to fracture occurred principally through the resin parallel to the fibers. While this is similar to delamination fracture, it is different in that crack growth does not occur through any resin rich region between plies. Rather it occurs mainly through the resin lean region within the plies. Thus, it represents a limiting case for crack growth where the resin rich region between plies approaches a zero thickness.

To produce sharp natural cracks in the split laminate specimens, they were loaded until a natural crack of approximately 2.5 cm. length was grown from the 2.5 cm. wide teflon strip on one end. A sharp, natural crack was introduced into the compact tension specimen at the root of the machined in notch by tapping gently on a razor blade held in the notch.

Mechanical Testing - Both types of specimens were tested in a MTS materials testing systems using appropriate fixtures. Load, displacement and crack length were all measured and recorded simultaneously using a Minc II laboratory computer. Displacement for the CT specimens was measured using a LVDT attached to the mouth of the slot. These displacement measurements were subsequently corrected to give load line displacement using the analysis of Saxena and Hudak [3]. The crack length on both types of specimens was measured both optically and using Krak gages (electrical resistance type gages). The load-displacement history was interrupted frequently to obtain unload/reload compliances on both types of specimens. All tests were conducted in displacement control to allow stable crack growth.

Mixed mode delamination was produced using asymmetrically loaded split laminates. Figure 2 shows how such a loading scheme can be analyzed using superposition to separate the mode I and mode II load contributions. Details of the experimental setup and procedures and analysis have been described elsewhere [4].

Fracture Mechanics Analysis - Using linear beam theory and superposition as shown in Figure 2, relationships for  $G_I$  and  $G_{II}$  may be derived in terms of variables that are easily measured experimentally. The results are as follows

$$G_I = \frac{8P_s^2 L_c^2}{BEI_1} \quad (2a)$$

$$G_{II} = \frac{6P_a^2 L_c^2}{BEI_1} \quad (2b)$$

where  $P_s = (P_u + P_L)/2$ ,  $P_a = (P_u - P_L)/2$ ,  $L_c$  is the length of the split portion of the laminate,  $B$  is the laminate width,  $E$  is the Young's modulus in the fiber direction and  $I_1$  is the moment of inertia of the uncracked portion of the laminate. It should be noted that equations 2a and 2b can also be used to analyze pure mode I loading in which case  $P_u = P_L$ , giving  $P_s = P_u = P_L$  and  $P_a = 0$ . Equation 2a is then identical to the previously published result for linear beam theory for pure mode I loading [5].

For pure mode I loading, generally equation 2a was used to calculate  $G_{IC}$ . However, in a few of the tests,  $G_{IC}$  was calculated using the compliance measurements and an analysis first suggested by Wilkins [6]. Wilkins' analysis and equation 2a gave essentially identical results in all cases where both were used. This is to be expected as long as linear beam theory behavior is observed.

The compact tension specimen results were analyzed using the standard relationship from LEFM

$$G_I = \frac{P^2}{2B} \frac{2C}{2a} \quad (3)$$

A load-displacement record with multiple unload/reload to give compliance information was required along with an independent measurement of the crack length throughout the test.

#### In-situ Delamination Fracture in SEM

A JEOL-35 scanning electron microscope equipped with a tensile stage was used to study the micromechanisms of the delamination fracture process. Smaller panels 8-10 plies thick were fabricated with specimens 3 cm. by 1.3 cm. cut from these for the in-situ fracture studies. A teflon crack starter was used. The edge of these specimens to be viewed during

delamination was carefully polished using standard metallographic materials and technique. Some specimens were coated using vapor deposition of a gold palladium film to improve the imaging characteristics of the surface.

Delamination was accomplished in the SEM by pushing the specimen into a stationary metal wedge, the wedge giving essentially mode I loading of the specimen as it delaminates. More experimental details are summarized elsewhere [7].

Preliminary studies were conducted to verify that the fracture behavior at the surface would be representative of bulk fracture behavior and that the coating was not the source of any of the fracture artifacts noted on the surface. Careful examination of the entire fracture surface after fracturing specimens and comparisons of the artifacts on the edge and at the center of the specimen showed no difference [8]. Such a result would be surprising in metals where the difference in plane stress at the surface and plane strain in the center of a specimen can result in very different fracture behavior. In graphite/epoxy composites, the magnitude of  $\sigma_3$  resulting from Poisson's contraction is quite small so that the variation in state of stress from the surface to the center is also small.

Several specimens were polished on edge and several thin strips of tape were placed on these edges before coating with gold/palladium. Subsequently, the tape was removed and the specimens were delaminated in the SEM. A video tape was made of the crack growth as observed on both the coated and uncoated portions of the surface. These were carefully studied, particularly as the crack propagated across an interface between a coated and an uncoated section. No differences in fracture artifacts were noted; however, a significant difference in image quality was observed. Thus, it was decided that the remainder of the study would be made using coated

specimens [9].

Results and discussion of these macroscopic and microscopic studies will be presented next.

## EXPERIMENTAL RESULTS AND DISCUSSION

### Macroscopic Measurements of Delamination and Transverse Fracture Toughness

The fracture toughness measurements made using split laminates and compact tension specimens are summarized in Table I.

Ductile Resins - For the two systems with ductile resin (F155 and F185), the predicted decrease in fracture toughness (for crack propagation parallel to the fibers) for decreasing thickness of resin rich region is observed. Note the neat material represents the limiting case of a material with an "infinitely" thick resin rich region whereas the transverse cracking corresponds to the opposite limit of an essential zero thickness resin rich region. Delamination represents an intermediate case between these extremes.

If one assumes (1) that the process zone for the neat material is the same size as that in the composite and (2) that the toughness comes principally through energy dissipation in the resin, then one might expect the decrease in toughness comparing neat material to delamination or transverse cracking to correlate with the volume fraction of fibers; i.e.

$$G_{IC} \text{ (delamination or transverse cracking)} = G_{IC} \text{ (neat material)} \times (1 - V_f) \quad (4)$$

where  $V_f$  represents the average volume fraction of fiber over the volume of the process zone. For these systems the average volume fraction of fiber over the whole composite is between 55 and 60%, which should also be the  $V_f$  used for transverse cracking. For delamination cracking, the process zone

Table I. Summary of mode I energy release rates for four materials and two types of tests.

Material	Type of Fracture	Avg. $\dot{a}$ (m/s)	$G_C$ J/m <sup>2</sup>
Neat 3502 Resin		$5.0 \times 10^{-5}$	69 [10]
AS1/3502	Delamination	$6.1 \times 10^{-5}$	155 [4]
AS1/3502	Transverse	$5.7 \times 10^{-5}$	225 [10]
AS4/3502	Delamination	$2.8 \times 10^{-5}$	225
AS4/3502	Transverse	$1.7 \times 10^{-5}$	120
Neat F155 Resin		*	730 [11]
T6C190/F155	Delamination	$3.5 \times 10^{-5}$	600
T6C190/F155	Transverse	$3.8 \times 10^{-5}$	410
Neat F185 Resin		*	6000 [12]
T6T145/F185	Delamination	$3.0 \times 10^{-5}$	2700
T6T145/F185	Transverse	$3.8 \times 10^{-5}$	1525

\*Test performed by others; crack growth rate not indicated.

averages the resin rich region between plies with the higher volume fraction of fibers within a given ply. The larger the process zone, the higher would be the average  $V_f$  value since a larger fraction of the total process zone would be ply rather than resin rich region between plies. A reasonable estimate for  $V_f$  might be 40% for delamination in the F185 and 30% for the F155, which has a smaller process zone. These estimates are based on the in-situ fracture results to be presented later.

The use in equation 4 of these values of  $V_f$  for transverse and delamination cracking of T6T145/F185 overestimates the observed  $G_{IC}$  results. This implies that the presence of the fibers further degrades the resin toughness in some other way(s). These might include the effect of fiber constraint in resin strain to fracture, fiber debonding prior to extraction of all of the intrinsic toughness from the resin, or reduction of the process zone size with the addition of fibers.

A similar analysis for T6C190/F155, again using equation 4 and the estimated values for  $V_f$ , underestimates the transverse and delamination toughness values as compared to those observed in the fracture mechanics testing. This implies that the additional increments of toughness must be due to fiber debond, tie zone formation and fiber breakage in addition to resin deformation. Note the net effect of fiber constraint on resin strain to fracture and fiber debonding leading ideally to tie zone formation and fiber fracture varies from system to system giving an increase in the F155  $G_{IC}$  but a decrease in the F185  $G_{IC}$ .

In summary, the trend in toughness from neat material to delamination to transverse cracking predicted by Equation 4 for ductile resins (based on effect of volume fraction of fibers on resin deforming in process zone) is well supported by the results of the two ductile resins, F155 and F185.

The lack of exact numerical agreement implies that other factors not accounted for by this equation are also important, as previously discussed.

Brittle Resins - For the two systems with brittle resins studied, the predicted increase in  $G_{IC}$  with fiber additions (for crack propagation parallel to the fibers) was observed. If one assumes (1) that the fracture energy is proportional to surface area on the fracture surface and (2) that the cracking occurs through the resin rather than at the interface, then the ratio of the  $G_{IC}$  for composite material compared to neat material would have a maximum value of  $\pi/2$  for a fully "corrugated" fracture surface compared to a flat one. The 3502 neat resin does give a glassy smooth fracture surface [10]; and the delamination of the composite gives a very corrugated fracture surface, as will be shown later in this paper.

The increases in  $G_{IC}$  with fiber additions reported in Table I for the 3502 resin system are much greater than the  $\pi/2$  prediction, which implies in general that crack tip interaction with the fibers, fiber debond and fiber breakage make a significant contribution to the total energy dissipation in the fracture process in a composite with a brittle resin. For AS1/3502 the predicted increase in  $G_{IC}$  with decreasing thickness of the resin rich zone (neat to delamination to transverse cracking) is observed. For AS4/3502 the transverse cracking actually gave a lower  $G_{IC}$ , possibly due to a significant amount of cracking at the fiber matrix interface rather than through the matrix itself. The AS4 fibers debonded much more readily than did the AS1 fibers, which almost never debonded in our study. The AS4 fibers are smoother fibers which give a higher strain to fracture and strength. However, the interfacial bonding in the graphite fiber/3502 system must have a significant mechanical contribution in the rougher fiber AS1/3502 which is substantially lost in the smooth fiber AS4/3502 system.



Mixed-Mode Delamination - The mixed mode delamination results are summarized in Figure 3. The expected increase in  $G_{Total} = G_I + G_{II}$  with increasing mode II shear is observed in the two systems with a brittle resin; namely, AS1 and AS4/3502. A slight increase in the T6C/F155  $G_{Total}$  with increasing mode II is noted whereas the  $G_{Total}$  for the T6T/F185 decreases. The reason for this last observation is not known and in fact seems to be at odds with results by O'Brien, Johnston, Morris and Simonds obtained with a different test coupon and analysis [12]. It is possibly significant that they were using a multidirectional lay up where we were using unidirectional.

#### Microscopic Observation of Fracture Process

T6T145/F185 - In-situ fracture of T6T145/F185 is shown in Figure 4 with post-mortem fractography shown in Figures 5 and 6. Figure 4 shows the crack tip region during delamination for a thin and thick resin rich region between plies. It has previously been suggested that the process zone (or damage zone) for this composite should be much larger than the resin rich region between plies. This is clearly seen to be the case. Typically microcracking can be seen over a region of  $\pm 3-5$  fiber diameters from the plane of the primary crack.

The extensive microcracking around the crack tip will result in the scalloped fracture surface often seen in delamination fracture if the resin rich region is not too thick. Where it is thicker and the resin is ductile the primary fracture will show more gross deformation and the fracture surface may resemble to some extent the dimpled fracture surface seen in ductile fracture of metals. Figure 5 shows this duplex appearance of the fracture surface due to variation in thickness of the resin rich region. At higher magnification, some scalloping that results from

coalescence of microcracks is seen.

Fiber breakage (or bundle breakage) is generally initiated by fiber debond which allows the fiber (or bundle) to span the crack opening. As the crack opening increases, the fiber is eventually bent until it breaks, as seen in Figure 6. Where the resin is fairly ductile and compliant, the bending of the fiber (or bundle) to the point of breaking is more difficult, allowing a significant tie zone to form behind the crack tip. Such a tie zone has the effect of increasing the energy dissipated in fracture, and thus, the delamination  $G_{IC}$ .

T6C190/F155 - In-situ fracture of the T6C190/F155 is seen in Figure 7. Note fracture in this region is occurring in a relatively thick resin rich zone between plies. It should also be noted that the damage zone is more localized than it was in the F185, giving a much lower delamination  $G_{IC}$ .

The toughening of the F155 and F185 is accomplished through the introduction of rubber particles with a bimodal size distribution. The fracture behavior in Figure 7 suggests that the rubber particle spatial distribution is heterogeneous, leaving the matrix hard and brittle in some regions and soft and ductile in others. Some fiber debond is also noted.

The heterogeneity in the fracture behavior that results from a nonuniform distribution of rubber particles, variation in thickness of resin rich region and variation in fracture mechanism (fiber debond versus resin rupture) is clearly seen in Figure 8 which shows post-mortem fractography.

AS4/3502 - In-situ fracture in the brittle AS4/3502 is seen in Figure 9. The volume fraction of fibers in this system is seen to be much greater than in the two ductile systems with no significant resin rich region. This is due to the fact that the 3502 resin during processing has a very low viscosity, allowing almost all excess resin to bleed off. The process

zone, or damage zone is seen to be very localized to the crack tip with no indication of microcracking elsewhere.

Post-mortem fractography seen in Figure 10 shows the expected corrugated fracture surface with some scalloping for matrix fracture between fibers. While it is not clear whether the fracture surface seen in Figure 10 is through the matrix or along the fiber/matrix interface, Figure 11 suggests debonding and fracture along the interface dominates. It should be noted that previously published fractography on AS1/3502 indicates fracture through the matrix, with very little debonding [4], in contrast to the results presented here for AS4/3502.

#### SUMMARY

The fracture process and resultant fracture toughness for delamination of graphite/epoxy composites is seen to be sensitive to the following factors: (1) resin toughness, (2) interfacial strength, and (3) thickness of resin rich region (or volume fraction of fibers). Ideally, the interfacial strength should be just strong enough to allow deformation of the resin to the point of fracture before debonding occurs. This would allow energy dissipation by both the matrix and the fibers. Too weak an interface will allow mainly fiber breakage without extraction of the resin's intrinsic toughness. Too strong an interface will allow energy dissipation from the matrix alone.

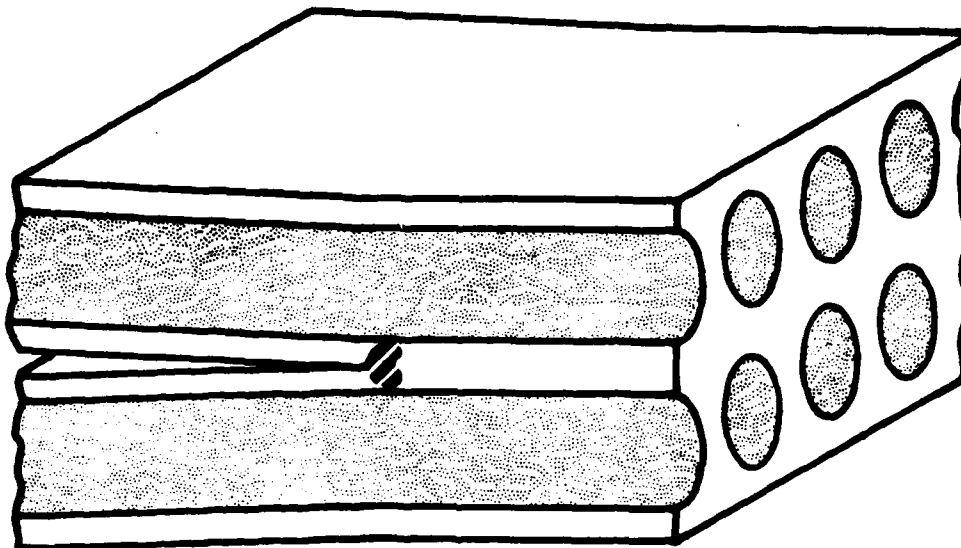
The optimal thickness of the resin rich region (thick versus thin) depends on whether the resin is ductile or brittle. For a ductile resin, a thicker resin rich region (or lower average volume fraction of fibers) will increase the resistance to delamination, though at the expense of stiffness and tensile strength. Recently completed work to be published elsewhere

[8] has indicated that the T6C190/F155 will have a 2x variation in delamination  $G_{IC}$  comparing a bled to an unbled panel. For a brittle resin the optimal thickness of the resin rich region between plies would be zero, or as small as processing can produce.

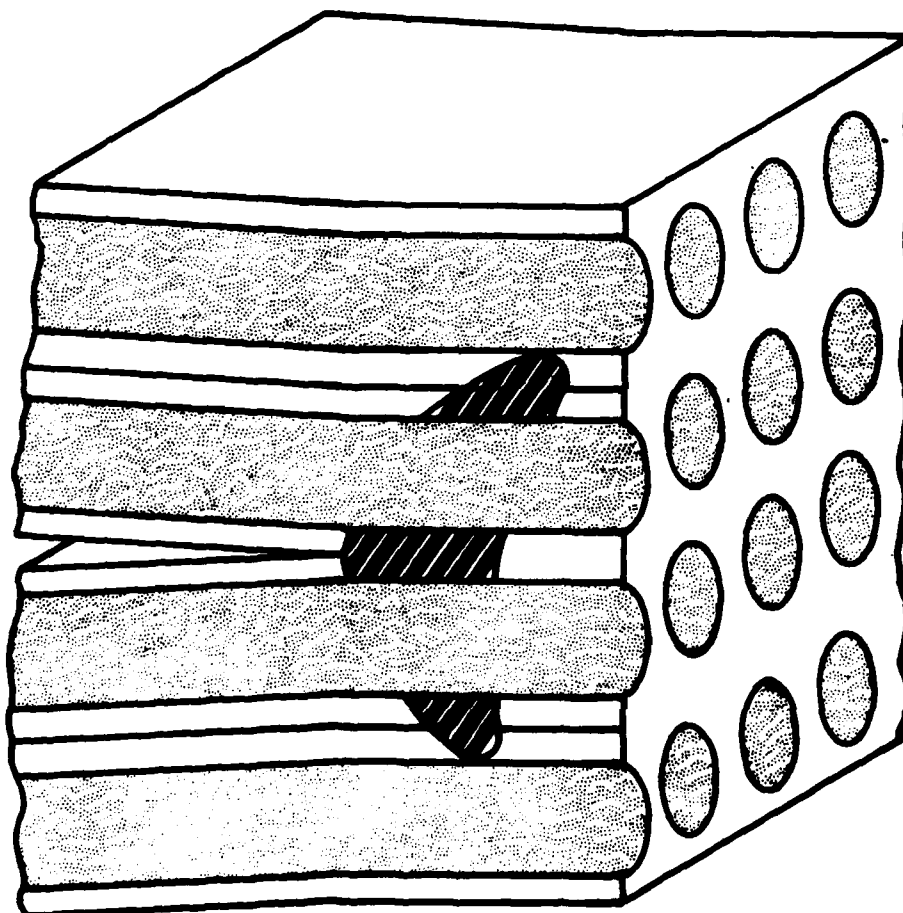
Finally, the lower delamination fracture toughness as compared to neat material toughness for a ductile resin can be rationalized principally in terms of a decrease in the volume of resin being deformed in the process zone due to the presence of fibers, with fiber constraint and debond also important in modifying the toughness.

## REFERENCES

1. Bascom, W.D., Ting, R.Y., Moulton, R.J., Riew, C.K. and Siebert, A.R., "Fracture of Epoxy Polymer Containing Elastomeric Modifiers", Journal of Composite Materials, Vol. 16, 1981, p. 2657.
2. Bascom, W.D., Bitner, J.L., Moulton, R.J. and Siebert, A.R., "The Interlaminar Fracture of Organic-Matrix Woven Reinforcement Composites", Composites, January 1980, p. 8.
3. Saxena, A. and Hudak, S.J., Jr., "Review and Extension of Compliance Information for Common Crack Growth Specimens", International Journal of Fracture, Vol. 14, No. 5, October, 1978.
4. Vanderkley, P.S., "Mode I - Mode II Delamination Fracture Toughness of a Unidirectional Graphite/Epoxy Composite", Master's Thesis, Texas A&M University, College Station, TX, December 1981.
5. Devitt, D.F., Schapery, R.A. and Bradley, W.L., "A Method for Determining the Mode I Delamination Fracture Toughness of Elastic and Viscoelastic Composite Materials", Journal of Composite Materials, Vol. 14, October 1980, p. 270.
6. Wilkins, D.J., Eisenmann, J.R., Camin, R.A., Margolis, W.S. and Benson, R.A., "Characterizing Delamination Growth in Graphite-Epoxy", Damage in Composite Materials: Basic Mechanisms, Accumulation, Tolerance and Characterization, ASTM STP 775, American Society for Testing and Materials, 1983.
7. Cohen, R.N., "Effect of Resin Toughness on Fracture Behavior of Graphite/Epoxy Composites", Master's Thesis, Texas A&M University, College Station, TX, December 1982.
8. Jordan, W.M. and Bradley, W.L., "Effect of Resin Content on the Delamination Fracture Behavior of Graphite Epoxy Laminates", to be presented at Annual SAMPE Meeting, Reno, April 1984.
9. Andler, M., Chakachery, E., Veeder, L. and Bradley, W., Unpublished research results obtained at Texas A&M University, Summer 1983.
10. Williams, D., "Mode I Transverse Cracking in an Epoxy and a Graphite Fiber Reinforced Epoxy", Master's Thesis, Texas A&M University, College Station, TX, December 1981.
11. Technical Information Bulletins from HEXCEL, 11711 Dublin Blvd., Dublin, CA., 94566, on epoxy resins F155 and F185.
12. O'Brien, T.K., Johnston, N.J., Morris, D.H. and Simonds, R.A., "Determination of Interlaminar Fracture Toughness and Fracture Mode Dependence of Composites Using Edge Delamination Test", Proceedings of Conference on Testing, Evaluation and Quality Control of Composites, TEQC 83, Sept. 1983, U. of Surrey, Guildford, United Kingdom (Butterworth Scientific Ltd.) pp. 223-232.



**A. Brittle Resin**



**B. Ductile Resin**

Figure 1. Schematic of crack damage zone size in a delaminating composite with a brittle matrix and in a delaminating composite with a ductile matrix.

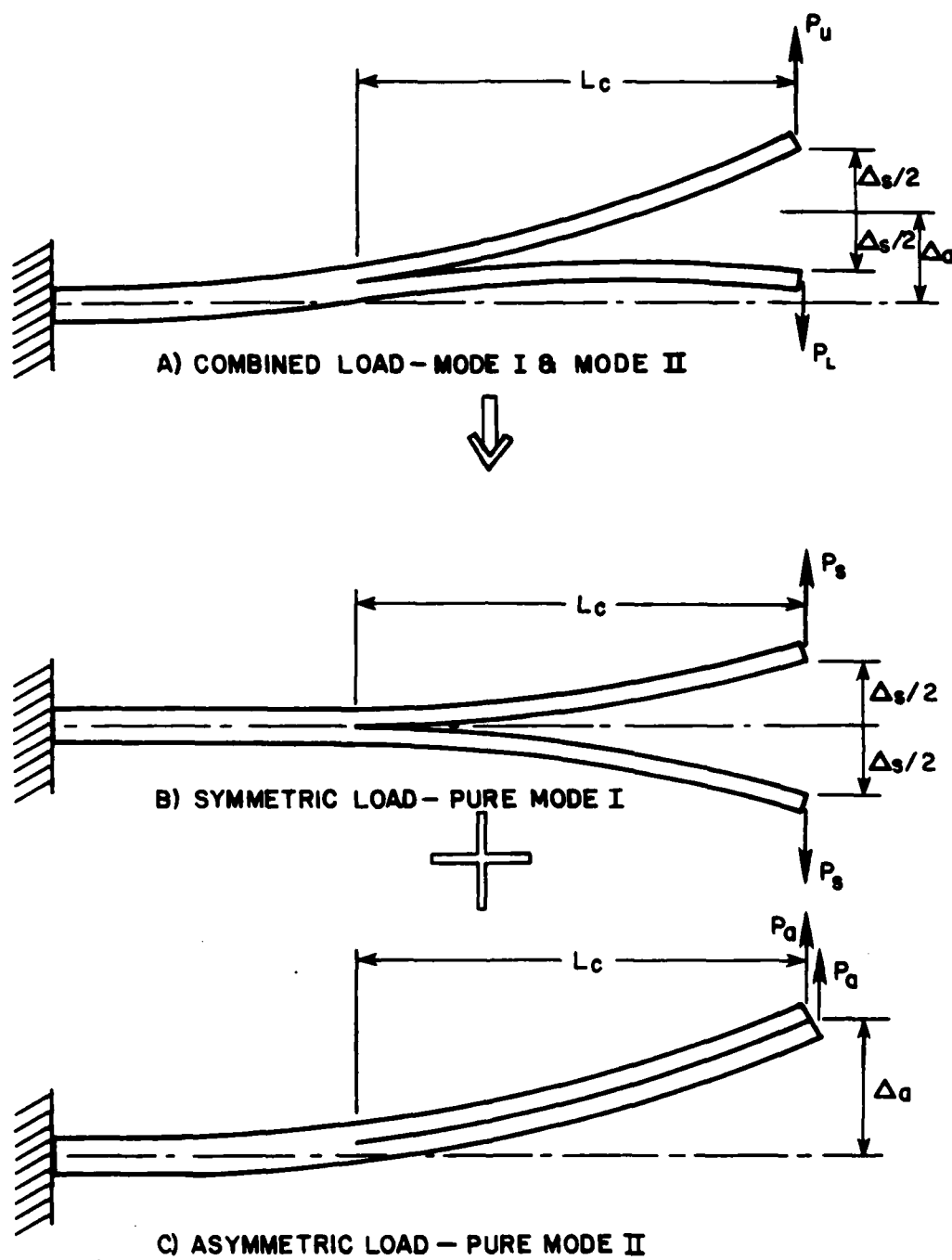


Figure 2. Schematic showing how asymmetric loading of split laminate can introduce a mixed mode I/mode II state of stress at the crack tip.

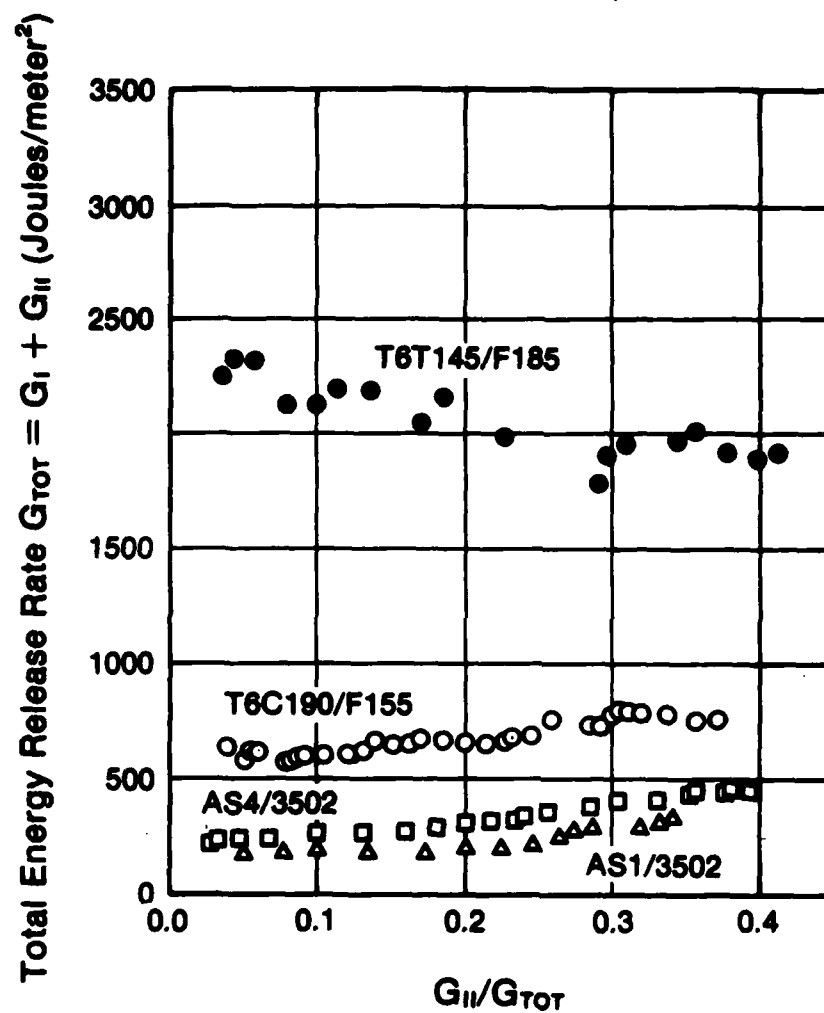


Figure 3. Total critical energy release rate for mixed mode delamination for four composite material systems.



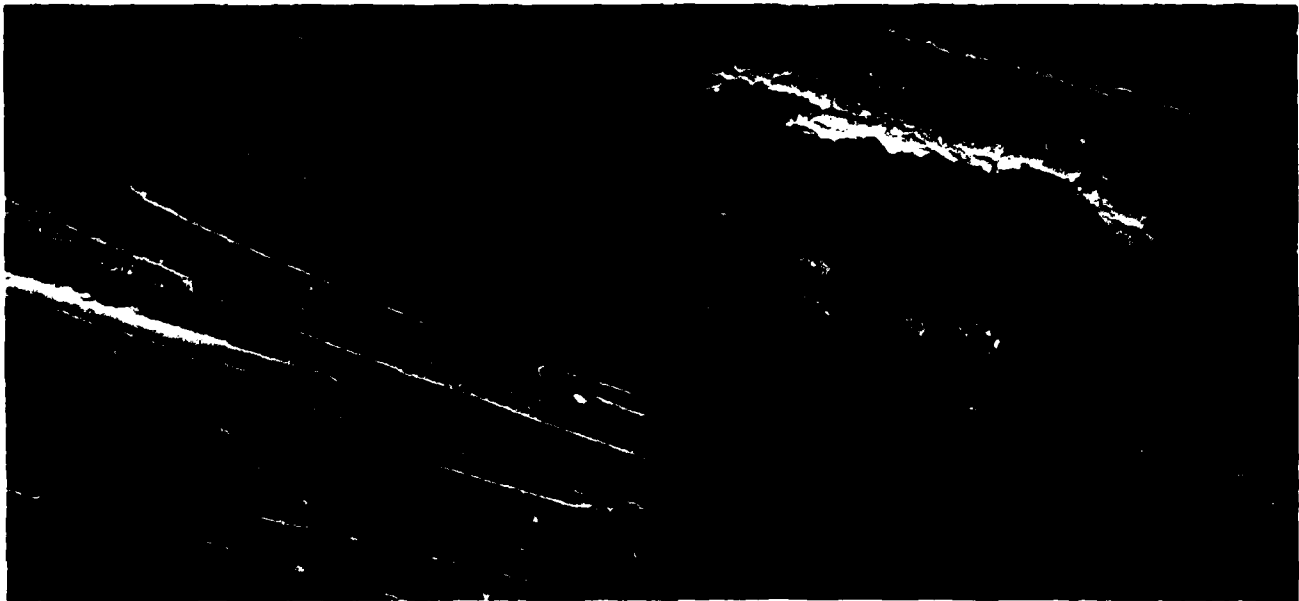


Figure 4. In-situ delamination fracture of T6T145/F185 composite at 500X (left) and 1000X (right). Note the extent of the damage zone as indicated by the secondary cracking.



Figure 5. Post-mortem fractography of delaminated T6T145/F185 composite material. Note great variety of artifacts on fracture surface due to variation in thickness of resin rich region. (Upper-left and right, 700X; lower-left, 1000X; lower-right, 2000X).



Figure 6. In-situ delamination showing bundle breakage in T6T145/F185 composite. Fiber or bundle breakage almost always begins with debond and follows the pattern shown in these pictures. (Upper-left, 500X; right, 1300X; center-500X).



Figure 7. In-situ delamination fracture in T6C190/F155. Heterogeneity of resin is apparent with hard brittle region just ahead of crack tip and soft, more ductile region further ahead of crack tip (left). (Left, 600X; right, 650X).



Figure 8. Post-mortem fractography of a delaminated T6C190/F155 composite. Note the variety of artifacts due to variations in thickness of resin rich region and variations in fracture mechanism: namely, debond versus resin fracture. Dimples are thought to be due to rubber particles rather than voids introduced during manufacturing. Scalloping is a result coalescence of microcracks.

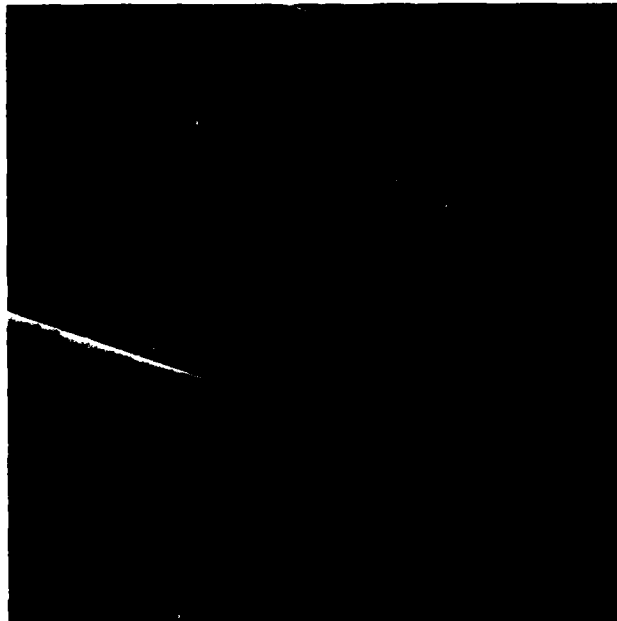


Figure 9. In-situ delamination fracture in AS4/3504. Because of brittle character of resin, crack opening displacement is very small and exact location of crack tip is uncertain. No damage zone around crack tip is indicated. 500X.



Figure 10. Post-mortem fractography of delaminated AS4/3502 composite. Note the smooth corrugations due to debond at the matrix/fiber interface with coalesced microcracks giving scalloped regions between the fiber debonds. 2000X

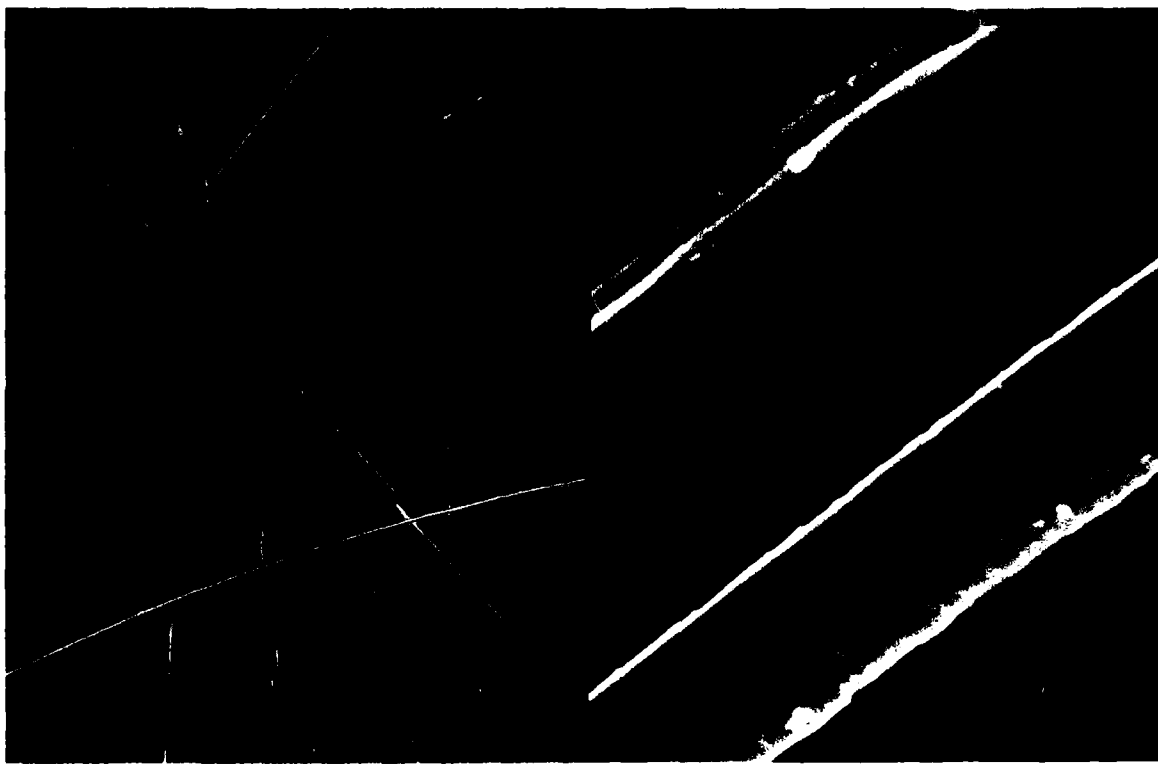


Figure 11. Post-mortem fractography of delaminated AS4/3502 composite emphasizing the weak interface in this system. Only in this system were loose fibers found strewn on the delaminated fracture surface. The enlargement shows the bare fiber resulting from debonding and the cracked resin between adjacent fibers. No such observations were ever made on the AS1/3502 composites, which apparently had much stronger interfacial bonding: (left, 100X; right, 4500X.)



Texas A&M University Report MM 4665-84-1  
January 1984

EFFECT OF RESIN CONTENT ON THE DELAMINATION  
FRACTURE BEHAVIOR OF GRAPHITE EPOXY LAMINATES

William M. Jordan\* and Walter L. Bradley\*\*

\*Graduate Student  
Mechanics and Materials Center  
Texas A&M University  
College Station, TX 77843

\*\*Professor of Mechanical Engineering  
Department of Mechanical Engineering  
Texas A&M University  
College Station, TX 77843

18)

## ABSTRACT

Jordan, W.M., and Bradley, W.L., Effect of resin content on the delamination fracture behavior of graphite epoxy laminates, 1984, SAMPE Quarterly, Volume ( , ).

Delamination fracture in Hexcel F155 graphite/epoxy composite is shown to be matrix (resin) dominated. Tests were run on laminates that were bled and unbled during curing. Unbled laminates have a higher resin content than bled laminates. In-situ delamination fracture was done in an SEM. This SEM was equipped with a tensile stage to enable real time observations of crack growth to be made. The unbled laminates have a smaller but much more heavily microcracked region near the crack tip. The more highly damaged crack tip region in the unbled laminates appears to be the major cause for them to have a higher  $G_{1C}$  than the bled laminates for delamination fracture.

## INTRODUCTION

Fiber reinforced laminates are of great interest to the aerospace industry because of their very high specific strength. However, a problem with fiber reinforced epoxy laminates has been their poor toughness transverse to the fiber direction. A proposed solution to this problem has been to toughen the resin by the addition of rubber particles. These particles can increase the toughness of the neat resin by several orders of magnitude [1, 2]. In contrast to the large toughness increase in a toughened resin, the composite often has a much more modest increase in toughness with the addition of rubber particles [1, 2]. The exact reasons are not clear but it appears to be related to the fiber-matrix interaction [3]. Cohen and Bradley [4, 5] have shown the toughness of a brittle resin may be increased by fiber addition; however, if the resin is already relatively tough, the fibers may actually decrease the toughness of the

material. In a brittle resin the presence of fibers restricts micro-crack growth, requiring more energy to be input before the crack will be able to grow further. In a tough resin, the deformation zone ahead of the crack tip may be significantly reduced in size by the presence of the fibers. Fracture at the fiber/resin interface could also potentially reduce the energy absorbed in crack growth.

Material processing can also affect fracture behavior. For example a bleeder cloth may be used in the fabrication process to control resin content [6]. By the use of a bleeder cloth it is possible to make laminates of the same resin but with different percentages of resin content. In this study two laminates were prepared with different proportions of resin content. The effect of resin content upon delamination fracture behavior was examined through the determination of the critical energy release rate  $G_c$ . In-situ fracture was studied in a scanning electron microscope to examine the micromechanisms of fracture.

#### MATERIALS AND METHODS

Two 16 ply unidirectional laminates were fabricated from Hexcel F155 resin with T3T145 carbon fibers. The manufacturer's suggested cure cycle was used. The laminates were cured at 127°C for 90 minutes. The heat up and cool down was at 3°C per minute. One laminate was made with a bleeder cloth and one without a bleeder cloth. The bled laminate had a smaller resin content than the unbled one. The supplier recommends the laminates not be bled during curing.

Teflon strips were placed in the centerline around the edge of the laminate during fabrication to provide a sharp initial crack. Small delamination samples approximately 1 cm. by 3 cm. were prepared for delamination in a JEOL 35 JSM scanning electron microscope. Crack growth

was accomplished by pushing a wedge into the sample as shown in Figure 1. A dull wedge was used so that the wedge itself would not affect fracture by breaking fibers.

Larger double cantilever beam samples (2.5 cm. x 30 cm.) were used to measure the critical delamination energy release rate ( $G_c$ ). Using the analysis developed by Devitt et.al. [7, 8] it was possible to calculate  $G_c$  from measured loads, displacements and crack lengths. These tests were conducted on an MTS tensile machine operated in stroke control. Exposed fracture surfaces were then examined in a JEOL 25 scanning electron microscope operated at 25 kv. The in-situ fracture samples as well as the fractured surface were sputter coated with gold-palladium to a thickness of 100-200 Å.

#### RESULTS

Fiber content was calculated two ways. The results are shown in Table 1. First, fiber content was estimated by measuring the density of the laminate. Knowing the individual fiber and resin densities, the volume percent of fibers was calculated. The second estimate of fiber content was obtained by a point count on a transverse photomicrograph of the laminates. An unfractured transverse view of the laminates is shown in Figures 2a and 2b. Both methods produced a higher fiber content in the bled laminates. The point count method produced higher fiber content values than did the density method. The bled laminate had a higher fiber content largely due to having a smaller resin rich region between plies as shown in Figure 2.

The critical energy release rate,  $G_{1c}$ , was calculated in two ways. First, the method developed by Devitt et.al. [7, 8] was utilized. Following the example of Hulsey [9] and Cohen [4] the laminates were tested in the geometrically linear region. At each load/unload the crack length was measured visually. A value of  $G_{1c}$  at each unload could then be

calculated. A second way  $G_{1C}$  was calculated was using the method developed by Wilkins [10] which involved the use of the data to curve fit an equation for compliance as a function of crack length. As shown in Table 2 both methods produce similar values for  $G_{1C}$ . The unbled material has a  $G_{1C}$  almost twice that of the bled material.

In-situ fracture in the SEM was carried out using samples with the same number of plies (and from the same fabricated panels) as used in the determination of  $G_{1C}$ .

Results of in-situ fracturing are shown in Figures 3-6. Figure 3 illustrates the fracture behavior of the unbled specimen. Crack growth occurred between Figures 3a and 3b. As the crack grew, the microcracks ahead of the crack tip grew in size and number. The microcracks had a  $45^\circ$  orientation with respect to the main crack, indicating failure under shear. Three other major cracks parallel to the main crack also grew significantly. Fiber debonding from the resin is also present. Figures 3c and 3d show the microcracking at the resin tip in more detail. Crack growth occurred between Figures 3c and 3d. Figure 4 shows the crack growth in the region of rubber particles which indicates the crack growth proceeds around both sides of the particle. When the resin finally tears away, there is a scalloped type appearance on both sides of the major crack.

In the unbled material microcracking only extends about 2 or 3 fiber dimensions to each side of the major crack. This is in contrast to the way the bled material fractured as shown in Figures 5 and 6. In the bled material the microcracks often tend to be perpendicular to the main crack rather than parallel to it. They also extend up to 10 fiber diameters away from the main crack as shown in Figure 6 where photomicrographs a, b and c were taken panning away from the main crack to the right. For the unbled

laminate, its damage zone (region of microcracking) is smaller than the bled material but has many more microcracks within that damaged region.

Figures 7-9 show the fracture surface of the bled and unbled samples fractured in the MTS. Two important observations should be noted. First, the artifacts on the fracture surface are essentially the same near the edge and in the center, as seen in Figures 7 a and b for the bled laminate and Figures 8 a and b for the unbled laminate. This clearly indicates that the fracture processes we are observing at the surface are representative of those taking place in the bulk.

The basic fracture mechanism appears to be the same in both materials as shown in Figures 7 and 8. The unbled laminate surface had more resin and fewer fibers than did the bled fracture surface. Its fracture surface was rougher and more faceted. In contrast the bled laminate fracture surface had more fiber breakage and fiber pullout.

In some materials  $G_c$  varies with respect to crack length [11]. Figures 8b and 8c were taken at 2 and 5 inches, respectively, from the initial crack position on the unbled laminate. They show very little change in fracture appearance with respect to crack length, which is consistent with our measured  $G_{1c}$  remaining relatively constant with respect to crack extension.

Figures 6 c and d and Figure 9 show the highly irregular surface of the torn resin with rubber particles and associated cracks which appear to go behind them as well. This correlates with the crack proceeding around the rubber particles as shown in Figure 4.

#### DISCUSSION

The density and point count methods for estimating fiber content produced different results. The density method assumed no voids in the material and would produce an estimate of fiber content that is too low.

The point count method did not include the thicker resin rich regions near the surface of the laminate which for our purposes are not relevant. Because the point count method can be localized to the bulk density where fracture is being studied, it is considered to be the more meaningful.

$G_{1C}$  values were the same for each calculation method, and thus, either method is deemed acceptable. The unbled laminate had higher values of  $G_{1C}$  than the bled laminate. Since the resin has some ductility, higher  $G_{1C}$  values would be expected due to the higher resin content. For this material, most of the cracking occurs in the resin, and the microcracks provide the major energy dissipative process. The many more microcracks in the unbled laminate would appear to dissipate much more energy as crack growth occurs.

In-situ fracture was conducted on a laminate with the same number of plies as the one on which  $G_{1C}$  was measured. By using the same number of plies the in-situ fracture analysis could be legitimately correlated with the macromechanical  $G_{1C}$  results.

The appearance of the fracture surface near the edge and near the center of the sample was the same. This aspect is important because the photomicrographs record only the growth of the edge of the crack. These observations indicate the crack mechanism is essentially the same across the sample width, thus enabling this in-situ method to be used to get an accurate representation of the material while it is cracking.

The unbled laminate had more resin on the fracture surface. This observation is expected because it has more resin with increased microcracking in the resin rich region (Figure 3). The unbled laminate shows little change in the fracture surface as the crack grew (Figure 8), producing good correlation with the macroscopic  $G_{1C}$  testing which showed

little change in  $G_{1C}$  with respect to crack length.

The rougher, more faceted surface on the unbled fracture surface (Figure 8) was caused by the many small microcracks in the resin (Figure 3). Those many microcracks and the cracking around the rubber particles (Figure 4) produced the rougher fractured surface (Figure 8).

The bled laminate had fewer microcracks (Figure 6), and therefore, less resin on the fracture surface (Figure 7). Figure 7c shows more broken fibers and fiber tear out. This correlates with the in-situ observation (Figure 6) which showed most of the microcracks to be near the fibers. These microcracks appear to be the beginning stages of the fiber debonding.

#### CONCLUSIONS

The present study has 3 major conclusions:

- (1) delamination failure in this material is matrix (resin) dominated;
- (2) in-situ (real time) fracture analysis yields useful information about the crack growth mechanism because the crack growth mechanism near the edge and center of the sample appears to be the same;
- (3) the critical energy release rate,  $G_{1C}$ , appears to be a function of the number and type of microcracking near the crack tip, the size of the damaged zone being less important than the number of microcracks within it. With this material, the thicker the resin rich region the higher the value of  $G_{1C}$ .

#### ACKNOWLEDGEMENTS

The authors acknowledge the financial assistance of the Air Force Office of Scientific Research who supported this research with AFOSR Contract F46920-82-C-0057. This contract was administered by Major David Glasgow.

They would like to thank the Texas A&M Electron Microscopy Center for technical assistance in this project. They would like to thank Laurie



AD-A150 002

RESEARCH ON COMPOSITE MATERIALS FOR STRUCTURAL DESIGN

(U) TEXAS A AND M UNIV COLLEGE STATION MECHANICS AND

MATERIALS RE. D ALLEN ET AL. APR 84 MM-4665-84-5

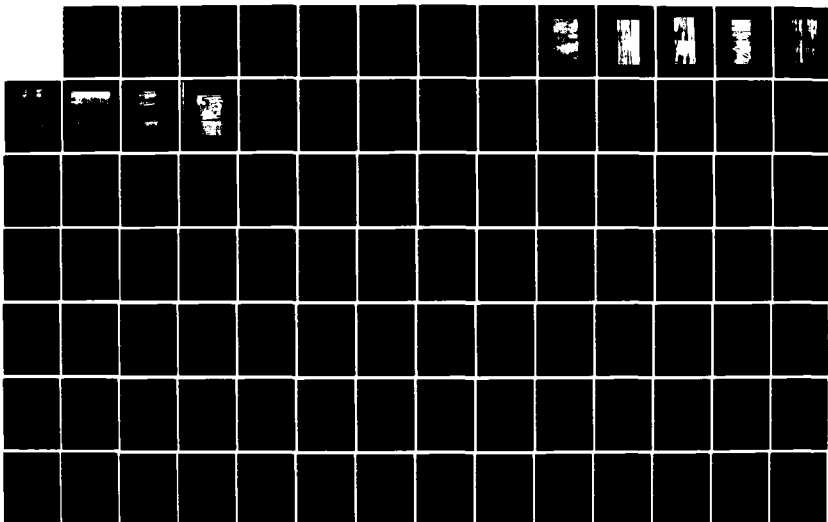
UNCLASSIFIED

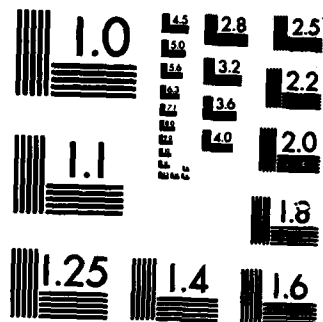
AFOSR-TR-85-0226 F49620-82-C-0057

F/G 11/9

NL

314





MICROCOPY RESOLUTION TEST CHART  
NATIONAL BUREAU OF STANDARDS-1963-A

Veeder, Kevin McRee, Mark Tanner and Keith Lund for their help in specimen preparation and testing.

Table 1

## RESIN CONTENT OF LAMINATES

Laminate	Composition by Density Calculations		Composition by Point Count of Transverse Photomicrograph	
	Volume % Fibers	Volume % Resin	Volume % Fibers	Volume % Resin
Bled	55.2	44.8	76.7	23.3
Unbled	41.6	58.4	61.7	38.3

## LITERATURE CITED

1. Bascom, W.D., Ting, R.Y., Moulton, R.J., Riew, C.K. and Siebert, A.R., "The Fracture of an Epoxy Polymer Containing Elastomeric Modifiers", Journal of Materials Science, Vol. 16, 1981, pp. 2657-2664.
2. Bascom, W.D., Bitner, J.L., Moulton, R.J. and Siebert, A.R., "The Interlaminar Fracture of Organic-Matrix Woven Reinforcement Composites", Composites, January 1980, pp. 8-18.
3. Bucknell, C.B., "Fracture and Failure of Multiphase Polymers and Polymer Composites", in Advances in Polymer Science #27, 1978, pp. 122-148.
4. Cohen, R.N., "Effect of Resin Toughness on Fracture Behavior of Graphite/Epoxy Composites", Master's Thesis, Texas A&M University, December 1982.
5. Bradley, W.L. and Cohen, R.N., "Delamination and Transverse Fracture in Graphite Epoxy Material", Fourth International Conference on Mechanical Behavior of Materials, Stockholm, Sweden, August 1983.
6. Loos, A.C. and Springer, G.S., "Curing of Epoxy Matrix Composites", Journal of Composite Materials, Vol. 17, March 1983, pp. 135-169.
7. Devitt, D.F., "Delamination Fracture Toughness of a Unidirectional Composite", Master's Thesis, Texas A&M University, August 1979.
8. Devitt, D.F., Schapery, R.A. and Bradley, W.L., "A Method for Determining the Mode I Delamination Fracture Toughness of Elastic and Viscoelastic Materials", Journal of Composite Materials, Vol. 14, 1980, pp. 270-285.
9. Hulsey, R.C., "Delamination Fracture Toughness of a Unidirectional Graphite/Epoxy Composite", Master's Thesis, Texas A&M University, December 1980.
10. Wilkins, D.J., Eisenmann, J.R., Camin, R.A., Margolis, W.S. and Benson, R.A., "Characterizing Delamination Growth in Graphite-Epoxy", in Damage in Composite Materials: Basic Methods, Accumulation, Tolerance and Characterization, ASTM STP 775, 1982.
11. Russell, A.J., and Street, K.N., "Moisture and Temperature Effects on the Mixed-Mode Delamination Fracture of Unidirectional Graphite/Epoxy", presentation given at ASTM Symposium on "Delamination and Debonding of Materials", Pittsburg, Nov. 1983.

Table 2

## CRITICAL ENERGY RELEASE RATE

 $G_c$  (J/m<sup>2</sup>)

Material	Bled (1"/min elongation rate)	Unbled (1.5"/min elongation rate)	Unbled (1"/min elongation rate)
$G_{lc}$ by Devitt Method (7)	553	955	1011
$G_{lc}$ by Wilkins Method (10)	552	947	1041

## Table of Figures

Figure 1	Tensile Stage Used to Delaminate Laminate in SEM
Figure 2a	Transverse View of Unfractured Bled Laminate Showing One Ply and Resin Rich Regions on Both Sides
Figure 2b	Transverse View of Unfractured Unbled Laminate Showing One Ply and Resin Rich Regions on Both Sides
Figure 3a	In-situ Fracture of Unbled Laminate Showing Crack Growth
Figure 3b	In-situ Fracture of Unbled Laminate Showing Crack Growth
Figure 3c	In-situ Fracture of Unbled Laminate Showing Microcracking Near Crack Tip
Figure 3d	In-situ Fracture of Unbled Laminate Showing Growth of Microcracks as Main Crack Grows
Figure 4a	In-situ Fracture of Unbled Laminate Showing Fracture Around Rubber Particles
Figure 4b	In-situ Fracture of Bled Laminate
Figure 5	In-situ Fracture of Bled Laminate
Figure 6a	In-situ Fracture of Bled Laminate
Figure 6b	In-situ Fracture of Bled Laminate (to right of 6a)
Figure 6c	In-situ Fracture of Bled Laminate (to right of 6b) Showing Microcracks up to 10 Fiber Diameters Away From Main Crack
Figure 7a	Bled Fracture Surface Near Edge
Figure 7b	Bled Fracture Surface Near Center
Figure 7c	Bled Fracture Surface Near Edge Showing Fiber Breakage and Tear Out
Figure 7d	Bled Fracture Surface Near Edge Showing Fracture of Resin Surface
Figure 8a	Unbled Fracture Surface Near Edge 2" from Initial Crack
Figure 8b	Unbled Fracture Surface Near Center 2" from Initial Crack

- Figure 8c      Unbled Fracture Surface Near Center 5" from initial Crack
- Figure 9a      Unbled Fracture Surface Near Edge Showing Significant  
Fracture of Resin Rich Region
- Figure 9b      Unbled Fracture Surface Near Edge Showing Ductile Type  
Fracture of Resin Rich Region



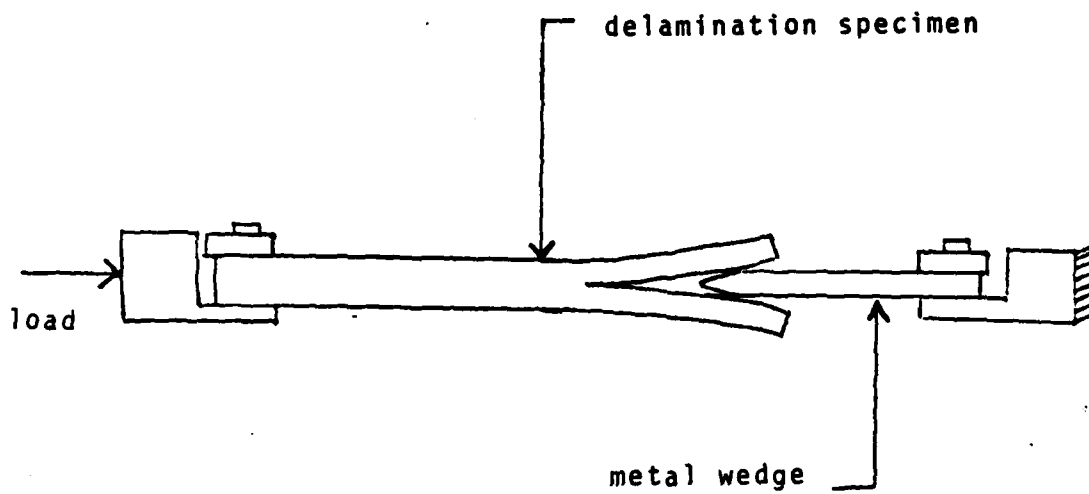
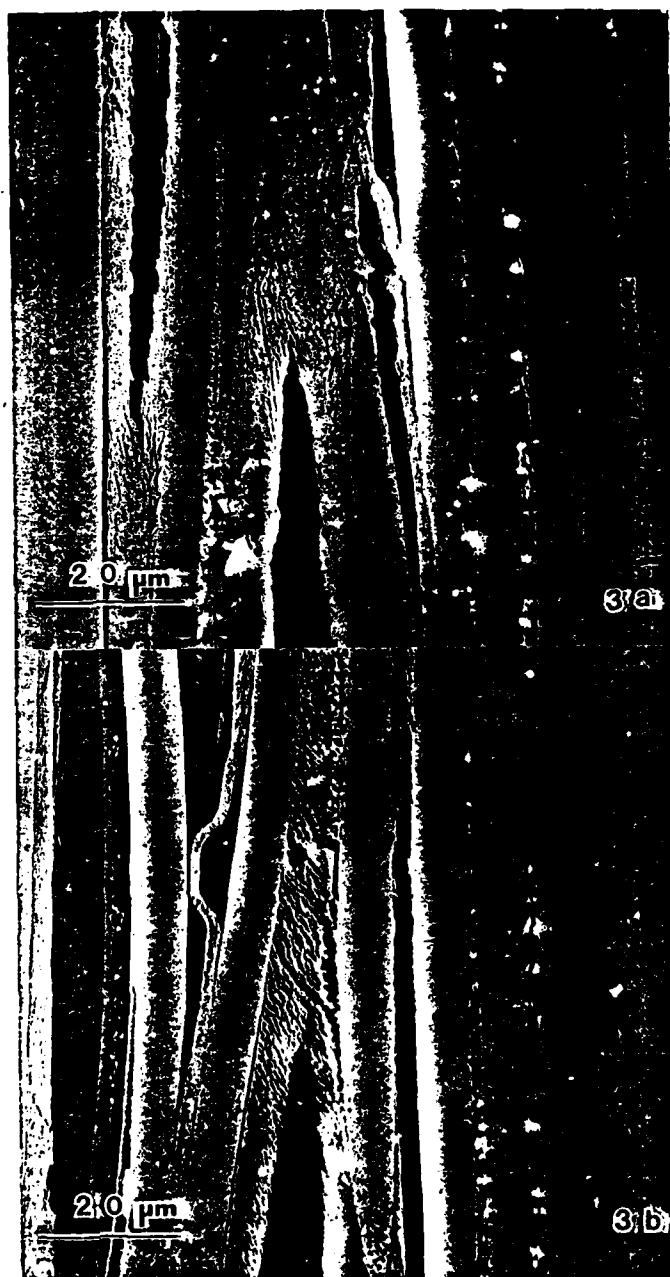
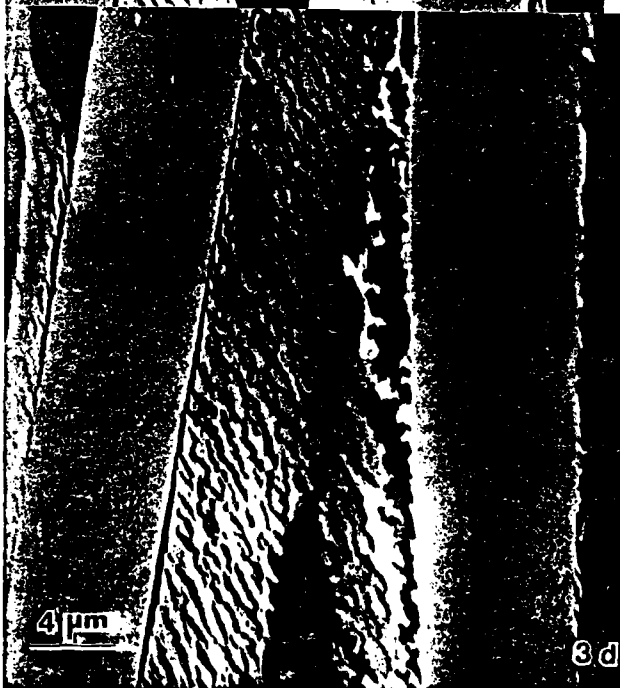
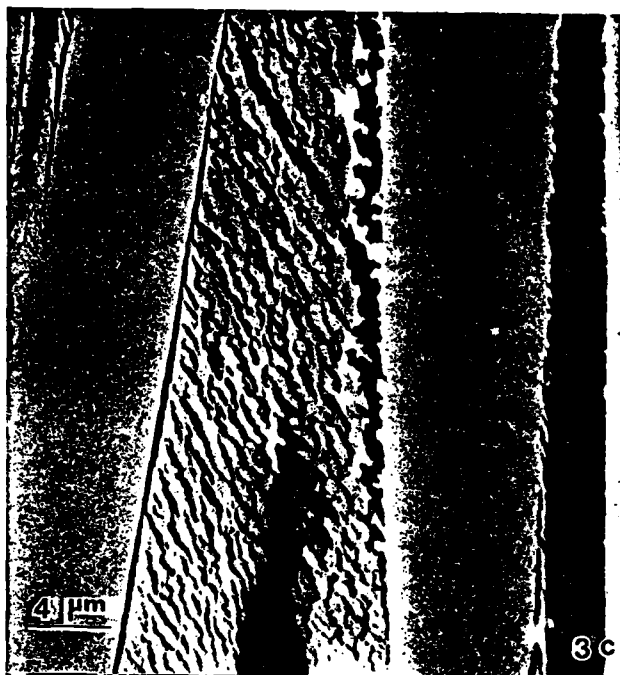


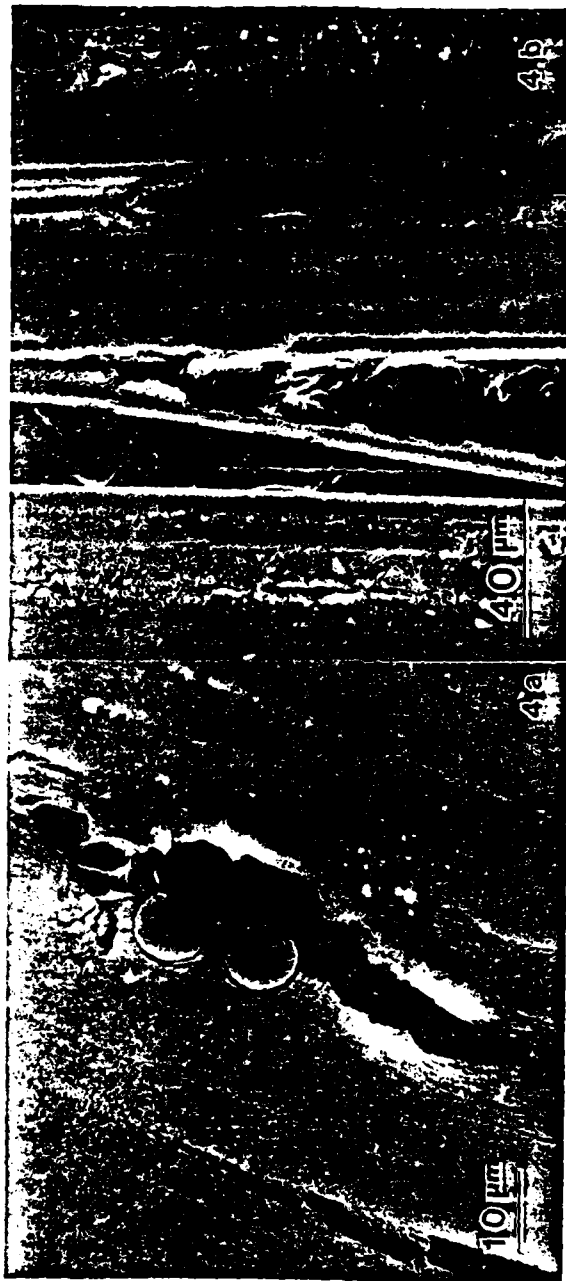
Figure 1

Tensile Stage Used for Delamination in the  
JEOL 35-TS2 Scanning Electron Microscope

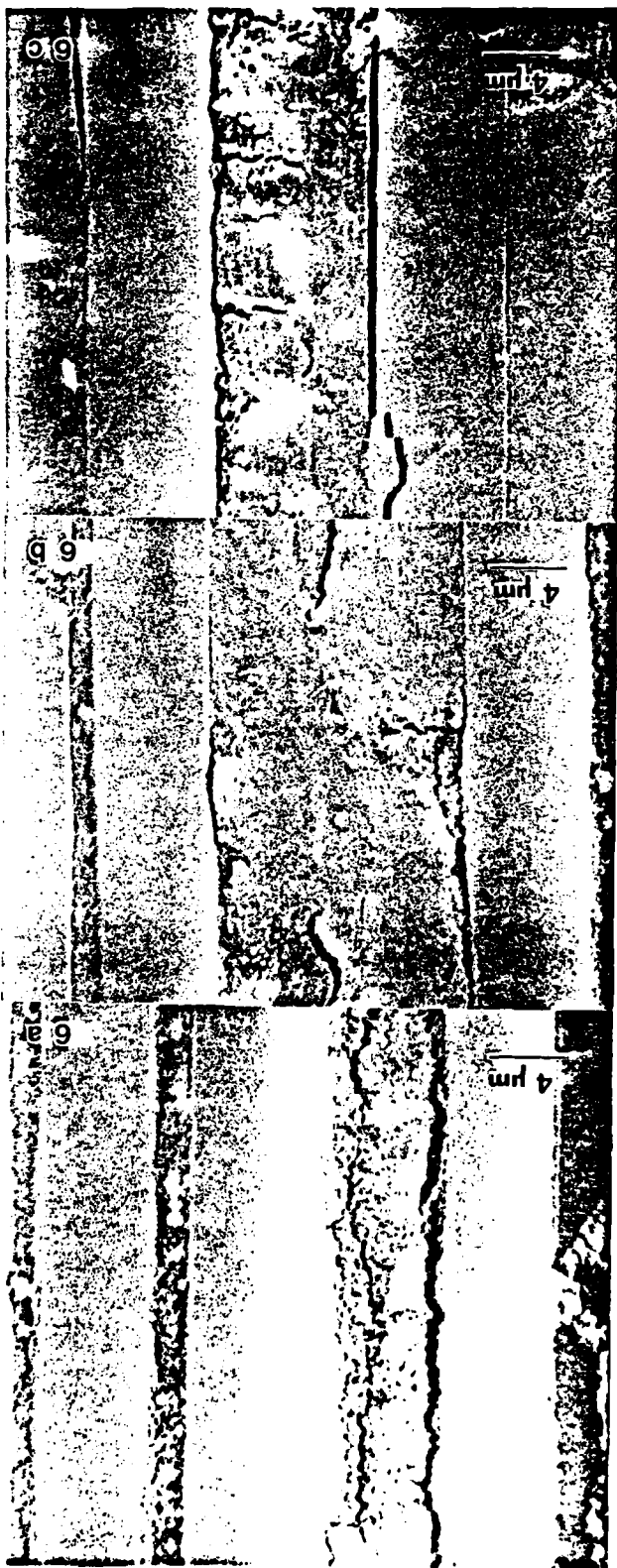


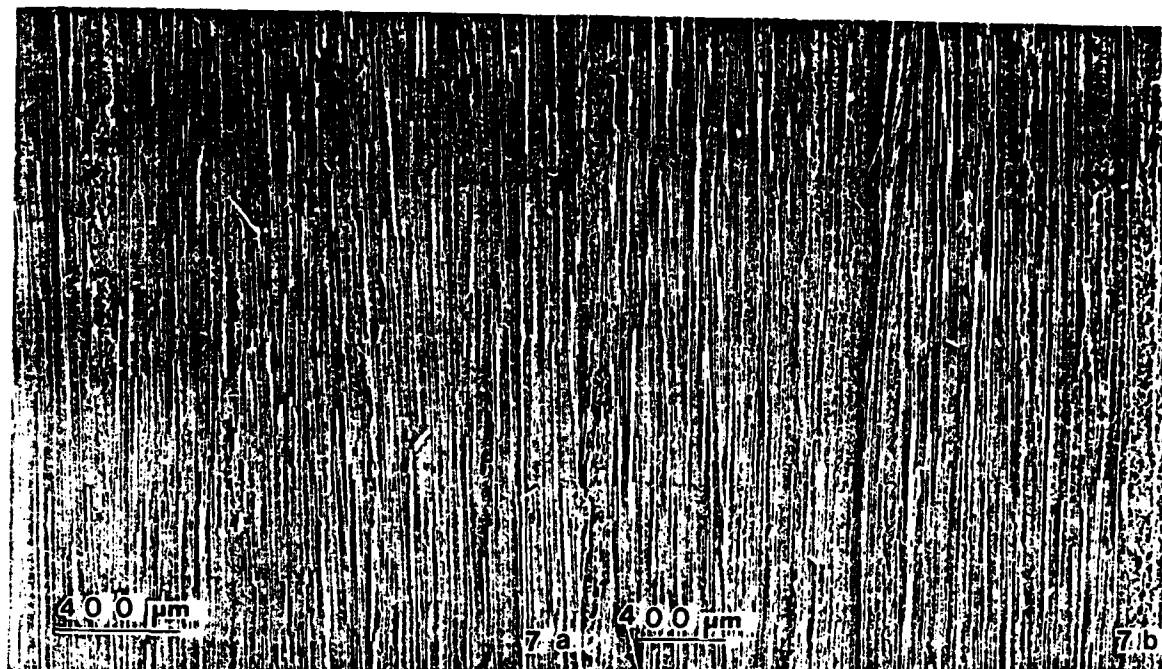


















A MOLECULAR MODEL FOR CREEP IN A VISCOELASTIC POLYMER

Joe S. Ham  
Dept. of Physics  
Texas A&M University

ABSTRACT

Some general molecular assumptions are used to derive the form for a stress relaxation function. Except for very short times, the shape closely approximates  $\exp(-at^{1/3})$  for the most reasonable approximation that the diffusive motion governs the relaxation. This is inverted to show that the creep function comes close to a power law with an exponent that becomes smaller as more nonrelaxing components are added. The primary assumptions are that the average stress of a chain that must move a length  $L$  to come into mechanical equilibrium will decay exponentially as  $\exp(-t/T)$ , where  $T$  is proportional to  $L^2$  for diffusive motion, and that the length  $L$  is a random variable distributed in an exponential form as  $\exp(-bL)$ .

Since the earliest studies of the properties of materials, efforts have been made to determine a general form to describe time-dependent properties of materials such as a creep function that would be applicable to a variety of materials with a minimum of adjustable parameters.<sup>1</sup> For the most part, these have been equations selected for their qualitative shape with sufficient empirical parameters to fit available experimental data. This is of most interest in polymeric materials where the time effects are particularly important.

In this paper, we will deduce from some rather general assumptions a form for the stress relaxation and creep functions for a molecular model. These approximate some of the empirical equations that have been proposed and, for example, show close to a power law dependence in creep. Since the power law has been used to represent the time dependence in many cases, a deduction of this mathematical form from a molecular model may indicate the conditions where this law is likely to be valid. The contribution of this paper is to offer a physical basis for this power law.

In order to explain how a non-equilibrium distribution of velocities in a gas could slowly evolve as a result of molecular collisions into the equilibrium distribution, Maxwell introduced a simple element consisting of a spring and a dashpot. The advantage of this element is its mathematical simplicity but neither it nor the related Voigt element should be considered to

represent any particular type of molecular motion. Nevertheless, we will discuss our model in terms of distributions of such elements as a mathematical convenience.

In a few cases, the theoretical models to represent the time dependent behavior of materials have been based upon the Maxwell or Voigt elements with elements added until quantitative agreement with experiment was obtained. Material behavior usually cannot be well represented by just a few of these theoretical elements and yet the introduction of a large number of empirical parameters casts doubt as to the physical basis for using such equations. Sometimes a continuous distribution of these elements is used in order to obtain a general model of the behavior but the density function of this distribution is difficult to determine from experimental data because large changes in the density function can yield almost identical experimental data. Therefore, criteria such as smoothness must be invoked to obtain a unique density function of the distribution.

Ngai<sup>2</sup> has developed a general theory of time-dependent processes which produce a family of functions that can be fitted to experimental data. Most of his work has been with the dielectric relaxation data, but he has also done some work with viscoelastic relaxation. The present work is a special case of his theory where more specific assumptions are made rather than the general assumptions of the shape of the phonon spectrum he

proposes whose significance are difficult to visualize in a polymer.

#### MODEL

We will consider either the amorphous state of a linear polymer of uniform molecular weight which is sufficiently high so that entanglements are important or a crosslinked system. The argument applies whether the system is either below or above the glassy transition temperature with some reinterpretation, but probably not within the temperature range where the relaxations of the glassy transition are present. In either the linear or the crosslinked system, the molecular chains are considered to interact in three distinct ways. First, there is the interaction that is a contact interaction such as occurs in any liquid. This interaction is the basis for the friction factors which affects the motion of one molecule relative to its neighbors. It will contain much of the temperature dependence of the motion.

Second, there are those entanglements which are so near permanent that they do not change during the course of a normal experiment. In a crosslinked system, this type of interaction is clearly important but even in a linear molecule an entanglement that persists beyond the time span of the experiment will be classified as of this type. This interaction affects the modulus but only indirectly influences any time dependent effects.

Third, there are those entanglements which can unravel or reform during the time of the measurements. These are the entanglements which give rise to the stress relaxation and creep. Even the first type of contact interactions can give rise to viscoelastic effects such as studied by Rouse<sup>3</sup> and Bueche.<sup>4</sup> When studying a material below the glassy transition, these relaxations are on a time scale short compared to the time scale we are discussing. They will dominate only when the molecular weight is so low that entanglements are rare. These motions become important near the glassy transition temperature.

Below the glassy transition temperature, the nature of the molecular motion is obscure. There can be motion of small segments of chains or side chains but the development of strains as large as several percent indicate that more than just bond bending and stretching must be occurring. Any time dependent behavior beyond what is due to the segmental motion giving rise to the absorption in dynamic studies below the glassy transition are presumed in this paper to come from molecular motion such as described above for the behavior well above the glassy transition. The difference is that below the glassy transition the entire material is much stiffer and so must be described by drastically different friction factors.

Of course, these three types of interactions have no sharp line of demarcation between them. They are a convenience to consider the interactions as either be those responsible for the

viscous drag, permanent crosslinking, or the transitory type. The transitory interactions give rise to the major part of the time dependence in solids at longer times. A change to a different temperature could imply one type of transition should be reclassified into another.

In stress relaxation, the sample is given a fixed strain and the stress is followed in time. The permanent crosslinks will show no stress relaxation but the transitory interactions will decay away with time. We will consider a typical chain in the sample while it is undergoing stress relaxation. If it is a linear molecule that has a free end, then the unravelling will be an unwinding of the chain so that the entanglement disappears. If there is a crosslinked structure, then a chain that is not at equilibrium in the stressed state will diffuse until it reaches this equilibrium position. While this is clearly a cooperative motion of the chain and its surroundings, we will approximate it by a single chain moving in its surroundings and represent the interaction with its surroundings by a friction factor.

This chain will be undergoing random motion coming from thermal excitation. It is not so much the motion of this individual molecule which is important but the average motion of many molecules of this same type. Due to the external stresses, they are not in mechanical equilibrium with their surroundings but will approach this equilibrium on the average. The force causing the approach to equilibrium is most likely only the



random motion coming from the thermal motion. This is likely to be much more significant in the approach to equilibrium than any mechanical stress on the individual molecular chain coming from the applied stress. The applied stress gives rise to a bias for the random wandering but the effect of the strain is more that once a chain has relaxed an entanglement, then it is unlikely to form one that will contain an appreciable stress. We will describe the relaxation of the stress by an exponential decay  $\exp(-t/T)$  where  $T$  will be a time constant.

One might argue that instead of this simple exponential decay, a step function should be used such that the stress remains constant until the time of unravelling at which time it goes to zero. But, the average stress in a large number of similar chains is likely to decrease up to the time of release in an exponential fashion. Certainly, one could imagine a model with a more complex time dependence but the effect of different assumptions for this time dependence will have little influence upon our final results as long as the function describes a decay within a time  $T$ . The exponential decay has both mathematical and physical advantages. By itself, such a single exponential suggests a Maxwell element but, this describes not just a single chain relaxing but how the average stress of many similar chains will evolve in time.

The length of chain that must unravel will govern the time constant. For a time constant coming from a random diffusion in one dimension, the time constant will vary as  $T = aL^2$  where  $L$  is the length of the chain. We also do some calculations for  $T = bL$  which would apply if the applied force dominated the diffusional terms so that the diffusion just depended upon how long a force would be required to move an object acted upon by an opposite viscous force. Sometimes we will also consider  $T = cL^3$  which is an approximation if the chain length  $L$  is also going to be involved in entanglements. That is, if the length of the chain is such that several entanglements can occur within this length so that multiple unravelling must occur. This is only qualitative and is more indicative of the effect of multiple entanglements would have than a quantitative relationship. This is similar to the assumption made in order to understand the molecular weight of viscosity of high molecular weight polymer melts.<sup>6</sup>

The most important contribution in our model is that rather than consider this typical molecular chain alone, we will take the length  $L$  as being a random variable strongly peaked at zero. This will give a distribution of relaxation times that is broad and strongly peaked at zero. The form of this distribution is exponential if entanglements occurred without any dependence upon previous entanglements along the length of the chain. The mathematical form is  $c \exp(-cL) dL$  for the probability of having a length between  $L$  and  $L+dL$ . The major assumption in the

deduction of this distribution is that an entanglement restricting the length can occur anywhere along the chain with equal probabilities independent of the presence or absence of nearby entanglements.

For our theoretical studies, we will rescale the time and length to dimensionless values so that the stress relaxation will be given by

$$\int_0^{\infty} \exp(-L-t/nL^n) dL$$

where  $n = 1, 2$  or  $3$  if

the relaxation is governed by the stress as dominant, diffusion as dominant or as an indication of multiple entanglements. As stated above, the most physical value is  $n = 2$  but the other values are used to show the directions and magnitudes of the effects to be expected if the assumptions in the model are relaxed.

The integrand at a positive  $t$  now vanishes at both  $L = 0$  and  $L = \infty$ . It has a peak at  $L=(t)^{1/n+1}$ . If the contribution comes from just this peak, the integral can be approximated by  $c \exp(-at^g)$  where  $g=1/2, 1/3$ , and  $1/4$  for the choices  $n = 1, 2$ , and  $3$ . This form for the stress relaxation is quite similar to the form  $d \exp(-bt^{1/3})$  suggested by some early workers as described in reference 1. Figure 4 tests this approximation by plotting the log of the stress relaxation versus the cube root of the time. Except for the very short times, a straight line results

indicating that this is a good approximation. The behavior at short times is obscured in experimental data by the process of applying the stress. Therefore, experimental data that obeyed the theory would be plotted without noting the deviation at small times. The creep function is sometimes fit to the inverse of this function. Since creep and stress relaxation functions are approximate reciprocals this choice has some theoretical justification although not very reliable. The numerical studies later in this paper show that a more careful conversion of the stress relaxation function to the related creep function results in a function closer to a power law.

The integral with  $n = 1$  can be evaluated analytically in terms of Airey functions. After attempting to carry out some more precise analytical evaluations of these integrals, we evaluated them numerically in order to see their predicted properties.

#### NUMERICAL ANALYSIS

By the introduction of  $\exp(-L)$  as a variable in the integral for the stress relaxation the domain becomes 0 to 1, and we can evaluate the stress relaxation numerically for  $n = 1, 2$  and 3. The results are shown in Figs. 1-3. The effect is as one would expect that as  $n$  increases, the initial drop is steeper but the long time tail is more pronounced. The plot<sup>1</sup> of the logarithm of this function versus  $t^{1/3}$  in Figure 4 shows that the

approximation of using just the peak value is an excellent approximation except at the very shortest times.

Most use is made of the creep function rather than the stress relaxation. Analytically, one can take the Laplace transform of the stress relaxation, take the reciprocal and then take the inverse transform to obtain the creep. Numerically, we chose the alternative of taking the integral equation in the form

$$(Eq. 1) \quad C(t) = 1 - \int_0^t E'(s) C(t-s) ds$$

where  $C(t)$

is the creep function and  $E'$  is the derivative of the stress relaxation function. The integral should not include at the upper limit the singularity in  $C(0)$ . The creep function on the right is at earlier times than at  $t$  except at the lower integration limit. Therefore, by breaking the integral into a summation and taking the first term which involves the creep function at time  $t$  to the other side of the equation, one has a numerical method to evaluate the creep from the stress relaxation in a process that steps along the parameter  $t$  to evaluate the creep function in terms of  $E'$  and values of  $C$  already calculated. If the time is broken into  $N$  divisions of  $h$  so  $Nh=t$  and the average of the integrand at the first and last of the interval is used, then

$$D(t) = \frac{1 - (h) \sum E'(nh) D(t-nh) + (h/2) E'(t) D(0)}{1 + (h/2) E'(0)}$$

where the summation is for  $n=1$  to  $N$ . The last term in the

numerator corrects the summation since the integrand at 0 and  $t$  occur only once. The other values of the integrand enter twice since the intervals on each side contribute to them.

The stress relaxation occurs as the derivative which means that it must be calculated carefully at  $s = 0$  since it has close to, if not actually a singularity at this point. We use a polynomial approximation to the stress relaxation passing through nearby points and then use this to evaluate the derivative numerically. This process will soften the singularity if there is one. The numerical result was checked against a model of two Maxwell elements which can be done analytically and the results agreed within the precision of the plotter. Nevertheless, it is likely that errors will accumulate during the integration so that this method should be restricted to only moderately long times.

The results are shown in the Figures 5-7. The same data is shown in a log plot in Figures 8-10. In these figures, a parameter  $\alpha$  is introduced to measure the fraction of the initial stress which can relax. This is to model the effects of the permanent crosslinks.  $\alpha$  equals one corresponds to where there are no permanent crosslinks and the stress relaxation should approach zero at long times.  $\alpha$  equals zero describes the effect of only elastic elements and so no creep but just the instantaneous displacement. A straight line in these Figures would indicate the frequently used power law. The presence of permanent crosslinks reduces the amount of creep and flattens the

curves. This will result in a smaller slope in this plot or exponent in the power law. For alpha equal one, that is, no permanent crosslinks, the slope is about 1/2, 1/3, and 1/4 for  $n=1, 2$ , or 3. A smaller alpha reduces this considerably.

The results show that the curves are very well approximated by straight line over the range of values shown for alpha equal one. The slopes for  $n=2$  vary from .33 for alpha = 1 down to less than 0.10 for alpha = 0.2. This range includes most of the observed values.

Even from the Rouse model<sup>3</sup> where one is concerned with just the contact type interaction, one will find a similar power law shape. Bagley and Torvik<sup>5</sup> shows the equivalent relationship that the dynamic modulus follows a power law in a variety of polymers. The theoretical slope they find is 1/2 for the Rouse type interactions. Experimentally, they find other values best fit the experimental data.

#### DISCUSSION

The feature which leads to the power law is determined more by the assumption of the exponential distribution of the lengths than by any other factor. The power of the length entering the relaxation time influences the magnitude of the slope but it is the distribution of lengths which is fundamental to the behavior. This is also the feature which has the most fundamental validity. Only by introducing an interaction between the entanglements so

that they tended to cluster or to spread out could one alter this distribution. This has the attraction that other details of the model need not be very precise, but, conversely, the results cannot be used to establish their presence. An exponential distribution of dimensions of domains of high or low modulus would probably result in similar results although not based upon any molecular basis.



## REFERENCES:

- <sup>1</sup>H. Leaderman, "Elastic and Creep Properties of Filamentous Materials and other High Polymers", The Textile Foundation, Wash. D. C. (1943).
- <sup>2</sup>K. L. Ngai, "Universality of Low Frequency Fluctuation, Dissipation and Relaxation Properties of Condensed Matter", Parts I and II, Comments Solid State Phys. 9, 127 (1979); 141 (1950).
- <sup>3</sup>P. E. Rouse Jr., J. Chem. Phys. 21, 1272 (1953).
- <sup>4</sup>F. Bueche, J. Chem. Phys. 22, 603 (1954).
- <sup>5</sup>R. L. Bagley and P. J. Torvik, "A Theoretical Basis for the Application of Fractional Calculus to Viscoelasticity", J. of Rheology, 27,201 (1983).
- <sup>6</sup>M. Doi, "Explanation for the 3.4-Power Law for Viscosity of Polymeric Liquids on the Basis of the Tube Model", J. Polymer Sci. (Physics), 21,667 (1983).

### CAPTIONS

FIGURE 1. Theoretical stress relaxation for  $n = 1$  and  $\alpha = 1$ .

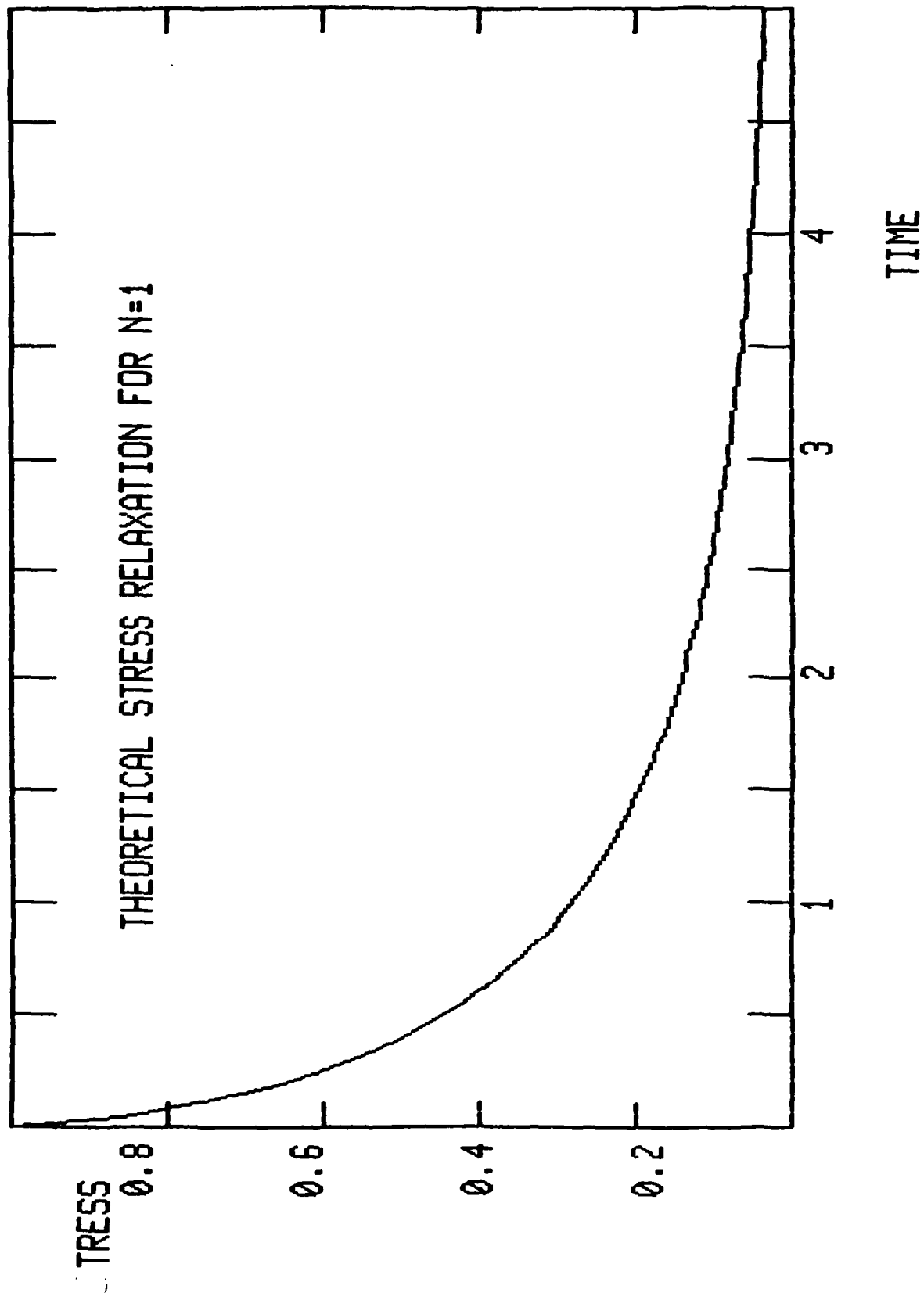
FIGURE 2. Same as Fig. 1 for  $n = 2$ . This is the value of  $n$  most likely from our model.

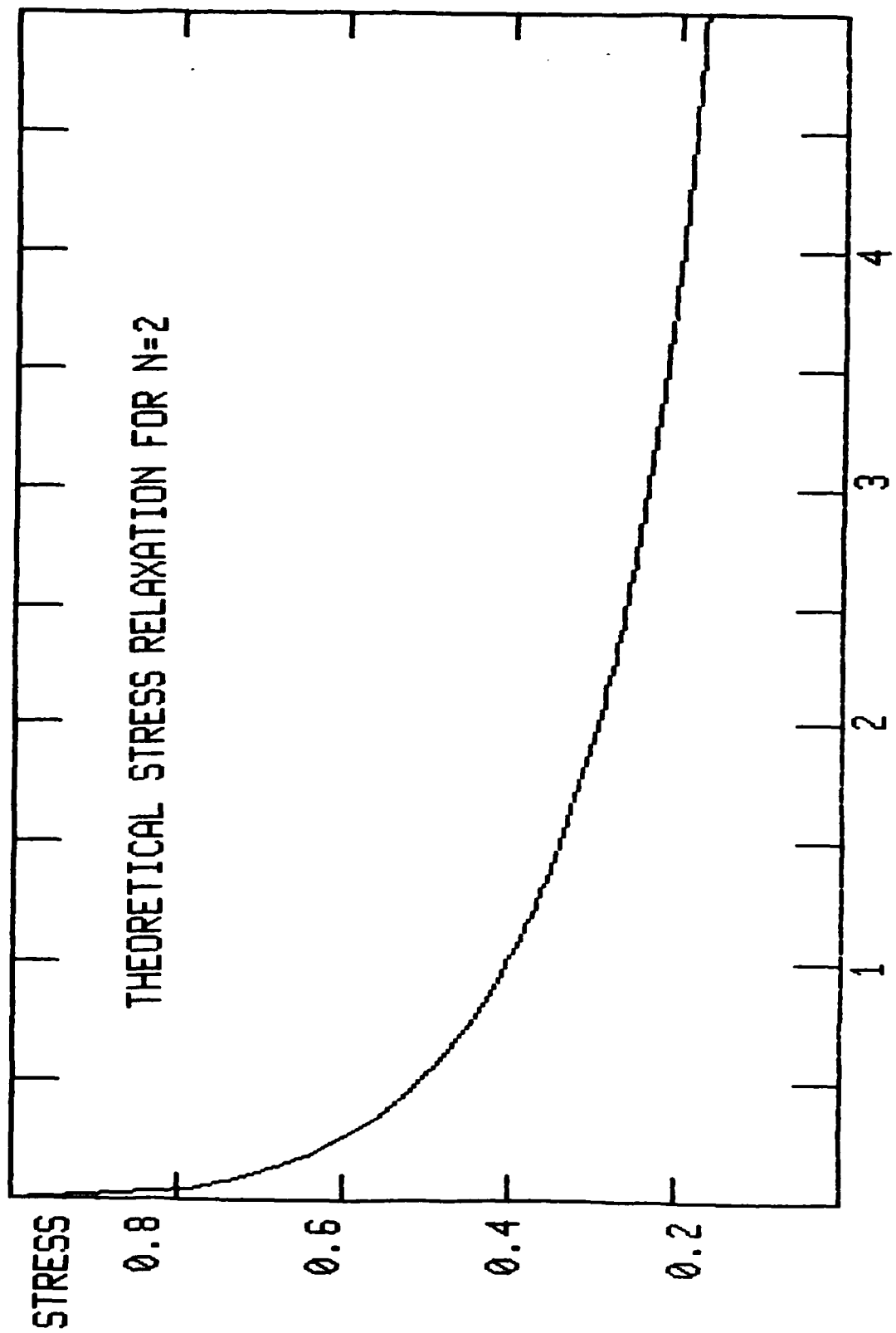
FIGURE 3. Same as Fig. 1 for  $n = 3$ .

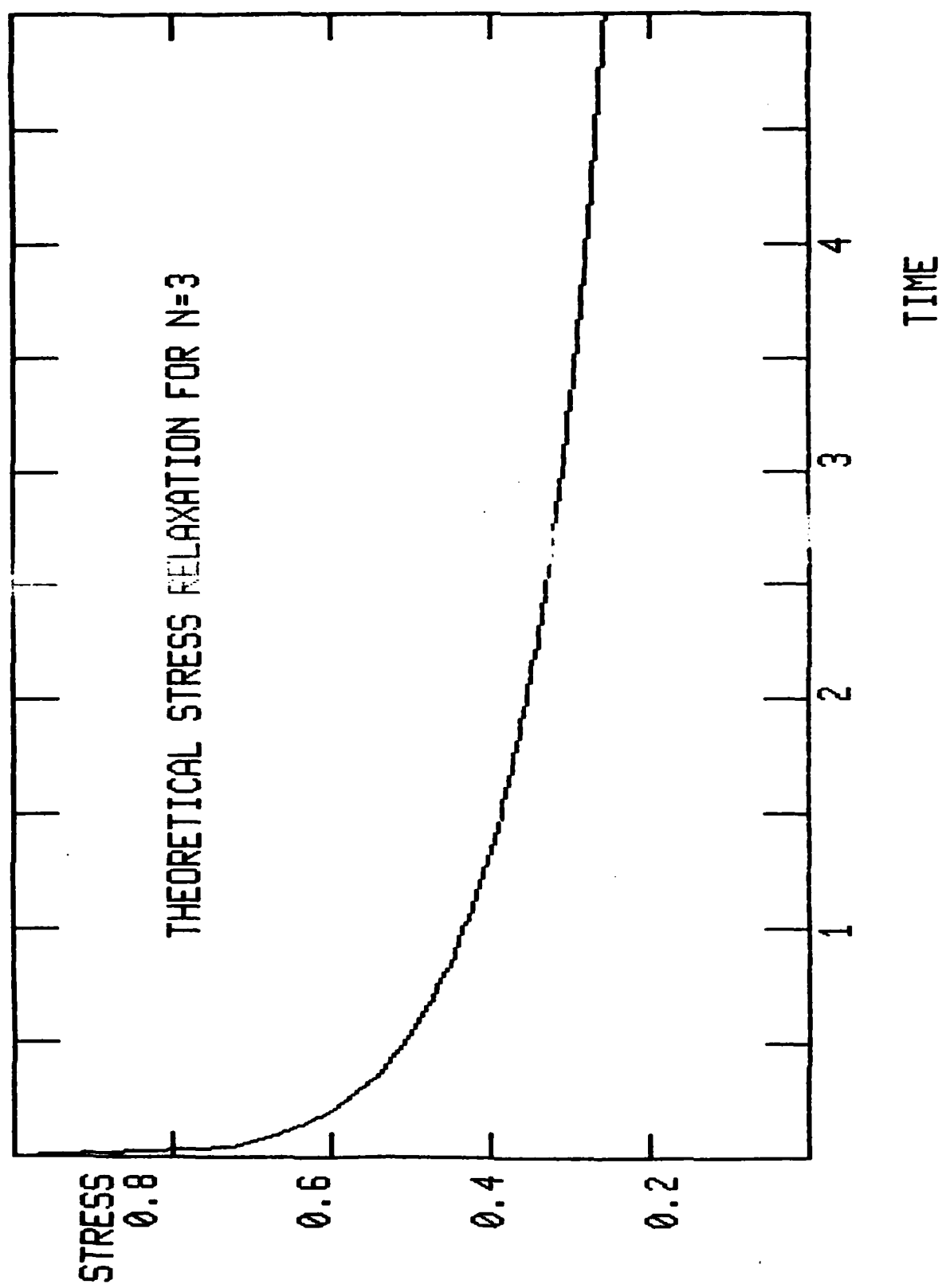
FIGURE 4. Theoretical stress relaxation curve for  $n=2$  where the logarithm of the stress is plotted versus the cube root of the time. Note that the plot is very close to a straight line except for very small times indicating that the function is close to  $\exp(-at^{1/3})$ .

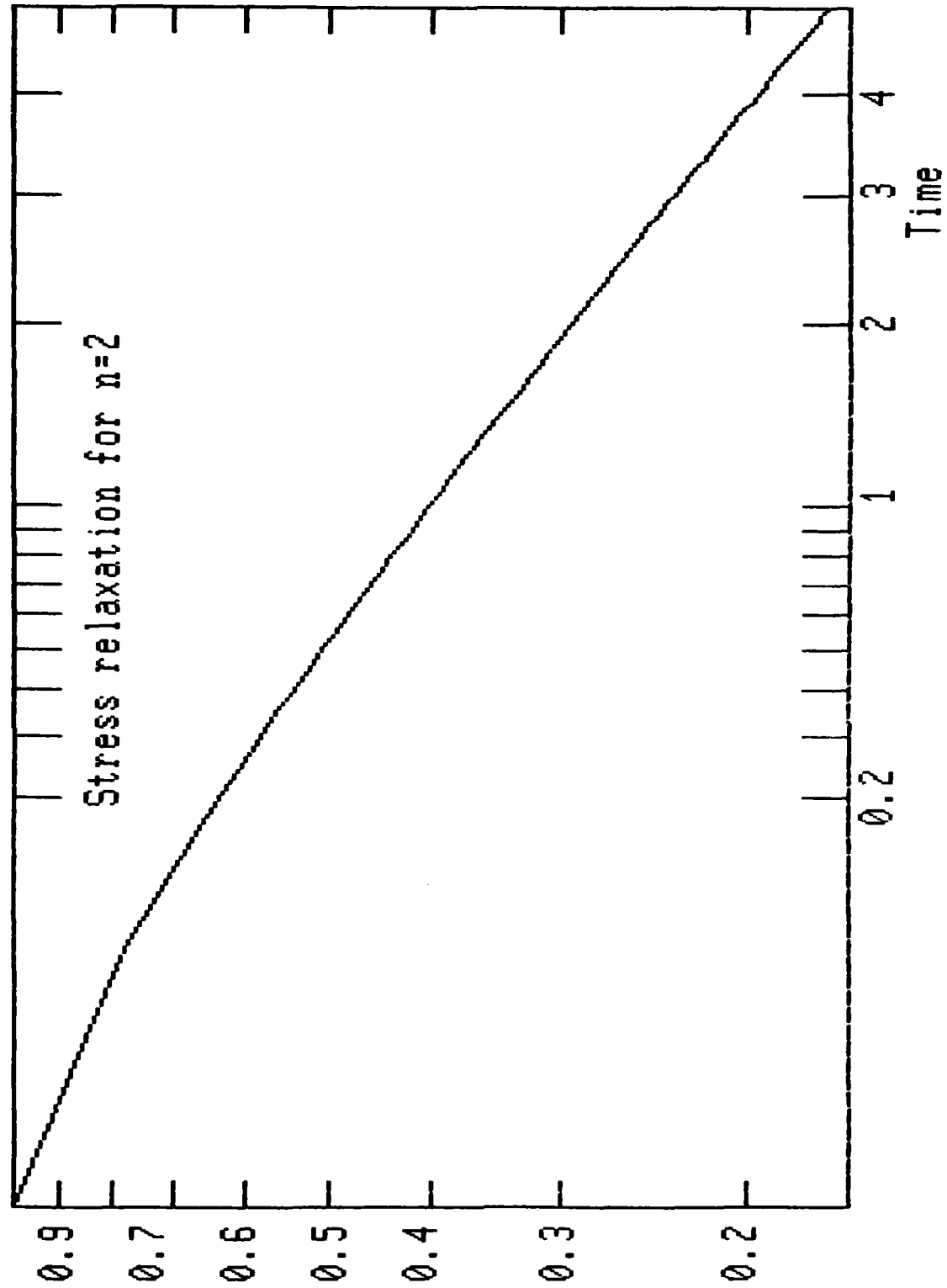
FIGURES 5-7. Creep curve obtained from numerical inversion of stress relaxation functions in Figs. 1-3. Fig. 4 has  $n=1$ . Fig. 5 has  $n=2$ . Fig. 6 has  $n=3$ . Alpha is taken as unity for all three meaning that no nonrelaxing entanglements or crosslinks are assumed.

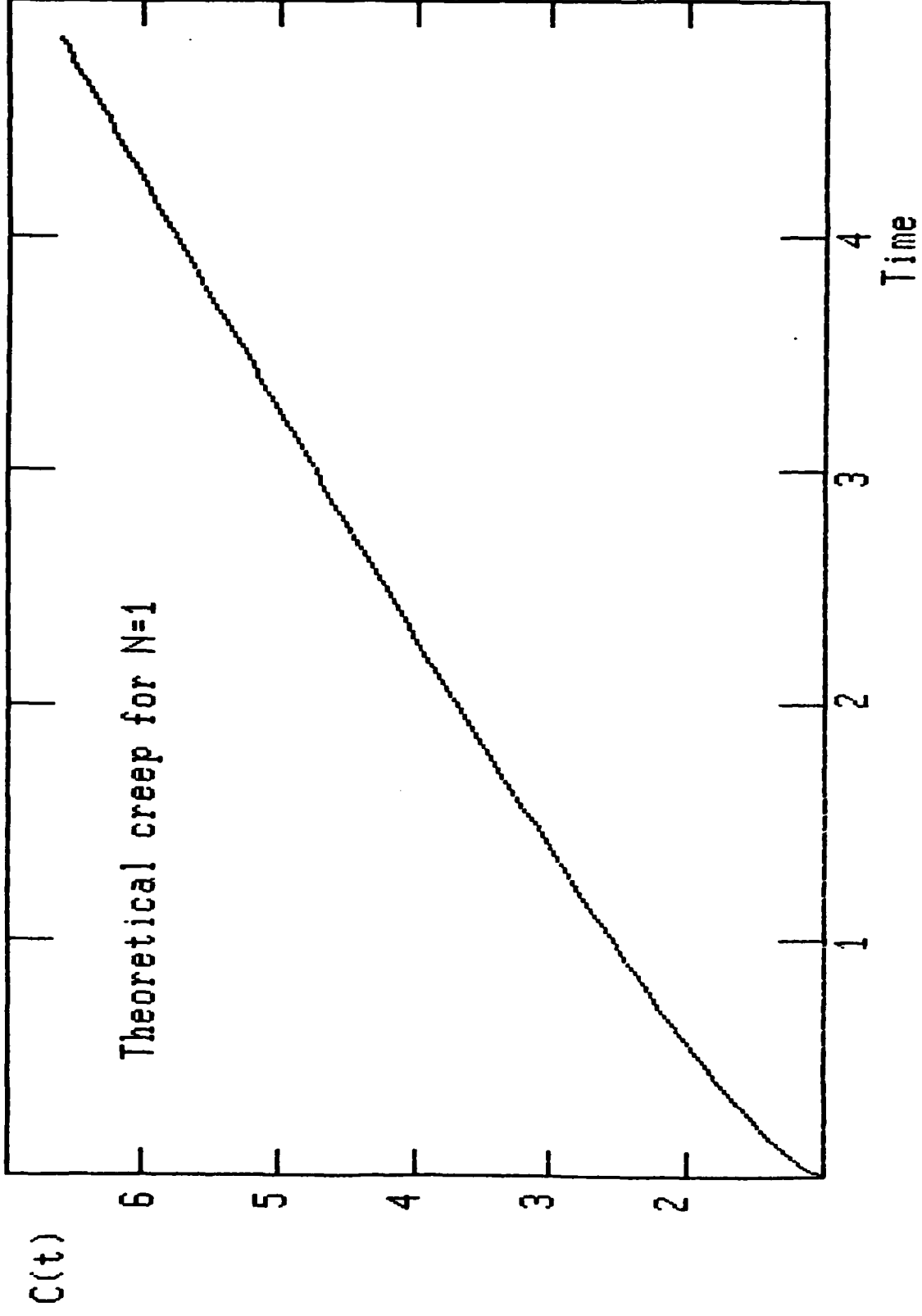
FIGURES 8-10. The creep curves from numerical inversion of the stress relaxation functions for various values of  $\alpha$  as marked. The curves are shifted vertically by an amount  $\log(\alpha)$  in order to display all curves on the same scale. Note the straightness of the curves for  $\alpha$  equal to 1 and how the slope drops to smaller values as  $\alpha$  decreases.

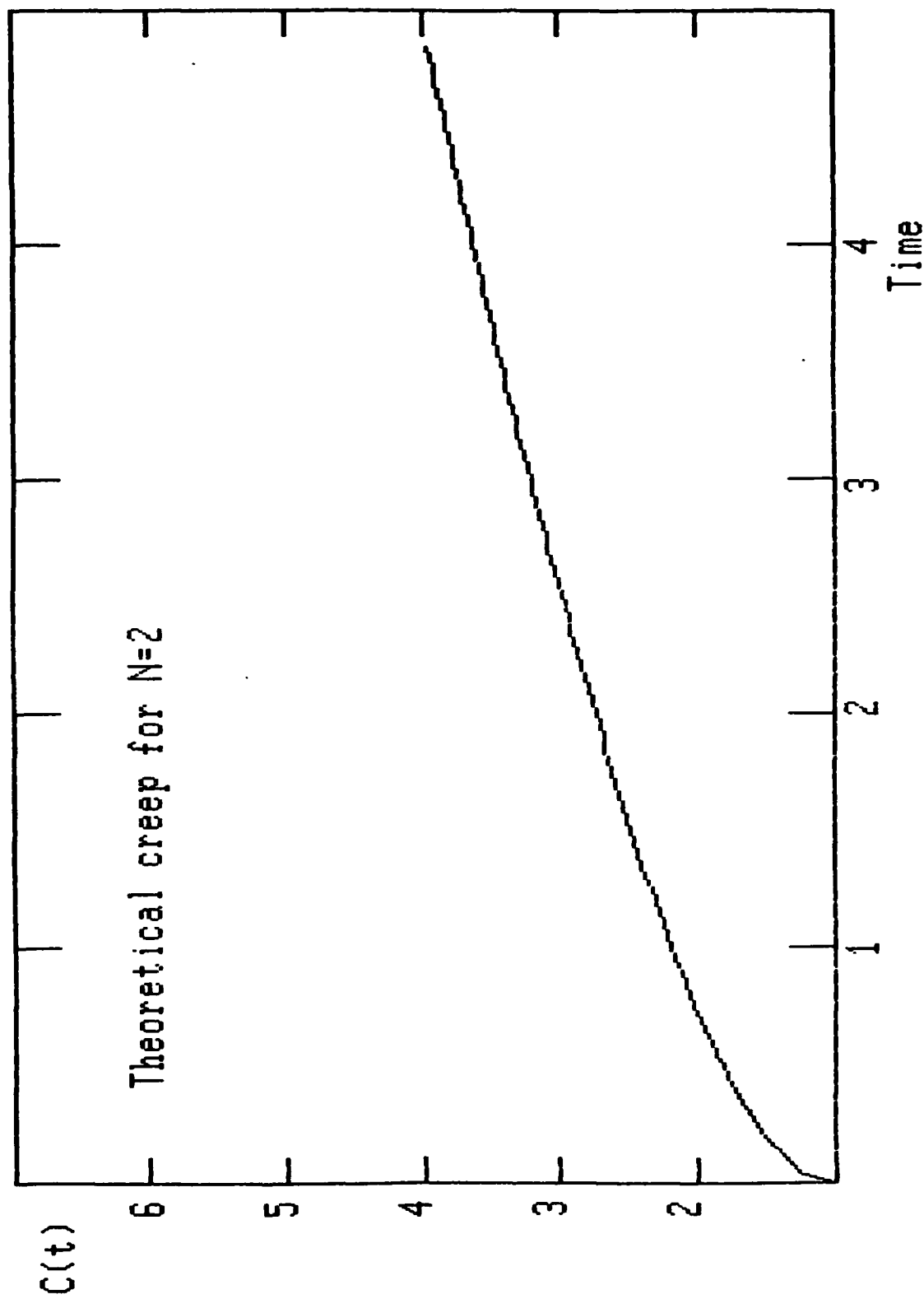




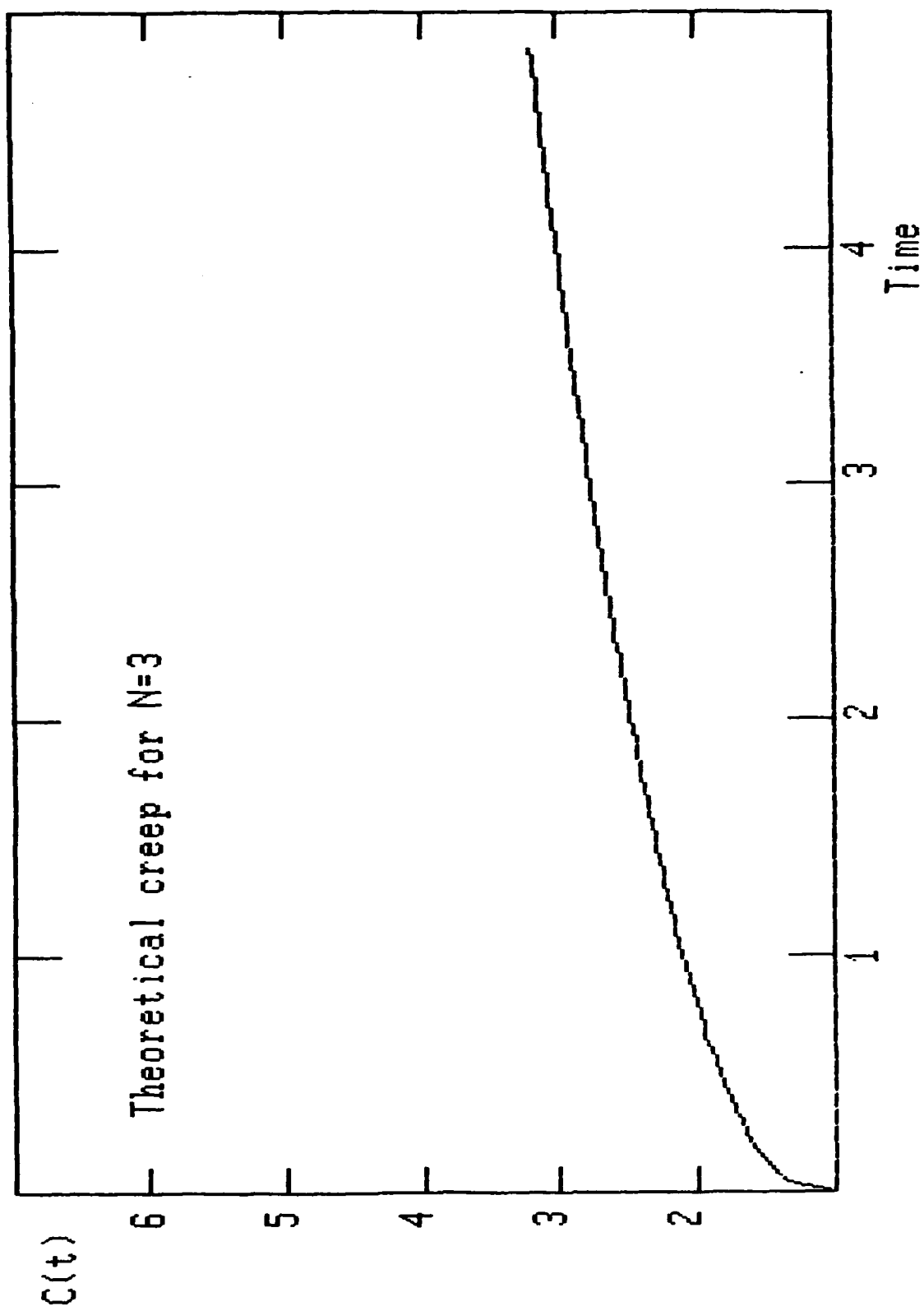


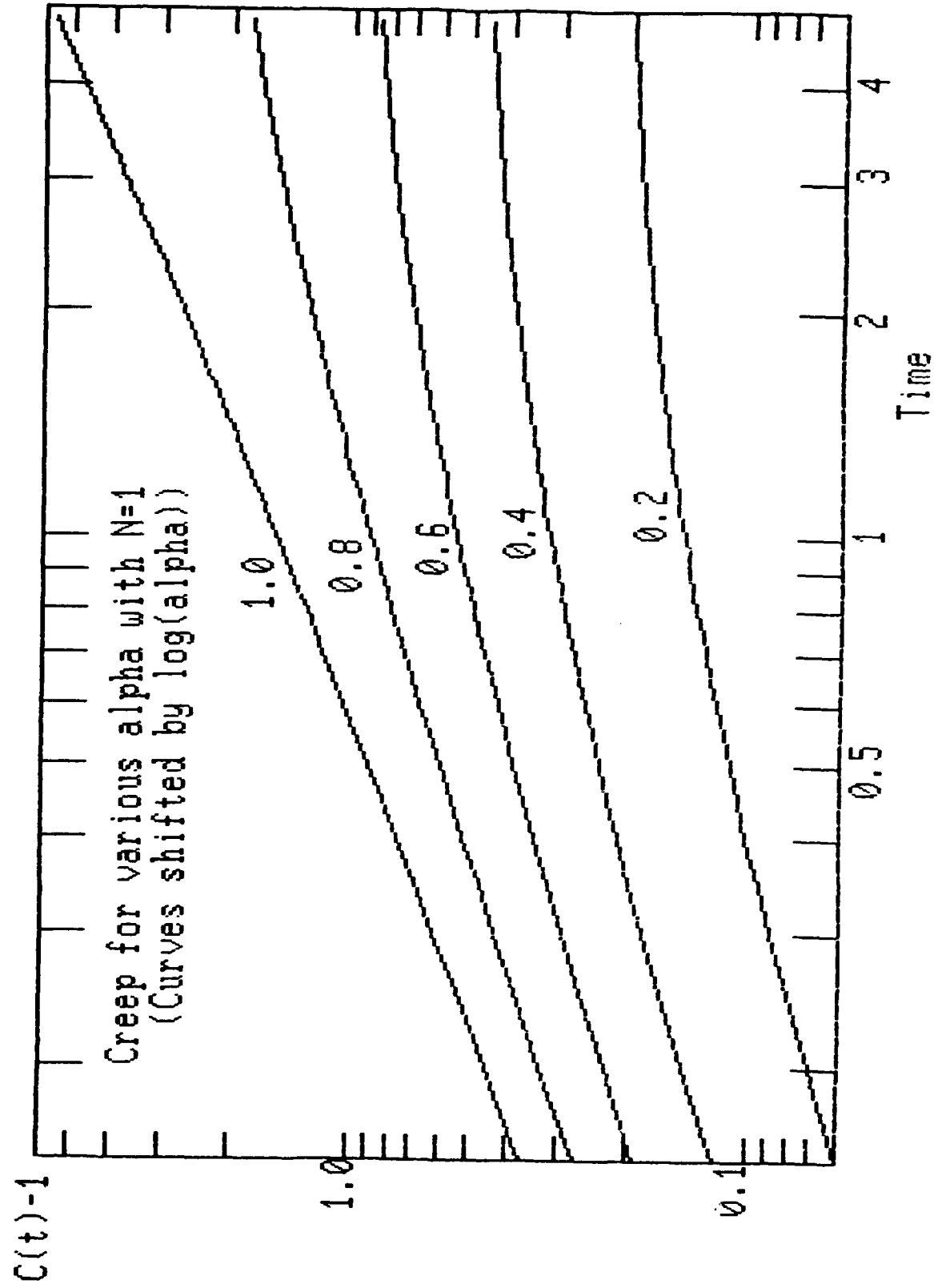












$C(t)-1$

Creep for various  $\alpha$  with  $N=2$   
(Curves shifted by  $\log(\alpha)$ )

1.0

0.8

0.6

0.4

0.2

1.0

0.1

0.05

0.02

0.5

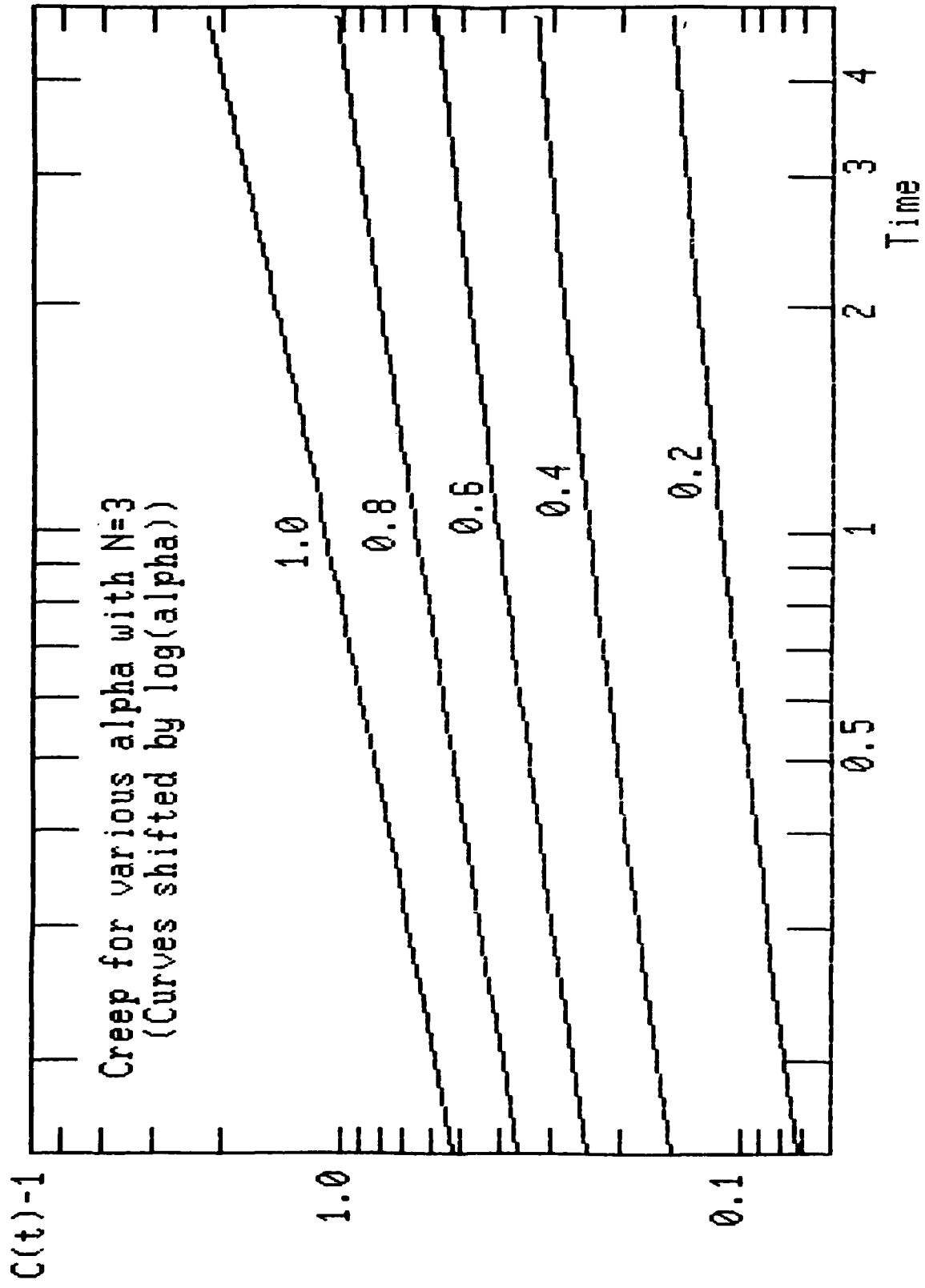
1

2

3

4

Time



A CHARACTERIZATION METHOD FOR A CLASS OF THERMORHEOLOGICALLY  
COMPLEX MATERIALS

by

B. D. Harper\* and Y. Weitsman\*\*

Abstract

This paper presents a method for modelling the response of a class of thermorheologically complex, viscoelastic materials. For the type of materials considered, all temperature effects can be correlated through horizontal and vertical shift factors. In addition, the proper evaluation of transient temperature response requires the vertical shift to be represented as a product of two temperature dependent functions.

It is shown that in order to obtain complete information it is necessary to conduct sharp temperature-drop tests in addition to isothermal creep and recovery experiments.

The method and its use are demonstrated for the specific case of Hercules 3502 epoxy resin.

---

\*Assistant Professor  
Department of Engineering Mechanics  
The Ohio State University  
Columbus, Ohio 43210-1181

\*\*Professor, Mechanics and Materials Center  
Civil Engineering Department  
Texas A&M University  
College Station, Texas 77843

## INTRODUCTION

Consider the problem of characterizing the time-dependent behavior of a viscoelastic bar under a uniform uni-axial stress  $\sigma$  and a spatially uniform, but time varying temperature  $T(t)$ . If all material properties which describe the mechanical response depend only on the instantaneous temperature  $T$ , the most general linear relation between the stress  $\sigma$  and the stress-induced strain  $\epsilon_\sigma$ , is [1].

$$\epsilon_\sigma = \int_{-\infty}^t D(t, \tau) \frac{d\sigma}{d\tau} d\tau \quad (1)$$

In (1),  $D(t, \tau)$  is the creep compliance which relates the stress-induced strain  $\epsilon_\sigma$  at time  $t$  to a unit stress applied at time  $\tau$ .

The characterization of  $D(t, \tau)$  in eqn. (1) involves a formidable experimental undertaking for it requires the conduction of a multitude of creep tests under different temperature histories, with loads applied at various initial times  $\tau_1, \tau_2, \dots$ .

For many materials, the strain-stress response under transient temperatures can be characterized solely from isothermal tests. In these cases, isothermal creep data can be coalesced to form a smooth "master curve" by appropriate shifts parallel to the horizontal axis of  $\log(\text{time})$  and to the vertical axis of  $\log(\text{strain})$ . The simplest, yet widely applicable, response involves only a horizontal shift. In such cases the material is denoted as "thermorheologically simple" (TSM) [1-3].

For the one-dimensional case, the TSM creep response under fluctuating temperature  $T$  and stress  $\sigma$  is given by

$$\epsilon_{\sigma} = \int_0^t D(\xi(t) - \xi(\tau)) \frac{d\sigma}{d\tau} d\tau \quad (2)$$

where  $\xi$  is defined by

$$\xi(u) = \int_0^u \frac{ds}{a_T(T(s))} \quad (3)$$

In (3)  $a_T$  is the shift factor, which depends on the instantaneous temperature  $T$  and  $\xi$  is the "reduced time". Accordingly, the only effect of temperature upon the compliance of a TSM is a stretch in the time-scale. The distinction between "real time" and "reduced time" depends on a rather arbitrary choice of a reference temperature  $T_R$ , where  $a_T(T_R) = 1$  by definition. For TSM the "master curve" for creep is formed by shifting isothermal creep data to the right when  $T > T_R$  and to the left when  $T < T_R$ . All the shifts are parallel to the  $\log t$  axis, as noted above.

It should be emphasized that formation of smooth master curves through horizontal shifting of isothermal data along the  $\log t$  axis is not sufficient to classify a material as thermorheologically simple. In addition, one must verify that equation (2) can be used to predict transient temperature behavior.

Simply stated, a thermorheologically simple material is one for which equation (2) applies. In view of this, it seems natural to define a thermorheologically complex material (TCM) as any viscoelastic material whose time-temperature dependence cannot be characterized by equation (2) [1]. It should be noted that some investigators prefer a more restricted designation for TCM, namely a material for which several viscoelastic mechanisms are possible, each having its own characteristic time-temperature dependence [4]. An example of this type of TCM would be a composite material

consisting of two or more TSM phases, each characterized by a different shift factor  $a_T$  [1,4].

From the view point of stress analysis, there is a clear distinction between TSM and all other forms of TCM. This stems from the fact that the correspondence principle remains applicable in many types of boundary value problems for the TSM case, but does not carry over to any TCM behavior. The stress analysis for any case which is not TSM is indeed very complex.

In many instances, isothermal creep data obtained at various temperatures are clearly not relatable through a horizontal shift factor function alone. However, for some materials it has been noted that smooth master curves may still be formed by using both vertical and horizontal shifts [5-7]. Before resorting to equation (1) to describe the response of such a material, one should first consider generalizations of equation (2) which can account for the observed vertical shifts in isothermal data. The most general constitutive relation of this type is [9]

$$\epsilon_\sigma = D_0 g_0 \sigma + g_1 \int_0^t \Delta D[\xi(t) - \xi(\tau)] \frac{d\{g_2 \sigma\}}{d\tau} d\tau \quad (4)$$

where  $\xi$  is the reduced time defined by (3) and  $g_0$ ,  $g_1$ ,  $g_2$  and  $a_T$  are empirically determined material properties which depend upon temperature. If these functions are "normalized" to be of unit magnitude at some arbitrarily selected reference temperature  $T_R$ , then  $D_0$  and  $\Delta D(t)$  define the isothermal creep compliance at  $T = T_R$ , namely  $D(T_R, t) = D_0 + \Delta D(t)$ . Eqn. (4) is grounded on both thermodynamic and continuum mechanics principles.

Our purpose here is to demonstrate a characterization method



for the linear thermoviscoelastic response described by (4). This characterization method employs isothermal tests together with specific transient temperature tests. The method is illustrated by characterizing the thermoviscoelastic response of Hercules 3502 epoxy resin. This material is also characterized solely from isothermal data obtained at several temperatures in order to demonstrate how such an approach may lead to significant errors in predicting transient behavior. The employment of transient temperature tests for the characterization of TCM response as expressed in eqn. (4) appears to be a new approach, which was not attempted until recently.

The experimental determination of the temperature dependent functions  $g_0, g_1, g_2$ , and  $a_T$  from a set of specialized characterization tests still requires verifications for the validity of eqn. (4). Such verifications are obtained by tests which differ from the experiments used for characterization. In the present case we employed three verification tests to check the characterization results obtained for Hercules 3502 epoxy. These tests involve both transient temperature and stress. The results of these tests are found to be in good agreement with predictions based upon equation (4).

## ANALYSIS

Consider eqn. (4) and assume further that the strain due to stress is  $\alpha\Delta T$  even in the viscoelastic case, namely that the thermal expansion does not depend on temperature history. In this case the total strain  $\epsilon$  is given by

$$\epsilon - \alpha\Delta T = D_0 g_0(T) \sigma + g_1(T) \int_0^t \Delta D[\xi(t) - \xi(\tau)] \frac{d\{g_2(T)\sigma\}}{d\tau} d\tau \quad (5)$$

Consider an isothermal creep test ( $\sigma = \sigma_0 H(t)$  and  $T = T_0$ ), in which case equation (5) reduces to

$$\epsilon = D_0 g_0(T_0) \sigma_0 + g_1(T_0) g_2(T_0) \Delta D(t/a_T(T_0)) \sigma_0 \quad (6)$$

If the log of the quantity  $\Delta\epsilon/\sigma_0 \equiv g_1(T_0) g_2(T_0) \Delta D(t/a_T(T_0))$  is plotted against  $\log t$  we see that the result may be shifted to predict the response at some reference temperature  $T_R$  (where  $g_0 = g_1 = g_2 = a_T = 1$ ) by vertical and horizontal amounts of magnitudes  $\log(g_1(T_0) g_2(T_0))$  and  $\log(a_T(T_0))$ , respectively. It is thus clear that an isothermal test will not enable the separation of the individual effects of  $g_1(T_0)$  and  $g_2(T_0)$ . However, a knowledge of the temperature dependence of  $g_1$  and  $g_2$  separately is required to predict transient temperature behavior through employment of (5). Therefore, additional tests - beyond isothermal experiments - are required to predict behavior under transient temperature conditions.

Many polymeric materials exhibit "power law" creep behavior [10-12]. For such materials the creep behavior at a reference temperature,  $T_R$ , is expressed by

$$\epsilon = D_0 \sigma_0 + D_1 \sigma_0 t^n \quad (7)$$

where  $D_0$ ,  $D_1$  and  $n$  are material constants. In this case equation (5)

gives

$$\epsilon - \alpha \Delta T = D_0 g_0(T) \sigma + g_1(T) D_1 \int_0^t (\xi(t) - \xi(\tau))^n \frac{d(g_2(T) \sigma)}{d\tau} d\tau \quad (8)$$

where  $\xi$  is given by (3).

Now consider an isothermal creep-recovery test at  $T = T_0$ , in which case

$$\sigma(t) = \sigma_0 [H(t) - H(t - t_1)] \quad (9)$$

whereby (8) gives

$$\epsilon_c(t) = D_0 g_0(T_0) \sigma_0 + g_1(T_0) g_2(T_0) D_1 \sigma_0 (t/a_T(T_0))^n \quad (10)$$

for  $0 < t \leq t_1$ .

and

$$\epsilon_r(t) = g_1(T_0) g_2(T_0) D_1 a_T^{-n}(T_0) [t^n - (t - t_1)^n] \sigma_0 \quad (11)$$

for  $t > t_1$

Denote the time dependent portion of  $\epsilon_c(t)$  by

$$\Delta \epsilon(t) = g_1(T_0) g_2(T_0) D_1 \sigma_0 (t/a_T(T_0))^n \quad (12)$$

Figure 1 shows a typical plot of  $\log (\Delta \epsilon / \sigma_0)$  versus  $\log t$ . The "apparent" horizontal shift  $\beta(T)$  is defined in terms of  $g_1$ ,  $g_2$  and  $a_T$  as

$$\beta(T) = \frac{a_T(T)}{(g_1(T) g_2(T))^{1/n}} \quad (13)$$

It is thus noted that isothermal creep data reduce to straight, parallel lines, with slope  $n$ , separated by a horizontal distance  $\beta(T)$ . Elevated temperature data can be related to reference temperature creep through a horizontal shift  $\beta(T)$ , however a vertical shift  $g(T) = \beta(T)^n$  is equally possible. In addition, any combination of a horizontal shift  $a_T(T) = (\beta(T))^q$  and a vertical shift  $g(T) = (\beta(T))^{n(1-q)}$  is also

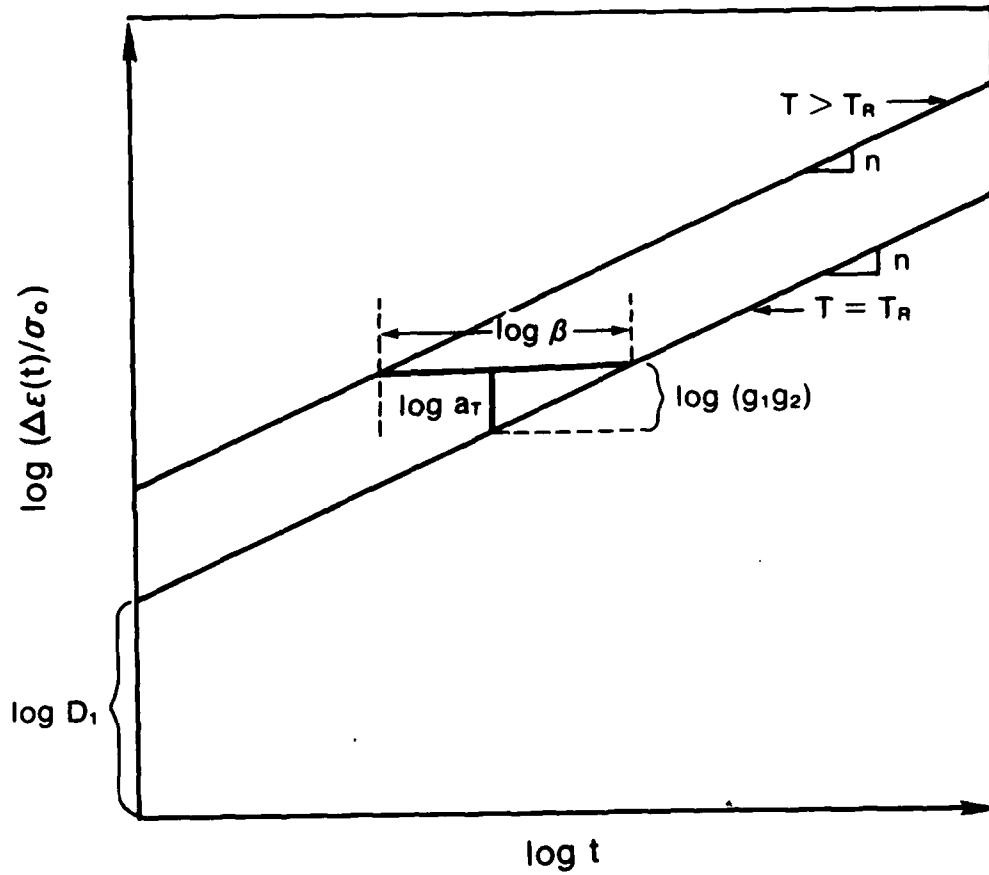


Figure 1. The time-dependent portion  $\Delta\epsilon(t)$  of the creep strain for a power law material.

acceptable. We therefore note that for power law creep, isothermal data alone does not determine the horizontal and vertical shifts  $a_T$  and  $g$ . Indeed, it is only possible to determine the "apparent" horizontal shift  $\beta(T)$  from such experiments.

The unique determination of the horizontal and vertical shifts  $a_T$  and  $g$ , as well as the "components" of the vertical shift  $g_1$  and  $g_2$  ( $g = g_1 g_2$ ), requires transient temperature characterization tests. One such test involves a typical creep recovery experiment (equation (9) accompanied by a simultaneous sudden temperature change (in our case a temperature drop). Experimentally it is impossible to achieve abrupt and instantaneous changes in temperature, so that a temperature history as schematically shown in figure 2 was considered. The specific temperature path in the time interval  $t_1 < t < t_2$  is unknown, however for the tests performed here this path was approximately linear, with  $t_2 - t_1 \approx 10$  sec.

For the stress history expressed in equation (9) and a temperature history sketched in figure 2, equation (8) gives

$$\epsilon_c(t) = D_0 g_0(T_2) \sigma_0 + D_1 g_1(T_2) (t/a_T(T_2))^n \sigma_0 \quad (14)$$

for  $0 < t < t_1$

and

$$\epsilon_r(t) = D_1 \sigma_0 g_1(T_1) g_2(T_2) \left\{ \left[ \frac{t_1}{a_T(T_2)} + J_a + \frac{t - t_2}{a_T(T_1)} \right]^n - \left[ J_a + \frac{t - t_2}{a_T(T_1)} \right]^n \right\} + \alpha(T_1 - T_2) \quad (15)$$

for  $t > t_2$

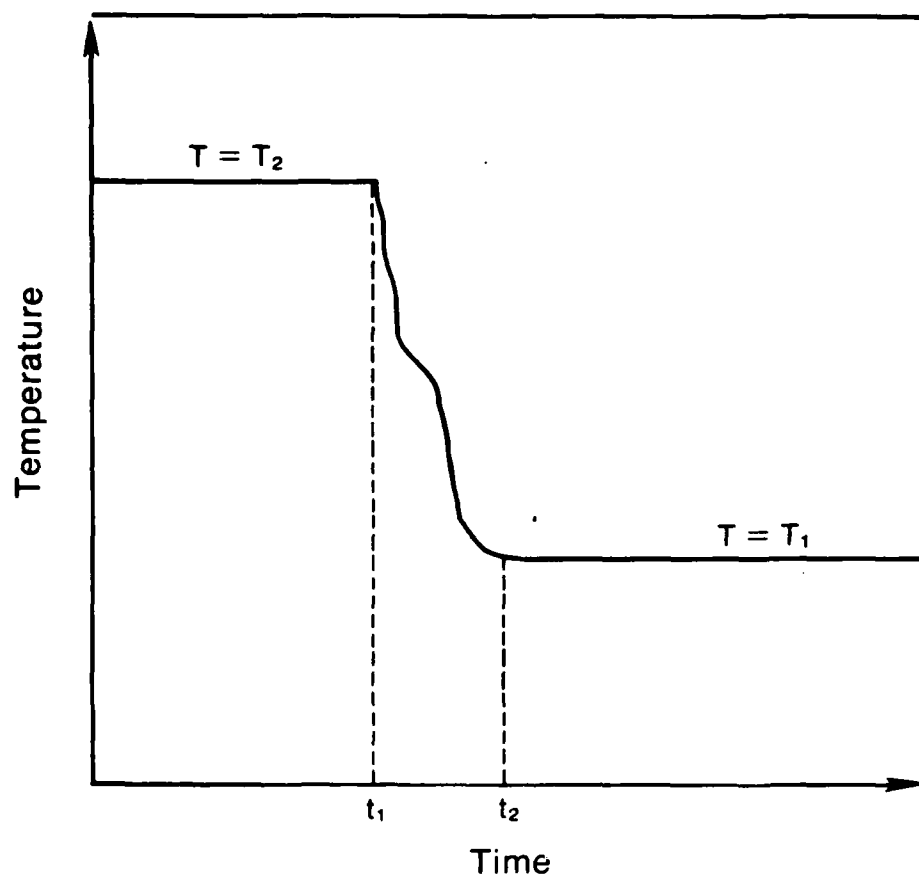


Figure 2. Assumed temperature history for the creep temperature-change experiment.

Since the temperature for  $t_1 < t < t_2$  is unknown, the term

$$J_a = \int_{t_1}^{t_2} \frac{ds}{a_T(\bar{T}(s))} \quad (16)$$

requires further consideration, as discussed later.

## CHARACTERIZATION SCHEME FOR POWER LAW CREEP

The thermoviscoelastic characterization requires the determination of the temperature dependent functions  $g_0$ ,  $g_1$ ,  $g_2$ , and  $a_T$ . In addition, it is necessary to obtain power law creep constants  $D_0$ ,  $D_1$  and  $n$ .

Without loss of generality, let us assume that the functions  $g_0$ ,  $g_1$ ,  $g_2$  and  $a_T$  are normalized to be of unit magnitude at some reference temperature  $T_R$  (in our case we took  $T_R = 303^\circ\text{K}$ ). To determine  $D_0$ ,  $D_1$  and  $n$  consider an isothermal creep recovery test at  $T = T_R$ . In view of (10)-(12) we have

$$\epsilon_c(t) = D_0 \sigma_0 + D_1 \sigma_0 t^n \quad 0 < t < t_1 \quad (17)$$

$$\epsilon_r(t) = D_1 t_1^n \sigma_0 [(1 + \lambda)^n - \lambda^n] \quad t > t_1 \quad (18)$$

and

$$\Delta \epsilon_1 \equiv \Delta \epsilon(t_1) = D_1 \sigma_0 t_1^n \quad (19)$$

$$\text{where } \lambda = \frac{t - t_1}{t_1}$$

In view of (18) and (19) we get

$$\log \Delta \epsilon_1 = \log \epsilon_r(t) - \log [(1 + \lambda)^n - \lambda^n] \quad (20)$$

Designate the right hand side of (20) as  $r(\lambda)$ , since  $\epsilon_r(t)$  is known experimentally and can be expressed as a function of  $\lambda$ . The quantity  $\log \Delta \epsilon_1$  is constant, whereas  $r(\lambda)$  will, in general, vary with  $\lambda$ . This dichotomy is overcome by choosing the "best" value for the power term  $n$  so as to minimize the square mean of the variation in  $r(\lambda)$ .



With  $n$  known,  $D_1$  may be found from (19) and (20). Once  $D_1$  and  $n$  have been determined, we can use creep data to determine the value of  $D_0$  in a similar manner.

At this stage it is possible to determine the "apparent" horizontal shift factor  $\beta(T)$ . Consider an isothermal creep recovery test at some elevated temperature  $T_0 > T_R$ , in which case equations (10) and (11) apply. In view of (11) and (13) we may write, for  $t > t_1$ .

$$\log (D_1 t_1^n) = \log \left\{ \frac{\epsilon_r(t)}{(1 + \lambda)^n - \lambda^n} \right\} + \log \beta(T_0) \quad (21)$$

The left side of (21) is constant, whereas on the right side only  $\beta(T_0)$  is unknown. The value of  $\beta(T_0)$  is selected so as to minimize the square mean error of the right hand side of (21)

In order to determine the temperature dependence of the functions  $g_0$ ,  $g_1$ ,  $g_2$  and  $a_T$  it is necessary to resort to transient temperature characterization tests. In particular consider the creep temperature change experiment. This test combines a temperature history as shown in figure 2 and a stress history given by  $\sigma(t) = [H(t) - H(t - t_1)]\sigma_0$ . Our purpose is to determine  $g_0$ ,  $g_1$ ,  $g_2$  and  $a_T$  at some temperature  $T_2$  when these functions are presumed known at  $T = T_1$  with  $T_2 > T_1$ .

Since by hypothesis  $g_0(T_R) = g_1(T_R) = g_2(T_R) = a_T(T_R) = 1$ , we begin by designating  $T_1 = T_R$ , and selecting  $T_2 = T_1 + \Delta T_e$ . In our case we selected the temperature increment  $\Delta T_e = 20^\circ\text{C}$ . Once the temperature dependent functions have been determined at  $T = T_2$ , both  $T_2$  and  $T_1$  can be increased by an amount  $\Delta T_e$  and the procedure repeated. By proceeding in this manner, values of  $g_0$ ,  $g_1$ ,  $g_2$  and  $a_T$  will always be known at  $T = T_1$  from the previous test.

Turning to details, suppose  $g_0$ ,  $g_1$ ,  $g_2$  and  $a_T$  are known at  $T = T_1$  and are to be determined at  $T = T_2$ . Consider first the quantity  $J_a$  in equations (15) and (16). The difficulty in determining  $J_a$  is due to the fact that both the actual temperature path for  $t_1 < t < t_2$  and  $a_T$  are unknown. However, since the time interval  $t_2 - t_1$  is relatively short (about 10 sec) consider, as a first approximation

$$J_a = \frac{t_2 - t_1}{2} \left( \frac{1}{a_T(T_1)} + \frac{1}{a_T(T_2)} \right) \quad (22)$$

where the only unknown is  $a_T(T_2)$ .

Substituting (22) into (15) and taking logs of the resulting expression we obtain, after some manipulations

$$\log Q = \log [\epsilon_r(t) - \alpha (T_1 - T_2)] - \log \left\{ \left[ 1 + \lambda_1 \frac{a_T(T_2)}{a_T(T_1)} \right]^n - \left[ \frac{t_2 - t_1}{2t_b} + \lambda_1 \frac{a_T(T_2)}{a_T(T_1)} \right]^n \right\} \quad (23)$$

$$\text{where} \quad Q = D_1 \sigma_0 g_1(T_1) g_2(T_2) \left[ \frac{t_b}{a_T(T_2)} \right]^n \quad (24)$$

$$\text{Also, in (23) and (24) } t_b = \frac{t_1 + t_2}{2} \quad \text{and} \quad \lambda_1 = \frac{t - t_b}{t_b}.$$

Since  $\log Q$  is constant we find  $a_T(T_2)$  through minimizing the square mean error of the right hand side of (23), as before. Once this is accomplished we have both  $a_T(T_2)$  and  $Q$ , so that  $g_2(T_2)$  can be found from (24).

Now consider the creep data at the elevated temperature  $T = T_2$ , from which we determine  $g_0(T_2)$  and  $g_1(T_2)$ . This can be accomplished in two ways, which we shall refer to as method A and method B.

In method A we obtain  $g_1(T_2)$  immediately from (13) since  $\beta(T_2)$ ,  $a_T(T_2)$  and  $g_2(T_2)$  are all known. The value of  $g_0(T_2)$  can then be

determined by fitting creep data to equation (14).

In method B, both  $g_0(T_2)$  and  $g_1(T_2)$  are obtained by fitting creep data to equation (14), without resort to  $\beta(T)$ . This is accomplished in a similar manner to that described above for determining  $a_T(T_2)$  and  $g_2(T_2)$  from recovery data.

Note that in method B the material is characterized through transient temperature tests alone, whereas method A incorporates both transient temperature and isothermal tests. For this reason it seems that method A is preferable.

In view of (22), the results obtained thus far are approximate. These approximate values of  $a_T$  can be inserted in (16) with the assumption that  $T$  varies linearly with time between  $t_1$  and  $t_2^*$  to attain improved accuracy. For the cases considered here, such corrections proved insignificant.

In addition to the characterization methods A and B outlined above, a characterization method (designated as method C) involving only isothermal creep and recovery data was also considered. This method represents the common approach used for thermoviscoelastic characterization, and results in only two temperature dependent functions  $g_0(T)$  and  $\beta(T)$ . The uniaxial constitutive equation for this case is

$$\epsilon - \alpha \Delta T = g_0(T) D_0 \sigma + D_1 \int_0^t (\zeta(t) - \zeta(\tau))^n \frac{d\sigma}{d\tau} d\tau \quad (25)$$

---

\*Some justification for this assumption of linearly varying temperature-time path can be deduced from thermal strain measurements on stress-free specimens during temperature change tests. In our case such free thermal strains were approximately linear during  $t_1 < t < t_2$ .

with

$$\zeta(u) = \int_0^u \frac{ds}{\beta(T(s))}$$

(26)

## RESULTS

For purposes of illustration, the characterization methods described earlier were applied to data obtained for Hercules 3502 epoxy. These data consisted of results from both isothermal creep and recovery tests and creep temperature-change tests. The specific details of experimental procedures used to obtain this data have been reported elsewhere [8,13]

Employing room temperature ( $T_R = 30^\circ\text{C} = 303^\circ\text{K}$ ) creep and recovery data we obtained, in view of (17) and (18)

$$\begin{aligned} D_0 &= 233 \times 10^{-6} (\text{MPa})^{-1} \\ D_1 &= 2.24 \times 10^{-6} (\text{MPa sec}^n)^{-1} \\ n &= 0.31 \end{aligned} \tag{27}$$

The above values are averages from six tests with a data scatter of about 3%.

Isothermal creep and recovery data obtained at temperatures of  $50^\circ\text{C}$ ,  $70^\circ\text{C}$ ,  $90^\circ\text{C}$ ,  $110^\circ\text{C}$  and  $130^\circ\text{C}$  provided the "apparent" horizontal shift factor  $\beta(T) \sim 1$ , independent of temperature, with data scatter of about 10%.

Thermal strain measurements on unstressed specimens provided the coefficient of thermal expansion,  $\alpha = 30 \times 10^{-6}/^\circ\text{C}$ .

The data from creep temperature-change tests were reduced according to the methods described earlier. Employing a least-square fitting routine, the results were then fit to the following forms

$$a_T = \exp \left[ -\gamma_0 \left( \frac{T - T_R}{T_R} \right)^{\gamma_1} \right]$$

$$\begin{aligned}
 g_0 &= \exp \left[ \beta_0 \left( \frac{T - T_R}{T_R} \right)^{\beta_1} \right] \\
 g_1 &= \exp \left[ -q_0 \left( \frac{T - T_R}{T_R} \right)^{q_1} \right] \\
 g_2 &= \exp \left[ r_0 \left( \frac{T - T_R}{T_R} \right)^{r_1} \right]
 \end{aligned} \tag{28}$$

Where  $T$  is in  $^{\circ}\text{K}$  and  $T_R = 303^{\circ}\text{K}$ . The constants in (28) are given in Table 1 for the two characterization methods A and B.

Table 1. Material Constants Resulting from Data Fit.

Constant	Method A	Method B
$\gamma_0$	13.7	12.9
$\gamma_1$	.985	.950
$\beta_0$	.675	.685
$\beta_1$	.787	.768
$q_0$	5.79	9.83
$q_1$	1.11	1.13
$r_0$	4.50	11.2
$r_1$	2.48	2.00

The functions  $g_0$ ,  $g_1$ ,  $g_2$ ,  $a_T$  are also plotted in figures 3-6. Dashed lines represent results based on characterization method A while solid lines are for characterization method B. The circles and triangles represent the average values determined from six different tests at the indicated temperature, triangles representing calculations for method A, circles for method B.

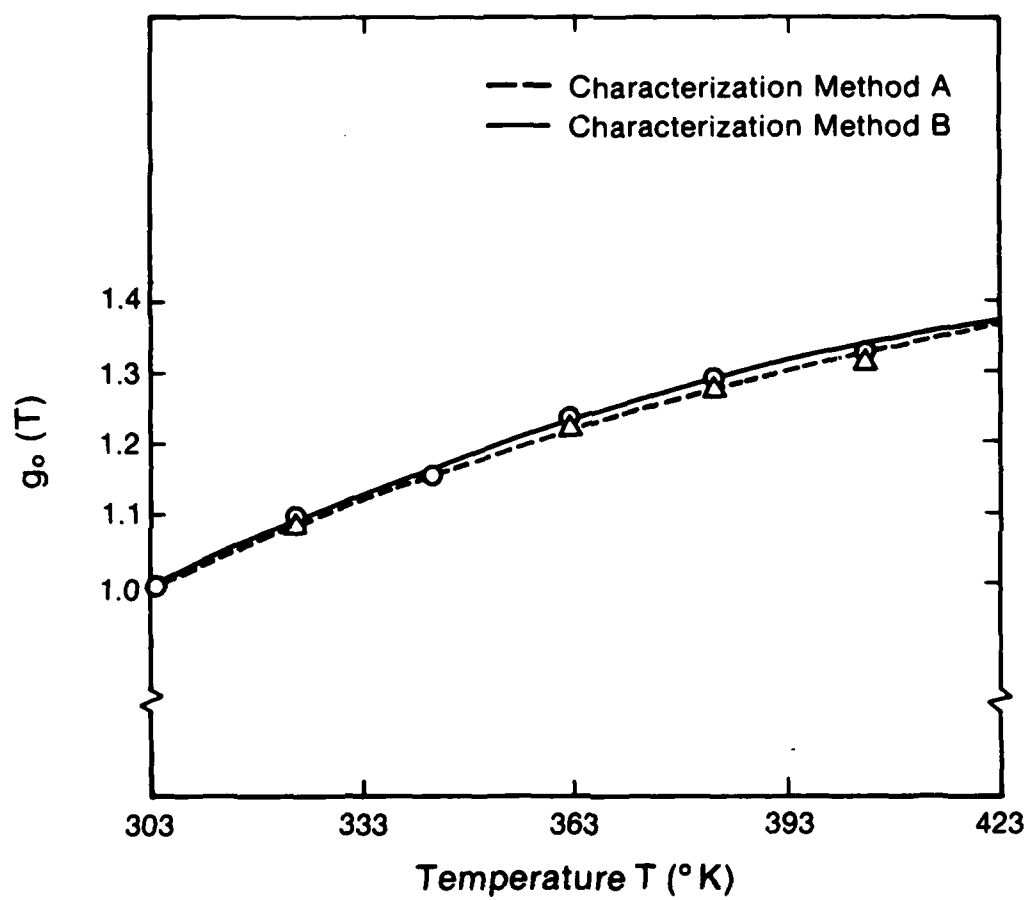


Figure 3. The temperature dependence of the function  $g_0$ .

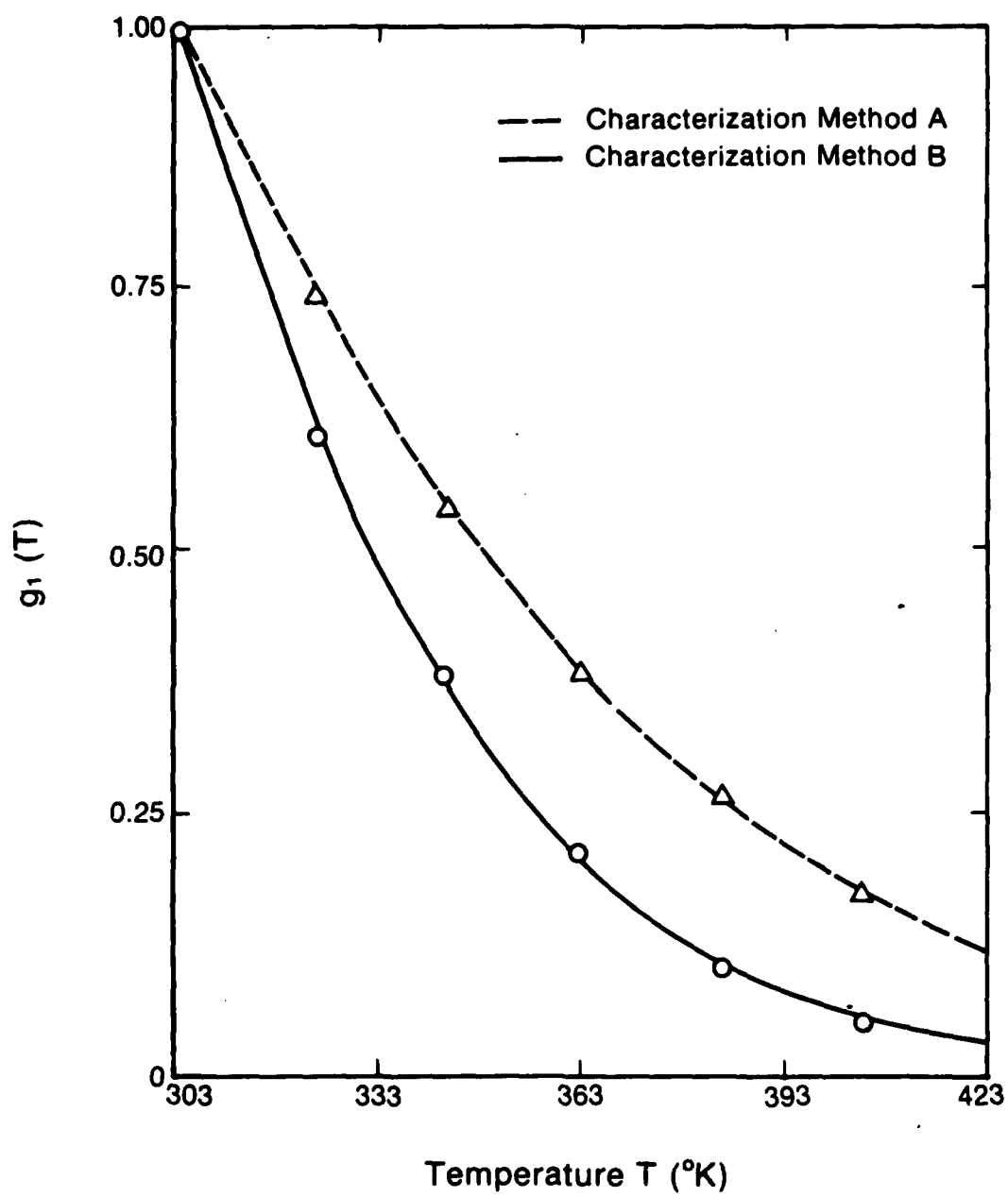


Figure 4. The temperature dependence of the function  $g_1$ .



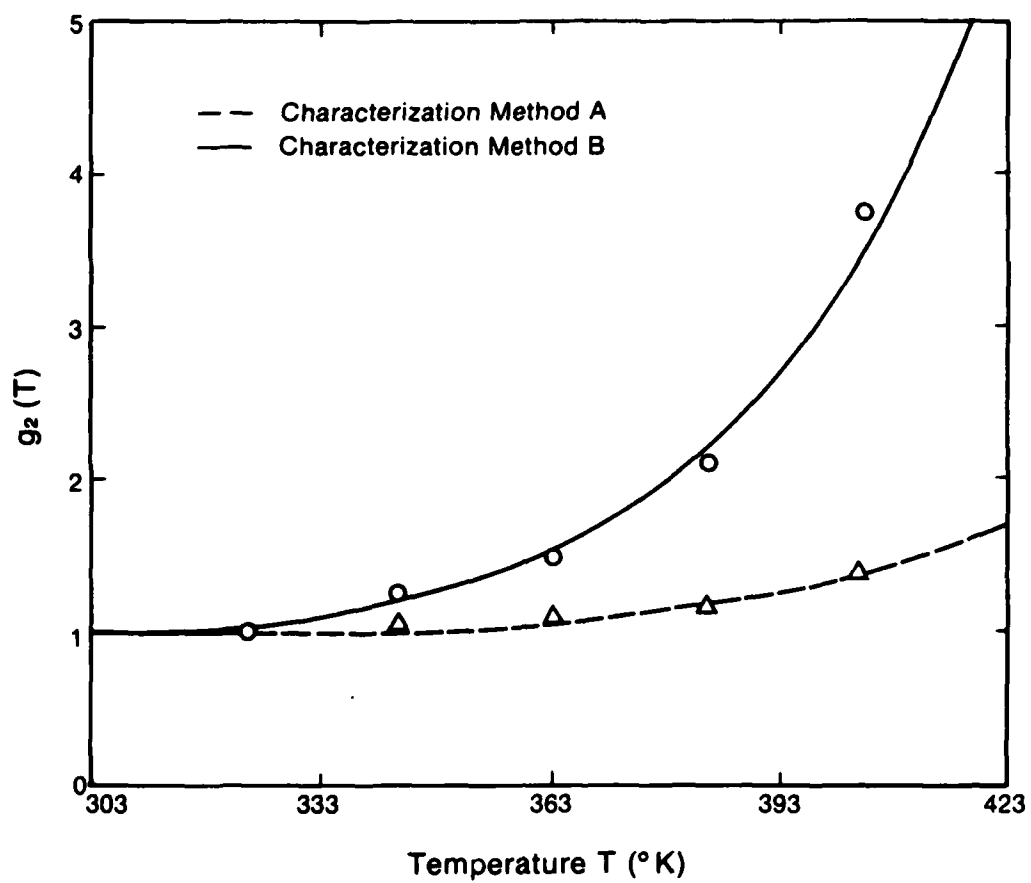


Figure 5. The temperature dependence of the function  $g_2$ .

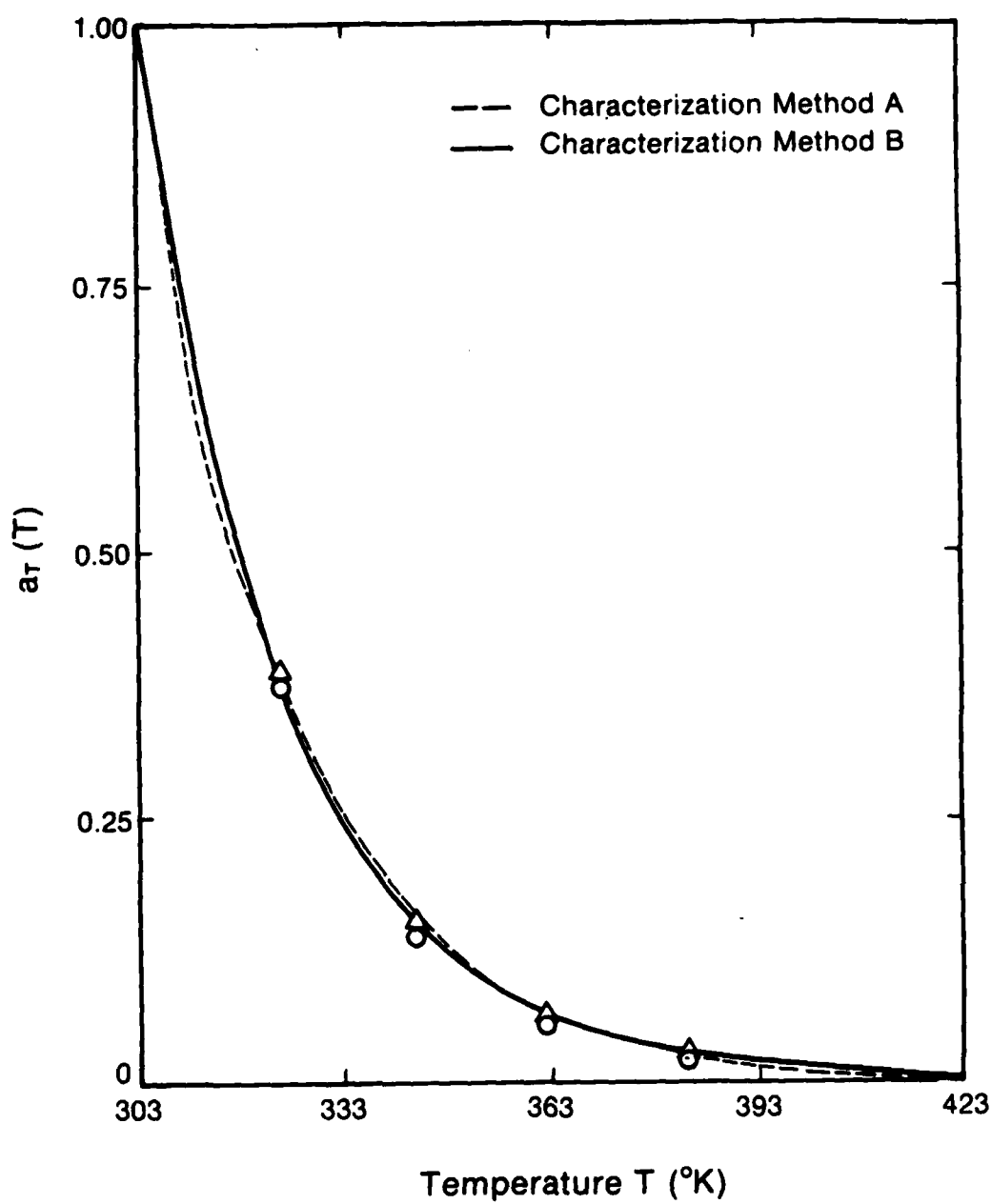


Figure 6. The temperature dependence of the function  $a_T$ .

Several tests were performed in order to compare model predictions with experimental results. These tests differed from those used for material characterization and involved both transient stress and temperature histories. The results of these tests are presented in figures 7-9, together with predictions based upon the results of the three characterization methods employed. The specific stress and temperature histories considered are also shown in each figure.

It is interesting to note in figures 7-9 that noticeable differences in predictions based upon the three different characterization schemes occur only after relatively sharp changes in temperature. When differences do occur, the characterizations involving transient temperature tests (methods A and B) predict the behavior better than the incomplete characterization (method C).

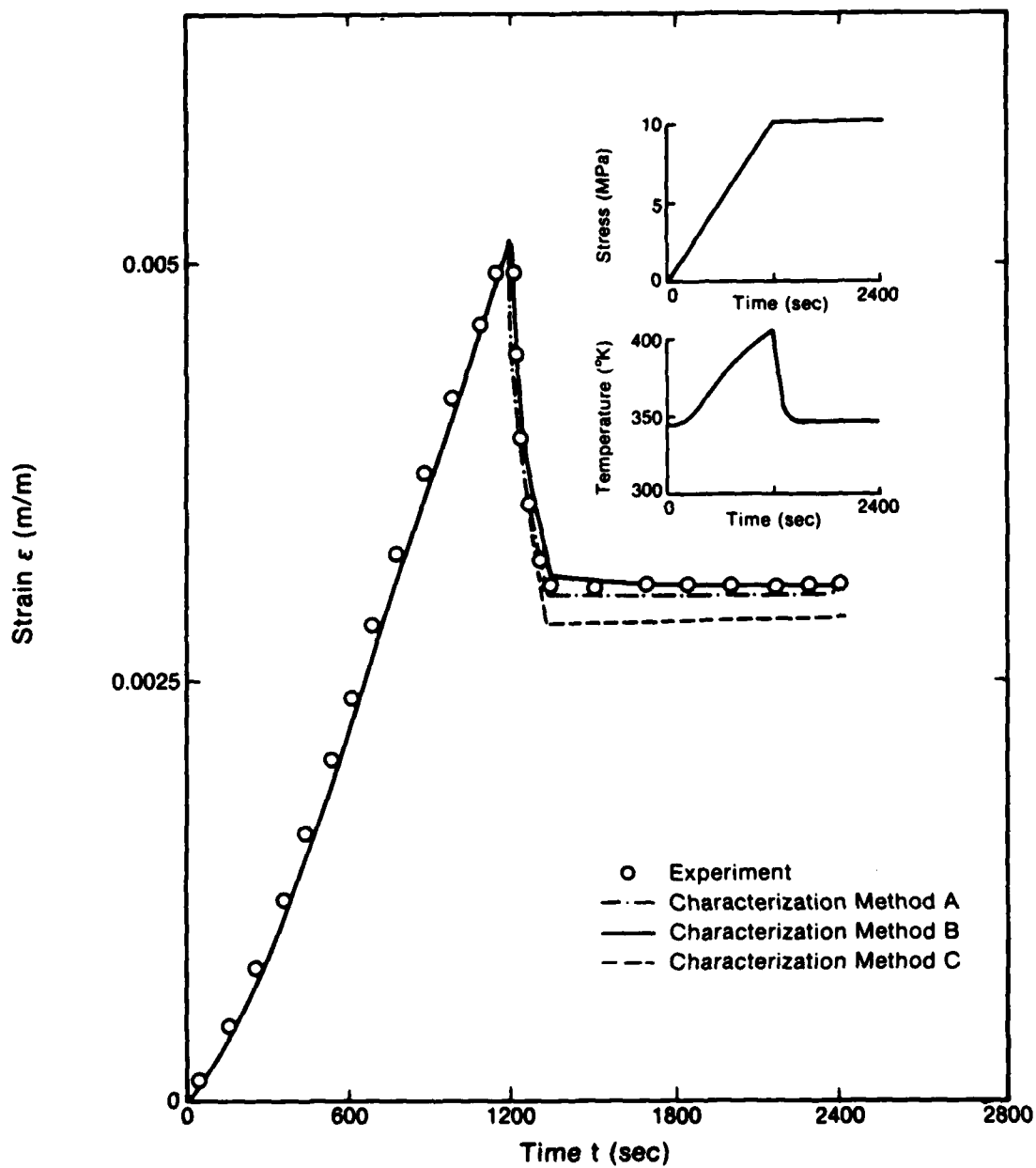


Figure 7. Results for the first verification test.

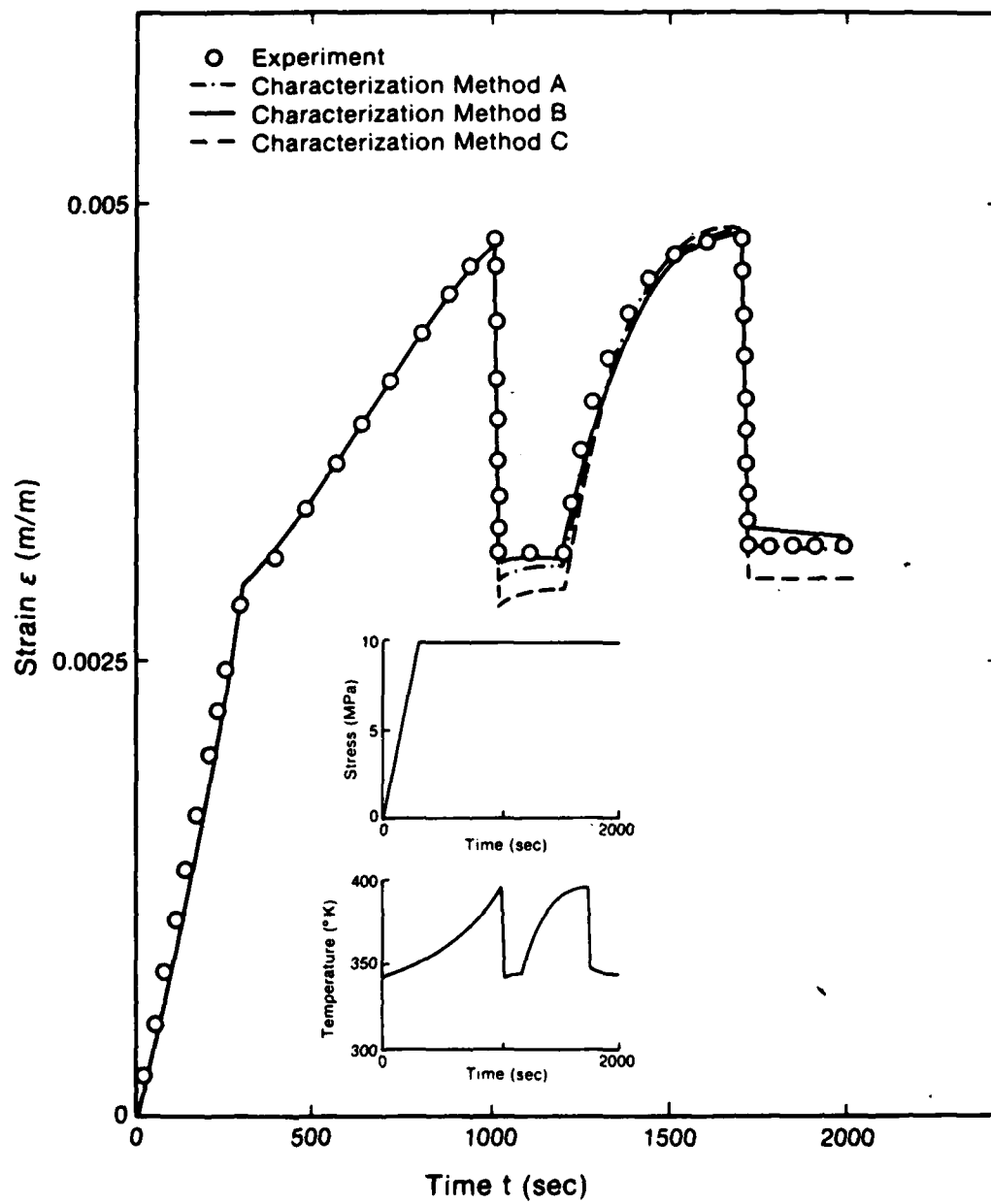


Figure 8. Results for the second verification test.

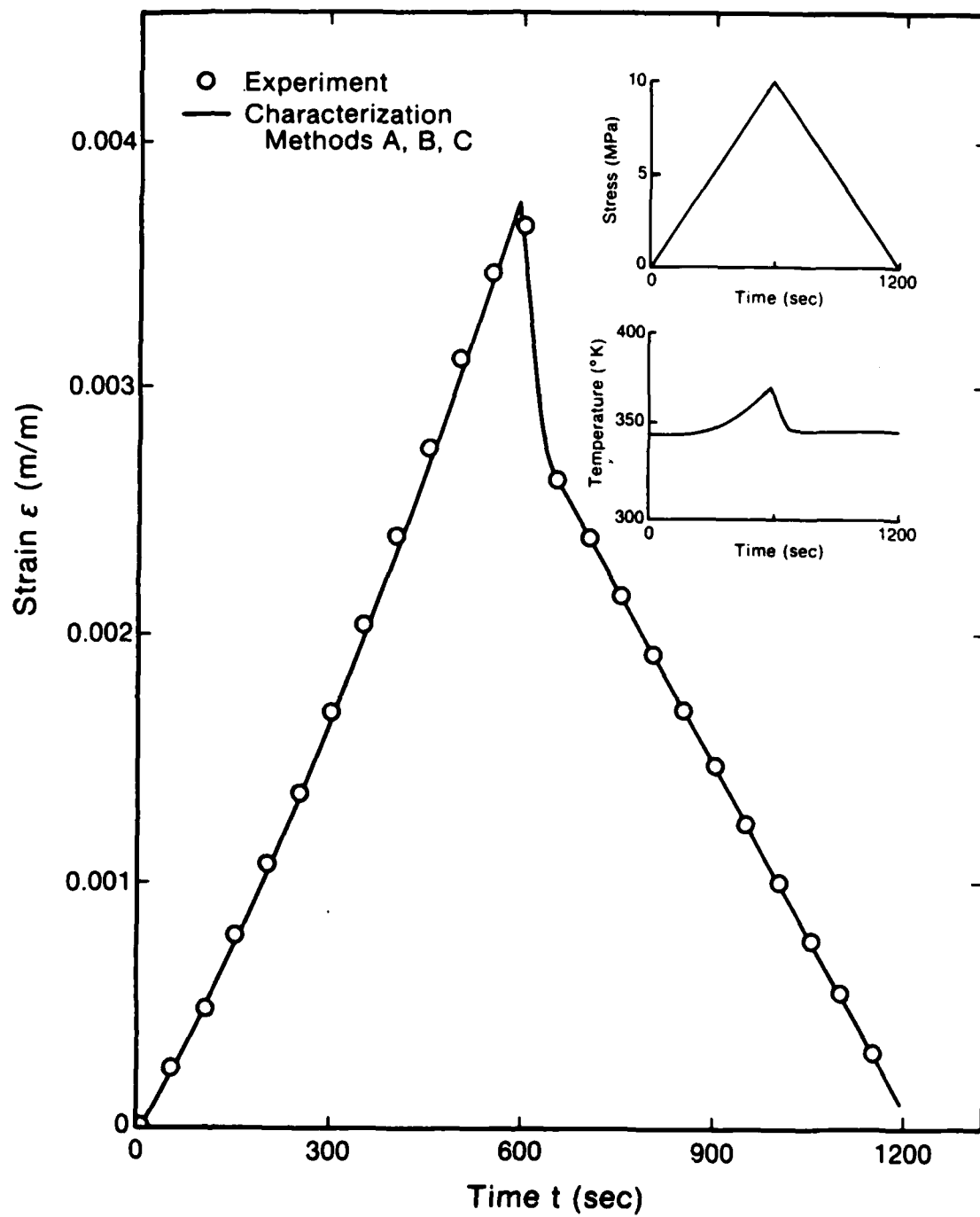


Figure 9. Results for the third verification test.

## CONCLUSIONS

In this paper we suggested a scheme to characterize the time-temperature behavior for a certain type of thermorheologically complex response. The details of this scheme were illustrated for Hercules 3502 epoxy resin. Three methods of characterization were employed, involving transient temperature data alone, a combination of transient temperature and isothermal data, and isothermal data alone. These three characterization methods predicted noticeable differences in the temperature dependence of the horizontal and vertical shift factors, while the temperature dependence of the instantaneous elastic response ( $g_0(T)$ ) was essentially the same for the various characterization schemes.

The verification tests employed to check the results of the thermoviscoelastic characterization indicated that noticeable discrepancies among the different characterization methods occur only after relatively rapid temperature changes. Actually, both of the characterization methods employing transient temperature tests, whether exclusively or in conjunction with isothermal tests, predicted the transient temperature thermoviscoelastic response of the material equally well. On the other hand, the characterization method which was based upon isothermal data alone departed from experimental results by as much as 17%. By contrast, the differences between predictions based upon transient temperature characterization and experimental data did not exceed 4%, and more often were less than 1%.

## ACKNOWLEDGEMENT

This work was conducted under Contract F49620-82-C-0057 from the Air Force Office of Scientific Research (AFOSR) whose support is gratefully acknowledged.



## REFERENCES

1. Schapery, R.A., "Viscoelastic Behavior and Analysis of Composite Materials," Mechanics of Composite Materials, Vol. 2, edited by G.P. Sendeckj, Academic Press, 1974.
2. Schwarzl, F. and Staverman, A.J., "Time-Temperature Dependence of Linear Viscoelastic Behavior," Journal of Applied Physics, Vol. 23, 1952, pp. 838-843.
3. Morland L.W. and Lee, E.H., "Stress Analysis of Linear Viscoelastic Materials with Temperature Variation," Trans. Soc. Rheology, Vol. 1 1960, pp. 233-263.
4. Caruthers, J.M. and Cohen, R.E., "Consequences of Thermorheological Complexity in Viscoelastic Materials", Rheologica Acta, Vol. 19, 1980, pp. 606-613.
5. Hufford, W.L. and Francis, C.E., "Thermal Mechanical Interaction Effects in Filled Polymers," In NSF Workshop on a Continuum Approach to Damage and Life Prediction, May 4-7, 1980, pp. 68-75.
6. McCrum, N.G. and Pogany, G.A., "Time-Temperature Superposition in the  $\alpha$ -region of an Epoxy Resin," Journal of Macromolecular Sci Phys., Vol B4, 1970, p. 109.
7. McCrum, N.G. and Morris, E.L., "On the Measurement of Activation Energy in Creep in Anelastic Solids," Phil. Mag., Vol. 7, 1962, pp. 2115-2118.
8. Peretz, D. and Weitsman, Y., "The Non-Linear Thermoviscoelastic Characterization of FM-73 Adhesives," Journal of Rheology, Vol. 27, No. 2, pp. 97-114 (April 1983).
9. Weitsman, Y., "On the Thermoviscoelastic Characterization of Adhesives and Composites," in Progress in Science and Engineering of Composites, edited by T. Hayashi et. al., ICCM-IV, Tokyo, 1982. pp. 771-779.
10. Lou, Y.C. and Schapery, R.A., "Viscoelastic Characterization of a Non-linear Fiber-Reinforced Plastic," Journal of Composite Materials, Vol. 5, 1971, p. 208.
11. Beckwith, S.W., "Viscoelastic Characterization of a Nonlinear Glass/Epoxy Composite, Including the Effect of Damage," Ph.D.Dissertation, Texas A&M University, December 1974.
12. Findley, W.N., Lai, J.S. and Onoran, K., Creep and Relaxation of Non-linear Viscoelastic Materials, North-Holland Pub. Co., 1976.
13. Harper, B.D., "On the Effects of Post Cure Cool Down and Environmental Conditioning on Residual Stresses in Composite Laminates," Ph.D.Thesis, Texas A&M University, August 1983.

ON THE EFFECTS OF ENVIRONMENTAL CONDITIONING ON  
RESIDUAL STRESSES IN COMPOSITE LAMINATES

by

B.D. Harper  
Assistant Professor  
Department of Engineering Mechanics  
The Ohio State University  
Columbus, Ohio 43210-1181

Y. Weitsman  
Professor, Mechanics and Materials Center  
Civil Engineering Department  
Texas A&M University  
College Station, Texas 77843

Abstract

This paper presents an experimental and theoretical investigation of moisture effects in graphite/epoxy composites. The experiments involved exposure of anti-symmetric, cross-ply laminates to various levels of fixed and fluctuating humidity and measurements of the resulting, time-dependent curvatures. Those data were compared with computed values based upon linear elasticity and linear, rheologically simple, viscoelasticity. Good agreement was noted between data and viscoelastic predictions during the moisture absorption stage from the initially dry condition. However, increasing disparity between theory and experiment developed during subsequent drying and humidity cycling conditions. This disparity is attributed to the growth of moisture-induced damage, indicating that drying and moisture cycling are more detrimental to the integrity of composites than moisture absorption, even though they may be associated with a smaller total moisture content.

## INTRODUCTION

Laminated composite materials have a tendency to develop residual thermal stresses as the laminate is cooled from its elevated cure temperature. Consider, for example, a  $(0/90)_s$  laminate. The thermal expansion coefficient in the direction of the fibers (longitudinal direction) is typically much smaller than the thermal expansion coefficient perpendicular to the fibers (transverse direction). In addition, the stiffness of the material parallel to the direction of the fibers is usually much greater than that transverse to the fibers. As the laminate is cooled from its elevated cure temperature, the individual laminae have a tendency to contract a much larger amount in the transverse direction relative to the longitudinal direction, however such transverse contraction is constrained by the adjacent perpendicularly directed laminae. These adjacent-ply constraints produce residual thermal stresses in the laminate.

Linear elastic stress analysis predicts that these residual thermal stresses may exhaust the strength of various laminae in a composite structure even before the application of external loads. Effects which were attributed to high residual thermal stresses in composite laminates have been reported by several investigators [1,2].\*

The polymer matrix material in composite laminates exhibits time-dependent behavior, especially at elevated temperatures or in the presence of moisture. Typically, this time-dependence reduces the magnitudes of the residual thermal stresses below those predicted by linear elasticity. There are situations, however, when this is not the case [3]. The use of elastic solutions as conservative estimates of the residual stress state in composite laminates is, therefore, often inappropriate.

\*Numbers in brackets indicate references listed at the end of this article.

It is common knowledge that the epoxy matrix material used in high performance graphite/epoxy composites absorbs moisture from a humid environment. This absorbed moisture produces expansional strains in the material which counteract the thermal contraction strains which result from the cool down of the material from its cure temperature and thus serve to relieve (or partially relieve) the residual thermal stresses which develop in these materials. In addition, moisture softens the epoxy matrix, substantially lowers its glass transition temperature, and accelerates its time-dependent behavior.

There is considerable evidence in the literature that, in some situations, moisture may cause irreversible time-dependent degradation of the properties of epoxy-matrix composites [4-20]. Permanent changes in certain mechanical properties [4-15] as well as changes in moisture sorption kinetics [9,16-20] have been attributed to the presence of such time-dependent degradation.

In most instances, the decrease in graphite/epoxy composite properties (e.g. stiffness, tensile strength, etc.) due to hygrothermal exposure has been attributed to some combination of matrix degradation, and a reduction of the fiber-matrix interfacial bond strength [4]. It is generally accepted that graphite fibers, unlike glass fibers [11], do not degrade by exposure to moisture.

This paper investigates the effects of post cure cool down and subsequent environmental conditioning upon residual stresses in composite laminates. The analysis incorporates linear viscoelastic, hygrothermorheologically simple material behavior with classical laminated plate theory to predict the time-dependent hygrothermal stresses as well as the mid-plane strains and curvatures of anti-symmetric cross-ply graphite/epoxy laminates. For comparison, the analysis is also performed assuming that the material behavior is linearly elastic.

Experimental assessment of residual stresses was provided by measurements of the time-dependent curvature of anti-symmetric cross-ply  $(0/90/0_4/90_4/0/90)_T$  AS/3502 graphite/epoxy laminates. These measurements were then compared with linear elastic and viscoelastic predictions.

Even though the elastic and viscoelastic analyses do not consider irreversible moisture induced degradation, careful attention was paid to all experimental data in order to detect the presence of such effects.

## ELASTIC FORMULATION

Consider an anti-symmetric cross-ply laminate, depicted in Figure 1, exposed to fluctuating ambient temperature  $T(t)$  and relative humidity  $\phi(t)$ . In view of the high thermal diffusivity and the small thickness of composite laminates employed in practice it is permissible to ignore the process of thermal diffusion and employ the approximation that  $T=T(t)$  throughout the laminate. On the other hand, the slowness of the process of moisture diffusion requires taking full account of transient moisture distributions. For laminates of thickness much smaller than in-plane dimensions moisture diffusion may be considered spatially one dimensional.

Employing the assumptions of classical laminated plate theory [21], the linear elastic stress/strain relations for the odd numbered, orthotropic plies in Figure 1 are

$$\begin{aligned}\sigma_x(z,t) &= C_L(\epsilon_x^0(t) + zk_x(t) - \alpha_L \Delta T(t) - \beta_L m_e(z,t)) \\ &\quad + C_{LT}(\epsilon_y^0(t) + zk_y(t) - \alpha_T \Delta T(t) - \beta_T m_e(z,t)) \\ \sigma_y(z,t) &= C_{LT}(\epsilon_x^0(t) + zk_x(t) - \alpha_L \Delta T(t) - \beta_L m_e(z,t)) \\ &\quad + C_T(\epsilon_y^0(t) + zk_y(t) - \alpha_T \Delta T(t) - \beta_T m_e(z,t))\end{aligned}\tag{1}$$

In (1),  $\sigma$  denotes stress,  $\epsilon^0$  and  $k$  the mid-plane strain and curvature respectively,  $C$  designates stiffness and  $\alpha$  and  $\beta$  are linear thermal and moisture expansion coefficients. Also  $\Delta T$  denotes temperature change and  $m_e$  the effective moisture content

$$\begin{aligned}m_e(z,t) &= m(z,t) - m_1 \quad \text{for } m(z,t) > m_1 \\ &= 0 \quad \text{for } m(z,t) \leq m_1\end{aligned}\tag{2}$$

where  $m(z,t)$  is the moisture content and  $m_1$  the "threshold" moisture content, below which no moisture expansional strains are observed. The subscripts L and T in Eq. (1) denote properties parallel and transverse to the direction of the fibers respectively, while subscripts x and y refer to the laminate coordinate system of Figure 1.

The stress/strain relations for the even-numbered plies are obtained by interchanging subscripts L and T in Eq. (1).

Since the laminate is assumed free of external loading, the net resultant forces and moments on the laminate must vanish, thus

$$\begin{aligned} N_x(t) &= \int_{-h_3}^{h_3} \sigma_x(z,t) dz = 0 \\ N_y(t) &= \int_{-h_3}^{h_3} \sigma_y(z,t) dz = 0 \\ M_x(t) &= \int_{-h_3}^{h_3} \sigma_x(z,t) z dz = 0 \\ M_y(t) &= \int_{-h_3}^{h_3} \sigma_y(z,t) z dz = 0 \end{aligned} \quad (3)$$

Appropriate substitutions into (3) followed by integration of the expressions yields four equations in the unknowns  $\epsilon_x^0$ ,  $\epsilon_y^0$ ,  $k_x$  and  $k_y$ . Solution of these equations yields

$$\begin{aligned} \epsilon_x^0(t) = \epsilon_y^0(t) &= \frac{1}{\Delta} [h_3^3 (C_L + C_T - 2C_{LT}) \{h_3 (P+Q) \Delta T(t) + (R+S) F(t)\} \\ &\quad - 3g_1 (C_L - C_T) \{g_1 (P-Q) \Delta T(t) + (R-S) G(t)\}] \\ k_x(t) = -k_y(t) &= \frac{3}{\Delta} [h_3 (C_L + C_T + 2C_{LT}) \{g_1 (P-Q) \Delta T(t) + (R-S) G(t)\} \\ &\quad - g_1 (C_L - C_T) \{h_3 (P+Q) \Delta T(t) + (R+S) F(t)\}] \end{aligned} \quad (4)$$

where  $P = C_L \alpha_L + C_T \alpha_T$

$$Q = C_{LT} \alpha_L + C_T \alpha_T$$

$$R = C_L \beta_L + C_{LT} \beta_T$$

$$S = C_{LT} \beta_T + C_T \beta_T$$

$$g_1 = \frac{1}{2} h_3^2 + h_1^2 - h_2^2$$

$$\Delta = h_3^4 \{ (C_L + C_T)^2 - 4C_{LT}^2 \} - 3g_1^2 (C_L - C_T)^2$$

$$F(t) = \int_0^{h_3} m_e(z, t) dz$$

$$G(t) = \int_0^{h_3} m_e(z, t) z dz - 2 \int_{h_1}^{h_2} m_e(z, t) z dz$$

Note that the moisture content profile  $m(z, t)$  is found independently by solving the diffusion equation.

Once  $\varepsilon_x^0$  and  $k_x$  are determined from (4), the stresses may be obtained by direct substitution into (1).



## VISCOELASTIC FORMULATION

For the viscoelastic case, the material behavior is assumed to be hygro-thermorheologically simple and linear. Making the assumptions of classical laminated plate theory and noting again that  $\epsilon_x^0 = \epsilon_y^0$  and  $k_x = -k_y$  due to the anti-symmetric cross-ply lay-up we have the following relations for the odd numbered plies

$$\begin{aligned}\sigma_x(z, t) &= \int_0^t C_L(\xi - \xi') \left\{ \frac{\partial \epsilon_x^0(\tau)}{\partial \tau} + z \frac{\partial k_x(\tau)}{\partial \tau} - \frac{\partial (\alpha_L \Delta T(\tau))}{\partial \tau} - \beta_L \frac{\partial m_e(z, \tau)}{\partial \tau} \right\} d\tau \\ &+ \int_0^t C_{LT}(\xi - \xi') \left\{ \frac{\partial \epsilon_x^0(\tau)}{\partial \tau} - z \frac{\partial k_x(\tau)}{\partial \tau} - \frac{\partial (\alpha_T \Delta T(\tau))}{\partial \tau} - \beta_T \frac{\partial m_e(z, \tau)}{\partial \tau} \right\} d\tau \\ \sigma_y(z, t) &= \int_0^t C_{LT}(\xi - \xi') \left\{ \frac{\partial \epsilon_x^0(\tau)}{\partial \tau} + z \frac{\partial k_x(\tau)}{\partial \tau} - \frac{\partial (\alpha_L \Delta T(\tau))}{\partial \tau} - \beta_L \frac{\partial m_e(z, \tau)}{\partial \tau} \right\} d\tau \\ &+ \int_0^t C_T(\xi - \xi') \left\{ \frac{\partial \epsilon_x^0(\tau)}{\partial \tau} - z \frac{\partial k_x(\tau)}{\partial \tau} - \frac{\partial (\alpha_T \Delta T(\tau))}{\partial \tau} - \beta_T \frac{\partial m_e(z, \tau)}{\partial \tau} \right\} d\tau\end{aligned}\quad (6)$$

Expressions for the even numbered plies are obtained by interchanging subscripts L and T in (6). In (6), the reduced times  $\xi$  and  $\xi'$  are defined by

$$\begin{aligned}\xi &= \xi(z, t) = \int_0^t \frac{ds}{a_{TM}(m(z, s), T(s))} \\ \xi' &= \xi'(z, \tau) = \int_0^\tau \frac{ds}{a_{TM}(m(z, s), T(s))}\end{aligned}\quad (7)$$

where  $a_{TM}$  is the combined temperature-moisture shift factor.

Requiring net resultant forces and moments to vanish at all times results in two integral equations

$$\int_0^t \left( \int_0^{h_3} F_1(\xi - \xi') dz \right) \frac{\partial \epsilon_x^0(\tau)}{\partial \tau} d\tau + \int_0^t \left( \int_0^{h_3} F_3(\xi - \xi') z dz \right. \\ \left. - 2 \int_{h_1}^{h_2} F_3(\xi - \xi') z dz \right) \frac{\partial k_x(\tau)}{\partial \tau} d\tau = R_1(t)$$

$$\int_0^t \left( \int_0^{h_3} F_3(\xi - \xi') z dz - 2 \int_0^{h_2} F_3(\xi - \xi') z dz \right) \frac{\partial \epsilon_x^0(\tau)}{\partial \tau} d\tau \\ + \int_0^t \left( \int_0^{h_3} F_2(\xi - \xi') z^2 dz \right) \frac{\partial k_x(\tau)}{\partial \tau} d\tau = R_2(t) \quad (8)$$

where,

$$R_1(t) = \int_0^t \left( \int_0^{h_3} F_4(\xi - \xi') dz \right) \frac{\partial [\alpha_T(T(\tau)) \Delta T(\tau)]}{\partial \tau} d\tau \\ + \int_0^t \left( \int_0^{h_3} F_5(\xi - \xi') dz \right) \frac{\partial [\alpha_L(T(\tau)) \Delta T(\tau)]}{\partial \tau} d\tau \\ + \int_0^t \left( \int_0^{h_3} (F_4(\xi - \xi') \beta_T + F_5(\xi - \xi') \beta_L) \frac{\partial m_e(z, \tau)}{\partial \tau} dz \right) d\tau \quad (9)$$

$$R_2(t) = \int_0^t \left( \int_0^{h_3} F_7(\xi - \xi') z dz - 2 \int_{h_1}^{h_2} F_7(\xi - \xi') z dz \right) \frac{\partial [\alpha_T(T(\tau)) \Delta T(\tau)]}{\partial \tau} d\tau \\ + \int_0^t \left( \int_0^{h_3} F_6(\xi - \xi') z dz - 2 \int_{h_1}^{h_2} F_6(\xi - \xi') z dz \right) \frac{\partial [\alpha_L(T(\tau)) \Delta T(\tau)]}{\partial \tau} d\tau \\ + \int_0^t \left\{ \int_0^{h_3} (F_7(\xi - \xi') \beta_T + F_6(\xi - \xi') \beta_L) \frac{\partial m_e(z, \tau)}{\partial \tau} z dz \right. \\ \left. - 2 \int_{h_1}^{h_2} (F_7(\xi - \xi') \beta_T + F_6(\xi - \xi') \beta_L) \frac{\partial m_e(z, \tau)}{\partial \tau} z dz \right\} d\tau$$

and

$$F_1 = C_L + C_T + 2C_{LT} \quad ; \quad F_5 = C_L + C_{LT}$$

$$F_2 = C_L + C_T - 2C_{LT} \quad ; \quad F_6 = C_L - C_{LT}$$

$$F_3 = C_L - C_T \quad ; \quad F_7 = C_{LT} - C_T$$

$$F_4 = C_T + C_{LT}$$

(10)

## MOISTURE DIFFUSION

For many epoxy resin composites the moisture sorption process was found to follow the classical diffusion equation [16]

$$\frac{\partial m}{\partial t} = D \frac{\partial^2 m}{\partial z^2} \quad (11)$$

where  $m$  is the moisture content,  $t$  denotes time, and  $z$  is the spatial coordinate for one-dimensional diffusion. Also,  $D$  is the moisture diffusion coefficient.

In many circumstances the equilibrium moisture content  $M_\infty$  was correlated to the ambient relative humidity  $\phi$  [19,22,23], and for the composite material at hand it was found [23]

$$M_\infty = 0.00268\phi^{1.325} \quad (12)$$

Finally, the coefficient  $D$  in equation (11) was found to vary most significantly with temperature [16,23]. For the present case we have [23]

$$D = D(T) = 1.67\exp(-5480/T) \quad (13)$$

In (13)  $T$  denotes temperature in  $^\circ\text{K}$  and  $D$  is in  $\text{mm}^2/\text{sec}$ .

The solution to (11) is well known [24,25] and can be evaluated most efficiently by a scheme proposed recently [26]. This scheme will be followed for calculating moisture profiles to be inserted in (1) and (6).

## NUMERICAL PROCEDURES

The complexity of the viscoelastic integral equations (8) necessitates the use of a numerical solution. Conventional numerical integration procedures are inappropriate because the unknown functions to be determined, namely  $\epsilon_x^0(t)$  and  $k_x(t)$ , appear as derivatives within the integral.

An approach often referred to as the "incremental time-marching scheme" has been employed on several occasions to solve integral equations of this type [23,27,28]. To illustrate this method consider one of the integral expressions in (8), namely

$$I(t) = \int_0^t \left( \int_0^{h_3} F_1(\xi(z,t) - \xi(z,\tau)) dz \right) \frac{\partial \epsilon_x^0(\tau)}{\partial \tau} d\tau \quad (14)$$

with

$$\xi(z,u) = \int_0^u \frac{ds}{a_{TM}(m(z,s), \bar{T}(s))} \quad (15)$$

First discretize the time domain into  $M$  time steps, not necessarily equal in magnitude. Evaluating (14) at time  $t=t_j$ , and allowing for the possibility of discontinuity at time  $t=0$ , we have

$$\begin{aligned} I(t_j) &= \int_0^{h_3} F_1(\xi(x,t_j)) dz [\epsilon_x^0(0^+) - \epsilon_x^0(0^-)] \\ &+ \sum_{k=0}^{j-1} \int_{t_k}^{t_{k+1}} \left( \int_0^{h_3} F_1(\xi(z,t_j) - \xi(z,\tau)) dz \right) \frac{\partial \epsilon_x^0(\tau)}{\partial \tau} d\tau \\ &= \int_0^{h_3} F_1(\xi(z,t_j)) dz [\epsilon_x^0(0^+) - \epsilon_x^0(0^-)] \\ &+ \frac{1}{2} \sum_{k=0}^{j-1} \left\{ \int_0^{h_3} [F_1(\xi(z,t_j) - \xi(z,t_{k+1})) \right. \\ &\quad \left. + F_1(\xi(z,t_j) - \xi(z,t_k))] dz \right\} [\epsilon_x^0(t_{k+1}) - \epsilon_x^0(t_k)] \end{aligned} \quad (16)$$

where  $t_0 \equiv 0^+$ .

The spatial integration in (16) is performed by discretizing the laminate half-thickness,  $h_3$ , into  $N$  divisions, again not necessarily equal in magnitude, for example

$$\int_0^{h_3} F_1(\xi(z, t_j) - \xi(z, t_k)) dz = \frac{1}{2} \sum_{i=0}^{N-1} \left\{ F_1(\xi(z_{i+1}, t_j) - \xi(z_{i+1}, t_k)) + F_1(\xi(z_i, t_j) - \xi(z_i, t_k)) \right\} (z_{i+1} - z_i) \quad (17)$$

where  $z_0 \equiv 0$  and  $z_N \equiv h_3$ .

Upon discretization of all terms in (8) it is finally possible to form two equations in the unknown quantities  $\epsilon_x^0(t_j)$  and  $k_x(t_j)$  that can be solved simultaneously. Note that at time  $t=t_j$ , all earlier values  $\epsilon_x^0(t_1), \dots, \epsilon_x^0(t_{j-1})$  and  $k_x(t_1), \dots, k_x(t_{j-1})$  are known from previous steps. With  $\epsilon_x^0(t_j)$  and  $k_x(t_j)$  known, one then increments the time to  $t=t_{j+1}$  and proceeds as above to find  $\epsilon_x^0(t_{j+1})$  and  $k_x(t_{j+1})$ . This procedure is repeated progressively until the mid-plane strain and curvature are found at any time of interest.

Note that this procedure requires solving for  $\epsilon_x^0$  and  $k_x$  at each time increment, even though these values may only be desired at the final time  $t=t_M$  or perhaps at only a few of the intermediate times. For this reason, this procedure is rather inefficient for very long hygrothermal histories.

In order to improve numerical efficiency, a method similar to that proposed by Schapery [29] was employed to solve equations (8) for the time-dependent mid-plane strains and curvatures. This method involves approximating the mid-plane strains and curvatures by the functions  $\epsilon_x^{(1)}$  and  $k_x^{(1)}$  defined through the following expressions

$$\left(\int_0^{h_3} F_1(\xi) dz\right) \epsilon_x^{(1)} + \left(\int_0^{h_3} F_3(\xi) z dz - 2 \int_{h_1}^{h_2} F_3(\xi) z dz\right) k_x^{(1)} = R_1(t) \quad (18)$$

$$\left(\int_0^{h_3} F_3(\xi) z dz - 2 \int_{h_1}^{h_2} F_3(\xi) z dz\right) \epsilon_x^{(1)} + \left(\int_0^{h_3} F_2(\xi) z^2 dz\right) k_x^{(1)} = R_2(t)$$

where  $R_1(t)$  and  $R_2(t)$  are given in (9) and  $\xi = \xi(z, t)$  is given in (7). Note that  $R_1(t)$  and  $R_2(t)$  can be evaluated exactly at any time of interest since the temperature and moisture history is known explicitly beforehand. Therefore the approximate quantities  $\epsilon_x^{(1)}$  and  $k_x^{(1)}$  do not need to be known at each intermediate time step in the numerical integration process, as was required in the previous procedure.

In order to estimate the error involved in using  $\epsilon_x^{(1)}$  and  $k_x^{(1)}$  as the mid-plane strain and curvature, define

$$\Delta \epsilon_x = \epsilon_x^0 - \epsilon_x^{(1)} \quad (19)$$

$$\Delta k_x = k_x - k_x^{(1)}$$

Manipulations of (8) and (18) then yield the following integral expressions for  $\Delta \epsilon_x$  and  $\Delta k_x$ ,

$$\begin{aligned} & \int_0^t \left( \int_0^{h_3} F_1(\xi - \xi') dz \right) \frac{\partial \Delta \epsilon_x}{\partial \tau} d\tau + \int_0^t \left( \int_0^{h_3} F_3(\xi - \xi') z dz \right. \\ & \quad \left. - 2 \int_{h_1}^{h_2} F_3(\xi - \xi') z dz \right) \frac{\partial \Delta k_x}{\partial \tau} d\tau = \int_0^t \left\{ \int_0^{h_3} (F_1(\xi) - F_1(\xi - \xi')) dz \right\} \frac{\partial \epsilon_x^{(1)}}{\partial \tau} d\tau \\ & \quad + \int_0^t \left\{ \int_0^{h_3} (F_3(\xi) - F_3(\xi - \xi')) z dz - 2 \int_{h_1}^{h_2} (F_3(\xi) - F_3(\xi - \xi')) z dz \right\} \frac{\partial k_x^{(1)}}{\partial \tau} d\tau \end{aligned} \quad (20)$$

$$\begin{aligned}
& \int_0^t \left( \int_0^{h_3} F_3(\xi - \xi') z dz - 2 \int_{h_1}^{h_2} F_3(\xi - \xi') z dz \right) \frac{\partial \Delta \epsilon_x}{\partial \tau} d\tau \\
& + \int_0^t \left( \int_0^{h_3} F_2(\xi - \xi') z^2 dz \right) \frac{\partial \Delta k_x}{\partial \tau} d\tau = \int_0^t \left\{ \int_0^{h_3} (F_3(\xi) - F_3(\xi - \xi')) z dz \right. \\
& - 2 \int_{h_1}^{h_2} (F_3(\xi) - F_3(\xi - \xi')) z dz \left. \right\} \frac{\partial \epsilon_x^{(1)}}{\partial \tau} d\tau + \int_0^t \left\{ \int_0^{h_3} (F_2(\xi) \right. \\
& \left. - F_2(\xi - \xi')) z^2 dz \right\} \frac{\partial k_x^{(1)}}{\partial \tau} d\tau
\end{aligned} \tag{21}$$

The solution of (20) and (21) for  $\Delta \epsilon_x$  and  $\Delta k_x$  will involve the same incremental time-marching procedure as mentioned previously, but since the "errors"  $\Delta \epsilon_x$  and  $\Delta k_x$  are presumably small in comparison with  $\epsilon_x^{(1)}$  and  $k_x^{(1)}$ , it is possible to employ cruder time-steps in the numerical integration.

If  $\Delta \epsilon_x \ll \epsilon_x^{(1)}$  and  $\Delta k_x \ll k_x^{(1)}$  then  $\epsilon_x^{(1)} + \Delta \epsilon_x$  and  $k_x^{(1)} + \Delta k_x$  may be taken as our solution. Otherwise, higher order increments  $\Delta^{(2)} \epsilon_x$  and  $\Delta^{(2)} k_x$  can be calculated in a similar manner.

In our case  $\Delta \epsilon_x$  and  $\Delta k_x$  provided sufficient accuracy since they resulted in corrections of no more than a few percentage points.



## SUMMARY OF MATERIAL PROPERTIES

Published data on the AS/3502 graphite/epoxy material [30] indicate that only the transverse compliance  $S_T$  shows any appreciable time-dependence. The compliances  $S_L$  and  $S_{LT}$  were both virtually constant with values given by

$$\begin{aligned} S_L &= 8.00 \times 10^{-6} \text{ MPa}^{-1} \\ S_{LT} &= 2.32 \times 10^{-6} \text{ MPa}^{-1} \end{aligned} \quad (22)$$

The dry transverse compliance data can be expressed in the following form

$$S_T(t) = S_o (t + t_o)^q \quad (23)$$

with

$$\begin{aligned} S_o &= 88.2 \times 10^{-6} \text{ MPa}^{-1} \cdot \text{min}^{-q} \\ q &= 0.00775 \\ t_o &= 1 \text{ min.} \end{aligned} \quad (24)$$

while wet transverse compliance data assumed the form

$$S_T(t) = D_o + D_1 t^n \quad (25)$$

with

$$\begin{aligned} D_o &= 88.2 \times 10^{-6} \text{ MPa}^{-1} \\ D_1 &= 1.662 \times 10^{-6} \text{ MPa}^{-1} \text{ min}^{-n} \\ n &= 0.14 \end{aligned} \quad (26)$$

The data also indicate that the AS/3502 material is hygrothermorheologically simple. The temperature dependent shift factor,  $a_T$  and moisture dependent shift factor  $a_M$  were expressed as follows

$$a_T = \exp(-T/A + B) \quad (27)$$

$$\text{and } a_M = \exp(-C_o m + C_1) \quad (28)$$

with

$$\begin{aligned}
 A &= 6.258 \\
 B &= 45.81 \\
 C_0 &= 5.2 \\
 C_1 &= .26
 \end{aligned}
 \tag{29}$$

In (27) and (28)  $T$  is the temperature in  $^{\circ}\text{K}$  and  $m$  is the moisture content in % weight gain.

It was also found that the combined temperature-moisture shift factor,  $a_{TM}$ , could be expressed as a product

$$a_{TM} = a_T a_M \tag{30}$$

Data from reference [30] also indicate that the thermal expansion coefficient varies linearly with temperature

$$\alpha_L = \alpha_{L0} + \alpha_{L1}T \tag{31}$$

$$\alpha_T = \alpha_{T0} + \alpha_{T1}T$$

with

$$\begin{aligned}
 \alpha_{L0} &= -.484 \times 10^{-6} \text{ cm/cm/}^{\circ}\text{K} \\
 \alpha_{L1} &= 0.72 \times 10^{-9} \text{ cm/cm/}^{\circ}\text{K}^2 \\
 \alpha_{T0} &= 9.05 \times 10^{-6} \text{ cm/cm/}^{\circ}\text{K} \\
 \alpha_{T1} &= 0.41 \times 10^{-7} \text{ cm/cm/}^{\circ}\text{K}^2
 \end{aligned}
 \tag{32}$$

Experimental data on AS/3502 graphite/epoxy [23] indicate that transverse moisture expansional strains may be expressed

$$\begin{aligned}
 \epsilon_T^H &= \beta_T(m-m_1) \quad \text{for } m > m_1 \\
 \epsilon_T^H &= 0 \quad \text{for } m \leq m_1
 \end{aligned}
 \tag{33}$$

where  $\epsilon_T^H$  is the transverse moisture swelling strain,  $m$  is the moisture content and  $m_1$  the threshold moisture content ( $m_1=0.1\%$ ). Also,  $\beta_T$  is the transverse moisture expansion coefficient ( $\beta_T=0.00324$  cm/cm/% moisture).

The longitudinal moisture expansional strain was negligibly small and we took  $\beta_L=0$  in all computations.

Since data for the AS/3502 material [30] are given in terms of creep compliances, we employed the quasi-elastic approximation [31] to express the relaxation moduli that are required for our viscoelastic analysis, namely

$$\begin{aligned} C_L(t) &= \frac{S_T(t)}{S_L S_T(t) - S_{LT}^2} \\ C_T(t) &= \frac{S_L}{S_L S_T(t) - S_{LT}^2} \\ C_{LT}(t) &= \frac{-S_{LT}}{S_L S_T(t) - S_{LT}^2} \end{aligned} \tag{34}$$

It has been shown [23] that for the AS/3502 material, the above approximation involves errors of less than 2%.

## EXPERIMENTAL PROCEDURE

Effects of residual stresses in composite materials can be detected by measuring curvatures of anti-symmetric laminates [2,4,23,28,32-34]. However, both lay-up and dimensions of the laminate must be chosen advisedly. For instance, the easiest conceivable lay-up, that of  $[0_n/90_n]_T$  is unsuitable because it develops premature cracks due to its low fracture toughness [2,28,33]. In addition, the deformation of plates with high length to thickness ratio departs from linearity, and may be even subjected to thermal buckling [35], while excessively thick plates require an impractically long time to reach moisture saturation.

Based on a multitude of considerations [23], square plates of in-plane dimensions of 0.1016 m (4") and the lay-up  $[0/90/0_4/90_4/0/90]_T$  were chosen as test specimens (see Fig. 1). Forty-five specimens were cut-up from larger panels that were manufactured and cured according to manufacturer's specifications.

Curvatures were determined from deflections that were measured periodically by means of dial gages attached to a rigid stand, as detailed elsewhere [23]. Deflection measurements yielded no more than 1% deviations in curvature values within each specimen and a scatter of  $\pm 4\%$  within each group of specimens. Also, the curvatures  $k_x$  and  $k_y$  deviated from their average values by no more than 4%.

Exposure to fixed levels of relative humidity was achieved by placing specimens above suitable salt solutions [36] within humidity chambers.\* Temperature control was achieved by placing the chambers in several rooms with different thermostat settings. A summary of the test environments is

\*The selected solutions were: LiCl (13%R.H.), NaCl (75%R.H.), and  $K_2SO_4$  (95%R.H.).

given in Table 1 below.

T(°K) \ RH(%)	0	13	75	95
298		X	X	X
327	X	X	X	X
339	X	X	X	X
346				X

Table 1. Combinations of Temperature and Relative Humidity Considered.

To assure initially dry conditions, all specimens were dessicated at 327°K (130°F) until reaching equilibrium weight. Upon exposure to moisture, weight gains were measured periodically, at equal  $\sqrt{t}$  intervals.

## RESULTS

Computational and experimental results for all environmental exposures are shown in Figures 2-11. In all those figures values of the non-dimensional curvature change  $h_3(k_{x_i} - k_x(t))$  are plotted vs. the square-root of time,  $t$  in days. In the above  $h_3$  is half the laminate thickness as before,  $k_{x_i}$  is the initial dry curvature and  $k_x(t)$  is the time-dependent curvature. The solid lines in the figures refer to elastic predictions whereas dashed lines represent viscoelastic evaluations. Experimentally determined curvatures had a typical data scatter of about 4-6% about the average values shown in the figures.

In those cases which include desorption (Figures 2-4) the desorption results were plotted with the time scale reset and measured as the square-root of time since the initiation of desorption.

In view of the observation that a geometrically constrained Hercules 3502 resin develops significant chemical shrinkage stresses during cure [37] the initial curvature, prior to exposure to moisture, is caused partly by the above mentioned chemical effect and partly by thermal cool-down. Since it is impossible to separate those effects, it was decided to relate all results in terms of departures from an initial curvature, rather than through absolute curvatures. Presented in this manner, the effects of initial stresses should disappear entirely in the elastic case. However, the uncertainty regarding initial stress effects must still be resolved when considering viscoelastic behavior. To overcome this ambiguity two sets of viscoelastic computations were performed. In the first set, the stress-free temperature was assumed to be the cure temperature of 455°K (350°F), while in the second set the stress-free temperature was assumed to be 25°K higher. It was found that

the results of the two sets of calculations yielded indistinguishable results for the curvature differences  $k_{x_i} - k_x(t)$  that are exhibited in Figs. 2-11.

Reproducibility of experimental results was checked by exposing two groups, of three specimens each, in two separate chambers to identical environmental conditions. The results for all four groups, averaging values between the three specimens within each group, are shown in Fig. 5. It is seen that the results coalesce to a continuous curve, proving consistent and reproducible data.

Note that, because of the way results are plotted in Figures 2-11, large values of the ordinate represent greater change of the curvature relative to the initial dry curvature, and thus smaller absolute values of curvature. It is interesting to note that elasticity predicts greater departures of curvature than viscoelasticity. In addition, during desorption the viscoelastic curvature exceeds its earlier value, prior to the onset of conditioning. These results seem contrary to intuitive notions that relaxation behavior should necessarily yield values that are smaller, however, they are typical of results obtained for problems in which an external agent (in this case moisture) acts as a stress inducing agent as well as a stress relaxing factor [3].

It can be seen from Figures 2-11 that data obtained during absorption at high temperature are closer to the elasticity predictions than to viscoelastic calculations. The data tend toward the viscoelastic results with the lowering of the conditioning temperatures. This trend indicates that, at least during initial absorption, the time-dependent behavior is predominantly viscoelastic, except under the more extreme environmental conditions. Under those more extreme conditions the fact that measured curvatures are smaller than viscoelastic predictions suggests the presence of some sort of moisture induced damage.

Figures 9-11 represent results obtained during absorption at a relative humidity of 13%. Since in this case the equilibrium moisture weight gain is 0.08%, which is below the threshold moisture content  $m_1=0.10\%$ , this circumstance is associated with no moisture induced strains. An elastic analysis, therefore, will predict no time-dependent changes in curvature, so that only viscoelastic results are plotted in Figures 9-11. The fact that the curvature was nevertheless observed to relax during exposure to a 13% relative humidity environment indicates that a time-dependent effect is inherently associated with moisture absorption, even in the absence of moisture expansional strains. Note the difference in scale between Figures 9-11 and Figures 2-8, indicating that under 13% R.H. the difference between experimental data and viscoelastic predictions is smaller than meets the eyes.

Periodic curvature measurements were also obtained from specimens conditioned dry at 339°K (150°F) and 327°K (130°F). The specimens were kept dry by placing a  $\text{CaCl}_2$  dessicant material in the environmental chambers. In these two situations, the measured curvature remained constant to within less than 1% of their original curvature for exposure times of approximately 6 months and 1 year, respectively. This shows that, for the AS/3502 graphite/epoxy material, time-dependent effects become significant only in the presence of moisture.

Note that, in Figures 2-4, the measured curvatures do not return to their original values after complete desorption, indicating a hysteresis-like material response. In Figure 2 the deviation of measured curvatures from viscoelastic predictions is about the same at the end of desorption as it is at the end of absorption. In Figures 3 and 4, however, the deviation from the viscoelastic predictions was larger at the end of desorption than it was at the end of absorption. This is especially apparent in Figure 4 where



measured values agreed well with viscoelastic predictions at the termination of the absorption phase, but differed significantly when desorption was complete. This observation is consistent with the fact that large tensile stresses develop at the surface of the laminate during the early stages of moisture desorption due to the steep moisture gradients which occur at this time [4]. These tensile stresses enhance matrix micro-cracking and fiber-matrix interface degradation, thus producing smaller curvatures than would be observed in the absence of these damage mechanisms.

All the curvature data obtained under environmental conditions in which moisture expansional strains develop (e.g. Figures 2-8) are plotted in Figure 12. In this figure, the ordinate and abscissa have been non-dimensionalized in such a way that the elastic results for all conditions fall on a single curve. The reduced time  $t^*$  is the non-dimensionalized quantity  $t^* = Dt/h_3^2$ ,  $m_1$  is the threshold moisture content ( $m_1 = 0.10\%$ ), while  $m_\infty$  is the equilibrium moisture content. The fact that the experimental data do not fall on a single curve provides further evidence that the material behavior is inelastic.

Additional tests were performed to measure curvatures of pre-saturated specimens under cyclic environmental exposures. In these experiments, specimens that were saturated at 95% R.H. were switched at regular time intervals between chambers with 0% and 95% R.H. All these tests were performed at a constant temperature of 327°K (130°F).

Results for the time-dependent curvature change obtained during these tests for cycles of 16 days and 9 days are shown in Figures 13 and 14. Note that in these figures time is measured from initial saturation (or the beginning of cycling). The elastic predictions are shown by solid lines, whereas viscoelastic predictions are given by dashed lines. Note that while initially the experimental results and viscoelastic predictions are in good

agreement, the discrepancy between the two sets of results increases as cycling continues. This suggests that repeated wetting and drying of composites enhances the moisture induced degradation of material properties.

This contention is further supported by the moisture uptake data obtained during the same environmental cycling tests, presented in Figures 15 and 16. The solid lines in these figures represent predictions based upon Fick's law. Note that the discrepancies between data and theory increase as cycling proceeds. This provides an indirect confirmation to the proposition of moisture induced damage.

RESEARCH ON COMPOSITE MATERIALS FOR STRUCTURAL DESIGN

(U) TEXAS A AND M UNIV COLLEGE STATION MECHANICS AND

MATERIALS RE. D ALLEN ET AL. APR 84 MM-4665-84-5

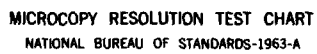
UNCLASSIFIED

AFOSR-TR-85-0226 F49620-82-C-0057

F/G 11/9

NL

END



**MICROCOPY RESOLUTION TEST CHART**  
**NATIONAL BUREAU OF STANDARDS-1963-A**

### CONCLUDING REMARKS

This paper presented an investigation of moisture effects on the mechanical behavior of polymeric composites. It was shown that the time-dependent material properties of the resin, which become more accentuated in the presence of moisture, play a very significant role on the response of the composite. This material time-dependence couples with the time-factor associated with the diffusion process to yield a very complicated history effect.

The drying of saturated composite laminates is accompanied by tensile stresses which, under appropriate combinations of time, temperature and humidity, exceed the tensile strength of the material - thereby causing matrix cracking or debonding between fibers and matrix. These cracks and debondings present new surfaces for moisture absorption during subsequent exposures, which lead to highly concentrated swelling strains at the newly formed tip zones. In this way the growth of damage may feed upon itself with each additional humidity cycle until reaching a critical level.

A detailed investigation of this highly complex damage mechanism should employ fracture mechanics and deserves further study.

# ACKNOWLEDGEMENT

This work was conducted under Contract F49620-82-C-0057 from the Air Force Office of Scientific Research (AFOSR) whose support is gratefully acknowledged.

## REFERENCES

1. C.C. Chamis, Residual Stresses in Angleplied Laminates and Their Effects on Laminate Behavior, NASA Report NASA TM-78835 (1978).
2. H.T. Hahn and N.J. Pagano, Curing Stresses in Composite Laminates, J. Comp. Mat. 9, 91 (1975).
3. Y. Weitsman, Effects of Fluctuating Moisture and Temperature on the Mechanical Response of Resin-Plates, J. Appl. Mech. 44, 571 (1977).
4. F.W. Crossman, R.E. Mauri and W.J. Warren, Hygrothermal Damage Mechanisms in Graphite-Epoxy Composites, Lockheed Palo Alto Research Laboratory, Final Report (1979).
5. C.H. Shen and G.S. Springer, Effects of Moisture on the Tensile Strength of Composite Materials, J. Comp. Mat. 11, 2 (1977).
6. C.Y. Lundemo and S. Thor, Influence of Environmental Cycling on the Mechanical Properties of Composite Materials, J. Comp. Mat. 11, 276 (1977).
7. C.E. Browning and J.T. Hartness, Effects of Moisture on the Properties of High Performance Structural Resins and Composites, Proceedings of the Third Conference on Composite Materials, ASTM (1974).
8. R.E. Mauri, F.W. Crossman and W.J. Warren, Assessment of Moisture Altered Dimensional Stability of Structural Composites, SAMPE Symp. 23, 1202 (1978).
9. C.E. Browning, The Mechanisms of Elevated Temperature Property Losses in High Performance Structural Epoxy Resin Matrix Materials After Exposures to High Humidity Environments, Polym. Eng. Sci. 18, 16 (1978).
10. D.H. Kaelble, P.J. Dynes, L.W. Crane and L. Maus, Interfacial Mechanisms of Moisture Degradation in Graphite-Epoxy Composites, J. Adhesion 7, 25 (1975).

11. K.H.G. Ashbee and R.C. Wyatt, Water Damage in Glass Fibre/Resin Composites, Proc. R. Soc. A 312, 553 (1969).
12. D.H. Kaelble, P.J. Dynes, L.W. Crane and L. Maus, Kinetics of Environmental Degradation in Graphite-Epoxy Laminates, Composite Reliability, ASTM STP 580, 247 (1975).
13. M.K. Antoon and J.L. Koenig, Irreversible Effects of Moisture on the Epoxy Matrix in Glass-Reinforced Composites, J. Polym. Sci.: Polym. Phys. 19, 197 (1981).
14. I.G. Hedrick and J.B. Whitesides, Effects of Environment on Advanced Composite Structures, Conference on Aircraft Structures: The Emerging Methodology for Structural Assurance, AIAA, 1 (1977).
15. J.R. Vinson, R.B. Pipes, W.J. Walker and D.R. Ulrich, The Effects of Relative Humidity and Elevated Temperature on Composite Structures, presented at the Workshop on the Effects of Relative Humidity and Elevated Temperature on Composite Structures, Delaware University, Newark, N.J. (1976).
16. C.D. Shirrel, Diffusion of Water Vapor in Graphite/Epoxy Composites, Advanced Composite Materials - Environmental Effects, ASTM STP 658, 21 (1978).
17. J.M. Whitney and C.E. Browning, Some Anomalies Associated with Moisture Diffusion in Epoxy Matrix Composite Materials, Advanced Composite Materials - Environmental Effects, ASTM STP 658, 43 (1978).
18. O. Gillat and L.J. Broutman, Effect of an External Stress on Moisture Diffusion and Degradation in a Graphite-Reinforced Epoxy Laminate, Advanced Composite Materials - Environmental Effects, ASTM STP 658, 61 (1978).
19. R. DeLasi and J.B. Whiteside, Effect of Moisture on Epoxy Resins and Composites, Advanced Composite Materials - Environmental Effects, ASTM STP 658, 2 (1978).



20. A. Apicella, L. Nicolais, G. Astarita and E. Drioli, Hygrothermal History Dependence of Moisture Sorption Kinetics in Epoxy Resins, Polym. Eng. Sci. 21, 18 (1981).
21. R.M. Jones, Mechanics of Composite Materials, Scripta Book Co. (1975).
22. C.H. Shen and G.S. Springer, Moisture Absorption and Desorption of Composite Materials, J. Comp. Mat. 10, 36 (1976).
23. B.D. Harper, On the Effects of Post Cure Cool Down and Environmental Conditioning on Residual Stresses in Composite Laminates, Ph.D. Thesis, Texas A&M University (1983).
24. A.V. Luikov, Analytical Heat Diffusion Theory, Academic Press (1968).
25. J. Crank, The Mathematical Theory of Diffusion, 2nd Ed. Oxford University Press (1975).
26. Y. Weitsman, A Rapidly Convergent Scheme to Compute Moisture Profiles in Composite Materials Under Fluctuating Ambient Conditions, J. Comp. Mat. 15, 349 (1981).
27. D.A. Douglass and Y. Weitsman, Stresses Due to Environmental Conditioning of Cross-Ply Graphite/Epoxy Laminates, Proc. Third International Conference on Composite Materials (ICCM3), 1, 529, Pergamon Press (1980).
28. R.S. Lott, Moisture and Temperature Effects on Curvature of Anti-Symmetric Cross-Ply Graphite Epoxy Laminates, Master's Thesis, Texas A&M University (1980).
29. R.A. Schapery, A Method of Viscoelastic Stress Analysis Using Elastic Solutions, J. Franklin Inst. 279 (1965).
30. K.G. Kibler, Time-Dependent Environmental Behavior of Graphite/Epoxy Composites, Final Report, General Dynamics Corporation, Fort Worth, Texas, Contract No. F33615-77-C-5109, Report No. AFWAL-TR-80-4052 (1980).
31. R.A. Schapery, Viscoelastic Behavior and Analysis of Composite Materials, Mechanics of Composite Materials, Vol. 2, Academic Press (1974).

32. F.W. Crossman, R.E. Mauri and N.T. Warren, Moisture Altered Viscoelastic Response of Graphite/Epoxy Composites, Advanced Composite Materials - Environmental Effects, ASTM STP 658, 205 (1978).
33. B.D. Harper and Y. Weitsman, Residual Thermal Stresses in an Unsymmetrical Cross-Ply Graphite/Epoxy Laminate, Proceedings of the 22nd SSD and Materials Conference (1981).
34. D.L. Flagg and F.W. Crossman, Analysis of the Viscoelastic Response of Composite Laminates During Hygrothermal Exposure, J. Comp. Mat. 15, 296 (1981).
35. M.W. Hyer, Calculations of the Room-Temperature Shapes of Unsymmetric Laminates, J. Comp. Mat. 15, 296 (1981).
36. F.E.M. O'Brien, The Control of Humidity by Saturated Salt Solutions, J. Scient. Instrum. 25, 73 (1948).
37. B.D. Harper, D. Peretz and Y. Weitsman, Assessment of Chemical Cure-Shrinkage Stresses in Two Technical Resins, AIAA/ASME, ASCE, AHS 24th Structures, Structural Dynamics and Materials Conference (1983).

## Figure Legends

- Figure 1. Geometry of anti-symmetric cross-ply laminate.
- Figure 2. Time-dependent curvature change of  $(0/90/0_4/90_4/0/90)_T$  AS/3502 graphite/epoxy laminates at  $346^\circ\text{K}$  ( $163^\circ\text{F}$ ). Absorption data is obtained at 95% relative humidity.
- Figure 3. Time-dependent curvature change of  $(0/90/0_4/90_4/0/90)_T$  AS/3502 graphite/epoxy laminates at  $339^\circ\text{K}$  ( $150^\circ\text{F}$ ). Absorption data is obtained at 95% relative humidity.
- Figure 4. Time-dependent curvature change of  $(0/90/0_4/90_4/0/90)_T$  AS/3502 graphite/epoxy laminates at  $339^\circ\text{K}$  ( $150^\circ\text{F}$ ). Absorption data is obtained at 75% relative humidity.
- Figure 5. Time-dependent curvature change of  $(0/90/0_4/90_4/0/90)_T$  AS/3502 graphite/epoxy laminates during absorption at  $327^\circ\text{K}$  ( $130^\circ\text{F}$ ) 95% relative humidity.
- Figure 6. Time-dependent curvature change of  $(0/90/0_4/90_4/0/90)_T$  AS/3502 graphite/epoxy laminates during absorption at  $327^\circ\text{K}$  ( $130^\circ\text{F}$ ) 75% relative humidity.
- Figure 7. Time-dependent curvature change of  $(0/90/0_4/90_4/0/90)_T$  AS/3502 graphite/epoxy laminates during absorption at  $298^\circ\text{K}$  ( $77^\circ\text{F}$ ) 95% relative humidity.
- Figure 8. Time-dependent curvature change of  $(0/90/0_4/90_4/0/90)_T$  AS/3502 graphite/epoxy laminates during absorption at  $298^\circ\text{K}$  ( $77^\circ\text{F}$ ) 75% relative humidity.
- Figure 9. Time-dependent curvature change of  $(0/90/0_4/90_4/0/90)_T$  AS/3502 graphite/epoxy laminates during absorption at  $339^\circ\text{K}$  ( $150^\circ\text{F}$ ) 13% relative humidity.
- Figure 10. Time-dependent curvature change of  $(0/90/0_4/0/90)_T$  AS/3502 graphite/epoxy laminates during absorption at  $327^\circ\text{K}$  ( $130^\circ\text{F}$ ) 13% relative humidity.
- Figure 11. Time-dependent curvature change of  $(0/90/0_4/90_4/0/90)_T$  AS/3502 graphite/epoxy laminates during absorption at  $298^\circ\text{K}$  ( $77^\circ\text{F}$ ) 13% relative humidity.
- Figure 12. Combined results for time-dependent curvature change of  $(0/90/0_4/90_4/0/90)_T$  AS/3502 graphite/epoxy laminates exposed to various environmental conditions.
- Figure 13. Time-dependent curvature change of  $(0/90/0_4/90_4/0/90)_T$  AS/3502 graphite/epoxy laminates during cyclic exposure to 0 and 95% relative humidities at  $327^\circ\text{K}$  ( $130^\circ\text{F}$ ), with cycle-interval of 16 days.

Figure 14. Time-dependent curvature change of (0/90/0<sub>4</sub>/90<sub>4</sub>/0/90)<sub>T</sub> AS/3502 graphite/epoxy laminates during cyclic exposure to 0 and 95% relative humidities at 327°K (130°F) with cycle interval of 9 days.

Figure 15. Moisture content (in % weight gain) during cyclic exposure to 0 and 95% relative humidities at 327°K (130°F), with cycle interval of 16 days.

Figure 16. Moisture content (in % weight gain) during cyclic exposure to 0 and 95% relative humidities at 327°K (130°F), with cycle interval of 9 days.

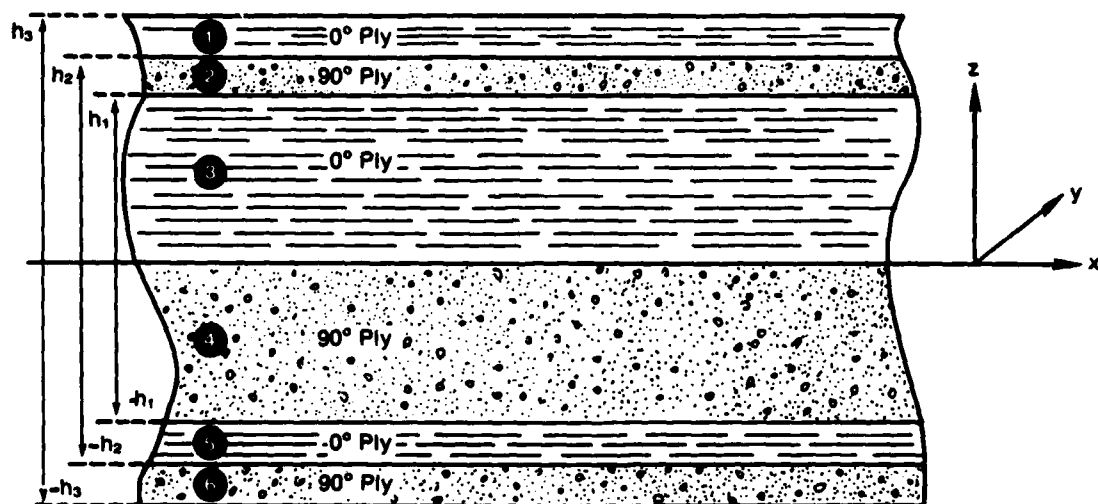


Figure 1. Geometry of anti-symmetric cross-ply laminate.

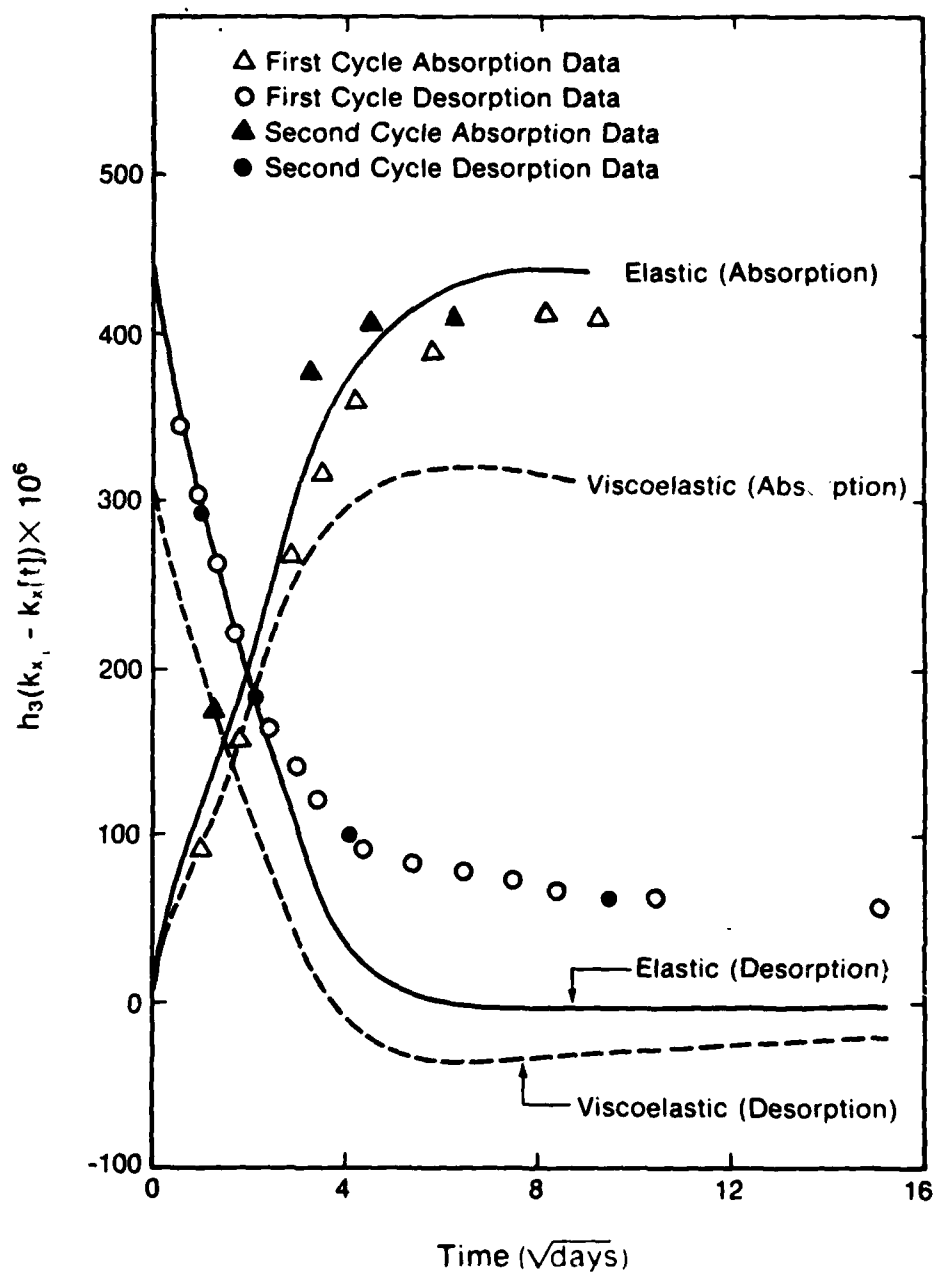


Figure 2. Time-dependent curvature change of  $(0/90/0_4/90_4/0/90)_T$  AS/3502 graphite/epoxy laminates at  $346^\circ\text{K}$  ( $163^\circ\text{F}$ ). Absorption data is obtained at 95% relative humidity.

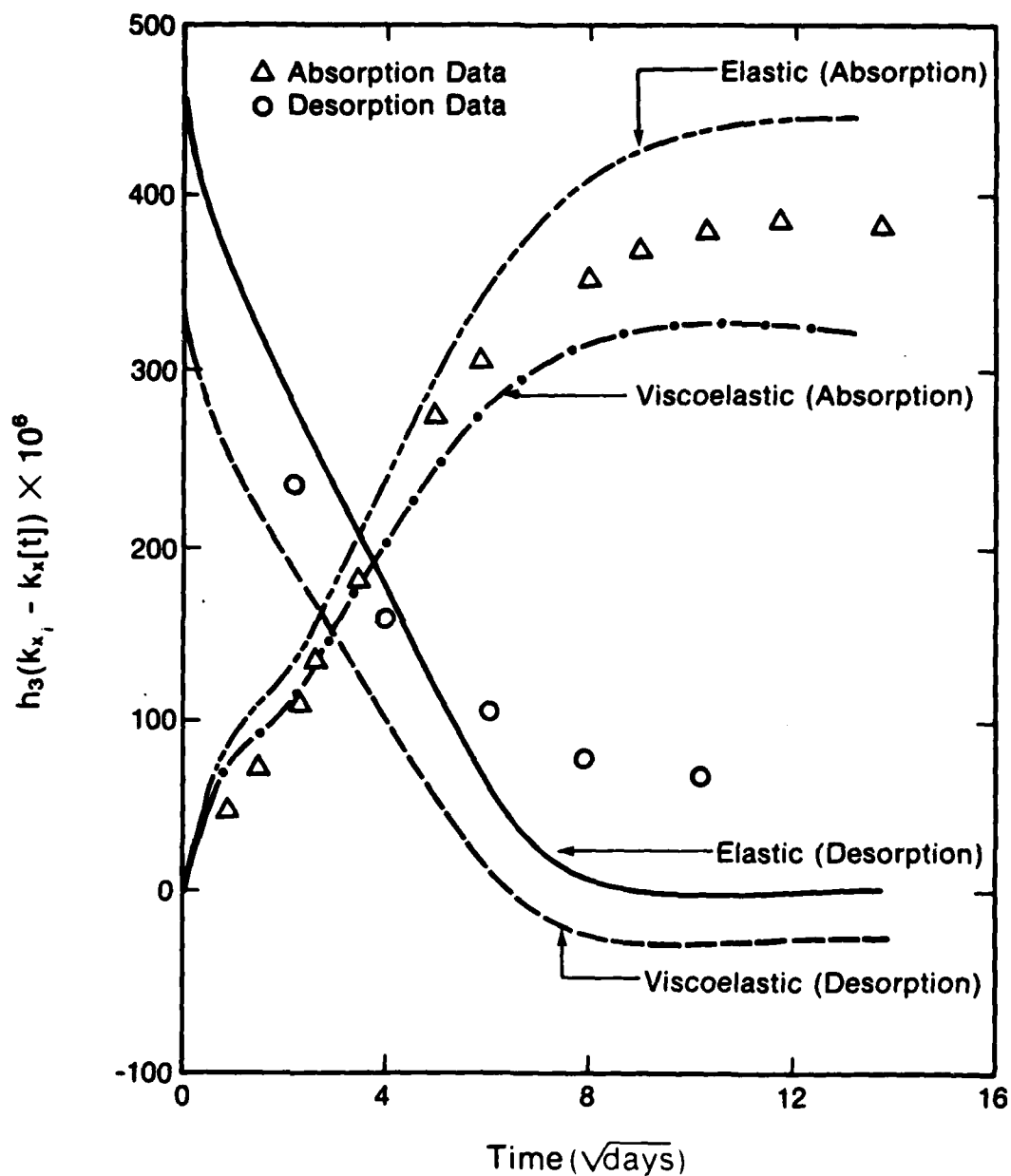


Figure 3. Time-dependent curvature change of  $(0/90/0_4/90_4/0/90)_T$  AS/3502 graphite/epoxy laminates at 339°K (150°F). Absorption data is obtained at 95% relative humidity.

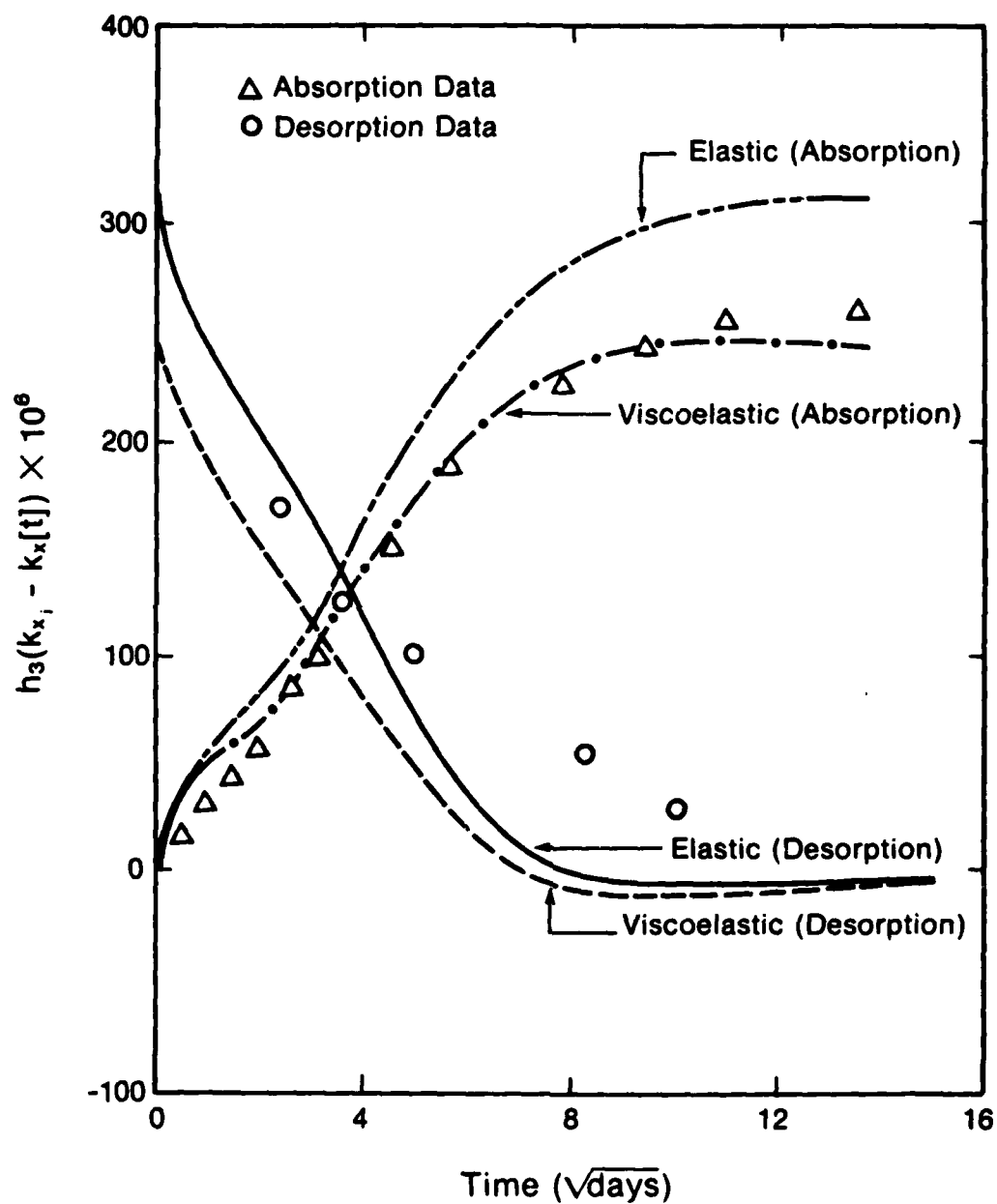


Figure 4. Time-dependent curvature change of  $(0/90/0_4/90_4/0/90)_T$  AS/3502 graphite/epoxy laminates at  $339^\circ\text{K}$  ( $150^\circ\text{F}$ ). Absorption data is obtained at 75% relative humidity.



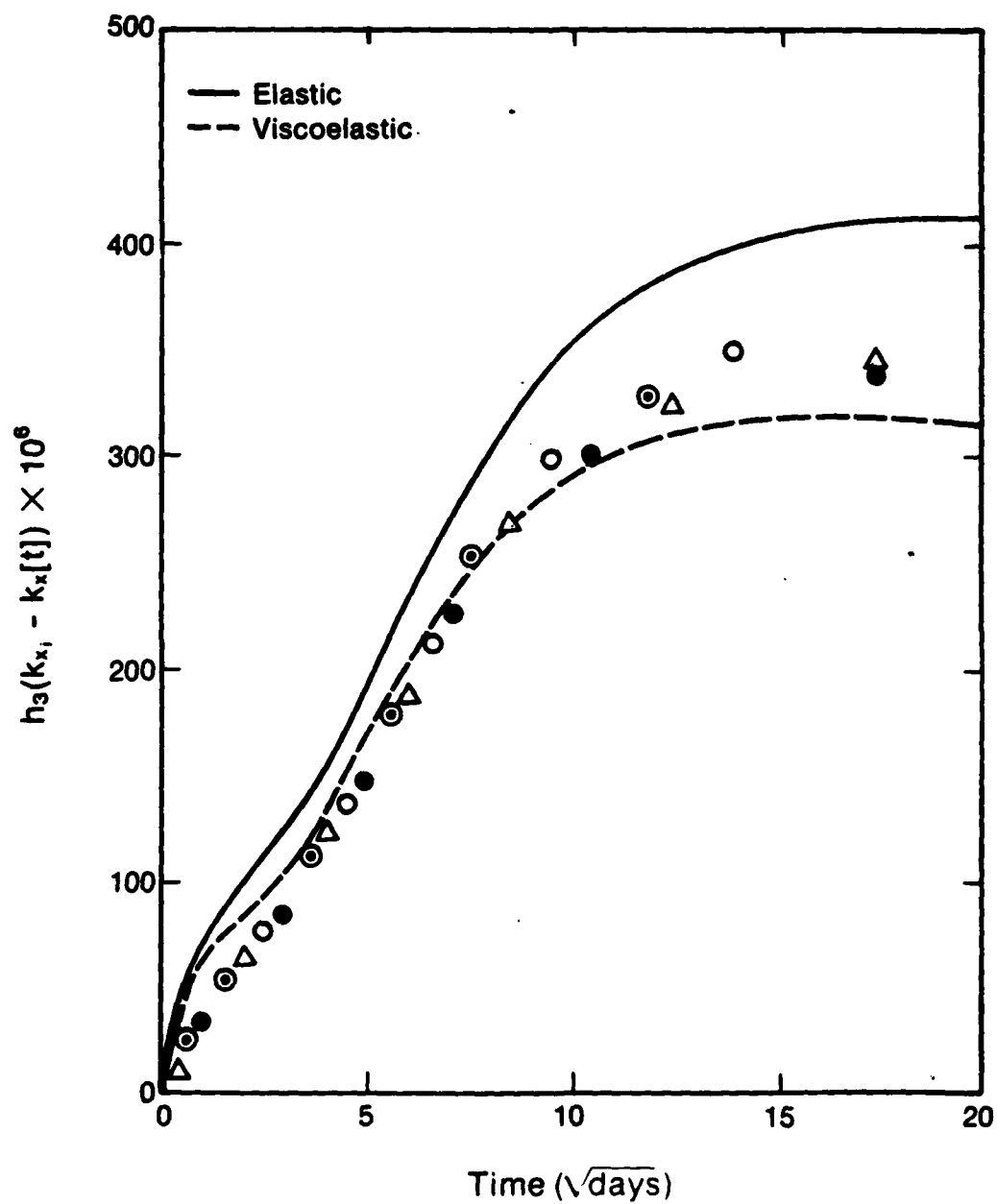


Figure 5. Time-dependent curvature change of  $(0/90/0_4/90_4/0/90)_T$  AS/3502 graphite/epoxy laminates during absorption at  $327^\circ\text{K}$  ( $130^\circ\text{F}$ ) 95% relative humidity.

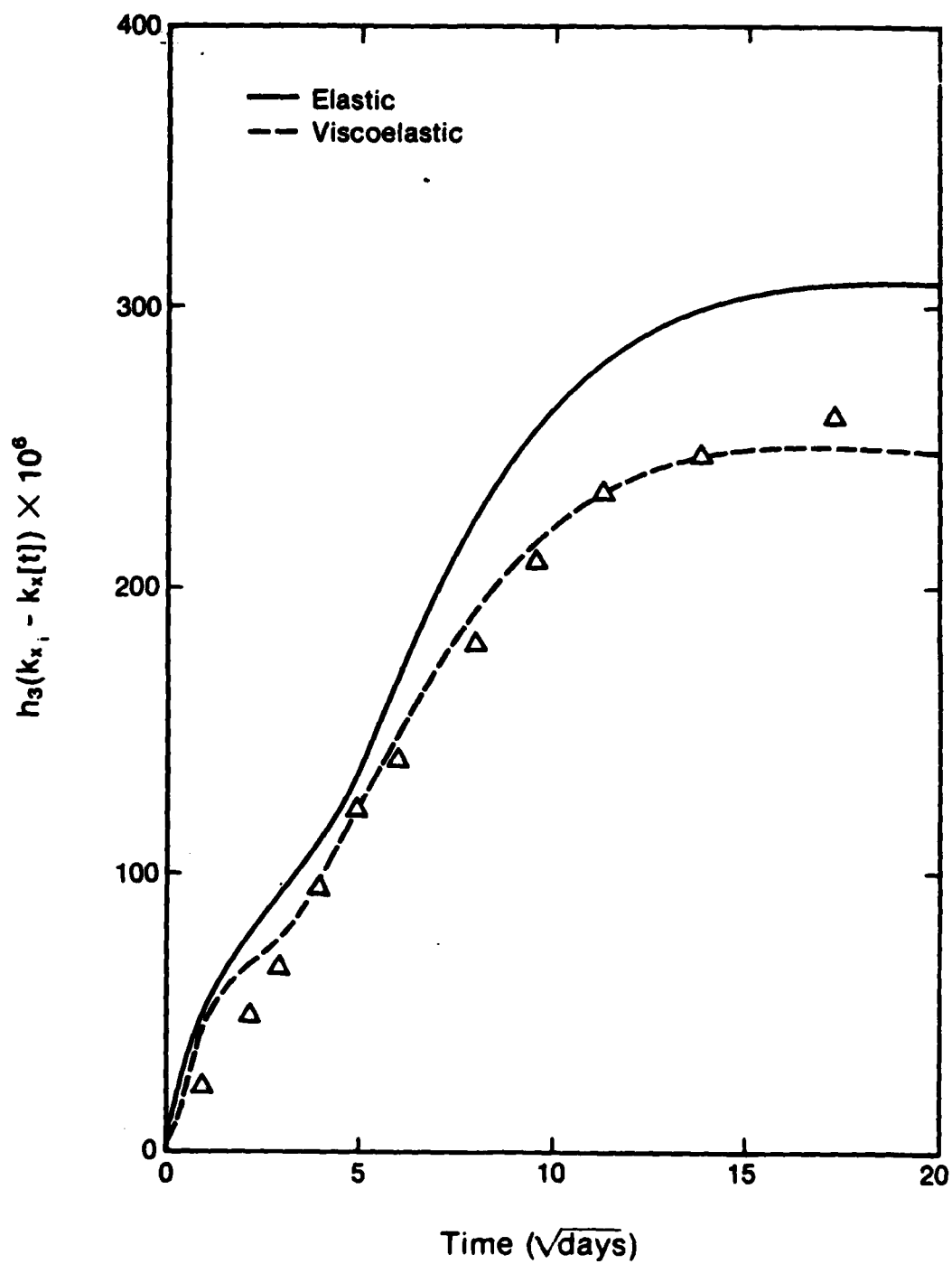


Figure 6. Time-dependent curvature change of  $(0/90/0_4/90_4/0/90)_T$  AS/3502 graphite/epoxy laminates during absorption at  $327^\circ\text{K}$  ( $130^\circ\text{F}$ ) 75% relative humidity.

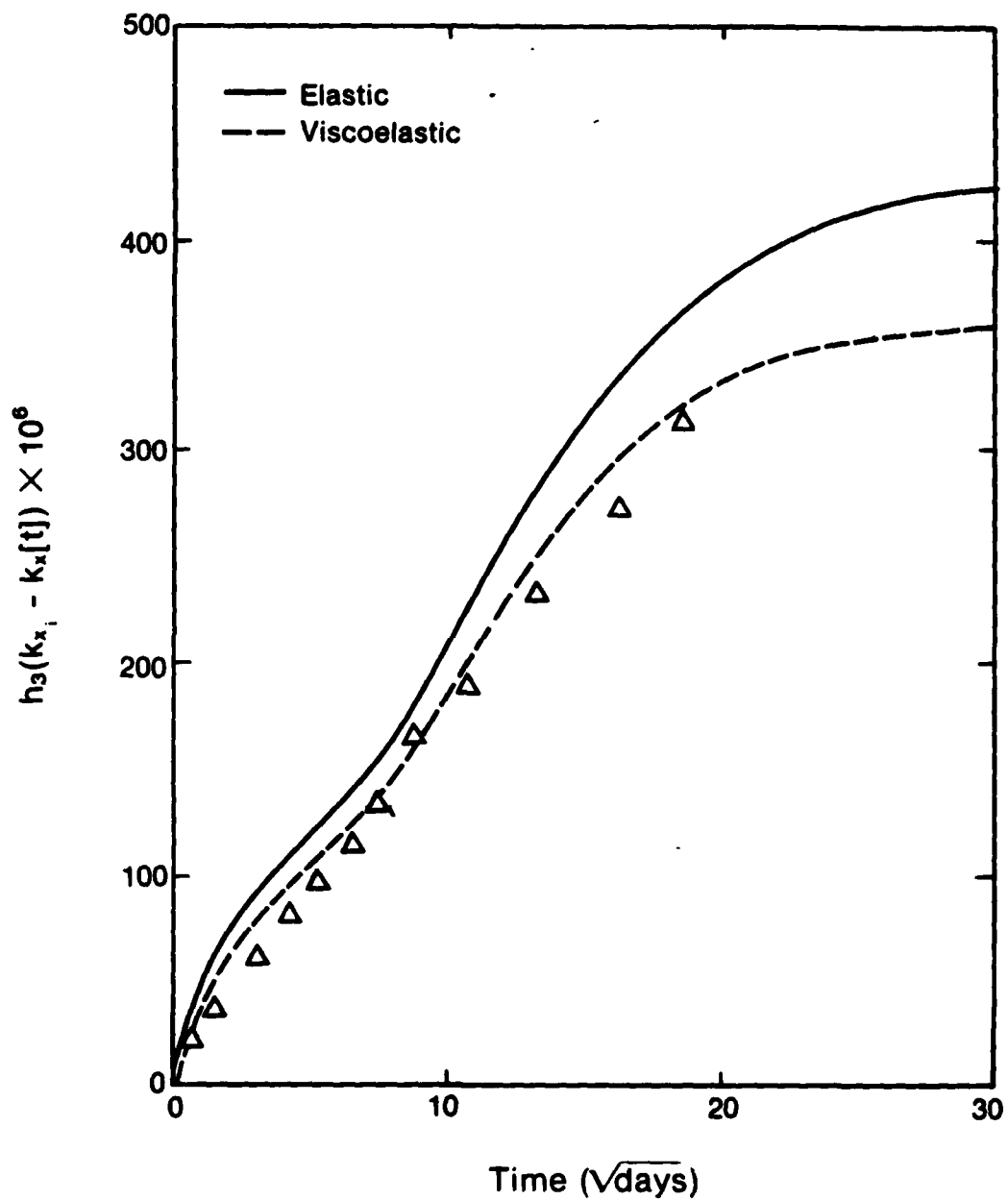


Figure 7. Time-dependent curvature change of  $(0/90/0_4/90_4/0/90)_T$  AS/3502 graphite/epoxy laminates during absorption at  $298^\circ\text{K}$  ( $77^\circ\text{F}$ ) 95% relative humidity.

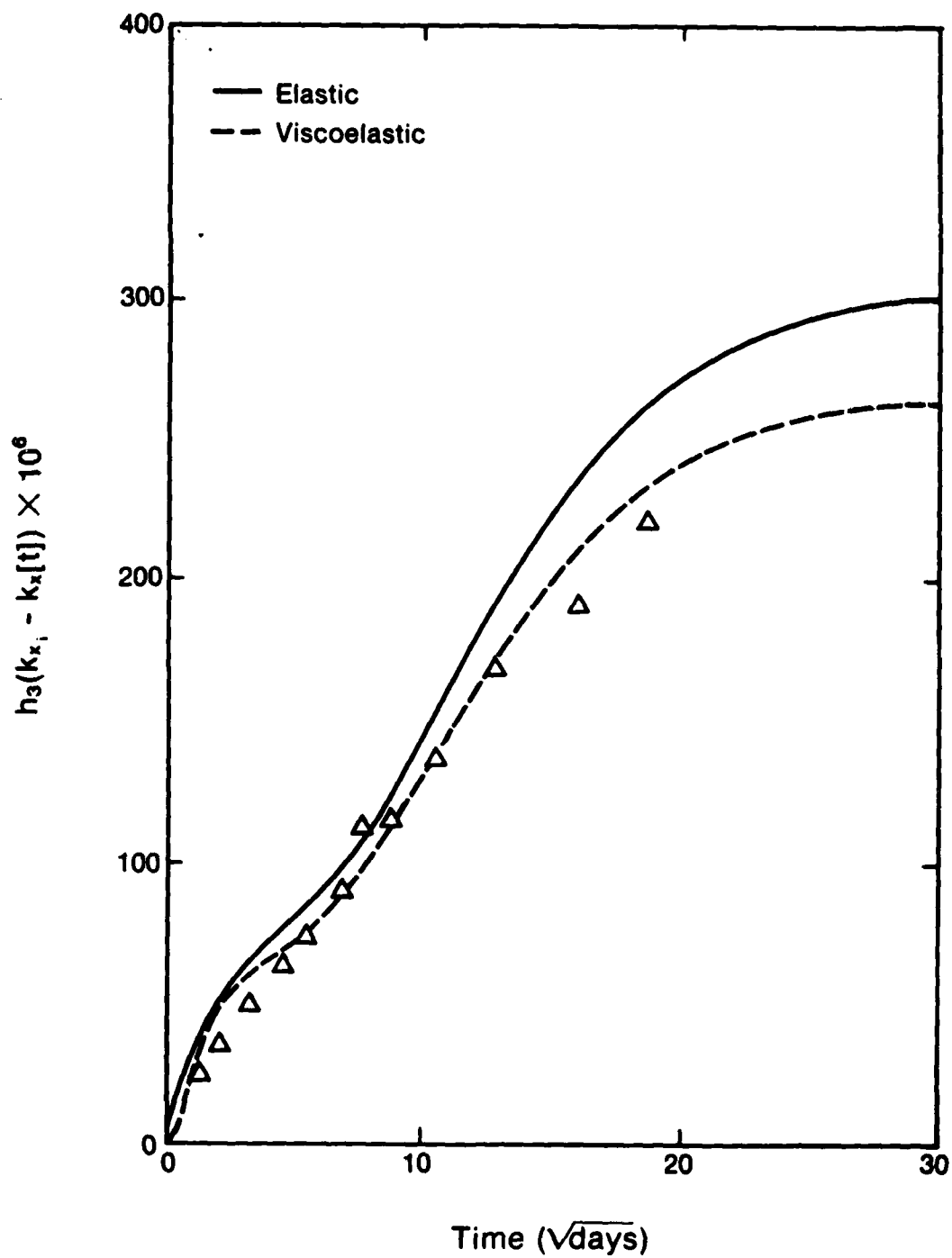


Figure 8. Time-dependent curvature change of  $(0/90/0_4/90_4/0/90)_T$  AS/3502 graphite/epoxy laminates during absorption at  $298^\circ\text{K}$  ( $77^\circ\text{F}$ ) 75% relative humidity.

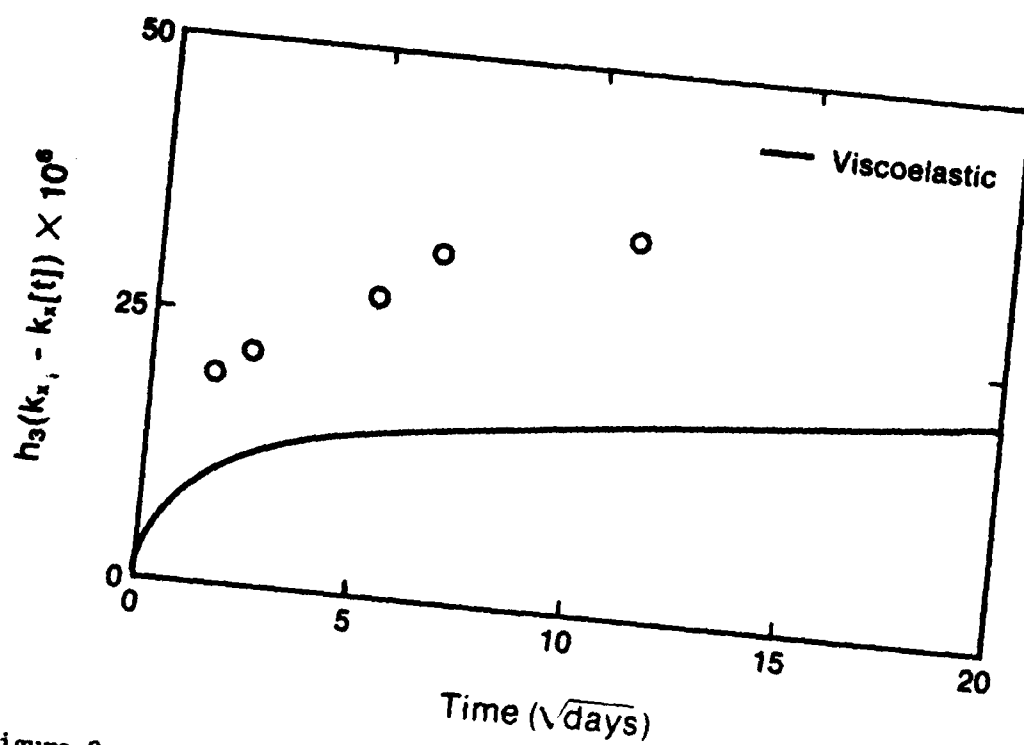


Figure 9. Time-dependent curvature change of  $(0/90/0_4/90_4/0/90)_T$  AS/3502 graphite/epoxy laminates during absorption at  $339^\circ\text{K}$  ( $150^\circ\text{F}$ ) 13% relative humidity.

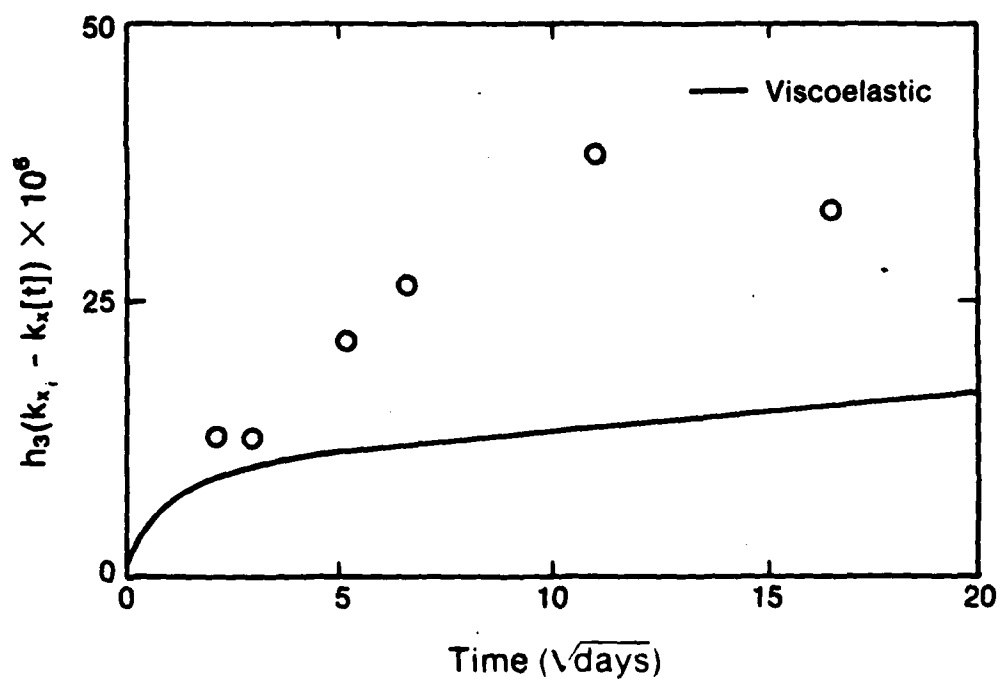


Figure 10. Time-dependent curvature change of  $(0/90/0_4/90_4/0/90)_T$  AS/3502 graphite/epoxy laminates during absorption at  $327^\circ\text{K}$  ( $130^\circ\text{F}$ ) 13% relative humidity.

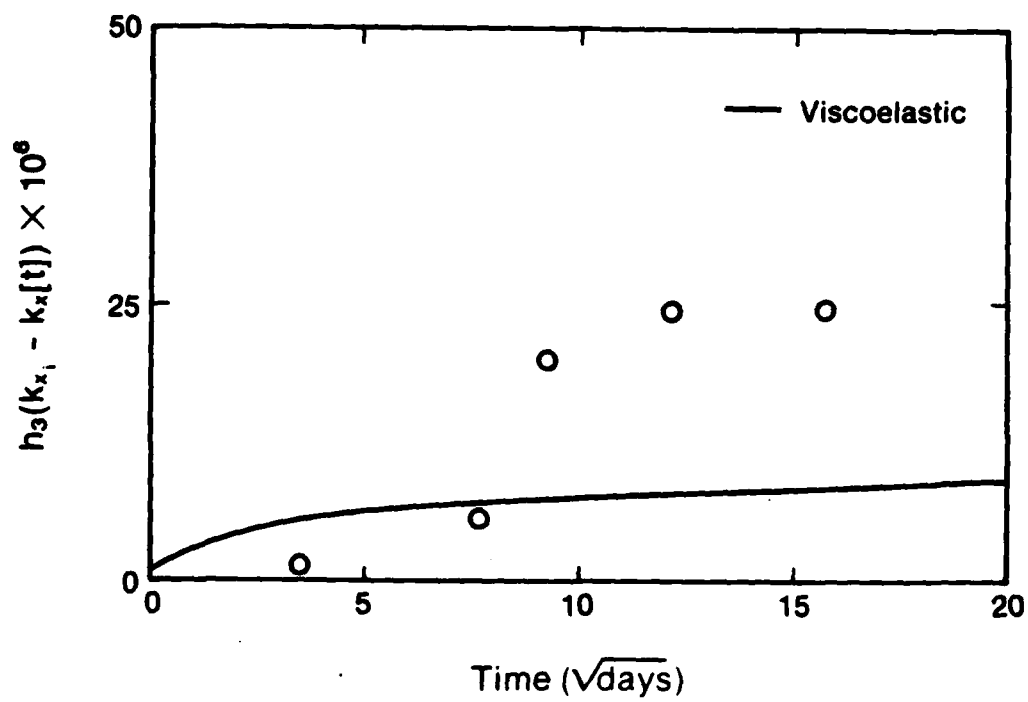


Figure 11. Time-dependent curvature change of  $(0/90/0_4/90_4/0/90)_T$  AS/3502 graphite/epoxy laminates during absorption at 298°K (77°F) 13% relative humidity.

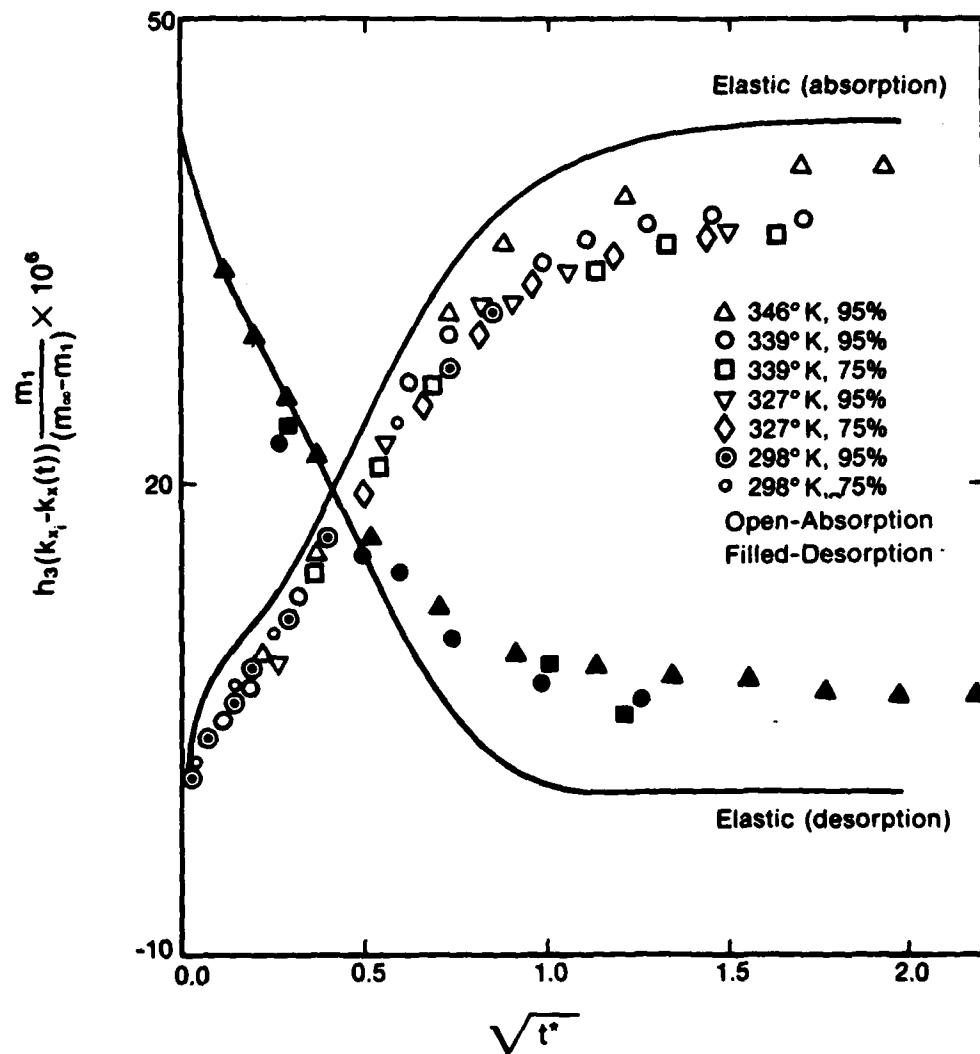


Figure 12. Combined results for time-dependent curvature change of  $(0/90/0_4/90_4/0/90)_T$  AS/3502 graphite/epoxy laminates exposed to various environmental conditions.



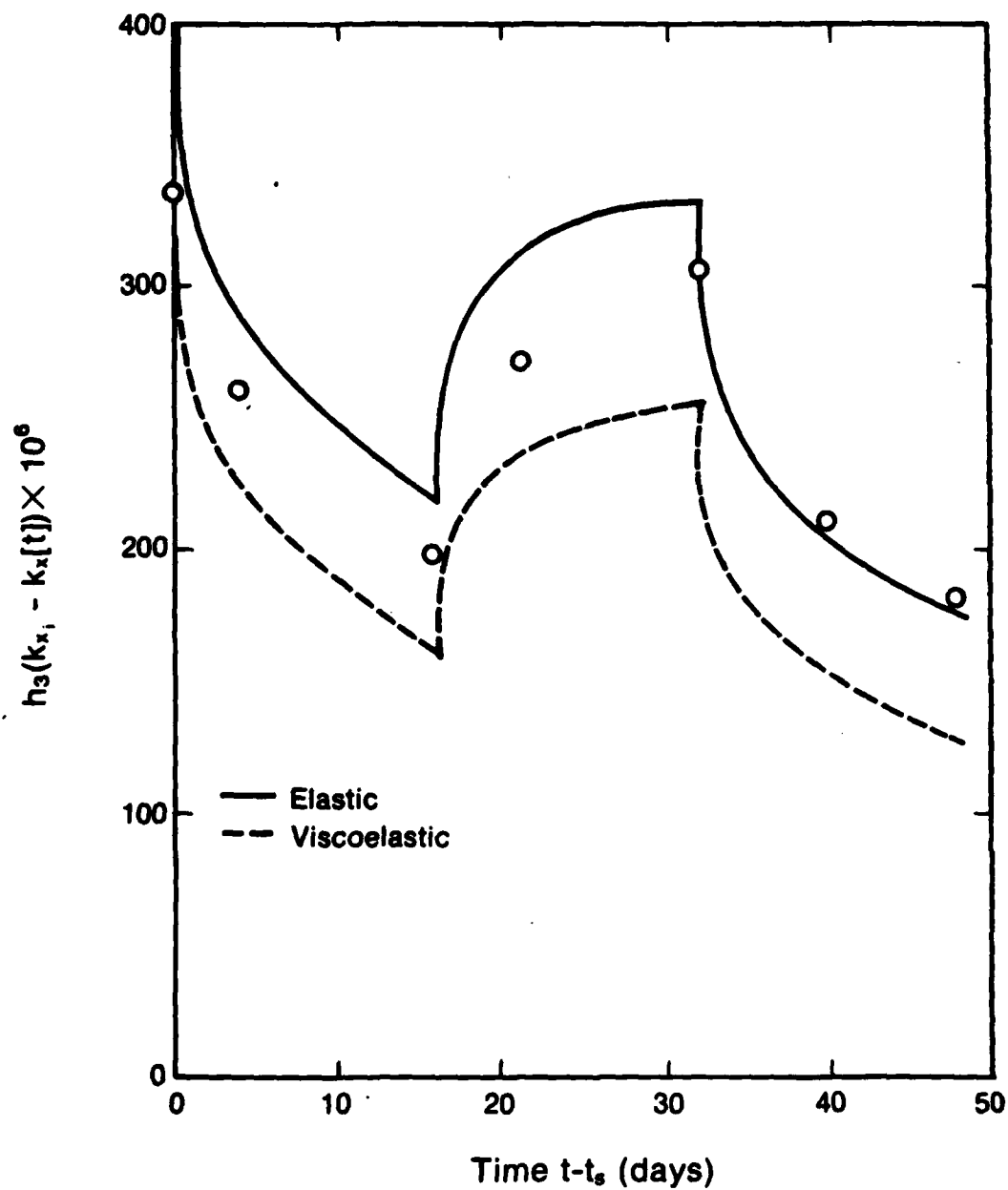


Figure 13. Time-dependent curvature change of  $(0/90/0_4/90_4/0/90)_T$  AS/3502 graphite/epoxy laminates during cyclic exposure to 0 and 95% relative humidities at 327°K (130°F), with cycle-interval of 16 days.

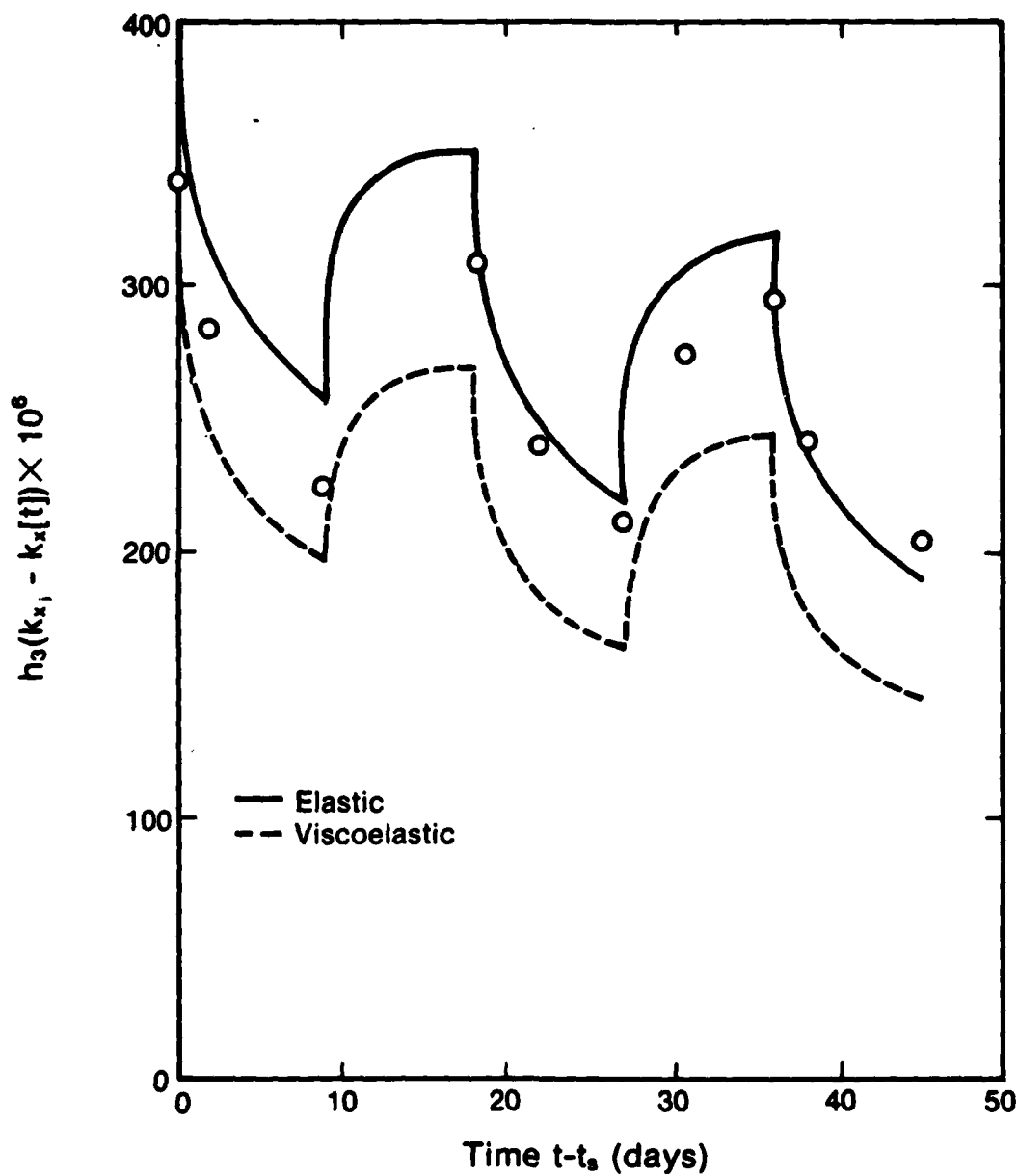


Figure 14. Time-dependent curvature change of  $(0/90/0_4/90_4/0/90)_T$  AS/3502 graphite/epoxy laminates during cyclic exposure to 0 and 95% relative humidities at 327°K (130°F) with cycle interval of 9 days.

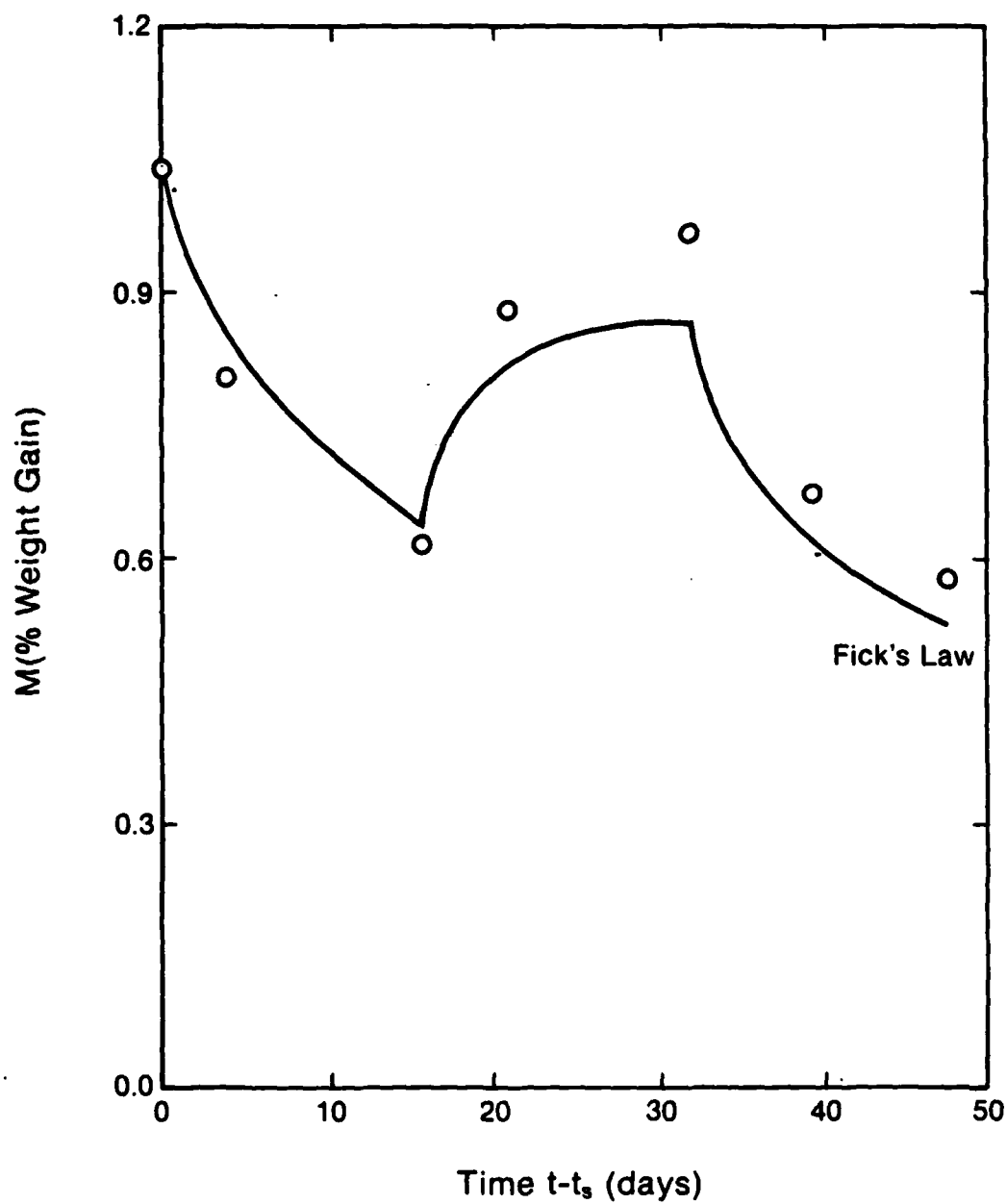


Figure 15. Moisture content (in % weight gain) during cyclic exposure to 0 and 95% relative humidities at 327°K (130°F), with cycle interval of 16 days.

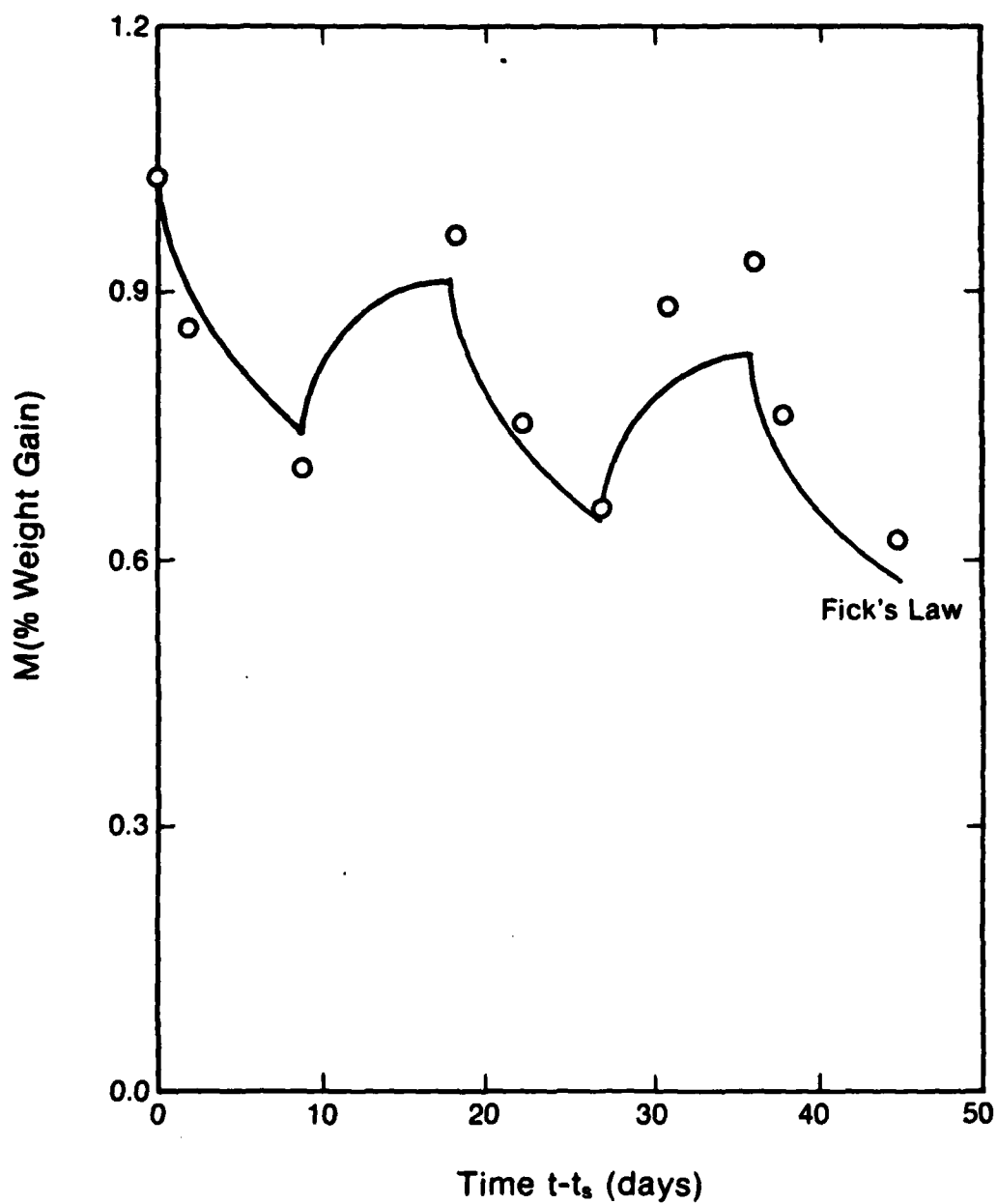


Figure 16. Moisture content (in % weight gain) during cyclic exposure to 0 and 95% relative humidities at 327°K (130°F), with cycle interval of 9 days.

**END**

**FILMED**

**3-85**

**DTIC**